# Decarbonisation of the Cement Production Process

**Franco Williams**

Supervised by Prof. Aidong Yang


Hertford College

Department of Engineering Science

University of Oxford

A thesis submitted for the degree of

Doctor of Philosophy

November 7th, 2025

# Abstract

Cement serves as the most consumed man-made material worldwide, with its production accounting for 8% of global anthropogenic carbon dioxide ($CO_2$) emissions. Clinker, constituting 95% of cement's composition, is the primary contributor to $CO_2$ emissions, making deep decarbonisation necessary to reduce climate change impacts. Although existing studies have tapped into fuel and calcination-oriented decarbonisation options, there is clearly a lack of a systematic comparative assessment of energy and $CO_2$ performances focusing on alternative fuels (carbon-neutral) and alternative clinkers (characterised by low limestone content) in distinct locations, to consistently quantify their potential. This thesis addresses the literature gap through a combination of process simulation, mathematical optimisation, geospatial analysis, along with energetic and gate-to-gate $CO_2$ performance assessments. In this thesis, fuel-based emissions were addressed through the use of hydrogen ($H_2$) and solar energy as alternatives to fossil fuel for clinker production. This was followed by the evaluation of alternative clinkers projected to reduce $CO_2$ emissions from limestone calcination. The findings reveal that using $H_2$ and solar energy as alternative energy sources enables $CO_2$ reductions of up to 27.6%. In contrast, both alternative fuel options demanded higher energy due to water electrolysis and operation of solar photovoltaics (PV) and concentrated solar power (CSP) systems. On the contrary, the use of alternative clinkers was able to achieve $CO_2$ reductions of up to 35%, and 45.5% in energy reductions. Similarly, $CO_2$ reductions of 45% was achieved through partial substitution of clinker with supplementary cementitious materials (SCMs) from $CO_2$ mineralisation. Notably, the economic analysis of the solar driven process shows that in high solar regions, costs can be ~47% lower than less favourable regions, highlighting the influence of location specific solar energy characteristics. These findings accentuate the limitation of fuel substitution

alone in clinker production and underscores the need for decarbonising the calcination process from the material perspective to achieve more substantial emission reductions. The collective contribution of this thesis involves insights into the carbon abatement potential from both the material and process perspectives, demonstrating the technical feasibilities of decarbonisation options.

# Acknowledgements

First and foremost, I am deeply grateful to my supervisor Prof. Aidong Yang for his invaluable guidance, encouragement in fostering critical thinking, and for consistently providing timely and constructive feedback throughout my DPhil journey. I extend my gratitude to Daya Ram Nhuchhen for his kind contribution in validating the research results and reviewing my first original research chapter. To Till Strunge for providing data on $CO_2$ mineralisation which supported the work on my third original research chapter.

I express my thanks to my friends and co-workers from the Systems Engineering Group at Oxford for their unwavering support and sharing knowledge through group seminars and discussions. To the Engineering Science Department for providing the facilities and software to conduct my research whilst offering technical IT support when required. A heartfelt gratitude is extended to my Mum and Dad, for motivating me throughout my DPhil career, inspiring me to pursue my dreams and continuously providing both financial and mental support to complete my studies.

This thesis is dedicated to the future generations, encouraging them to be empowered in innovating sustainable solutions for climate change and lead the way towards a carbon-neutral world for all.

# Publications

Williams, F., Yang, A., Nhuchhen, DR. (2024). Decarbonisation pathways of the cement production process via hydrogen and oxy-combustion. *Energy Conversion and Management, 300, 117931.* https://doi.org/10.1016/j.enconman.2023.117931.

Williams, F., & Yang, A. (2024). Potential of reducing $CO_2$ emissions in cement production through altering clinker compositions. *Ind. Eng. Chem. Res. 2024, 63, 40, 17158–17167.* https://doi.org/10.1021/acs.iecr.4c01885.

Williams, F., & Yang, A. (2025). Substituting fossil fuels from cement production with solar energy to reduce carbon emissions. *Under review.*

# Nomenclature

## Abbreviations

| | |
|---|---|
| $Al_2O_3$ | Aluminium oxide |
| Ar | Argon |
| AAMs | Alkali activated materials |
| AAC | Alkali activated cement |
| ASU | Air separation unit |
| BD | Beam down |
| BR | Brazil |
| BYF | Belite-ye'elimite ferrite |
| $C_2S$ | Belite or dicalcium silicate |
| $C_3A$ | Aluminate or tricalcium aluminate |
| $C_3S$ | Alite or tricalcium silicate |
| $C_3S_2$ | Rankinite |
| $C_4A_3S$ | Ye'elimite |
| $C_4AF$ | Ferrite or tetra-calcium aluminoferrite |
| $Ca_2Al_2SiO_7$ | Gehlenite or melilite |
| $CaCO_3$ | Limestone or calcium carbonate |
| CaO | Calcium oxide |
| $Ca(OH)_2$ | Calcium hydroxide |
| CAPEX | Capital expenditure |
| C-A-S-H | Calcium aluminum silicate hydrate |
| CCS | Carbon capture and storage |
| CCUS | Carbon capture utilisation and storage |
| CFD | Computation fluid dynamics |
| $CH_4$ | Methane |
| CM | Calcined meal |
| CN | China |
| $CO_2$ | Carbon dioxide |
| $CO_2eq$ | Carbon dioxide equivalent |

| | |
|---|---|
| COP | Coefficient of performance |
| CPC | Compound parabolic concentrator |
| CSA | Calcium sulphoaluminate |
| CS, $CaSiO_3$ | Wollastonite |
| CSC | Calcium silicate clinker |
| C-S-H | Calcium silicate hydrate |
| CSP | Concentrated solar power |
| $CSP_{th}$ | CSP thermal heat |
| DNI | Direct normal irradiation |
| EG | Exhaust gas |
| el | Electrical |
| ETS | Emission trading system |
| EU | European Union |
| $Fe_2O_3$ | Iron oxide |
| FGR | Flue gas recirculation |
| GAMS | General Algebraic Modelling System |
| GGBS | Ground granulated blast furnace slag |
| GHG | Greenhouse gases |
| GWP | Global warming potential |
| $H_2$ | Hydrogen |
| $H_2O$ | Water |
| HFC | High ferrite clinker |
| IEA | International energy agency |
| KG | Kiln gas |
| LCA | Life cycle analysis |
| LCOC | Levelised cost of clinker |
| LHV | Lower heating value or calorific value |
| $\dot{m}$ | Mass flow |
| MBM | Meat and bone meal |
| MEA | Monoethanolamine |
| $MgCO_3$ | Magnesium carbonate |
| Mg | Magnesium |
| MgO | Magnesium oxide |

| | |
|---|---|
| $(Mg_3Si_2O_5(OH)_4)$ | Serpentine |
| $(Mg,Fe)_2SiO_4$ | Olivine |
| mol. | Mole |
| N-A-S-H | Sodium aluminosilicate hydrate |
| $N_2O$ | Nitrous oxide |
| NG | Natural gas |
| $NO_x$ | Nitrogen oxide |
| $O_2$ | Oxygen |
| OPC | Ordinary Portland cement |
| OPEX | Operational expenditure |
| ORC | Organic Rankine cycle |
| PA | Primary air |
| PFD | Process flow diagram |
| PH | Pre-heater |
| PM | Particulate matter |
| PV | Photovoltaics |
| PV-T | Hybrid photovoltaic-thermal |
| PVGIS | Photovoltaic Geographical Information System |
| PZ | Blended piperazine |
| PZ-AMP | 2-amino-2-methyl-1-propanol |
| RDF | Refuse derived fuel |
| RH | Re-heater |
| RM | Raw meal |
| SA | Secondary air |
| SCMs | Supplementary cementitious materials |
| SC | Solar calciner |
| $SiO_2$ | Silicon dioxide |
| $SO_2$ | Sulphur dioxide |
| $SO_x$ | Sulfur oxide |
| SS | Sewage sludge |
| TA | Tertiary air |
| TDF | Tyre derived fuel |
| TES | Thermal energy storage |

| | |
|---|---|
| th | Thermal |
| TT | Top of tower |
| UK | United Kingdom |
| UNFCCC | United Nations Framework Convention on Climate Change |
| US | United States |
| vol. | Volume |
| VRM | Vertical roller mill |
| w/c | Water to cement ratio |
| WBCSD | World Business Council for Sustainable Development |
| wt.% | Weight percentage |

# Units

| | |
|---|---|
| °C | Celsius |
| clk | Clinker |
| g | Grams |
| GJ | Gigajoule |
| h, hr | Hour |
| J | Joule |
| K | Kelvin |
| kg | Kilogram |
| kJ | Kilojoule |
| kmol | Kilo-mole |
| kW | Kilowatt |
| kWh | Kilowatt-hour |
| $m^2$ | Square metre |
| MJ | Megajoule |
| mol | Mole |
| MPa | Megapascal |
| MW | Megawatt |
| MWh | Megawatt-hour |
| t | Tonne |
| USD | United States Dollar |

# Table of Contents

# List of Figures

# List of Tables

# Chapter 1. Introduction

## 1.1. Background and Rationale

ement has been the most utilised man-made material worldwide since the 21st century, as it is prominently used in the construction industry (Gagg, 2014). Rapid urbanisation and population growth has propelled the increase in cement consumption in the last two decades, notably from 1.6 billion tonnes in 2000 to 4.1 billion tonnes in 2023 (Jaganmohan, 2024b), with projections to increase by 12 – 23% of 2020 levels by 2050 (Cheng *et al.*, 2023). Cement production, however, is carbon dioxide ($CO_2$) intensive, accountable for 2.9 billion tonnes of global $CO_2$ emissions in 2021 (Supriya *et al.*, 2023), and 8% of global anthropogenic $CO_2$ emissions (Cormos, 2022). To give perspective, if cement was a nation, it would rank as the world's third-largest emitter, closely following China and the United States (Rodgers, 2018). Clinker, the dominant component of cement (at 95% by weight (wt.) (British Geological Survey, 2005)), releases an average of 866 kilograms (kg) of $CO_2$ into the atmosphere per tonne of clinker produced (Summerbell, Barlow and Cullen, 2016). The $CO_2$ intense nature of clinker production has drawn significant attention in the construction and cement industries where the aim to meet net-zero greenhouse gas (GHG) emissions targets by 2050 has become necessary whilst simultaneously complying with the Paris Agreement to limit global warming to 1.5 °C above pre-industrial levels (UNFCCC, 2015).

Rapid decarbonisation of the clinker production process involves addressing two main pathways, namely fuel and calcination induced emissions, responsible for ~26% (Williams, Yang and Nhuchhen, 2024), and 60% (Cavalett *et al.*, 2024) of the total emissions from

clinker production, respectively. Currently, the majority of clinker processes use fossil fuels (including coal and natural gas) as their main energy source to operate the respective combustion stages of calcination and kiln combustion. The substitution of fossil fuels with cleaner resources, for instance, hydrogen ($H_2$) or solar energy would enable the elimination of $CO_2$ from fuel combustion (Guo *et al.*, 2024), and significantly reduce energy-based emissions. In contrast, the emissions from the calcination stage stem from the decomposition of limestone, namely calcium carbonate ($CaCO_3$) to calcium oxide (CaO) and $CO_2$ (Cavalett *et al.*, 2024), where ~0.44 tonnes of $CO_2$ is produced per tonne of $CaCO_3$ calcined (Simoni, 2022). Therefore, it is imperative to tackle emissions in cement calcination through the reduction of the limestone content in clinker raw meal, using alternative clinkers (Antunes *et al.*, 2022).

Fuel induced emissions are correlated with the energy intensity of combustion, subject to high combustion temperatures reaching up to 1500 °C (Nhuchhen, Sit and Layzell, 2022a). $H_2$ as a fuel is expected to bring substantial $CO_2$ reductions of up to 26% (Williams, Yang and Nhuchhen, 2024), mainly due to $H_2$ reacting with oxygen (both from water electrolysis) to form water vapour, eliminating the release of $CO_2$ in the combustion process (Williams, Yang and Nhuchhen, 2024). $H_2$ can also be used along-side natural gas (El-Emam and Gabriel, 2021), promoting the gradual shift towards low carbon clinker production whilst reducing $CO_2$ emissions. Alternatively, solar energy through concentrated solar power (CSP) can be used to facilitate the energy requirements of the clinker combustion stages. This results in $CO_2$ savings due to the low carbon nature of renewable energy without compromising the required temperatures for combustion (Moumin *et al.*, 2020). Although CSP systems rely on sunshine availability, a thermal energy storage system can be integrated into the clinker production process, allowing operations to continue even during periods

without sunshine (Moumin *et al.*, 2020). In contrast, the use of electrification to replace fossil fuel combustion is forecasted to bring $CO_2$ savings while maintaining combustion temperatures required for the calciner. While electrification alone is unable to achieve the high temperatures required for kiln combustion, incorporating plasma gas technology can bridge this gap, enabling combustion temperatures to reach up to 2000 °C (Antunes *et al.*, 2022). In addition, it is worth noting that carbon capture utilisation and storage (CCUS) is a widely adopted decarbonisation option for the clinker production process. In particular, the current lineup of CCUS technologies includes amine-based capture and calcium looping (Hills *et al.*, 2016). Although these technologies are capable of capturing over 90% of $CO_2$ released from clinker flue gases (Gardarsdottir *et al.*, 2019), they do not address the mitigation of $CO_2$ produced during the clinker production process. This is because CCUS cannot address the $CO_2$ emitted at source, namely, during the limestone calcination and fuel combustion.

Deep decarbonisation of clinker production necessitates the reduction of $CO_2$ emissions from the calcination stage. This reduction can be achieved through the use of alternative clinkers and the direct replacement of clinker with supplementary cementitious materials (SCMs), where both options lead to lower limestone contents (Antunes *et al.*, 2022). Alternative clinkers (including belite-ye'elimite ferrite (BYF) clinker, calcium silicate clinker (CSC) and high ferrite clinker (HFC)) not only reduce the limestone content but also enables the use of lower sintering temperatures during kiln combustion (Elakneswaran *et al.*, 2019; Sahu and Meininger, 2019; Antunes *et al.*, 2022). This decreases the total enthalpy of formation, hence reducing the energy demand for combustion (Jain, Seth and DeCristofaro, 2019) without compromising the mechanical compressive strength (Elakneswaran *et al.*, 2019; Sahu and Meininger, 2019). Furthermore, the substitution of

clinker with SCMs, particularly those derived from $CO_2$ mineralisation offers both clinker reduction and partial $CO_2$ capture of cement flue gases during the mineralisation process (Strunge, Renforth and der Spek, 2022).

Whilst the above-mentioned alternative fuels (including $H_2$ and solar energy) and alternative clinkers promise reduced inherent $CO_2$ emissions from fuel combustion and calcination, existing systematic assessment of these methods has not included both their energy and $CO_2$ performance and compared them using process simulation modelling, to quantify the potential of these options on a consistent basis. Similarly, despite available techno-economic analyses in literature on the use of solar energy and electricity to support combustion phases in the clinker process, research gaps exist in developing optimisation models (that account for the details of variable solar energy availability) to minimise the total solar based clinker process costs. These gaps in research targeting the reduction of fuel and calcination induced emissions were the rationale for the research described in this thesis.

## 1.2. Objectives

The thesis's overarching aim is to conduct academic research to facilitate the decarbonisation of the cement production process by evaluating technical decarbonisation options with energetic and economic advantages. More specifically, the purpose of this work is to provide an in-depth assessment of and develop technical options for reducing $CO_2$ emissions resulting from both fuel combustion (including substitution of conventional fuel with $H_2$ and solar based-energy) and clinker calcination (including introduction of low-lime alternative clinkers). This is conducted through mathematical process simulations and optimisation modelling with geospatial assessments, targeting the major contributors to $CO_2$

emissions in the cement production process. The modelling results are based on standardised assumptions and validated process parameters. The research objectives supporting the aim are defined as follows:

(1) Review emerging decarbonisation options for cement production from the environmental and energetic points of view.
(2) Explore the energetic and $CO_2$ performance impact of substituting fossil fuels via electrolysis derived $H_2$ fuel coupled with oxygen combustion, complemented by carbon capture systems through process simulation modelling.
(3) Optimise the techno-economics of renewable solar energy-based fuels whilst assessing the energy and $CO_2$ performance through optimisation modelling, including an analysis of region-specific potential.
(4) Assess the decarbonisation of cement calcination from the introduction of alternating clinkers through process simulation modelling and elucidate the critical components in alternative clinkers impacting the energy and $CO_2$ performance.
(5) Synthesise findings about optimal decarbonisation options and provide critical insights for industry implementation and policy development.

## 1.3. Thesis Structure

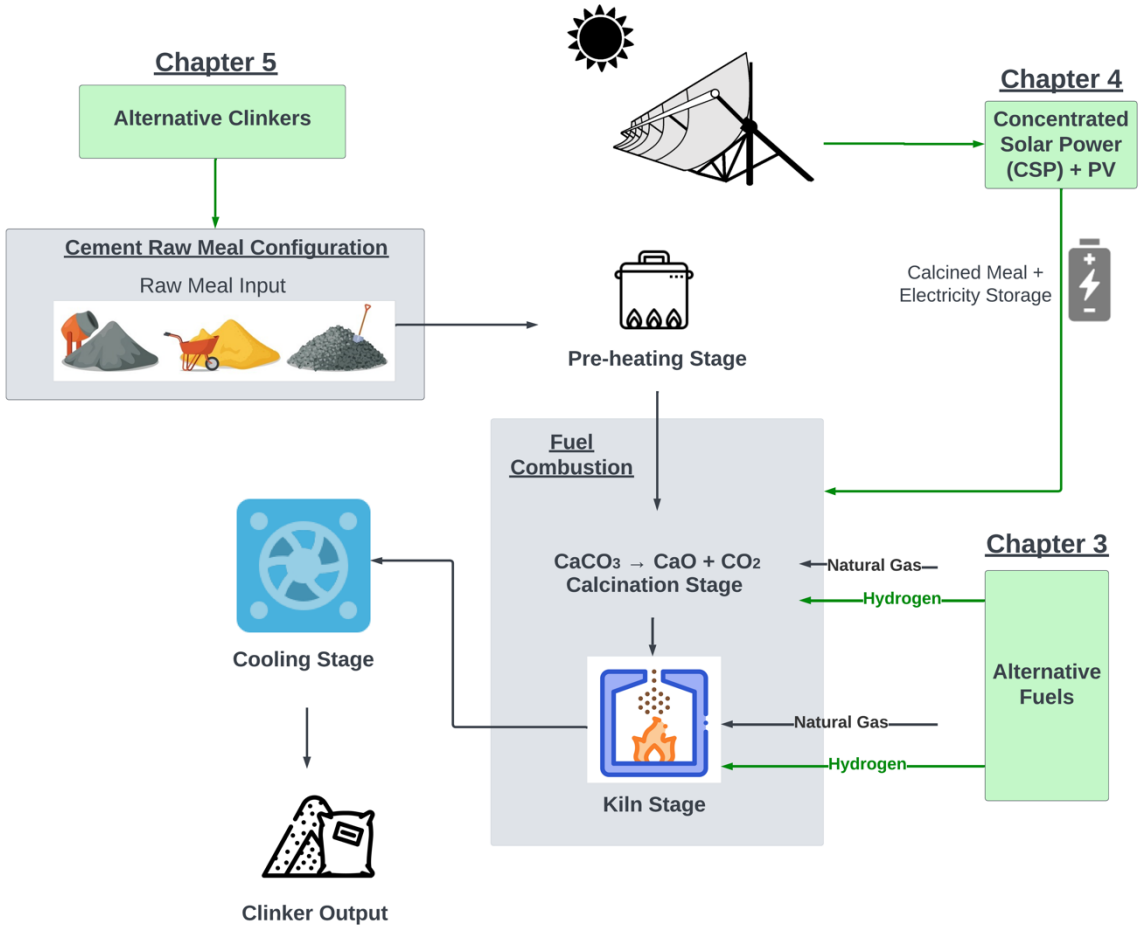


***Figure 1.1. Links between the three original research chapters****. These include Chapter 3 on alternative fuel replacement of $H_2$, Chapter 4 on solar energy fuel replacement, and Chapter 5 on the use of alternative clinkers.*

This thesis comprises of six chapters: an introduction (Chapter 1) and a literature review (Chapter 2) followed by three original research Chapters (3)–(5), and the overall conclusion (Chapter 6). The thesis objectives are met in hierarchical order, where objectives (1)–(4) each aligns with the respective Chapters (2)–(5), with objective (5) being addressed amongst all chapters (shown in Figure 1.1). An integrated thesis format has been adopted, where the original research chapters consist of published, and under-review papers. The structure of the thesis is outlined as follows:

**Chapter 1** presents the research background and motivation, complemented by a structured overview.

**Chapter 2** provides an in-depth review of relevant literature on technologies and engineering methods for decarbonising cement production, including fossil fuel substitution (through $H_2$ and solar energy) and cement substitution (including utilisation of alternative clinkers and SCMs). This chapter addresses the research gaps identified in the literature and proposes research methods to address these gaps.

**Chapter 3** explores the decarbonisation impacts of substituting conventional fossil fuels with $H_2$ involving oxygen combustion. To determine the impact on the energy and $CO_2$ performance, the variance of energetic and $CO_2$ respective to the substitution percentage of $H_2$ was assessed, complemented by an investigation of indirect and direct combustion methods. The cement production process was simulated to provide a basis for the energy and $CO_2$ assessment, whilst establishing a process simulation foundation for the subsequent work in Chapters 4 and 5.

**Chapter 4** constructs and solves a series of optimisation models across three geospatial regions aiming to minimise the techno-economic costs of a solar driven cement process. The focus was on the cost optimisation of the solar calciner and kiln subsystems, where the subsystems sourced energy from concentrated solar power (CSP), and photovoltaics (PV)-driven plasma gases, respectively. The optimisation models also determined the minimum feasible capacities (including CSP, calciner and storage), in the calciner subsystem and in the kiln subsystem (including PV and electricity storage).

**Chapter 5** targets the carbon reduction of cement calcination through the assessment of distinct technically feasible alternative clinkers. Specifically, the focus is on assessing the energy consumption and $CO_2$ emissions of high ferrite, belite-ye'elimite-ferrite, and calcium silicate clinkers across three geographical regions. The aim was to identify the key factors influencing their energy efficiency and $CO_2$ performance without compromising the mechanical compressive strength. Partial substitution of clinker with supplementary cementitious materials (SCMs) from $CO_2$ mineralisation was also explored to determine further implications on $CO_2$ savings and energetic performance.

**Chapter 6** summarises the key results presented in this thesis, underscoring the key contributions and importance of the research conducted. Research limitations are also addressed along with suggestions of potential areas for future work.

# Chapter 2. Literature Review

This chapter provides an in-depth review of the literature to date on technical options for the decarbonisation of the cement production process. The purpose is to identify research gaps that must be filled in order to optimise solutions to reduce energy and carbon dioxide ($CO_2$) emissions in the cement production process whilst providing rationale for the thesis. Initially, traditional fossil fuel-based cement production is reviewed, with a specific focus on identifying opportunities for fuel replacement in terms of their technical viability, carbon and energy reductions. Carbon capture strategies and technologies for cement flue gas are also covered, emphasising their integration pathway into the cement production process. This is followed by a review of the energetic and carbon implications, and the economic feasibility of utilising concentrated solar power and electrification for the calciner and kiln subsystem, respectively. Subsequently, this chapter dives into a review of relevant modelling and experimental studies on alternative clinkers, supplementary cementitious materials (SCMs), alkali activated materials (AAMs), and $CO_2$ mineralisation, targeting $CO_2$ reduction in the calcination stage, evaluating their contributions in decarbonising cement production. In addition, methods to improve the energy efficiency such as improving the kiln performance and recovering waste heat are also discussed.

## 2.1. Carbon emissions and energy demand from cement production

Since the Industrial Revolution, mankind has entered a phase of rapid industrial development and urbanisation. The construction industry, as the key driver, reached a total production value of 9.7 trillion USD globally in 2022, and is forecasted to rise to 13.9 trillion

USD by 2037 (Fearnely, Robinson and Leonard, 2023). This is primarily due to the global growth in population urbanisation, which reached 4.52 billion in 2022, an increase of 20% compared to the 2010 levels at 3.59 billion (Ritchie, Samborska and Roser, 2024). This demanded increased resource consumption (Uwasu, Hara and Yabar, 2014), with cement being the most consumed man-made material worldwide (Global Cement and Concrete Association, 2024). Global cement production has increased over 3-fold since the past decade (Jaganmohan, 2024b), currently sitting at 4.05 billion tonnes in 2023 (Research Department, 2023) (see Figure 2.1). The cement industry contributes to 2.3 billion tonnes of $CO_2$ emissions globally each year (Cavalett *et al.*, 2024), a noteworthy increase from 1.63 billion tonnes in 2020 (see Figure 2.2), contributing to 8% of anthropogenic emissions (Moumin *et al.*, 2020; Cheng *et al.*, 2023). From an economic perspective, the cost of clinker production sits at ~84 USD per tonne of clinker produced, with energy costs accounting for ~15% of the total production costs (Nhuchhen, Sit and Layzell, 2022a), (see Table 2.1 for a cost breakdown structure).

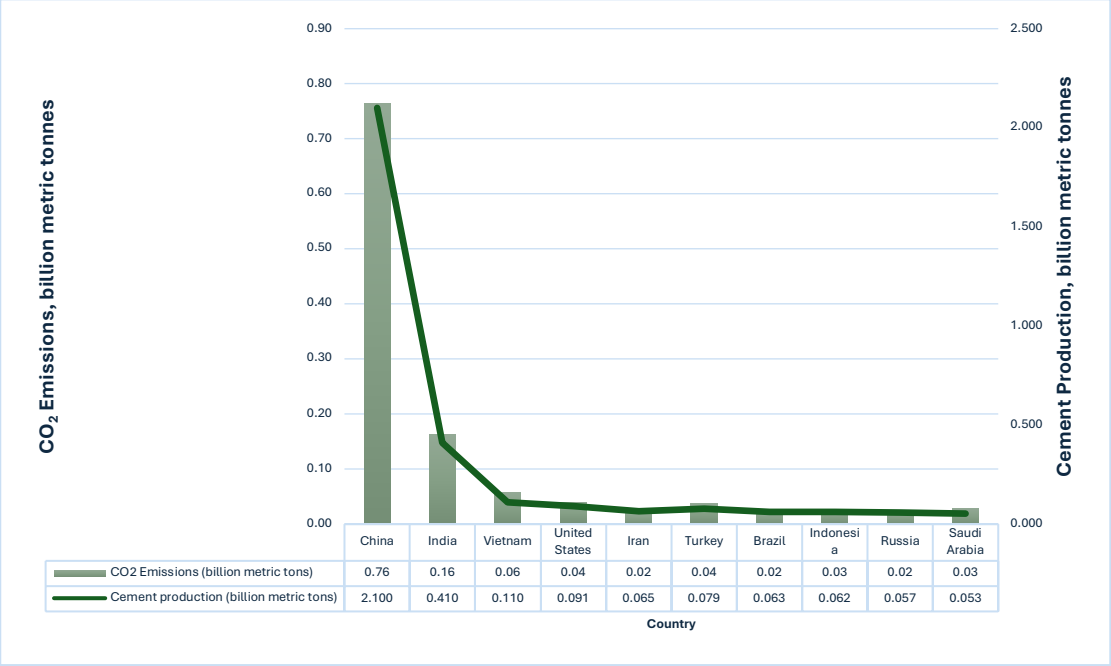


***Figure 2.1. Global cement induced $CO_2$ emissions and cement production.*** *Comparisons of annual cement produced and $CO_2$ trends across top ten worldwide cement producers (Global Carbon Budget, 2023; Research Department, 2023).*

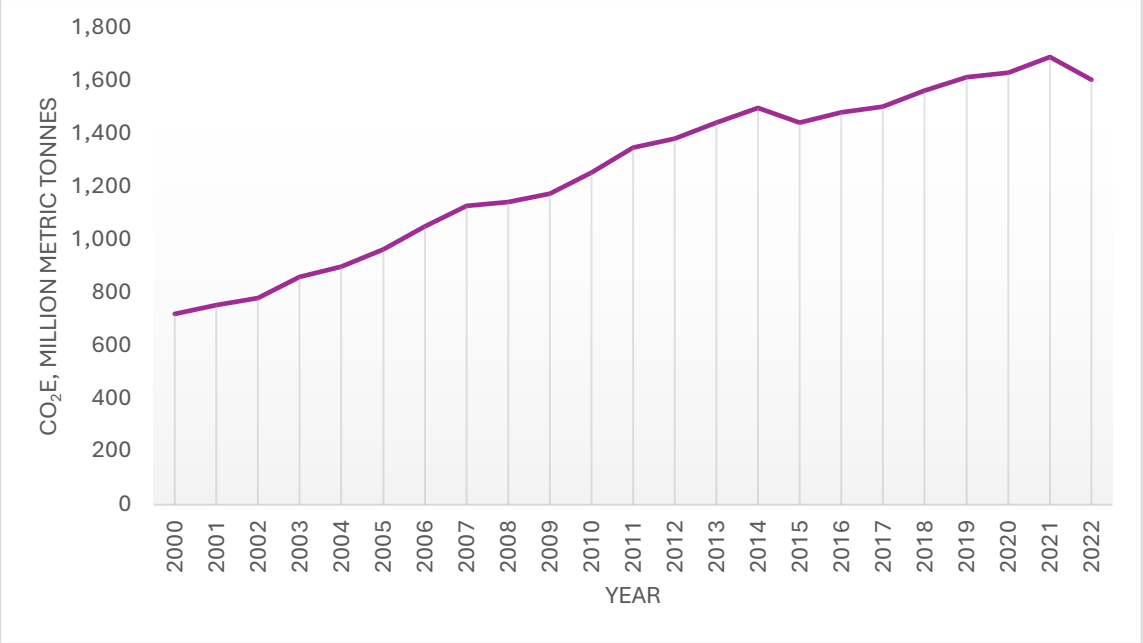


***Figure 2.2. Global $CO_2$ emissions from cement production.*** *Ranging from 2000–2022 (Tiseo, 2023a).*

***Table 2.1. Cost breakdown structure of conventional fossil*** *(i.e., natural gas) based clinker production (Nhuchhen, Sit and Layzell, 2022a).*

| Cost | USD/t clinker |
|---|---|
| Capital expenditure (CAPEX), capital | 17.26 |
| Fixed annual maintenance | 14.99 |
| Operational expenditure (OPEX), variable operational (non-energy) | 38.24 |
| Natural gas | 6.44 |
| Electricity | 6.72 |
| Total | 84.54 |

According to (Madlool *et al.*, 2011), the production of clinker accounts for a thermal energy demand of 4.6 GJ/tonne of clinker and electrical energy demand of 141 kWh/tonne of clinker in the United States. For the last three decades, although Europe has partially relied on the use of alternative fuels for thermal energy (Cembureau, 2023), the global cement industry is

still largely dependent on fossil fuels for combustion, with coal and gas as the main dominators (Chatterjee and Sui, 2019). Studies have shown that clinker, the primary constituent of cement, is responsible for producing 866 kilograms of $CO_2$ per tonne (Summerbell, Barlow and Cullen, 2016). According to (Uratani and Griffiths, 2023), cement production collectively commanded 7% of global energy demand, where energy related emissions accounted for 700 Mt $CO_2$ (Cheng *et al.*, 2023). This emphasises the urgency to implement $CO_2$ mitigation and energy efficiency measures to address climate change impacts and global warming issues, to comply with the Paris Agreement targets and limit global warming to 1.5 °C above pre-industrial levels (UNFCCC, 2015), whilst producing cleaner cement.

## 2.2. Overview of decarbonisation options

Deep decarbonisation from the global cement sector necessitates a transition to cleaner production by reducing dependency on fossil fuels (Chatterjee and Sui, 2019), and calcination induced emissions to mitigate global climate change impacts (Cavalett *et al.*, 2024). The cement production process involves the pre-heating of raw meal (input) to 800 °C (in the pre-heater), predominantly from the calciner exhaust gas (see Figure 2.3). A typically used pre-heater in the industry is multi-stage cyclone pre-heater (of six cyclones), for gas and solid mixing, heat exchange and separation (Agico Cement, 2024). The pre-heated raw meal then enters the calciner, where limestone decomposition occurs at 900 °C (Vikström, 2021). The calcined meal moves on to the kiln (long, cylindrical, rotating furnace (Juangsa *et al.*, 2022)), where it is further converted through three stages, namely, decomposition, transition, and sintering, with the last stage operating at ~1500 °C (Faria *et al.*, 2022). Here, clinkerisation reactions occur (i.e., formation of alite ($C_2S$), belite ($C_3S$),

ferrite ($C_4AF$), and aluminate ($C_3A$)) (Mujumdar *et al.*, 2007). The calcined meal moves toward the hotter zone of the kiln's flame, where the kiln's temperature increases from the feed end and decreases towards the discharge end (Stadler, Poland and Gallestey, 2011). The clinker from the kiln is then cooled down to 100 °C through cooling air in the cooler where the final product exits the process. This process is shown in Figure 2.3, aligning with (Boesch, Koehler and Hellweg, 2009), which states that for every tonne of clinker produced, 1.6 tonnes of raw meal input is required. Although carbon capture, utilisation and storage (CCUS) can remove ~90% of $CO_2$ emissions from cement production (Ozcan, Brandani and Ahn, 2014; Gardarsdottir *et al.*, 2019), it does not eliminate the underlying $CO_2$ generation inherent to cement production.

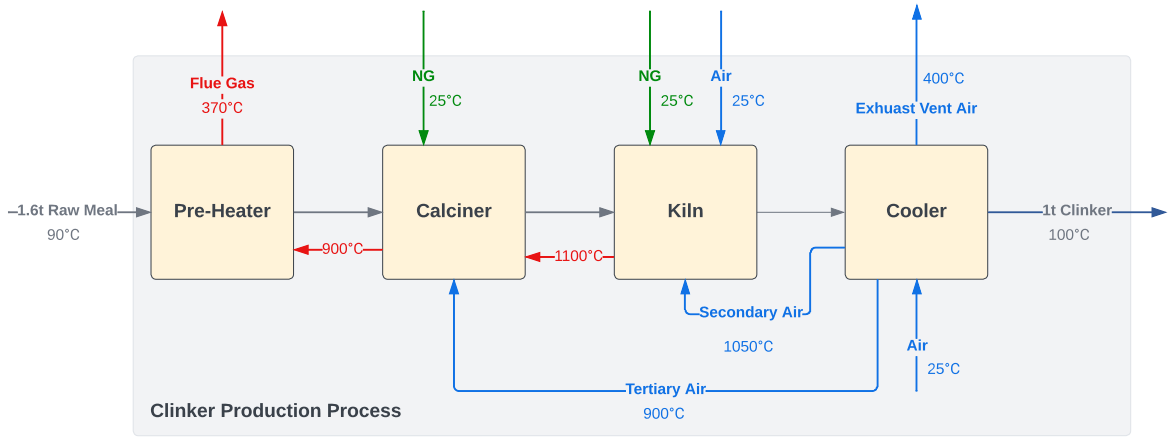


***Figure 2.3. Clinker production process flow diagram (PFD).*** *Material flows are represented in grey, gases in red, air in blue and natural gas (NG) inputs in green (Nhuchhen, Sit and Layzell, 2022a).*

The combustion of fuels (predominantly coal or natural gas) in the calciner and kiln accounts for 25 – 30% of $CO_2$ emissions from clinker production (Damtoft *et al.*, 2008; Psomopoulos and Themelis, 2014). These emissions are attributed to the energy intense nature of the calcination and kiln combustion stages (both being endothermic), requiring high temperatures of 900 °C and 1500 °C, respectively (Nhuchhen, Sit and Layzell, 2022a). Here, the emissions can be reduced through the use of alternative fuels (targeting fuel emissions

as depicted in Figure 2.4), with substantially lower carbon content, such as hydrogen ($H_2$) (El-Emam and Gabriel, 2021; Juangsa *et al.*, 2022), biomass, and waste fuels (Chatterjee and Sui, 2019; Kusuma *et al.*, 2022). $H_2$ combustion only produces water vapour (Jibran and Mahat, 2023), whereas biomass (Rahman *et al.*, 2015) still releases $CO_2$ when burned, although its biogenic nature reduces the net emissions. In addition, waste derived fuels (including refuse derived fuel (RDF), tyre derived fuel (TDF), meat and bone meal (MBM), and sewage sludge (SS)), can contribute to $CO_2$ emission reductions, however unlike $H_2$, they cannot achieve net zero $CO_2$ emissions from combustion and vary in supply (Chatterjee and Sui, 2019). Moreover, $H_2$ fuel provides consistent quality and efficiency (El-Emam and Gabriel, 2021), allowing for stable temperatures to be achieved. A modelling study by (Juangsa *et al.*, 2022) achieved significant $CO_2$ reductions by about 30%, compared to the conventional fossil fuel (through natural gas) process (Nhuchhen, Sit and Layzell, 2022a), by eliminating fuel combustion emissions through the use of $H_2$ fuel. Additionally, the substitution of fossil fuels with solar energy (targeting fuel emissions as depicted in Figure 2.4), shifts the cement production towards achieving zero fuel related $CO_2$ emissions (Moumin *et al.*, 2020), where up to 35.5% of $CO_2$ can be reduced (Nikolakopoulos *et al.*, 2022). In contrast, replacing fossil fuels with electrification (harnessing direct electrical energy to supply heat energy through plasma) can reduce $CO_2$ emissions by 25% compared to conventional fossil-based cement production (Quevedo Parra and Romano, 2023).

Cement production is energy intensive, making efficiency improvements and reducing heat loss essential. In particular, implementing kiln efficiency improvements through measures such as insulation, use of alternative fuels, and indirect combustion can propose energy savings of up to 0.22 GJ/t clinker (Saidur *et al.*, 2011; Sahoo, Kumar and Samsher, 2022), and $CO_2$ savings up to 12% (Sahoo, Kumar and Samsher, 2022; Georgiades et al., 2023).

More significantly, implementing waste heat recovery systems, particularly an organic Rankine cycle (ORC) can recover ~21% of the electrical energy used in cement production (Sztekler *et al.*, 2016; Poggianti, Palazzolo and Moliner, 2024).

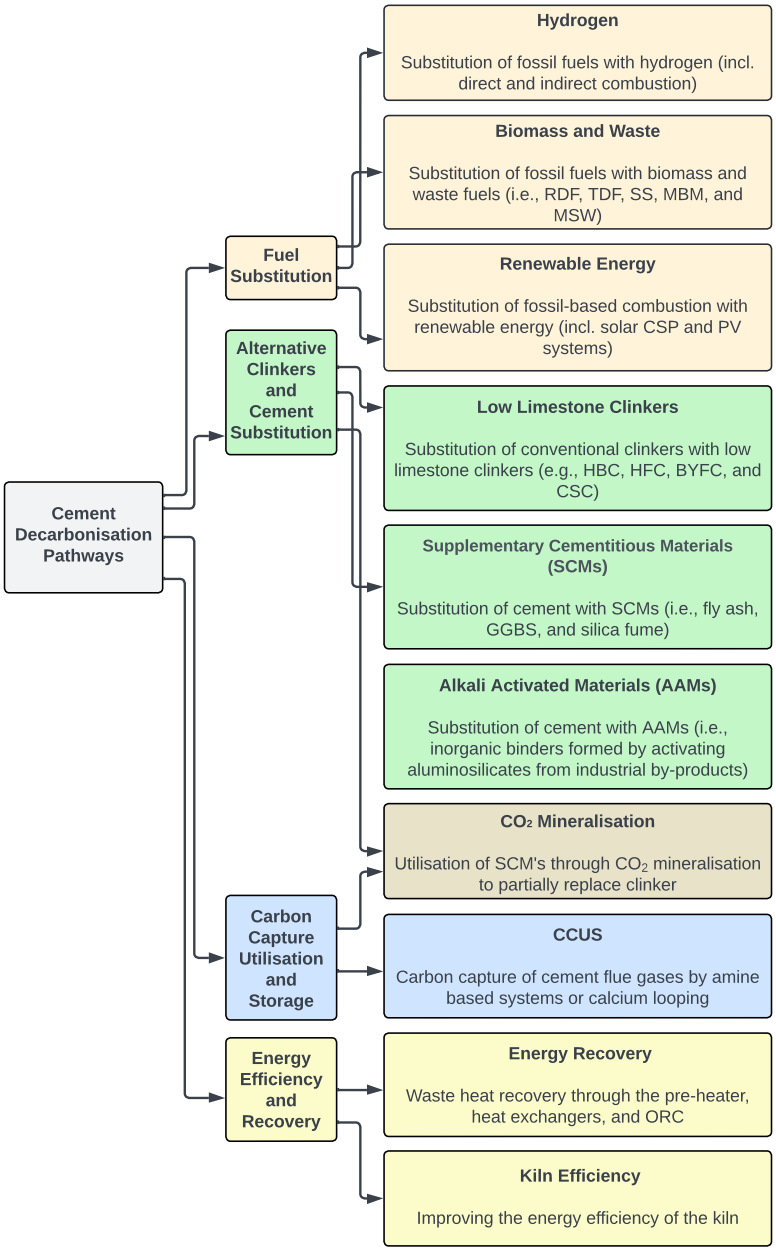


***Figure 2.4. Decarbonisation options for the cement production process.*** *The pathways present process (fuel emissions, CCUS, $CO_2$ mineralisation, energy recovery, and kiln efficiency improvements) and materials side (including alternative clinkers, SCMs, and AAMs) decarbonisation methods.*

The decomposition of limestone ($CaCO_3$) to calcium oxide (CaO), a process known as calcination, alone contributes to 60% of $CO_2$ emissions from clinker production (Cavalett *et*

*al.*, 2024). This stage is inherently carbon intensive as one molecule of $CO_2$ is released for every molecule of $CaCO_3$ decomposed (Faria *et al.*, 2022) (shown in Equation 2.1), whilst demanding a high temperature of 900 °C (Nhuchhen, Sit and Layzell, 2022a).

*Equation 2.1. Limestone decomposition reaction.*

$$CaCO_3(s) \rightarrow CaO(s) + CO_2(g)$$

The reduction of emissions in the calcination stage involves the utilisation of alternative clinkers (targeting calcination emissions as depicted in Figure 2.4), such as high ferrite clinker (Zhang *et al.*, 2021), belite-ye'elimite ferrite clinker (Sabbah and Zhutovsky, 2022), and calcium silicate clinker (Sahu and Meininger, 2019). Studies as per (Sahu and Meininger, 2019; Zhang *et al.*, 2021; Sabbah and Zhutovsky, 2022) have advocated that these clinkers support the reduction of limestone decomposition up to 13%, sintering temperatures down to 1250 °C, and $CO_2$ reductions of up to 30%.

Moreover, partial substitution of conventional clinkers with Supplementary Cementitious Materials (SCMs) can offer $CO_2$ reductions of up to 40% depending on the extent of clinker replaced and type of SCMs used (Lothenbach, Scrivener and Hooton, 2011; Juenger and Siddique, 2015; Samad and Shah, 2017; Kusuma *et al.*, 2022). In comparison, alkali activated cements (AACs) derived from industrial by-products can achieve $CO_2$ savings ranging from 50 – 80% compared to OPC (Ding, Dai and Shi, 2016; Ślosarczyk *et al.*, 2023). However, the widespread adoption of both SCMs and AACs are constrained by the limited availability when compared to OPC (Benhelal *et al.*, 2013; Duchesne, 2021; Pol Segura *et al.*, 2023; Snellings, Suraneni and Skibsted, 2023). In addition, SCMs derived from $CO_2$ mineralisation, substituting cement by up to 25%, can further reduce $CO_2$ emissions by up to 33% (Strunge, Renforth and der Spek, 2022). SCMs are generally used as partial

replacement of clinker in cements (Juenger, Snellings and Bernal, 2019), and $CO_2$ mineralisation involves the process of utilising captured $CO_2$ whilst reacting with activated minerals to form stable carbonate minerals (Strunge, Renforth and der Spek, 2022).

Noteworthily, life cycle assessments (LCAs), applied from a cradle-to-gate perspective, have demonstrated that by 2050, $CO_2$ emissions from cement production could be reduced by 42% through clinker substitution, 25% with alternative fuels, and 12% from kiln efficiency improvements relative to 2020 levels (Georgiades *et al.*, 2023). LCAs are widely used to quantify the environmental performance impact of various decarbonisation options in cement production (Georgiades *et al.*, 2023), by assessing stages from raw material extraction and transport to cement production and concrete batching (cradle-to-gate) (Olsson, Miller and Kneifel, 2024).

## 2.3. Alternative fuels

### 2.3.1. Fossil fuels in cement production

Since the 20$^{th}$ century, fossil fuels have been relied upon to support high temperature combustion in the clinker production process (Harder, 2023). As depicted in Figure 2.5, the majority of thermal energy for clinker production has come from fossil fuels and non-renewables since 2010 (Cumbrera, 2023). Specifically, coal has been the key fuel source in the cement industry since 1895 (Harder, 2023), where coal combustion releases 3.2 kg of $CO_2$ for every kg burned (Moseman and Surendranath, 2023). Coal currently represents 70% of the total energy consumption in the cement industry followed by natural gas and oil at 24% (Kusuma *et al.*, 2022). Fuel combustion in cement comprises of two methods, indirect

and direct combustion; whilst indirect combustion avoids direct contact between the combustion gases and raw materials, with the former offering higher $CO_2$ capture efficiencies (Ozcan, Brandani and Ahn, 2014). Although the cement industry is steadily transitioning from coal to natural gas combustion, the combustion of natural gas (primarily methane) still releases 2.75 kg of $CO_2$ for every kg of natural gas burned (Bradbury, Clement and Down, 2015). The use of finite resources such as coal and natural gas plays a crucial role in the depletion of natural resources and climate change impacts such as air quality degradation, health hazards, and greenhouse gases (Mohamad *et al.*, 2021). With respect to (Canvi Climatic, 2019), 0.18 kg of $CO_2$ is emitted per kWh of natural gas (methane) compared to coal (bituminous) at 0.36 kg $CO_2$ per kWh of energy, highlighting greater $CO_2$ emissions from coal. Studies have demonstrated the feasibility of achieving complete substitution of fossil fuels with alternative fuels in the cement production process (Aranda Usón *et al.*, 2013; Rahman *et al.*, 2015; Zieri and Ismail, 2018). In particular, the use of alternative fuels may require kiln flame temperature control, through adjusting air to fuel ratios (Juangsa *et al.*, 2022), using pure oxygen (which increases the flame temperature) (Nhuchhen, Sit and Layzell, 2022a), mass flow rates adjustments, and monitoring the volatility of the fuels (where low volatile fuels require more energy to reach the desired combustion rates) (Schumacher and Juniper, 2023). Modelling work done through computation fluid dynamics (CFD) showed that utilising alternative fuels consisting of $H_2$ (20% vol.) alongside 70% biomass, and 10% plasma gas led to the elimination of fossil fuel related $CO_2$ emissions (Association and Ltd, 2019). In contrast, the use of biomass and waste derived fuels can achieve up to ~30% of $CO_2$ reductions when replacing conventional fossil fuels (Aranda Usón *et al.*, 2013; Chatterjee and Sui, 2019; Wojtacha-Rychter, Kucharski and Smolinski, 2021). In addition, as per an LCA (cradle-to-gate) study (Pitre, La and Bergerson, 2024), the replacement of natural gas with alternative fuels such as biomass can achieve 7 –

13% greenhouse gas emission (GHG) reduction. This highlights the necessity to utilise environmentally friendly alternative fuels to steer the cement industry towards cleaner production for the future generations.

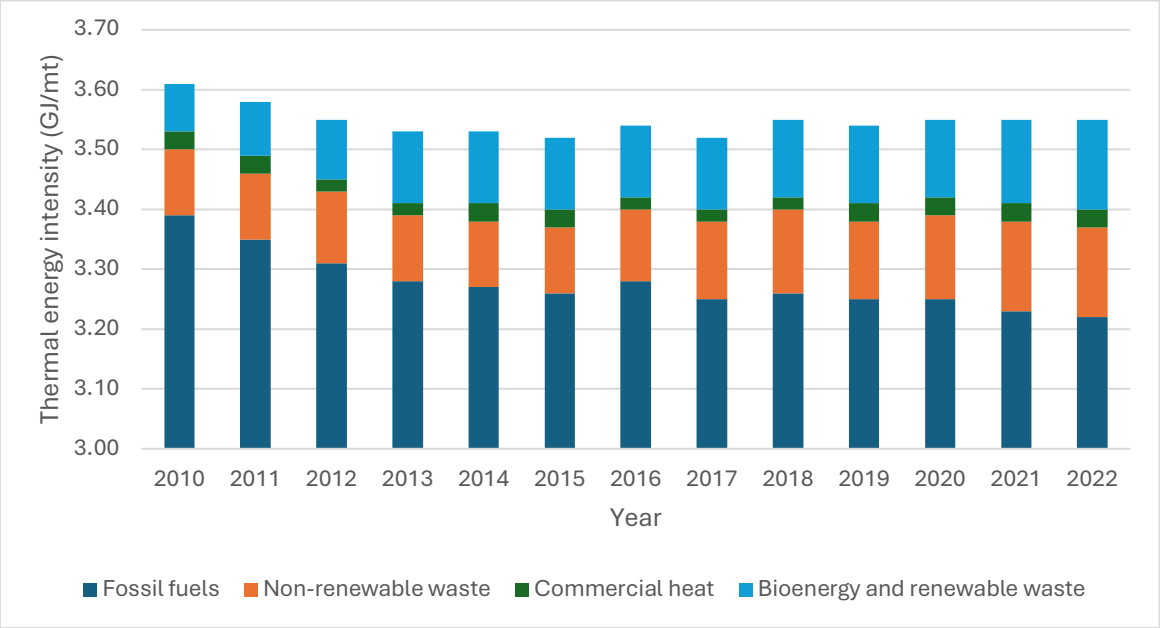


***Figure 2.5. Thermal energy intensity of clinker production worldwide 2010–2022*** *(Cumbrera, 2023). Four different types of energy are included: fossil fuels, non-renewable waste, commercial heat, and bioenergy with renewable waste.*

## 2.3.2. Oxygen combustion

Oxygen combustion (hereafter oxy-combustion) in cement production involves utilising pure oxygen, substituting air for fuel combustion (Carrasco-Maldonado *et al.*, 2016; Faria *et al.*, 2022). The flue gas stream from oxy-combustion predominantly produces $CO_2$ and water vapour, as opposed to air combustion where the flue gas additionally contains nitrogen. This enables production of purer $CO_2$ in the flue gas, increasing the efficiency and reducing the energetic demand for capture (Faria *et al.*, 2022). Here, oxy-combustion offers $CO_2$ capture rates up to 95% (Schneider *et al.*, 2023), which are normally higher compared to air combustion. Higher combustion efficiencies from oxy-combustion improves the

thermal efficiencies and reduces the fuel requirements, leading to $CO_2$ reductions (Nhuchhen, Sit and Layzell, 2022a).

A study by (Faria *et al.*, 2022), achieved reductions of 9.1 kg$CO_2$/t clinker through the use of oxy-combustion in the cement production process. Modelling studies in (Carrasco-Maldonado *et al.*, 2016) have clarified that the electrical energy demand of oxy-combustion is significantly dependent on the use of an air separation unit (ASU) (electric unit used to extract oxygen from air) (Nhuchhen, Sit and Layzell, 2022a). Furthermore, (Domingues *et al.*, 2023) suggested that increasing the oxygen concentration in air ($O_2$-enrichment) from 21 – 27% by volume can increase clinker production by 7% whilst increasing the fuel efficiency. However, as stated by (Nhuchhen, Sit and Layzell, 2022a), although oxy-combustion prevents nitrogen induced emissions and produces a concentrated $CO_2$ stream for easier capture, it requires an ASU unless sourcing oxygen elsewhere, thus increasing the cement production cost. More specifically, adopting oxy-combustion in cement production, was shown to cost 119 USD/t clinker, which is about 42% higher than the cost of conventional cement production at 84 USD/t clinker (Nhuchhen, Sit and Layzell, 2022a). Despite this, oxy-combustion based cement production results in a lower $CO_2$ avoidance cost at ~70 USD/t $CO_2$ when $CO_2$ emission taxes range from 70 – 92 USD/t $CO_2$ (Cormos, 2022).

### 2.3.3. Hydrogen ($H_2$)

Studies have demonstrated that low emission fuels particularly $H_2$ (Association and Ltd, 2019; Juangsa *et al.*, 2022), can effectively replace fossil fuels (including coal and natural gas) while significantly reducing $CO_2$ emissions associated with fuel combustion (Schneider *et al.*, 2023), contributing to the transition towards net zero cement production. $H_2$ as a fuel

is primarily produced through electrolysis (Khadka, 2021), with alkaline water electrolysis being the predominately utilised technology, where the water input produces an output of hydrogen and oxygen. Notably, current electrolysis efficiencies range from 60% (Institute of Power Engineering, 2022) to 80% (Khadka, 2021), where almost 100% purity can be achieved (Khadka, 2021). Previous literature (Association and Ltd, 2019; Khadka, 2021) has investigated the applicability of utilising $H_2$ fuel through water electrolysis to eliminate $CO_2$ from fuel emissions, providing direct heat transfer during combustion. Hydrogen production from water electrolysis co-generates oxygen (8kg of $O_2$ per kg of $H_2$), supporting oxy-combustion based CCUS (Cavalett *et al.*, 2024), whilst decreasing the electrical energy demand in the air separation unit. Additionally, $H_2$ utilisation through water electrolysis demands 55 kWh of electrical energy to produce 1 kg of $H_2$ (Franco and Giovannini, 2023). The literature has shown that $H_2$ is optimally produced through water electrolysis whilst the oxygen produced is used for oxy-combustion. Specifically, there are two pathways for fuel combustion: direct and indirect combustion (Ozcan, Brandani and Ahn, 2014), where direct combustion involves burning fuel in direct contact with limestone. On the other hand, indirect combustion involves separately burning the fuel for heat and decomposing limestone, with the latter process producing a purer $CO_2$ stream by avoiding mixing with combustion by-products.

One study (Juangsa *et al.*, 2022), achieved reductions in $CO_2$ emissions by 44% through the use of $H_2$ completely replacing fossil fuels. Another work by (Okeke *et al.*, 2024), achieved 6% $CO_2$ emissions reduction through the use of 20% $H_2$ replacement of fossil fuel. The difference in $CO_2$ savings was primarily attributed the first study comparing $CO_2$ savings with a coal-based clinker process where 0.95 $kgCO_2$/t clinker was assumed (Juangsa *et al.*, 2022), whilst the second study assumed 0.75 $kgCO_2$/t clinker. Correspondingly, another

study (El-Emam and Gabriel, 2021), showed that a reduction of up to 19% $CO_2$ emissions was achieved by introducing hydrogen enriched with natural gas replacing fossil fuels in the cement process. Notably, a report by Hanson Cement (Hanson, 2022), successfully demonstrated the replacement of fossil fuels with $H_2$ based net zero fuels (including $H_2$, biomass, and plasma energy) at Hanson's Ribblesdale plant in the United Kingdom (UK) where it was able to save about 180,000 tonnes of $CO_2$ annually at the site. Another project by Limak Çimento in Turkey (Perilli, 2024), demonstrated success utilising $H_2$-blended fuel to replace 50% of fossil fuels in the cement production process which is projected to reduce $CO_2$ emissions by 700,000 tonnes annually. Regardless, $H_2$ itself is not yet widely used as fuel in the cement industry (Association and Ltd, 2019; Schneider *et al.*, 2023) due to its current higher electrical energy demand and initial costs (Schneider *et al.*, 2023). More specifically, in terms of the costs, hydrogen fuel is about two times more expensive compared to natural gas (Clark *et al.*, 2024), at 4 USD per kg (Pal *et al.*, 2024). Despite the range of studies available in the literature and industrial projects, research on the application of $H_2$ in cement is currently limited, particularly on full $H_2$ replacement of fossil fuels in the cement process, where systematic comparative assessments with other decarbonisation options are required.

### 2.3.4. Biomass

Biomass is currently utilised as an alternative fuel, compromising of over 5% of the total energy consumption and accounting for 90% of renewable heat sources consumed in the cement sector (Kusuma *et al.*, 2022). Biomass fuels are derived from non-fossilised and biodegradable organic materials from plants, animals, microorganisms and organic waste (Chatterjee and Sui, 2019). Biomass can be combusted in the kiln without significant

changes in the equipment or process, due to the kiln's long residence times at high temperatures and alkaline environment (Chatterjee and Sui, 2019). The use of biomass has shown potential in achieving 12 – 25% of $CO_2$ reductions when compared to fossil fuels (Chatterjee and Sui, 2019; Wojtacha-Rychter, Kucharski and Smolinski, 2021), and about 20 – 30% fuel substitution is recommended without comprising the clinker's quality (Aranda Usón *et al.*, 2013; Kusuma *et al.*, 2022). The combustion of biomass releases $CO_2$ equivalent to the amount obtained from air during its photosynthetic growth (Abbasi and Abbasi, 2010), without a net addition of $CO_2$ from combustion itself. In addition, biomass can reduce $NO_x$ and $SO_x$ emissions compared to fossil fuel combustion (Rahman *et al.*, 2015). In particular, a study by (Cavalett *et al.*, 2024), demonstrated climate change mitigation of up to ~30% through the use of biomass in contrast with fossil fuels, where the biogenic content of the fuel was considered. Modelling work by (Association and Ltd, 2019), demonstrated alternative fuel replacement in the kiln with 50% hydrogen and 50% biomass where 83.3% biomass and 16.7% plasma were used in the calciner, leading to removal of fuel related $CO_2$ emissions, where biogenic carbon was not included. This shows that $H_2$ can be used alongside biomass without compromising the mitigation of $CO_2$ emissions. Specifically, Siam City Cement in Thailand utilised biomass fuel (considering biogenic carbon) for cement production, replacing 20.5% of thermal energy with biomass in 2023 (ICR Newsroom, 2024). A project was launched, namely, Siam Cement Biomass Project in Thailand (Climate Friendly, 2024), which utilised biomass fuel in cement and projected to save upwards of 600,000 tonnes of $CO_2$ emissions per year.

On the other hand, biomass poses several challenges involving the maintenance of particles or combustion velocities, fuel burnout (Kusuma *et al.*, 2022), and the requirement for additional treatment from its lower calorific value compared to fossil fuels (Pamenter and

Myers, 2021). Besides, the availability is dependent on regional factors and is subject to seasonal fluctuations (Rahman *et al.*, 2015). In terms of the techno-economics, biomass fuel is about two times more expensive compared to natural gas (Clark *et al.*, 2024). Notably, studies commonly consider process-based $CO_2$ emissions and assumes biogenic carbon to be carbon neutral. This implies that emissions from biomass sources used in the cement production process are considered to be offset by the carbon absorbed during the biomass growth phase (Shahbaz *et al.*, 2021). This assumption could potentially underestimate the actual environmental impact as carbon released during biomass combustion may remain in the atmosphere for more than a century before being fully absorbed (Kouchaki-Penchah *et al.*, 2023).

### 2.3.5. Waste fuels

Prominent cement companies such as Lafarge group are currently using waste, predominantly from industrial by-products, as an alternative fuel, followed by Heidelberg and Holcim (Rahman *et al.*, 2015), allowing diversion of materials from landfills and promoting circular economy practices. Waste fuel is currently widely acknowledged as an alternative fuel in European cement plants where 64% of cement plants use waste materials as alternative fuels (Aranda Usón *et al.*, 2013). It is thanks to the kiln's alkaline environment and resistance to high temperature, waste materials can be combusted (Rahman *et al.*, 2015).

Meat and bone meal (MBM) is a type of non-hazardous waste fuel which is produced by processing animal by-products through grinding and sterilisation (Hiromi Ariyaratne *et al.*, 2014; Tan *et al.*, 2023). According to (Rahman *et al.*, 2017), MBM can substitute up to 40% of fossil fuels in cement production and is more readily available compared to other alternative fuels. Moreover, the high calcium content in MBM reduces the sulfur dioxide

($SO_2$) emissions during combustion. On the energy perspective, incorporating MBM at 20% share in the fuel mix could result in a ~6% reduction in thermal energy demand of the cement production process (Rahman *et al.*, 2017). Combusting MBM results in a lower gas temperature in contrast with coal, primarily a result of the high moisture and ash content, along with a greater air demand caused by its lower oxygen levels (Ariyaratne *et al.*, 2015). Whilst the combustion of MBM reduces the $CO_2$ produced by ~33% when compared to coal at 100% replacement (Aranda Usón *et al.*, 2013), it is accountable for a ~35% higher content of $NO_x$ (Gulyurtlu *et al.*, 2005), with increased emissions of CO and $SO_2$, from its higher nitrogen content compared to coal (Rahman *et al.*, 2015). Another drawback is the increased chlorine content, which has the potential to result in material build-up and blockages in the preheater impacting the cement plant's efficiency (Rahman *et al.*, 2015).

An alternative type of non-hazardous waste fuel is sewage sludge (SS), which is a by-product of wastewater treatment (Tan *et al.*, 2023). SS primarily consists of water and organic matter and a high moisture content in its raw form. $CO_2$ reductions of 0.88 tonne per tonne of coal replaced by SS can be realised (Rahman *et al.*, 2015). Moreover, the utilisation of SS as an alternative fuel in cement production results in reduced $NO_x$ emissions without impacting the quality of clinker (Tan *et al.*, 2023). SS also contains a low calorific value comparable to MBM, therefore releases less energy per unit mass (Rahman *et al.*, 2015). Despite this, the use of SS increases the $SO_x$ emissions (Rahman *et al.*, 2015; Zieri and Ismail, 2018).

A waste product from the automotive sector, tyres, are normally disposed in landfills which poses environmental, health, and safety risks from rodent and insect infestation (Aranda Usón *et al.*, 2013; Zieri and Ismail, 2018). Tyre derived fuel (TDF) does not impact the chemical composition of clinker produced and is notably more cost effective compared to

natural gas and coal (Rahman *et al.*, 2015). TDF utilisation can lead to a reduction of fuel consumption (Chatterjee and Sui, 2019), and ~10% $CO_2$ emissions reduction (Rahman *et al.*, 2015), in contrast with conventional fossil fuels. However, the combustion of TDF was seen to increase $SO_2$ and $NO_x$ emissions (Zieri and Ismail, 2018), whilst generating approximately 35% more CO compared to conventional fossil fuels (i.e., coal and natural gas) (Rahman *et al.*, 2015).

Refused derived fuel (RDF) is a by-product of municipal solid waste (MSW), enabling the reuse of waste materials. RDF is a non-hazardous alternative fuel produced by extracting non-combustible components from MSW. For instance, waste from plastic bottles can be incinerated directly or processed into RDF (Shehata *et al.*, 2022). RDF is a widely adopted alternative fuel, primarily due to its high calorific value, offering high energy output and improved combustion efficiency (Chaves *et al.*, 2022). RDF has the potential to reduce coal consumption by 10 – 30% in cement production. Studies have shown that replacing coal with RDF can reduce carbon dioxide emissions by 1.61 – 2.25 kg for every kg of RDF substituted (Karpan, Abdul Raman and Taieb Aroua, 2021; Chaves *et al.*, 2022). However, one of the key challenges in using RDF in cement kilns is its chlorine content, as chlorine can compromise the strength of cement through weakening and accelerate corrosion of steel reinforcements in concrete (Ziaee *et al.*, 2016). Furthermore, RDF is reliant on the availability of MSW, therefore the procurement costs can vary according to the market conditions (Chaves *et al.*, 2022).

Whilst studies (Wiloso *et al.*, 2016), including LCAs, typically treat biogenic carbon from alternative fuels as carbon-neutral, this assumption can artificially lower the life cycle greenhouse gas emissions by 7.2% (Pitre, La and Bergerson, 2024). Carbon neutrality was assumed as biogenic carbon is absorbed by plants during growth and eventually released in

equal amounts, resulting in no net increase in atmospheric greenhouse gases (Wiloso *et al.*, 2016).

### 2.3.6. Properties of alternative fuels

According to (Rahman *et al.*, 2015; Chatterjee and Sui, 2019; Luo *et al.*, 2024), key properties of alternative fuels that influence energy efficiency, combustion efficiency, and $CO_2$ emissions include the calorific value or lower heating value (LHV), moisture content, and ash content (see Table 2.2). Fuels with high LHV, low moisture and ash contents are generally preferred (Rahman *et al.*, 2015), since they provide faster burning rates, requires less fuel, enable improved kiln control, and offer higher fuel efficiencies (Chatterjee and Sui, 2019).

In particular, high ash content increases dust generation, which can impact the clinker product quality and burnability, requiring dust control measures (Luo *et al.*, 2024). These ashes may also be incorporated into the clinker product during kiln combustion, potentially affecting the cement strength or causing prolonged setting times (Tan *et al.*, 2023). Similarly, high moisture content reduces the LHV and requires preprocessing and drying steps for moisture evaporation, leading to increased specific heat demand, fuel, and costs (Tan *et al.*, 2023). As shown in Table 2.2, $H_2$ stands out with the highest calorific value, lowest moisture and ash content whilst producing the least amount of $CO_2$ per GJ of energy. In contrast, the other alternative fuels listed in Table 2.2, offer limited $CO_2$ reduction compared to coal.

***Table 2.2. Properties of alternative fuels.*** *Including the calorific value (LHV), moisture content, ash content, and $CO_2$ produced. Varies suggest that the carbon released depends on the amount initially absorbed from the atmosphere which is applicable to biomass and MBM based alternative fuels.*

| Fuel | Lower heating value (LHV) (MJ/kg) | Moisture Content (wt. %) | Ash Content (wt.%) | $CO_2$ Produced ($kgCO_2/GJ$) | Reference |
|---|---|---|---|---|---|
| Coal | 27.89 – 30 | 9.20 | 8.85 | 96 | (Chatterjee and Sui, 2019; Luo *et al.*, 2024) |
| Natural gas | 46.8 – 53.8 | N/A | 0 | 54.2 | (Rahman *et al.*, 2015, 2017; Chatterjee and Sui, 2019; Luo *et al.*, 2024) |
| Hydrogen ($H_2$) | 120 | N/A | 0 | 0 | (Abdin *et al.*, 2020) |
| Biomass | 13.50 | 9.96 | 20.61 | varies | (Rahman *et al.*, 2015; Chatterjee and Sui, 2019; Luo *et al.*, 2024) |
| Tyre-derived fuel (TDF) | 27 – 37.8 | 0.62 | 4.78 – 4.81 | 85 | (Rahman *et al.*, 2015, 2017; Georgiopoulou and Lyberatos, 2018; Chatterjee and Sui, 2019; Tan *et al.*, 2023; Luo *et al.*, 2024) |
| Municipal solid waste (MSW) | 6.21 – 15.40 | 50 – 80 | 31.2 – 35.17 | 8.7 | (Palanivel and Sulaiman, 2014; Rahman *et al.*, 2015, 2017; Chatterjee and Sui, 2019; Tan *et al.*, 2023) |
| Refuse-derived fuel (RDF) | 12 – 26 | 3 – 7.8 | 10.9 | ~44.6 – 96.7 | (Rahman *et al.*, 2015; Georgiopoulou and Lyberatos, 2018; Alfè *et al.*, 2022; Brożek *et al.*, 2022; Tan *et al.*, 2023) |
| Sewage sludge (SS) | 14.8 – 16.7 | 0.2 – 10 | 71.0 | ~52.7 – 59.7 | (Valderrama *et al.*, 2013; Rahman *et al.*, 2015; Luo *et al.*, 2024) |
| Meat and bone meal (MBM) | 13.06 – 10.71 | 1.35 – 6.80 | 10.54 – 34.4 | varies | (Rahman *et al.*, 2015, 2017; Chatterjee and Sui, 2019; Luo *et al.*, 2024) |

The use of alternative fuels such as hydrogen, biomass, and waste in cement production offer substantial climate change benefits by reducing $CO_2$ emissions and reducing consumption

of finite resources. With regards to climate change impacts, $SO_x$ and $NO_x$ emissions are notably reduced in biomass fuels when compared to coal (Aranda Usón *et al.*, 2013), with MBM waste fuels accounting for a higher content of $NO_x$ (Gulyurtlu *et al.*, 2005). In contrast, the combustion of $H_2$ achieves zero climate change impacts (Jibran and Mahat, 2023). This is because hydrogen fuel combustion does not produce $CO_2$ as it reacts with $O_2$ where the only product is water (Habib *et al.*, 2024). However, its overall carbon footprint depends on how it is produced. Green hydrogen, made with renewable energy, is near-zero carbon, whereas grey hydrogen relies on natural gas and blue hydrogen involves capturing carbon emissions from production, both of which emit minor levels of $CO_2$ emissions (Hulst, 2019).

Whilst alternative fuels such as biomass and waste (including MBM, SS, TDF, and RDF) produce notably less $CO_2$ emissions as opposed to coal, they are unable to achieve net zero $CO_2$ emissions from combustion and vary in supply in contrast with $H_2$ fuel. In addition, the utilisation of waste fuels in practice such as MBM, SS, and RDF can increase the chlorine content in the cement process and result in clogging in the pre-heater and resulting in efficiency losses (Chatterjee and Sui, 2019). Furthermore, the use of waste-based alternative fuels can lead to minor changes in the clinker product as their combustion by-products can become incorporated into the clinker (Rahman *et al.*, 2013, 2015). The comparative information in Table 2.2 was used to inform the selection of $H_2$ as the alternative fuel. The key reason is because, in terms of climate change impacts and transitioning towards cleaner cement production, $H_2$ was seen to be the most optimal alternative fuel option among current trends from its high LHV, carbon neutral combustion, and absence of ash formation.

## 2.4. Concentrated solar power (CSP) and electrification

### 2.4.1. Solar as fuel (including CSP and PV)

Meeting climate change targets necessitates substantial growth of renewable energy and substitution of fossil fuels in the cement industry. In particular, solar energy, harnessed from the sun's radiation, is one of the most abundant and sustainable energy sources available. There are two main types of modern solar energy technologies: Concentrated Solar Power (CSP) and Photovoltaic (PV) systems (Kurkute and Priyam, 2022). A CSP system uses mirrors (known as heliostats) to reflect and concentrate sunlight into a specific area (concentrator), where the concentrated energy is used as thermal energy (Sahoo, Kumar and Samsher, 2023). On the contrary, a PV system converts sunlight directly into electrical energy using semiconductor materials, where electrical energy is generated once sunlight hits the PV cells (Parida, Iniyan and Goic, 2011). Solar energy accounts for three-quarters of the total global renewable energy supply in 2023, exceeding other renewable sources such as wind power and expected to double by 2028 in contrast with 2022 levels (IEA, 2024).

Advancements in solar technologies and heightened demand for climate change mitigation have led to the use of solar power in the cement industry. In particular, a project by CEMEX and Synhelion has demonstrated the feasibility and $CO_2$ mitigation performance of utilising solar energy in cement production through investments in pilot plants. Carbon emission reduction of 40% compared with conventional fossil-based processes was observable in the project, where it adopted the use of CSP solar systems (Global Cement and Concrete Association, 2023). Modelling works by (Gonzalez, Switzerland and Flamant, 2013), and (Nikolakopoulos *et al.*, 2022) have demonstrated ~40% $CO_2$ savings from CSP-based

alternative fuel in the cement calcination stage, although it demands a higher energetic performance compared to fossil-based fuel. Although PV systems can supply electrical energy to support the cement process, electrical energy only accounts for ~10% of the total energetic demand of the process (Nhuchhen, Sit and Layzell, 2022a). In contrast, utilising electrical energy to facilitate plasma gas energy for the cement kiln can bring about $CO_2$ savings of ~25% compared to the conventional fossil-based process whilst meeting the high temperature required of the kiln combustion at 1500 °C (Quevedo Parra and Romano, 2023). With the increase in popularity of solar energies in the industrial sectors as the dominant renewable energy source (IEA, 2024), as depicted in Figure 2.6, the transition towards adopting solar as partial fossil fuel replacement will be the backbone of efforts aimed at greener cement production.

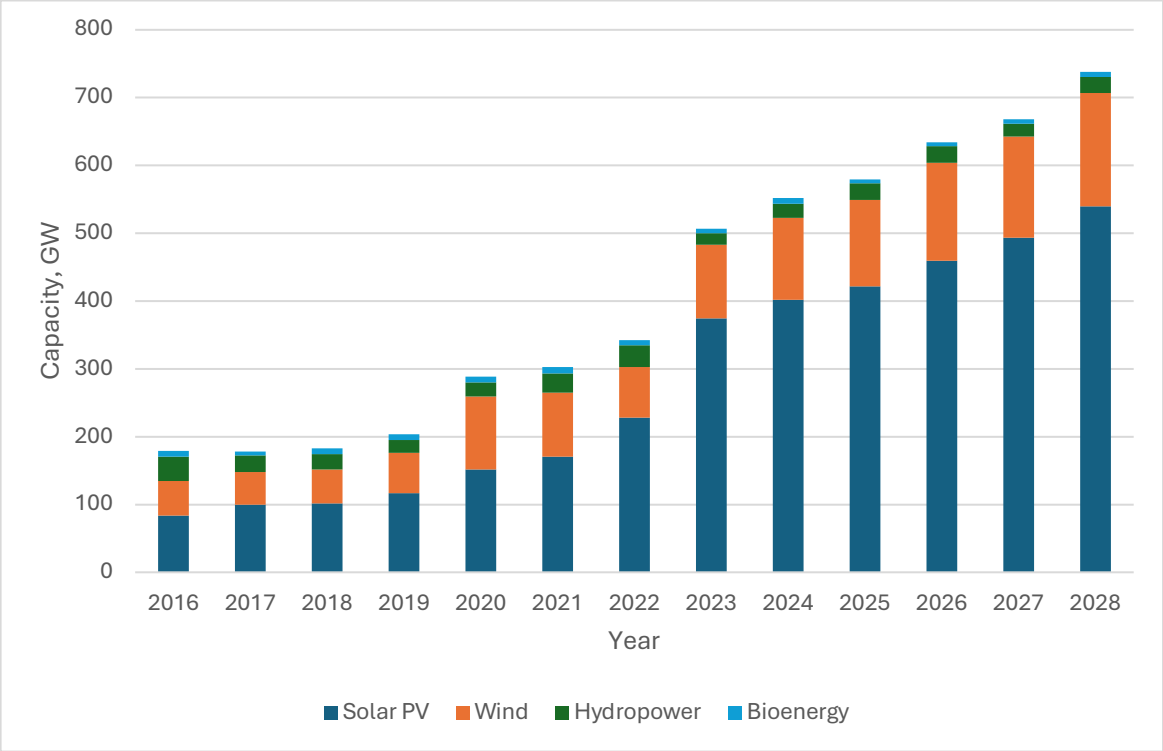


***Figure 2.6. Renewable electricity capacity by technology and type, 2016–2028.*** *Data adapted from IEA (IEA, 2024).*

## 2.4.2. Concentrated solar power (CSP)

Previous studies (Tregambi *et al.*, 2018; Moumin *et al.*, 2020; Nikolakopoulos *et al.*, 2022) have highlighted the dominant role of CSP-based fuel in targeting the calcination stage of cement production (accountable for 60% of total $CO_2$ emissions (Cavalett *et al.*, 2024)). In a CSP-based cement process, two tower systems are available, notably the top of tower (TT) and beam down (BD) systems (Moumin *et al.*, 2020). The TT system involves placing the solar calciner on top of a tower (shown in Figure 2.7), whereas in the BD system, the reactor, positioned on the ground, receives solar energy reflected by heliostats atop a tower. However, the losses of solar flux are increased, and the reactor requires additional investment in the BD system in contrast with the TT system (Moumin *et al.*, 2020).

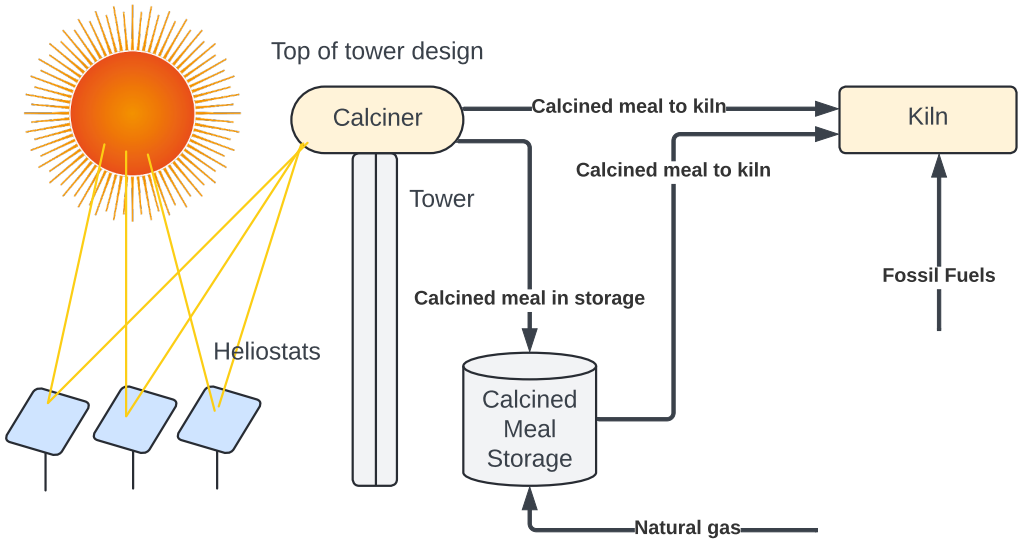


***Figure 2.7. Process flow diagram (PFD) of the CSP-based cement production process.*** *The represented PFD is based on the TT system for the solar calciner with energy for the kiln being sourced from fossil fuels (including coal or natural gas). The thermal energy storage method adopted is the calcined meal storage, where the calcined meal is over-produced during the daytime and stored for use during night-time.*

A hybrid process involving a solar and fossil calciner was assessed in a 3000 tonne per day clinker capacity plant (with 86% calciner efficiency), demonstrating 9% of $CO_2$ savings from a 28% replacement of fossil fuel with solar energy in 2020 (Moumin *et al.*, 2020). It

was shown by (Moumin *et al.*, 2020), that the implementation of the solar calciner in the cement industry can achieve up to 17% $CO_2$ avoidance. Another study by (Meier, Gremaud and Steinfeld, 2005), shows the elimination of 95% of fossil-based emissions from lime calcination by utilising a CSP-based solar calciner (TT system). Utilising solar energy to support the calcination stage in cement production could lower $CO_2$ emissions by up to 35.5% (Nikolakopoulos *et al.*, 2022), while maintaining the necessary temperature conditions of the cement calciner and kiln. Likewise, a sharp decrease in climate change impacts of 48% and decline in fossil fuels by 75% is achieved through a solar calciner where energy requirements were met through CSP (Tomatis *et al.*, 2020). This underscores the positive climate change impacts of utilising CSP to decarbonise the calcination stage in cement production.

The thermal energetic demand of the CSP system is higher in contrast with a fossil-based process due to the high energy demand of maintaining continuous thermal energy storage and solar calcination (Sahoo, Kumar and Samsher, 2023). Conversely, the energy required for calcination in the solar driven process aligns with the fossil-based process at 3182 kJ/kg of CaO (Sahoo, Kumar and Samsher, 2023). It is evident from (Gonzalez, Switzerland and Flamant, 2013), that as the substitution of fossil fuel with solar energy increases, there is a corresponding rise in energy demand, primarily driven by the increased energy demand of the solar reactor and thermal storage systems. Whilst CSP offers higher energy efficiency in contrast with PV systems (Awan *et al.*, 2019), it requires direct sunlight to function as opposed to PV systems which can utilise both direct and diffuse sunlight (Desideri and Campana, 2014).

Whilst CSP in the cement industry is currently in its infancy, there are notable projects by CEMEX in conjunction with Synhelion (Global Cement and Concrete Association, 2023),

and Holcim Cement (Schoeck, 2023), whom have implemented a solar driven system in the cement production process. Noteworthily, CEMEX and Synhelion's project successfully operated a cement plant sourcing all fuel from CSP systems whilst aiming to achieve green cement by 2050. This project eliminated all fossil fuels in the calciner and kiln stages with high temperature solar heat whilst meeting the temperature requirements of 900 °C and 1500 °C for combustion, respectively (Global Cement and Concrete Association, 2023). Holcim cement is projected to install a 25 MW solar array to support the energy demand of cement production enabling the existing facility to self-generate 75% of its electrical energy requirements from renewable solar energy (Schoeck, 2023). In addition, an EU-funded project, namely, SOLPART, demonstrated the feasibility of utilising solar thermal energy in the calcination stage to meet combustion temperatures of 900 °C in the cement production (Flamant, 2020).

### 2.4.3. Plasma gas electrification

The transition to electrification in the cement production process represents a step closer towards reducing $CO_2$ emissions, as it addresses the cement industry's reliance on fossil fuels and introduces electricity as an alternative (Antunes *et al.*, 2022). Electrification harnesses direct electrical energy to supply heat energy through resistive heating or plasma. When electricity is provided from a renewable source, such electrification leads to a reduction in $CO_2$ emissions by eliminating the need for fossil-based fuels (Huismans and Voswinkel, 2023). Noteworthily, a report by (Roelofsen *et al.*, 2020), suggested that about 50% of fuel consumed in the industrial sectors (including cement) can be electrified with present technologies. A study by (Quevedo Parra and Romano, 2023), utilised an electrified calciner coupled with plasma gas for kiln combustion where grid electricity is the key source

of energy. The findings showed that the complete electrification of the cement process is significantly more electrical energy-intensive, requiring 1341 kWh/t of clinker (electrical energy) in contrast to 131.7 kWh/t clinker (electrical energy) in the fossil-based process. In this system, the electrified calciner and plasma burners collectively contributed to 1152.78 kWh/t clinker (~75% of the total energy), due to the high flowrates of plasma air and high combustion temperatures (Quevedo Parra and Romano, 2023). On the contrary, it is important to note that the $CO_2$ produced is 647.4 kg$CO_2$/t clinker, 25% less compared with the fossil process (Quevedo Parra and Romano, 2023). Focusing on the economics, $CO_2$ avoidance costs of ~135 USD/t clinker were demanded, primarily attributed to the electricity price of ~58 USD/MWh in 2022. The cost increase is attributed to the substantially higher electrical energy demand and costs of the plasma generator (Quevedo Parra and Romano, 2023).

Furthermore, in a notable project, CemZero, confirmed the feasibility of adopting the plasma technology in clinker production, allowing the generation of plasma gas temperatures up to 2000 °C (Antunes *et al.*, 2022), where the ability to reach this temperature was also confirmed in a separate notable study (Nozaki, Kim and Chen, 2024). As complete electrification of both the calciner and kiln combustion stages is more energy intensive compared to fossil-based production (Lechtenböhmer *et al.*, 2016), studies advocate for a selective approach. Specifically, electrifying the calcination stage is suggested (Antunes *et al.*, 2022), which allows $CO_2$ savings to be realised although demanding additional electricity. Another study (Vermeiren *et al.*, 2024), recommended the use of electrification through microwave technology by converting electric current into electromagnetic radiation which can reduce up to 40% the energy required in the cement process. This was stated by (Antunes *et al.*, 2022), enabling microwave heating to reach temperatures of up to 1160 °C.

These studies underscore the potential of electrification as a promising option for decarbonising the cement industry, although achieving carbon neutrality depends on using renewable energy sources for electricity and necessitates a shift away from traditional grid electricity (Jacob and Tokheim, 2023).

### 2.4.4. Solar thermal energy storage

Solar energy is limited to the availability of sunshine received (hereafter solar irradiation) throughout the day (Moumin *et al.*, 2020), and varies depending on the season and weather changes. Therefore, for solar-heat driven processes, Thermal Energy Storage (TES) is required to operate the cement process during periods of low to zero solar irradiation (Moumin *et al.*, 2020). Existing TES systems include the use of molten salt as the storage medium (typically a mixture of sodium and potassium nitrate) or calcined meal storage (Moumin *et al.*, 2020). Utilising molten salts involves heating them to high temperatures in insulated tanks which are then circulated through a heat exchanger to supply heat when needed (Gonzalez, Switzerland and Flamant, 2013). Conversely, calcined meal storage entails producing excess calcined meal during daylight hours, therefore the solar reactor needs to be oversized to support the storage of thermal energy during night-time operations (Moumin *et al.*, 2020). The oversized solar reactor operates during the photovoltaic hours daily, producing calcined meal for the cement process and for storage in silo. During periods of no sunshine, the stored calcined meal is re-heated to 900 °C using natural gas to facilitate the calcination process (Sahoo, Kumar and Samsher, 2023). Utilising hot calcined meal storage enhances the efficiency whilst decreasing energy losses and permitting higher temperatures to be achieved by avoiding the use of intermediate fluids such as molten salts (Gonzalez, Switzerland and Flamant, 2013).

### 2.4.5. Market competitiveness of solar driven systems

With regards to the economic competitiveness, the solar driven system incurs the additional costs of the heliostats, tower, solar calciner, compound parabolic concentrator (CPC), and land costs, while the costs of the rest of the clinker production system remains comparable to the conventional system (Moumin *et al.*, 2020). More specifically, it was estimated that additional annualised capital expenditure (CAPEX) and operational expenditure (OPEX) costs totalling 14.84 USD/t clinker are induced when operating the solar driven process as opposed to the fossil-based process in (Moumin *et al.*, 2020). Accordingly, $CO_2$ avoidance costs are 127.78 USD/t and can reach 80.13 USD/t depending on the reactor efficiency and solar irradiation in 2020. Current storage costs for calcined meal storage and molten salts are 9.64 USD/kWh and 21.44 USD/kWh respectively in 2020 (Moumin *et al.*, 2020), with the former benefiting from no storage medium being required (Gonzalez, Switzerland and Flamant, 2013). In contrast, PV battery storage costs via lithium ions is 200 USD/kWh (International Renewable Energy Agency, 2017), substantially higher compared to calcined meal storage costs, indicating that calcined meal storage is more cost efficient. Although currently higher initial costs exist for solar based systems, governmental incentives and rising $CO_2$ taxes will guide the shift towards the implementation of the solar driven processes in the cement industry (Moumin *et al.*, 2020) for greener cement production.

## 2.5. Energy efficiency and carbon capture

### 2.5.1. Kiln efficiency improvements

Kilns are one of the most energy-intensive parts of cement production, demanding about ~3000 MJ/t clinker. Therefore, enhancing their energy efficiency is of prominent importance in the cement industry (Saidur *et al.*, 2011). The type of kiln is one of the key contributors in determining the energy demand of the cement production process, where the dry process is more energy efficient utilising 3.40 GJ/t clinker, compared to the wet process utilising 5.29 GJ/t clinker. The typical energy mix in the dry process consists of 75% thermal and 25% electrical energy (Sahoo, Kumar and Samsher, 2022). The efficiency of the kiln decreases as the pre-calcination increases where higher pre-calcination reduces the enthalpy of the raw meal, air, and flue gases (Anacleto *et al.*, 2021).

In particular, the kiln is responsible for multiple sources of heat loss including the flue gases, leakage air (ambient air) (Adeniran *et al.*, 2019), and heat radiated from the kiln's surface. To mitigate heat loss from the kiln, advanced insulated refractories based on the raw material, operating conditions and fuel type allow for 0.12 – 0.63 GJ/t of thermal energy savings and 10.3 – 15.5 kg/t of $CO_2$ emission reductions to be realised (Sahoo, Kumar and Samsher, 2022). In accordance with (Sahoo, Kumar and Samsher, 2022), thermal energy savings of up to 0.22 GJ/t clinker were achievable through the use of indirect firing in the kiln, and electrical energy savings of about 13% when using alternative fuels composed of rice husk and waste-derived materials. Similarly, the use of alternative fuels such as biomass can offer 3% energy efficiency improvement whilst decreasing the $CO_2$ produced by 3.5% (Rahman *et al.*, 2016). In contrast, harnessing waste heat can improve the thermal efficiency,

and offer 12% of $CO_2$ emissions reduction (Sahoo, Kumar and Samsher, 2022; Georgiades *et al.*, 2023), whilst offering reduced fuel usage and costs (Sztekler *et al.*, 2016; Adeniran *et al.*, 2019; Al-Rawashdeh *et al.*, 2019).

### 2.5.2. Organic Rankine cycle (ORC)

Cement production is a highly energy-intensive process, consuming between 3 – 5 GJ per tonne of cement, with clinker production accounting for about 80% of this demand. To address this, energy recovery processes such as waste heat recovery systems are increasingly being explored among studies to enhance the energy efficiency and reduce the energy demand (Al-Rawashdeh *et al.*, 2019). An organic Rankine cycle (ORC) presents a promising solution for waste heat recovery in clinker production, offering conversion of low to medium temperature heat from 80 °C – 300 °C, into electricity (Ahmed *et al.*, 2018) and $CO_2$ emission reductions of 0.74% (Wang *et al.*, 2015). Moreover, it has been demonstrated by (Poggianti, Palazzolo and Moliner, 2024), that waste heat recovery has the potential to recover about 21% of the cement plant's electrical energy.

In a typical cycle of an ORC, heat is added to the organic fluid in the evaporator at constant pressure, where the fluid undergoes isentropic expansion in the turbine. The working fluid releases heat to the cooling water in the condenser at constant pressure and then compressed isentropically by the pump before returning to the evaporator to begin a new cycle. The selection of organic fluids is critical as it impacts the efficiency of the ORC and isentropic fluids have shown to generate high power output. Unlike conventional steam-based Rankine cycles that utilises water as the working fluid, ORCs typically offer lower operational maintenance, costs, higher efficiencies and better commercial adaptability (Moreira and Arrieta, 2019). ORCs also provide improved energetic performance compared to the water-

vapor Rankine cycles (Wang *et al.*, 2015), as the evaporation process requires less heat, lower pressure, and temperature (Ahmed *et al.*, 2018).

### 2.5.3. Carbon capture utilisation and storage (CCUS)

Carbon capture, utilisation and storage (CCUS) offers carbon capture efficiencies of over 90% of flue gases derived from clinker production (Gardarsdottir *et al.*, 2019), through the use of amine-based or calcium looping solutions. Amine-based CCUS systems primarily utilise amine solutions to chemically absorb $CO_2$ from the cement flue gases (Rolfe *et al.*, 2018). A modelling study by (Jiang *et al.*, 2024) through Aspen Plus simulations, demonstrated the feasibility of increasing the $CO_2$ capture efficiency to 99.7%, using advanced amine-based capture through the utilisation of blended piperazine (PZ) and 2-amino-2-methyl-1-propanol (AMP) (PZ-AMP) solution. The use of PZ-AMP solvent resulted in improved energy performance, $CO_2$ capture capacity, and economic competitiveness due to 18% lower $CO_2$ avoided cost, in comparison with the conventional Monoethanolamine (MEA) solution used for amine systems (Jiang *et al.*, 2024). Although the capture cost through the PZ-AMP solution is 56 USD/tonne $CO_2$, it retains cost effectiveness in contrast with the MEA based solution (Jiang *et al.*, 2024). Correspondingly, CCUS through calcium looping, used as a post combustion system into a cement kiln, offers capture efficiencies of 90%. This system utilises the reversible reaction between calcium oxide (CaO) and carbon dioxide ($CO_2$) to capture and release $CO_2$ (Rolfe *et al.*, 2018), targeting the calcination reactions and involving liquid to gas reactions. Although current CCUS systems capture $CO_2$ from air combustion, oxygen combustion (hereafter oxy-combustion) allows more concentrated $CO_2$ to be produced from cement flue gases, leading to higher capture efficiencies (Faria *et al.*, 2022). This was shown by (Rolfe *et al.*, 2018),

where oxy-combustion achieved a 100% $CO_2$ capture rate, when compared to calcium looping at 94%, although calcium looping offered better energy performance. Whilst CCUS through amine-based through MEA (Jiang *et al.*, 2024), or calcium looping pathways (Lena, Spinelli and Romano, 2018) can capture most of the $CO_2$ from clinker flue gases, it does not prevent the generation of $CO_2$ but mitigates its release to the atmosphere.

## 2.6. Alternative clinkers and cement substitution

### 2.6.1. $CO_2$ from cement calcination

It has been widely noted in the literature (Hanein *et al.*, 2021; Antunes *et al.*, 2022; Cavalett *et al.*, 2024), that about 60% of $CO_2$ from the cement production process results from calcination. In the calcination stage, the decomposition of limestone occurs at 900 °C (shown in Equation 2.1), where $CaCO_3$ is decomposed to CaO and $CO_2$ (Nehdi, Marani and Zhang, 2024). During this stage one mole of $CaCO_3$ produces one mole of $CO_2$, with an average of 0.5 – 0.7 tones of $CO_2$ produced per tonne of clinker (Barbhuiya *et al.*, 2024). $CaCO_3$ accounts for ~80% of the raw meal composition in clinker (Faria *et al.*, 2022), where the extensive use of limestone amplifies the total $CO_2$ emissions. This emphasises the importance of reducing the amount of limestone calcined whilst shifting the focus to determining alternative clinkers with lower limestone content (Antunes *et al.*, 2022).

### 2.6.2. Alternative clinkers and their performance

In ordinary Portland cement (OPC) clinker, alite is the primary component (Antunes *et al.*, 2022), and accounts for the production of 579 $kgCO_2/t$ (Scrivener, John and Gartner, 2018). The secondary component of clinker is belite, which accounts for 512 $kgCO_2/t$ (Scrivener,

John and Gartner, 2018). Other components are tricalcium aluminate and ferrite, contributing to 489 $kgCO_2/t$ and 362 $kgCO_2/t$, respectively (Scrivener, John and Gartner, 2018). Clinker is produced from raw meal; its typical composition is ~80% $CaCO_3$, 14% $SiO_2$, 3.5% $Al_2O_3$, and 2.5% $Fe_2O_3$ (Mastorakos *et al.*, 1998). Given the rising concern on climate change issues, it is imperative to examine the modification of the clinker composition or introduce alternative clinkers (see Table 2.3) with reduced limestone content to effectively reduce these emissions.

***Table 2.3. Energy and $CO_2$ performance of alternative clinkers in comparison with OPC clinker,*** *respective of sintering temperatures, phase, and oxide clinker compositions. With regards to the HFC, the ranges of the mineral compositions for the three HFC types are outlined and the amorphous content in CSC refers to the non-crystalline phases in clinker.*

| Alternative clinker | Energy savings (%) | $CO_2$ savings (%) | Sintering temperature (°C) | Phase composition (wt%) | Oxide composition (wt%) | Source |
|---|---|---|---|---|---|---|
| High belite clinker | 12 | 5.2 – 10 | 1350 | 30% $C_3S$<br>45% $C_2S$<br>23% $C_4AF$ | 73.70 $CaCO_3$<br>23.59 $SiO_2$<br>4.84 $Al_2O_3$<br>7.54 $Fe_2O_3$ | (Popescu, Muntean and Sharp, 2003; Gartner and Sui, 2018; Kian *et al.*, 2021; Antunes *et al.*, 2022) |
| Belite ye'elimite ferrite clinker | 20 | 20 – 40 | 1350 | 49.70% $C_2S$<br>19.90% $C_4AF$<br>28.80% $C_4A_3S$ | 64.20 $CaCO_3$<br>12.50 $SiO_2$<br>13.80 $Al_2O_3$<br>4.70 $Fe_2O_3$<br>4.81 $CaSO_4$ | (Sabbah and Zhutovsky, 2022; Wang *et al.*, 2023) (Wang *et al.*, 2023) |
| High ferrite clinker | 5 – 20 | 5 – 18 | 1350 – 1375 | 37.06 – 59.10% $C_3S$<br>8.60 – 32.86% $C_2S$<br>2.80 – 8.50% $C_3A$<br>15.17 – 18.10% $C_4AF$ | 77.33 – 78.46 $CaCO_3$<br>12.85 – 15.80 $SiO_2$<br>3.14 – 4.73 $Al_2O_3$<br>3.72 – 4.34 $Fe_2O_3$ | (Elakneswaran *et al.*, 2019; Zhang *et al.*, 2021; Yang *et al.*, 2022) |
| Calcium silicate clinker | 30 | 30 | 1250 | 2.96% $C_2S$<br>52.30% CS<br>13.38% $C_3S_2$<br>24.20% Amorphous | 61.86 $CaCO_3$<br>35.62 $SiO_2$<br>1.93 $Al_2O_3$<br>0.59 $Fe_2O_3$ | (Sahu and Meininger, 2019) (Gartner and Sui, 2018) |

High-belite clinkers (HBC) have similar compositions to OPC clinker whilst offering reductions of up to 10% limestone and lower combustion temperatures of 1350 °C (10% lower than OPC clinker), reducing up to 10% $CO_2$ process-based emissions (Antunes *et al.*, 2022). High-belite clinkers typically have lower early age strengths from their slower hydraulic kinetics (Antunes *et al.*, 2022), and lower heat of hydration compared to OPC

clinker (Gartner and Sui, 2018). It produces similar compressive strength to OPC at 28 days (Scrivener, John and Gartner, 2018). On the other hand, belite is harder than alite, therefore 5% more energy is required for grinding (Gartner and Sui, 2018).

Similarly, belite-ye'elimite-ferrite (BYF) clinker provides $CO_2$ mitigation while having relatively similar compressive strength to OPC (Morin *et al.*, 2017) at 24 hours (Antunes *et al.*, 2022), without compromise of a slower hydration process (Antunes *et al.*, 2022). Ye'elimite hydration results in the formation of ettringite and contributes to the development of early-age strength (Wang *et al.*, 2023). BYF contains 20 – 30% less limestone content in contrast with OPC clinker, reducing $CO_2$ emissions by up to 20% from the calcination stage. The rapid hydration property of ye'elimite compensates for the low early age strength of belite (Antunes *et al.*, 2022). Other studies reported $CO_2$ reductions by BYF clinkers at 28% (Nehdi, Marani and Zhang, 2024) and 25% (Morin *et al.*, 2017), respectively. Additionally, the kiln combustion temperature of BYF clinkers is 1250 °C – 1350 °C (Sabbah and Zhutovsky, 2022; Nehdi, Marani and Zhang, 2024), 10 – 17% less compared to OPC clinker, whilst having improved grindability (Morin *et al.*, 2017). The composition of BYF can be seen in Table 2.3.

Another alternative to OPC clinker is high ferrite clinker (HFC), which contains double the amount of ferrite whilst cutting the belite content by 50% as opposed to OPC clinker (Elakneswaran *et al.*, 2019). Noteworthily, one composition of HFC is 59.1% $C_3S$, 8.6% $C_2S$, 8.5% $C_3A$, and 17.2% $C_4AF$. It can reduce the kiln combustion temperature to 1350 °C, which reduces the energy consumption by 5% in contrast with OPC clinker (Elakneswaran *et al.*, 2019) (detailed in Table 2.3). According to X-ray diffraction based experimental studies by (Elakneswaran *et al.*, 2019), HFC has identical degrees of hydration and develops comparable mechanical strength to OPC after 28 days. Ferrite in HFC offers high early-age

compressive strength but slows later strength development (Yang *et al.*, 2022). Another study investigating HFC with distinctive compositions through experimental methods through X-ray diffraction (Zhang *et al.*, 2021), found that a kiln combustion temperature of 1375 °C can be achieved whilst achieving a compressive strength of 72.7 MPa, comparable to OPC after 28 days of curing. The composition of this HFC is 42.1% $C_3S$, 28.4% $C_2S$, 2.8% $C_3A$, and 18.1% $C_4AF$ (see Table 2.3) offering high hydration reactivity. Moreover, it was able to achieve energy and $CO_2$ reductions of up to ~20% and ~19%, respectively (Zhang *et al.*, 2021), through the reduction of alite and belite contents along with the sintering temperature. Similarly, work by (Yang *et al.*, 2022) on HFC demonstrated comparable mechanical compressive strength compared to OPC, whilst offering lower alite content. This HFC has the composition of 37.06% $C_3S$, 32.86% $C_2S$, 4.32% $C_3A$, and 15.17% $C_4AF$ (Yang *et al.*, 2022).

Calcium silicate clinkers (CSC) comprise a higher amount of low calcium silicate phases such as wollastonite (CS) and rankinite ($C_3S_2$), whilst having lower alite and belite contents in contrast with OPC clinker (detailed in Table 2.3). This allows for a lower limestone content of 30% as opposed to OPC clinker as CSC only requires 45% CaO compared to 70% in OPC (Wang, Guo and Ling, 2022). This reduces $CO_2$ emissions by 30%, while having comparable mechanical compressive strength to OPC at 24 hours (Gartner and Sui, 2018; Sahu and Meininger, 2019). Furthermore, another study suggested that CSC clinkers can achieve 31.7% $CO_2$ reductions when compared to OPC clinker (Antunes *et al.*, 2022). CSC distinctively requires kiln combustion temperatures of 1250 °C, ~17% less compared to OPC clinker (Sahu and Meininger, 2019). CSC clinkers can be produced in cement plants without cement process modifications as only the raw material inputs are changed (Antunes *et al.*, 2022). While HBC, BYF, and HFC clinkers develop strength through hydration in the

presence of water (Antunes *et al.*, 2022; Sabbah and Zhutovsky, 2022; Yang *et al.*, 2022), CSC gain strength through carbonation and is cured in a $CO_2$-rich atmosphere (Gartner and Sui, 2018; Scrivener, John and Gartner, 2018). During carbonation, the low-lime (i.e., wollastonite, rankinite) and amorphous phases react with $CO_2$ to form calcite ($CaCO_3$) and silica ($SiO_2$) (Ashraf, Olek and Sahu, 2019; Sahu and Meininger, 2019).

The utilisation of alternative clinkers not only provides lower $CO_2$ emissions but also less energy demand, thanks to its lower combustion temperatures and limestone content (see Table 2.3). Whilst some alternative clinkers such as MgO-based clinker (Gartner and Sui, 2018), and calcium sulfoaluminate (CSA) clinker (Lv *et al.*, 2021), has the potential to reduce the early or overall compressive strength of cement, others such as HFC (high ferrite clinker), BYF clinker (belite-ye'elimite-ferrite), and CSC (calcium silicate clinker) have demonstrated compressive strength comparable to Portland cement under certain conditions and mixes (Elakneswaran *et al.*, 2019; Sahu and Meininger, 2019; Zhang *et al.*, 2021; Yang *et al.*, 2022; Wang *et al.*, 2023), as explained in Chapter 5. However, the performance of alternative clinkers is context-dependent, and strength trade-offs could still be present. The costs of implementation are low as no process modifications are necessary, only the raw material composition changes. Overall, the use of alternative clinkers offers climate change mitigation benefits and increased energetic performance.

### 2.6.3. Supplementary cementitious materials (SCMs)

Supplementary cementitious materials (SCMs) play a similar role to alternative clinkers, in that they displace the use of conventional $CO_2$-intensive OPC clinker. SCMs are materials which are typically derived from other industrial processes and contain lower calcium content compared to OPC, where their use reduces $CO_2$ emissions, conserves non-renewable

resources, and diverts waste from landfills (Lothenbach, Scrivener and Hooton, 2011; Juenger and Siddique, 2015). Similar to cement, SCMs are inorganic materials that contribute to the hydration reactions through pozzolanic or hydraulic routes, enhancing the mechanical strength and durability (Juenger and Siddique, 2015; Duchesne, 2021). Common SCMs include industrial by-products such as coal fly ash, granulated blast furnace slag (GGBS), and silica fume (Lothenbach, Scrivener and Hooton, 2011; Juenger and Siddique, 2015; Kusuma *et al.*, 2022), which has been shown to significantly reduce carbon emissions in contrast with OPC (shown in Table 2.4).

Fly ash and GGBS typically exhibit lower early age compressive strengths compared to cement, however, exceeds the strength of OPC in the long term (Miller, 2018; Fode, Chande Jande and Kivevele, 2023). This behaviour is attributed to the slower pozzolanic reactions in fly ash and GGBS, resulting in reduced initial calcium silicate hydrate (C-S-H) formation relative to OPC. Nonetheless, long-term strength improvements occur as ongoing pozzolanic reactions produce additional C-S-H and increases in the products from the pozzolanic reactions are realised (Ramzi and Hajiloo, 2023). In addition, the fine pore structure of SCMs contributes to a filler effect which accelerates the reaction of the clinker phases by increasing the space available relative to the clinker content (Lothenbach, Scrivener and Hooton, 2011; Duchesne, 2021). The filler effect offers improved hydration kinetics of cement and increased durability (Juenger and Siddique, 2015).

In accordance with literature, fly ash and GGBS can offer cement replacements of up to 30% (Fode, Chande Jande and Kivevele, 2023), and 50% (Samad and Shah, 2017), respectively. Noteworthily, higher replacement levels may compromise the strength and durability (Snellings, Suraneni and Skibsted, 2023), largely due to the slower hydration kinetics relative to cement (Ramzi and Hajiloo, 2023). Studies have shown (Flower and Sanjayan,

2007; Yang *et al.*, 2015), the $CO_2$ reduction potential of fly ash and GGBS of 15% and 22%, at 25% and 40% replacement levels, respectively, when compared to OPC (Fode, Chande Jande and Kivevele, 2023). Despite these environmental benefits, the availability of fly ash is declining due to the gradual decommissioning of coal-fired power plants, while GGBS is constrained by its reliance on the steel industry (Juenger and Siddique, 2015; Samad and Shah, 2017; Fantilli and Jóźwiak-Niedźwiedzka, 2021; Fode, Chande Jande and Kivevele, 2023).

Additionally, silica fume (by-product of silicon and ferro-silicon alloy industries) (Hamada *et al.*, 2023), characterised by its fine particles and large surface area, refines the pore structure of concrete, resulting in a denser matrix that enhances both durability and compressive strength (Duchesne, 2021; Fode, Chande Jande and Kivevele, 2023). In terms of the decarbonisation potential, silica fume can substitute cement at 10 – 25%, allowing for mitigation of equivalent $CO_2$ emissions associated with cement production (Singh and Singh, 2024). In particular, the porosity of cement reduces when silica fume replacement levels are under 10% due to the pore size refinement of concrete and over 20% replacement leads to the silica fume decreasing the compressive strength of cement (Singh and Singh, 2024). Conversely, it is reported in literature that, silica fume demands more water for concrete due to their ultra fine particle size, therefore can compromise the cement's workability and induce shrinkage (Hamada *et al.*, 2023).

In accordance with a cradle-to-gate LCA study assessing the global warming potential (GWP) (Terán-Cuadrado *et al.*, 2024), the findings have shown that incorporating SCMs can reduce $CO_2$ emissions by ~37% (on a kg $CO_2$-eq/tonne cement basis), compared to OPC. Despite the $CO_2$ reductions realised, the availability of SCMs tends to be region specific and limited in supply compared to conventional cement (Benhelal *et al.*, 2013; Duchesne, 2021;

Snellings, Suraneni and Skibsted, 2023). Higher replacement levels of SCMs can also lead to extended setting times, disrupting construction schedules (Duchesne, 2021).

***Table 2.4. Carbon emission factor of SCMs from industrial by-products.*** *Where it represents the amount of $CO_2$ equivalent ($CO_2e$) emitted per kilogram of a given material, quantifying the environmental impact of producing 1 kg of the specific material (Lin, Lyu and Fang, 2025).*

| Material | Emission factor ($kgCO_2/kg$) |
|---|---|
| Ordinary Portland clinker | 0.735 |
| Fly ash | 0.010 |
| Ground granulated blast-furnace slag | 0.083 |
| Silica fume | 0.008 |

### 2.6.4. Alkali-activated materials (AAMs)

Alkali-activated materials (AAMs) can also serve as partial or complete replacements for traditional Portland cement. AAMs are inorganic binders formed at relatively low temperatures, typically between 25 – 100 °C (Faridmehr *et al.*, 2021), through activating aluminosilicates from industrial by-products, such as coal fly ash or blast furnace slag with highly alkaline solutions (i.e., hydroxides or silicates, or carbonates) (Ding, Dai and Shi, 2016; Mendes *et al.*, 2021; Pol Segura *et al.*, 2023; Ślosarczyk *et al.*, 2023). During this activation process, silicon and aluminium dissolve and re-polymerise into C-A-S-H gel (in high calcium systems) or N-A-S-H gel (in low calcium systems) in the presence of alkaline. These gels, when mixed with aggregates, form alkali-activated concrete without the need for conventional combustion (García-Lodeiro, Fernández-Jiménez and Palomo, 2013; Pol Segura *et al.*, 2023).

According to (Pol Segura *et al.*, 2023), AAMs through calcined clays, and industrial by-products (i.e., fly ash and GGBS) can lower emissions by up to 68% and 75%, respectively (Pol Segura *et al.*, 2023). LCAs further show that fly ash based AAMs produced less $CO_2$ (45.5 kg $CO_2/m^3$) compared to GGBS based AAMs (70.6 kg $CO_2/m^3$) (Faridmehr *et al.*, 2021), both significantly lower than OPC (436.8 kg $CO_2/m^3$). $CO_2$ reductions of using alkali activated cements, ranging from 50 – 80% compared to OPC (Ding, Dai and Shi, 2016; Ślosarczyk *et al.*, 2023), are particularly attributed to the exclusion of limestone calcination and kiln combustion (Pol Segura *et al.*, 2023).

Moreover, AAMs offer high early strength and improved durability, including resistance to sulfate attack (Faridmehr *et al.*, 2021). However, at elevated temperatures, alternative binders in mortar and concrete may experience strength loss caused by thermal incompatibility between the binder and aggregates (Ding, Dai and Shi, 2016; Faridmehr *et al.*, 2021; Song, Guo and Ling, 2022; Pol Segura *et al.*, 2023). Despite their environmental benefits, the widespread adoption of AAMs faces challenges, particularly from the limited availability of industrial by-products such as fly ash and slag (Pol Segura *et al.*, 2023). Additionally, the cost of producing AACs using coal fly ash or GGBS is about 1.9 – 2.15 times higher than OPC (Pol Segura *et al.*, 2023).

### 2.6.5. $CO_2$ mineralisation

$CO_2$ mineralisation is a process that involves storing $CO_2$ in solid forms of calcium and magnesium carbonates, which are thermodynamically stable under atmospheric conditions, thus providing a permanent solution for $CO_2$ storage (Ostovari *et al.*, 2021; Zajac *et al.*, 2022), from their exothermic reaction (Strunge, Renforth and der Spek, 2022). $CO_2$ from cement flue gases is stored through CCUS technologies (including amine-based) and

directly used for $CO_2$ sequestration (see Figure 2.8). This sequestration process involves $CO_2$ reacting with calcium or magnesium that exists in the forms of silicate minerals such as olivine ($(Mg,Fe)_2SiO_4$), wollastonite ($CaSiO_3$), and serpentine ($Mg_3Si_2O_5(OH)_4$) (Zajac *et al.*, 2022). The sizing classification centrifuge in the $CO_2$ mineralisation separates the silica ($SiO_2$) (0-1 μm) from magnesium carbonate ($MgCO_3$) (1-5 μm) based on the particle size. More specifically, parametric studies conducted using Aspen Plus were employed to determine the appropriate particle sizes for various throughputs, utilising a disc centrifuge (Strunge, Renforth and der Spek, 2022).

$CO_2$ mineralisation involves two methods, in situ and ex situ, where in situ involves the use of geological formation for permanent storage of solids, and ex situ converts $CO_2$ to carbonates (Zajac *et al.*, 2022). The cement production process is accountable for process emissions surpassing 2.2 Gt $CO_2$ annually (Ostovari *et al.*, 2021), making it ideal for $CO_2$ mineralisation while promoting circular economy. Natural silicate rocks, such as those mentioned above, are ideal feedstocks for $CO_2$ mineralisation due to their abundancy and stable composition (Strunge, Renforth and der Spek, 2022).

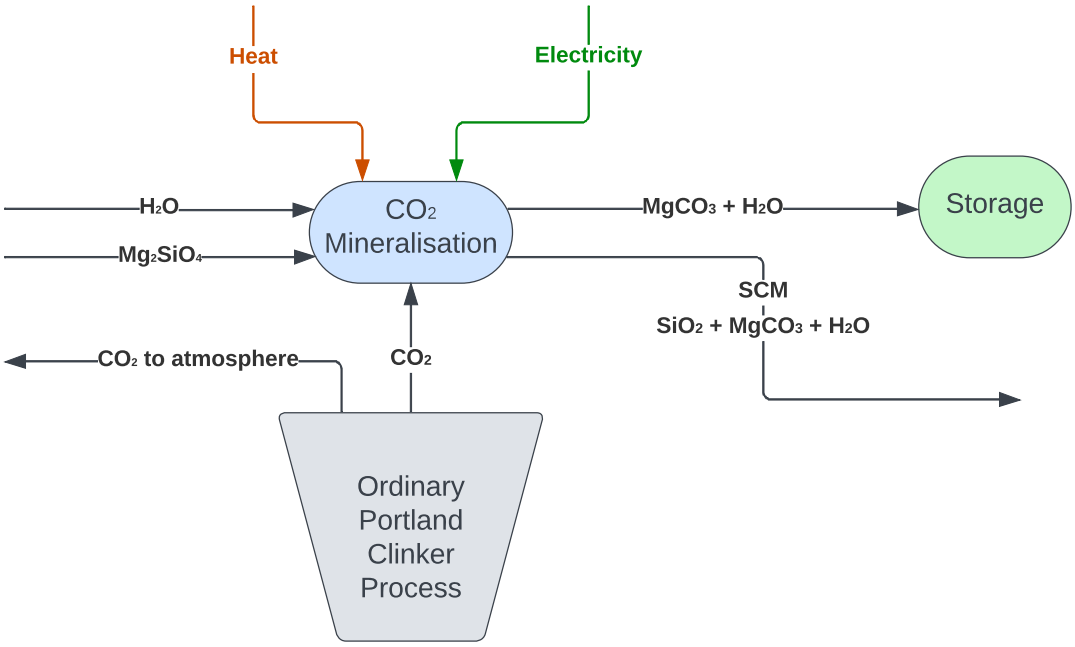


***Figure 2.8. $CO_2$ mineralisation process flow diagram (PFD).*** *The inputs (including $CO_2$ from cement flue gases, carbonates, water, and energy) and outputs (including carbonates to storage and SCM) are presented as per (Strunge, Renforth and der Spek, 2022).*

It was shown by (Strunge, Renforth and der Spek, 2022), that 25% of cement can be replaced with SCMs without compromising the performance, such as the mechanical strength and curing time. In particular, a study by (Ostovari *et al.*, 2021), clarified that $CO_2$ mineralisation could reduce the cement industry's carbon footprint by 44% with higher substitution of clinker with mineralisation products, with the potential to capture 90% of GHG emissions from the cement plant (Ostovari *et al.*, 2021). Distinctively, work by (Strunge, Renforth and der Spek, 2022), demonstrated $CO_2$ emission reductions of up to 33% from $CO_2$ mineralisation of silicate minerals to store $CO_2$. A modelling study by (Bremen *et al.*, 2022), presented GHG emissions reduction of up to 54% with the optimisation of a direct mineral carbonation process. Therefore, producing SCM via $CO_2$ mineralisation and partially replacing clinker with SCM provides both reduction of $CO_2$ process emissions from clinker production whilst reducing the limestone input to the calcination stage (Ostovari *et al.*, 2021), a step closer to greening the cement industry. Although $CO_2$ mineralisation is not yet

widely applied in the cement industry (Zajac *et al.*, 2022), because the process is not yet reaching maturity (Strunge, Renforth and der Spek, 2022), the implementation of successful pilot projects and emission trading system (ETS) credits would incentivise cement companies to gradually adopt $CO_2$ mineralisation. Conversely, $CO_2$ mineralisation also generates additional profits of 37 USD/t cement produced from the utilisation of $CO_2$ mineralisation products as SCMs and the applicability to quality for carbon credits and incentives (Strunge, Renforth and der Spek, 2022).

## 2.7. Process modelling

Process modelling offers a simulation of the cement production process, to determine the combustion air requirements, overall energy demand (Kääntee *et al.*, 2004), and $CO_2$ produced based on the feed requirements (Kaddatz, Rasul and Rahman, 2013). This modelling approach can be used for process optimisation and impact analysis (Kääntee *et al.*, 2004; Hökfors, Eriksson and Viggh, 2014), along with determining the impacts of fuel switching without the need for full-scale trials in the cement plant (Kääntee *et al.*, 2004; Sharma, Sheth and Sen, 2023). Process models can articulate the physical and chemical reactions taking place during combustion in the calciner or kiln. It can also be used to analyse the material and energy flows, including the emissions from the flue gas constituents (Zhang *et al.*, 2011; John, 2020; Nhuchhen, Sit and Layzell, 2022a).

Although distinctive software's exist for process modelling including, Aspen Plus (Zhang *et al.*, 2011; John, 2020; Nhuchhen, Sit and Layzell, 2022a), Microsoft Excel (Kaddatz, Rasul and Rahman, 2013), and computational fluid dynamics (CFD) (Mikulčić *et al.*, 2012; Chandra Kahawalage, Melaaen and Tokheim, 2017), the most prominently used amongst

studies is Aspen Plus (Kääntee *et al.*, 2004). Aspen Plus is generally used for process modelling as it contains a diverse range of property databases from physical parameters to combustion products while offering flexible unit operation modules (Zhang *et al.*, 2011). It can visually present the flow of each process stage, enabling easy modifications without requiring a new model (Kaddatz, Rasul and Rahman, 2013; John, 2020). In particular, Aspen Plus allows for the simulation of chemical reactions across solid, liquid, and vapour phases, whilst allowing for an integrated modelling of solids and fluids within a single process (John, 2020).

On the other hand, CFD thermodynamic modelling is limited to the models available in the simulators and simulations are limited by the calculation of the physical properties. CFD alone is not sufficient for comprehensive process simulation, unlike Aspen Plus (Vaquerizo and Cocero, 2018). Notably, an Excel-based model is limited to input-output analysis and cannot factor in changes to the chemical reactions, compositions, and thermal properties (Kaddatz, Rasul and Rahman, 2013). It is important to note that, in process simulations, the produced product is ~2% higher compared to operational data as the entrainment of particles during the gas phase is not considered in the simulations. In addition, the amount of leakage air maybe underestimated in the simulations in contrast with operational data (Hökfors, Eriksson and Viggh, 2014). However, these minor deviations are not expected to impact the results.

## 2.8. Research gaps

The shift towards greener cement production is becoming more popular, driven by the increasing climate change impacts and market demands. Alternative fuels such as biomass,

MBM, TDF, SS, and RDF do not achieve carbon neutrality upon combustion, whereas $H_2$ offers carbon free combustion with higher calorific value and lower moisture content, positioning it as a cleaner and more efficient alternative fuel option. Despite industrial trials and use of $H_2$ in research, there exists a gap in a systematic comparison of different $H_2$ schemes coupled with oxy-combustion. This involves the performance impacts (including $CO_2$) of varying $H_2$ fuel replacement, integrated with the facilitation of $CO_2$ separation and capture. Whilst previous research has explored indirect calcination with fossil fuels (Ozcan, Brandani and Ahn, 2014) to reduce oxygen demand and enable combustion separately from limestone decomposition (ensuring higher $CO_2$ concentration for capture), utilisation of its application with $H_2$ has not been studied. Moreover, process simulations of energetic performances among distinct fuel substitution options, centred around $H_2$, with $CO_2$ capture is yet to be carried out, which this thesis seeks to address in Chapter 3.

Prior studies have investigated solar calcination separately through CSP (Moumin *et al.*, 2020), and kiln electrification through distinct methods (Quevedo Parra and Romano, 2023), with plasma gas as the most prominent to achieve high combustion temperatures (Nozaki, Kim and Chen, 2024). However, their integration has not yet been explored, calling for a more complete assessment of the energy and $CO_2$ performance of a combined solar driven system comprising both solar calcination and kiln electrification. Despite techno-economic analyses in literature concerning the $CO_2$ avoidance costs and solar calciner costs (Moumin *et al.*, 2020; Sahoo, Kumar and Samsher, 2023), along with cost analysis for the electrified kiln subsystem (Quevedo Parra and Romano, 2023), there been no studies, according to the author's knowledge, developing optimisation models that account for the details of variable solar energy availability, specifically, optimisation models across distinct countries, aiming

to minimise the total solar driven process costs (including solar calciner and electrified kiln) through the use of solar energy. These gaps are addressed in Chapter 4 of this thesis.

Although SCMs and AAMs from industrial by-products have demonstrated potential in reducing $CO_2$ emissions by substituting cement, they do not address emissions generated during the calcination of limestone, which accounts for a substantial portion of emissions from cement production. In contrast, alternative clinkers (including BYFC, HFC, and CSC) offer promising climate reduction benefits from the reduction of calcination induced $CO_2$ emissions, to the author's knowledge, their comparative $CO_2$ and energetic performances are yet to be systematically assessed through process simulation modelling. This noteworthy research gap underscores the necessity to implement consistent modelling simulations to provide a comparative evaluation of alternative clinkers in contrast with OPC. It is worth mentioning that, the projected carbon reduction benefits of $CO_2$ mineralisation open a pathway for research towards the use of SCMs through mineralisation of carbonates integrated with alternative clinkers. Although literature has suggested that reduced limestone use and lowered sintering temperatures (Antunes *et al.*, 2022), enabled $CO_2$ reductions, other $CO_2$ and energetic reduction factors are yet to be explored, motivating this thesis to fill in these gaps throughout Chapter 5.

# Chapter 3. Decarbonisation pathways of the cement production process via hydrogen and oxy-combustion

## Summary

This chapter features the subsequent published manuscript which was edited to include further clarifications: Williams, F., Yang, A., Nhuchhen, DR. (2024). Decarbonisation pathways of the cement production process via hydrogen and oxy-combustion. *Energy Conversion and Management, 300, 117931.* https://doi.org/10.1016/j.enconman.2023.117931. The corresponding Supplementary Information can be found in Appendix A.

Among the authors who contributed to this chapter, Franco Williams conceptualised the study involving the methodology, developed the models, analysed the results, and wrote the manuscript; Aidong Yang supported with the conceptualisation, supervision, provided feedback on the modelling, and revised the manuscript; Daya Ram Nhuchhen validated the results and revised the manuscript.

The first original work chapter evaluates various technical options for achieving deep decarbonisation in a clinker production process by utilising hydrogen ($H_2$) as an alternative fuel to replace fossil fuels and by integrating an oxy-combustion technique with carbon capture and storage (CCS). Using Aspen Plus process simulations, we examined the extent of decarbonisation and assessed the thermal and electrical energy demands. This was

achieved by incorporating an amine-absorption-based $CO_2$ capture to a conventional natural gas fuelled reference plant, implementing oxyfuel-combustion of natural gas, and exploring four different scenarios for replacing fossil fuel with $H_2$. The processes utilising $H_2$, except for the case of indirectly heated pre-calcination, employed oxyfuel combustion. The results indicated that the natural gas-fuelled oxyfuel-combustion process had the lowest total energy input at 4.92 GJ/t clinker, approximately 35% lower than that of the reference plant. Processes using $H_2$ reduced energy demand by 11 – 33%, depending on the substitution percentage. The process with indirect calcination required 6.24 GJ/t clinker, about 8% more $H_2$ fuel than direct calcination but helped eliminate the need for an air separation unit (ASU). The results also reveal that greater $H_2$ substitution led to higher total process energy requirements due to the inefficiencies of the electrolysis process. While the $H_2$-using processes could reduce the $CO_2$ generation by up to 559 $kgCO_2$/t clinker, this represents only about 27.6% of the $CO_2$ reductions relative to the reference plant. These findings underscore the limitation of $H_2$ fuel substitution alone in cement production and emphasises the need for the adoption of other renewable alternative fuels based on solar energy and implementation of alternative clinkers to target calcination induced $CO_2$ emissions.

## 3.1. Introduction

Tackling climate change requires the rapid reduction of greenhouse gas (GHG) emissions from all sectors of the global economy. The construction sector faces significant challenges, as it is projected to consume 35 – 60% of the remaining carbon budgets for the 2 °C scenario over the decades leading to 2050. This projection is driven by anticipated population growth and socioeconomic progress (Churkina *et al.*, 2020). Cement production, which is responsible

for about 8% of global carbon dioxide ($CO_2$) emissions (El-Emam and Gabriel, 2021), has widely been identified as a primary target for progressive decarbonisation efforts.

In the conventional cement production process, $CO_2$ emissions primarily result from the production of clinker, the main component of Portland cement (Nhuchhen, Sit and Layzell, 2021). Specifically, two main sources of $CO_2$ emissions exist: (1) process emissions from the calcination process, where limestone ($CaCO_3$), a key component in the raw meal for clinker production, decomposes into lime (CaO) and $CO_2$, and (2) energy emissions from the combustion of fossil fuels (mainly coal or natural gas) to provide the required thermal energy for both the calciner and the kiln, where calcining and sintering reactions occur. Extensive research has explored ways to reduce $CO_2$ emissions from calcination by replacing clinker with supplementary cementitious materials (Pamenter and Myers, 2021), like fly ash (Bouaissi *et al.*, 2020), and ground granulated blast furnace slag (GGBS) (Velpuri, Jyothishya and Vinod, 2021), which do not involve limestone decomposition (Teixeira *et al.*, 2016).

Regarding energy consumption, the cement industry's substantial demand, averaging approximately 4 GJ per tonne of cement (Khurana, Banerjee and Gaitonde, 2002), contributes to 12 – 15% of total global industrial energy consumption (Nie *et al.*, 2022), primarily from fossil fuels. Various strategies have been proposed to reduce GHG emissions and energy consumption (Chatterjee and Sui, 2019), including improvements in fuel efficiency (Rahman *et al.*, 2017), such as heat recovery from flue gases using the Organic Rankine Cycle (ORC) (Sanaye *et al.*, 2020), and the use of alternative fuels such as biomass (Pamenter and Myers, 2021), and hydrogen ($H_2$) (Juangsa *et al.*, 2022). An ORC captures the waste heat from the hot flue gases from the clinker production process and generates electricity to support the process (Nhuchhen, Sit and Layzell, 2022a), using an organic

working fluid with a low boiling temperature. This reduces the heat loss and effectively increases the energy efficiency of the clinker production process (Moreira and Arrieta, 2019). Conversely, alternative fuels have different physical and chemical properties, where the selection of alternative fuels that have minimal impacts on combustion phenomena and the overall cement production process is critical (Benhelal, Shamsaei and Rashid, 2021).

To address unavoidable emissions from calcination or fuel combustion, carbon capture and storage (CCS) become essential (Faria *et al.*, 2022). Oxyfuel combustion (Ying *et al.*, 2018), where combustion is with pure oxygen instead of air (Nhuchhen, Sit and Layzell, 2022a), has been considered a favourable approach for CCS, preventing the mixing of nitrogen with $CO_2$ from calcination or fuel combustion (Ditaranto and Bakken, 2019).

In line with other industrial sectors emphasising the decarbonisation of the thermal energy supply (El-Emam and Gabriel, 2021), the use of $H_2$ as a zero-carbon fuel in cement production has gained significant interest from both academia (Khadka, 2021), and industry (Association and Ltd, 2019). A modelling study by the Mineral Products Association (Association and Ltd, 2019), evaluated the reduction in coal consumption in the kiln by replacing thermal energy demand with 20% $H_2$, 70% biomass, and 10% plasma energy, resulting in the elimination of 100% fossil $CO_2$ emissions. Another study (Juangsa *et al.*, 2022), achieved a 44% reduction in $CO_2$ emissions for the total system by entirely replacing coal-based fuel with $H_2$ in the kiln. Furthermore, research conducted by (El-Emam and Gabriel, 2021), utilised $H_2$ from alkaline electrolysis to obtain natural-gas-enriched hydrogen (10% $H_2$ in volume) in the kiln, replacing 50% of coal by weight and estimating a 15% to 20% reduction in $CO_2$ emissions compared to pure coal-based cement production. In the industry, Hanson conducted trials at a cement plant using a mixture of 20% $H_2$ in volume mixed with biomass and plasma energy at Ribblesdale Cement Works, aiming to

supply net zero carbon concrete by 2050. The results indicated that if this mixture were applied in the kiln, approximately 180,000 tonnes of $CO_2$ could be saved annually (Hanson, 2022).

Despite these emerging explorations, research on the use of $H_2$ in cement production is currently limited, and there is a lack of systematic comparisons of possible $H_2$-based technical schemes and other decarbonisation options. In this work, we present technical modelling of six process options, distinguished by fuel, oxygen combustion supply, and $CO_2$ capture arrangement, for clinker production. We then assess and compare their energy consumption and $CO_2$ production. To our knowledge, this is the first study to compare process options with different levels of $H_2$ substitution for natural gas in oxyfuel combustion (which facilitates $CO_2$ separation and capture) with the conventional process equipped with amine-based (post-combustion) carbon capture and oxyfuel combustion. Previous studies have considered the use of oxygen as a by-product of water electrolysis (Nhuchhen, Sit and Layzell, 2022a), as a potentially advantageous alternative to an energy-intensive air separation unit (ASU) for supplying oxygen to cement production (Faria *et al.*, 2022). In our study, on-site water electrolysis was assumed to supply both $H_2$ and $O_2$ for feeding the oxyfuel combustors. To reduce the demand for oxygen, one of the novel process options includes indirect calcination, where combustion for heat supply occurs separately from the decomposition of limestone. This separation keeps combustion products separate from the $CO_2$ produced by calcination, ensuring high $CO_2$ purity in the captured $CO_2$ stream. While previous research has explored indirect calcination in connection with fossil fuels (Ozcan, Brandani and Ahn, 2014), our study investigates its application with $H_2$. Overall, the results of this work provide a consistent comparison of the energy consumption and $CO_2$ production

among the selected process options, serving as a foundation for future techno-economic assessments.

## 3.2. Methods

In this section, we first provide a brief overview of the technical options for clinker production assessed in this work (Section 3.2.1), followed by a detailed description of the modelling of these options as implemented in Aspen Plus (Section 3.2.2 – Section 3.2.5). Subsequently, the approach to modelling $CO_2$ separation and compression associated with the clinker production processes (Section 3.2.6) and quantifying energy consumption (Section 3.2.7) are presented, along with the key assumptions adopted in modelling and analysis (Section 3.2.8).

### 3.2.1. Overview of technical options

This work involves the technical modelling of six process options for clinker production, which were differentiated based on fuel use, combustion oxygen ($O_2$) supply, and $CO_2$ capture arrangements. Table 3.1 provides an overview of the characteristics of these compared processes. Concerning the extent of $H_2$ substitution, it is worth noting that there are significant differences in combustion characteristics between $H_2$ and conventional fuels, which has raised caution about extensive $H_2$ usage in clinker production (Juangsa *et al.*, 2022), particularly in the kiln (El-Emam and Gabriel, 2021). However, there is limited experimental evidence available to determine the feasible range. Among the process options involving $H_2$, three processes ($H_2$-a, $H_2$-b, and $H_2$-c) reduced the natural gas usage in the kiln to a conservative 80% (by vol.) of the oxyfuel process, with the remaining thermal

energy met by the supplementary $H_2$. In contrast, $H_2$-d represents a hypothetical scenario exploring the potential outcome of complete $H_2$ substitution. In terms of the calciner, the process $H_2$-a did not incorporate $H_2$ substitution, while the other three $H_2$ processes assumed the use of 100% $H_2$, a configuration that had previously been examined through theoretical modelling of calcination as a standalone process (i.e., not as part of clinker production) (Khadka, 2021).

***Table 3.1. Process parameters adopted in Aspen simulation.*** *The selected cases represent a progressive transition from conventional natural gas combustion to hydrogen and oxygen combustion systems. The studied cases involve fuel substitution, oxygen combustion, and $CO_2$ capture configurations, identifying their $CO_2$ and energetic impacts in clinker production, under consistent conditions.*

| **Process Options** | **Combustion** | | **Oxygen supply** | **Calcination Mode** | **$CO_2$ capture** |
|---|---|---|---|---|---|
| | **Calciner** | **Kiln** | | | |
| NG (reference case) | Fuel mix = Natural gas, Combustion agent = Air | Fuel mix = Natural gas, Combustion agent = Air | N/A | Direct | Amine-based capture + compression |
| Oxy | Fuel mix = Natural gas, Combustion agent = Pure oxygen | Fuel mix = Natural gas, Combustion agent = Pure oxygen | Air separation unit | Direct | Compression, cooling, and separation (with refrigeration for water separation) |
| $H_2$-a | Fuel mix = Natural gas, Combustion agent = Pure oxygen | Fuel mix = 80% Natural gas + 20% hydrogen, Combustion agent = Pure oxygen | Air separation unit + electrolysis | Direct | |
| $H_2$-b | Fuel mix = hydrogen, Combustion agent = Air | Fuel mix = 80% Natural gas + 20% hydrogen, Combustion agent = Pure oxygen | Electrolysis | Indirect | |
| $H_2$-c | Fuel mix = hydrogen, Combustion agent = Pure oxygen | Fuel mix = 80% Natural gas + 20% hydrogen, Combustion agent = Pure oxygen | Air separation unit + electrolysis | Direct | |
| $H_2$-d | Fuel mix = hydrogen, Combustion agent = Pure oxygen | Fuel mix = hydrogen , Combustion agent = Pure oxygen | Electrolysis | Direct | |

### 3.2.2. Modelling of clinker production processes

The mathematical modelling in this study was based on literature data, primarily sourced from a plant in Alberta, Canada, which produces 4,200 tonnes of clinker in a day (Nhuchhen, Sit and Layzell, 2022a). As shown in Figure 3.1, the process involves preheating the raw meal to 800 °C (in the pre-heater) using the calciner exhaust gas before it enters the calciner, where limestone decomposition occurs at 900 °C, achieving 95% calcination (Vikström, 2021). The solid output from the calciner then enters the kiln, where further decomposition, transition and sintering reactions take place (Faria *et al.*, 2022), reaching a sintering temperature of 1500 °C (Nhuchhen, Sit and Layzell, 2022a). While the resulting clinker from the kiln is cooled to approximately 100 °C by cooling air (in the cooler), the exhaust gas from the kiln is fed into the calciner. Both the cooling air and the preheater exhaust gas undergo heat recovery processes by the ORC. The specific configuration of this heat recovery system varies depending on the chosen process and must provide a hot gas flow of 1,762 kg/tonne clinker at 176.85 °C to operate the vertical roller mill (VRM) (Ghalandari *et al.*, 2021).

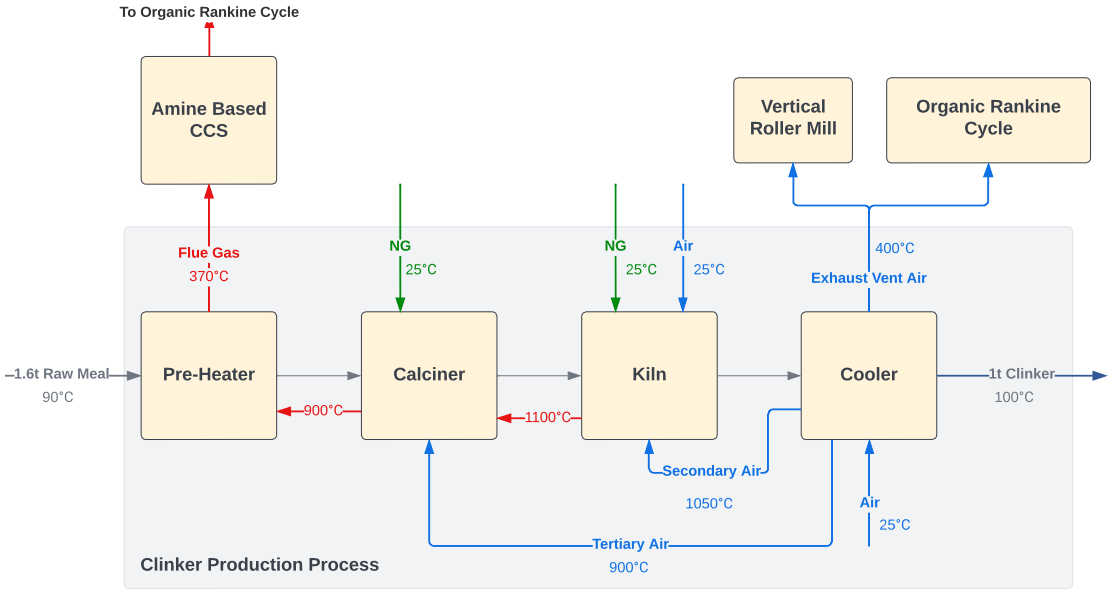


***Figure 3.1. NG cement production process flow diagram*** *(natural-gas reference case), adopting amine-based carbon capture (See Figure A.1 for Aspen Flowsheet).*

All six process options (Figures 3.1 – 3.6) were simulated (refer to Appendix Figure A.1 – A6 for the detailed Aspen models) with an input of 1.6 tonnes/hr of raw meal and a clinker output of 1 tonne/hr. Linear scaling of the process performance was adopted on a per tonne of clinker basis, consistent with the Aspen simulation approach used, where the key chemical reactions were modelled with fixed conversion ratios independent of scale. This modelling approach and linear scaling adoption is in line with other studies (Nhuchhen, Sit and Layzell, 2022a). Nevertheless, this approach simplifies the real-world process as conversion rates may vary with scale; this complexity has not been considered in this work. The energy or $CO_2$ performance is not impacted as it provides a consistent, "per tonne" reference point. It is important to note that all produced $CO_2$ was captured in its pure form at 150 bar with 100% capture efficiency, preparing it for subsequent transport and storage. $CO_2$ transport and storage after capture was not modelled as transport and storage steps are outside cement production sites and not relevant to the on-site comparisons among different fuel-substitution approaches. It is worth noting that, in real-world cement plants, $CO_2$ transport,

and storage requirements could influence the overall $CO_2$ savings and energy performance, which is beyond the scope of the current study.

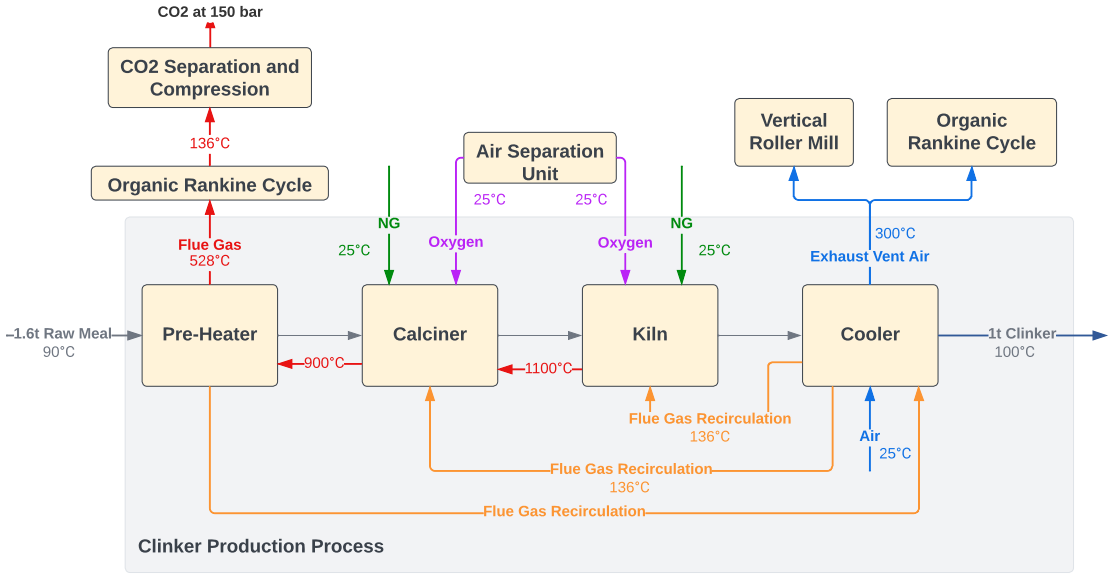


***Figure 3.2. Oxy cement production processes flow diagram*** *(oxyfuel-combustion based), with $CO_2$ separation and compression (See Figure A.2 for Aspen Flowsheet).*

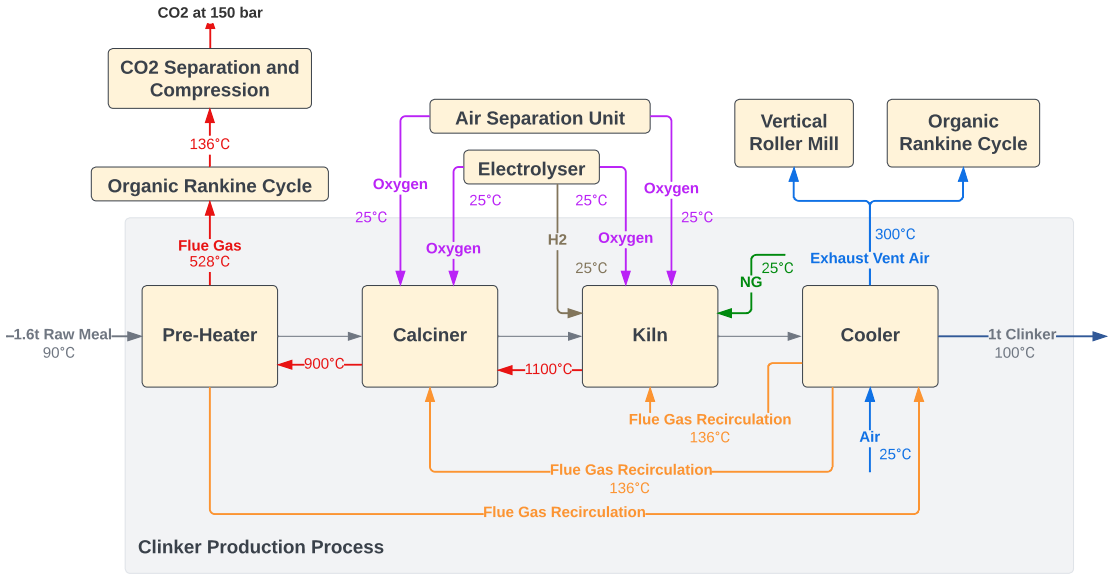


***Figure 3.3. $H_2$-a cement production process flow diagram*** *(20% hydrogen replacement of natural-gas in the kiln coupled with oxygen combustion) with $CO_2$ separation and compression, (See Figure A.3 for Aspen Flowsheet).*

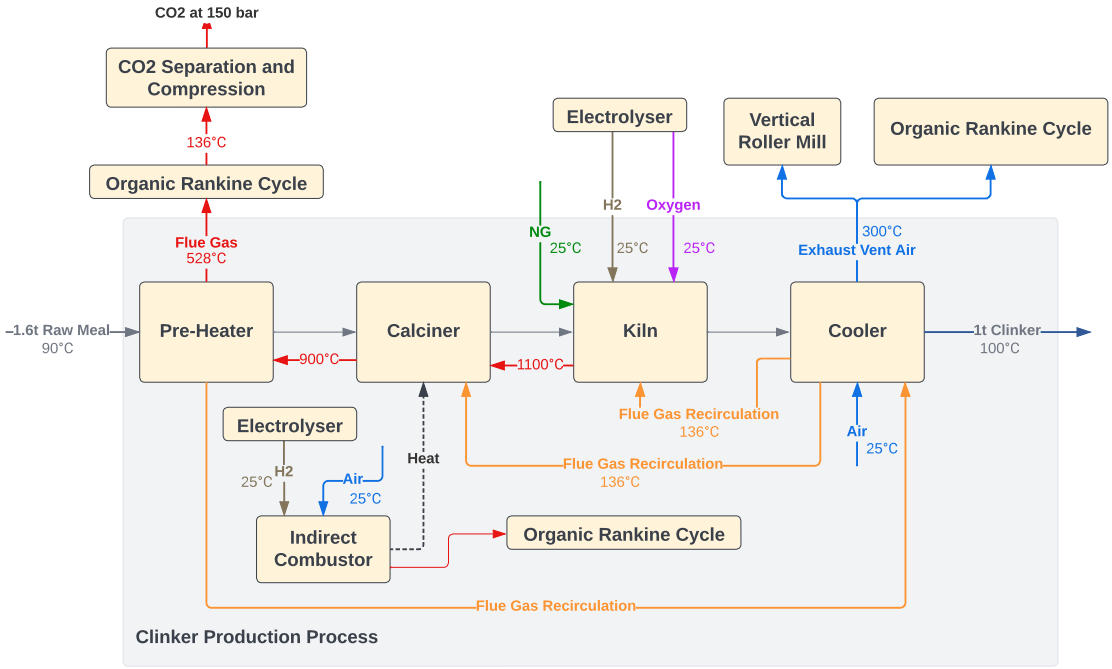


***Figure 3.4. $H_2$-b cement production process flow diagram*** *(indirect calcination using hydrogen for the calciner and direct combustion of hydrogen in the kiln), with $CO_2$ separation and compression (See Figure A.4 for Aspen Flowsheet).*

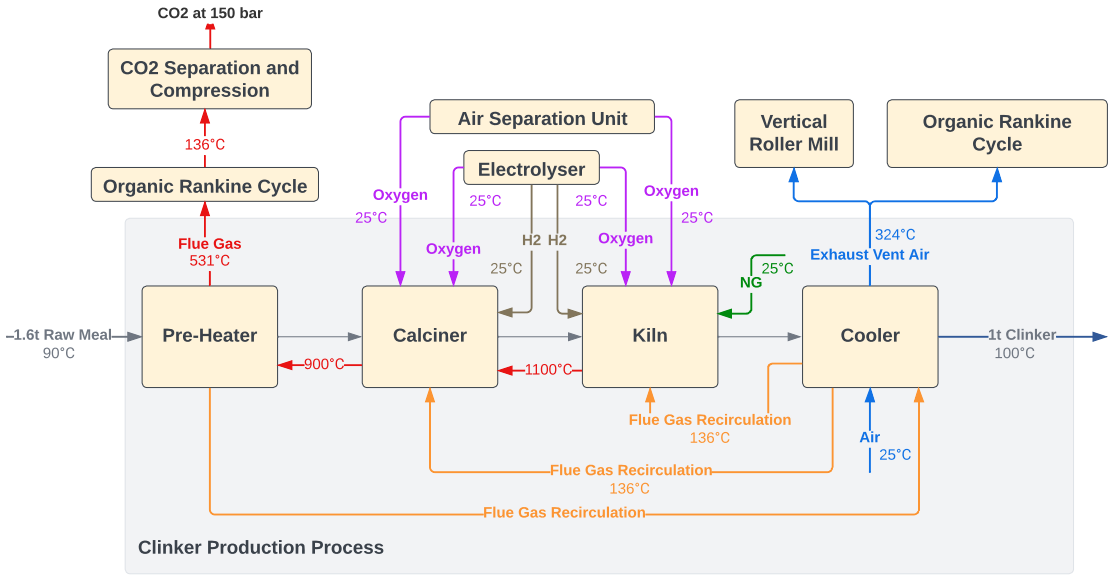


***Figure 3.5. $H_2$-c cement production process flow diagram*** *(20% natural-gas replaced with hydrogen in the kiln), with $CO_2$ separation and compression (See Figure A.5 for Aspen Flowsheet).*

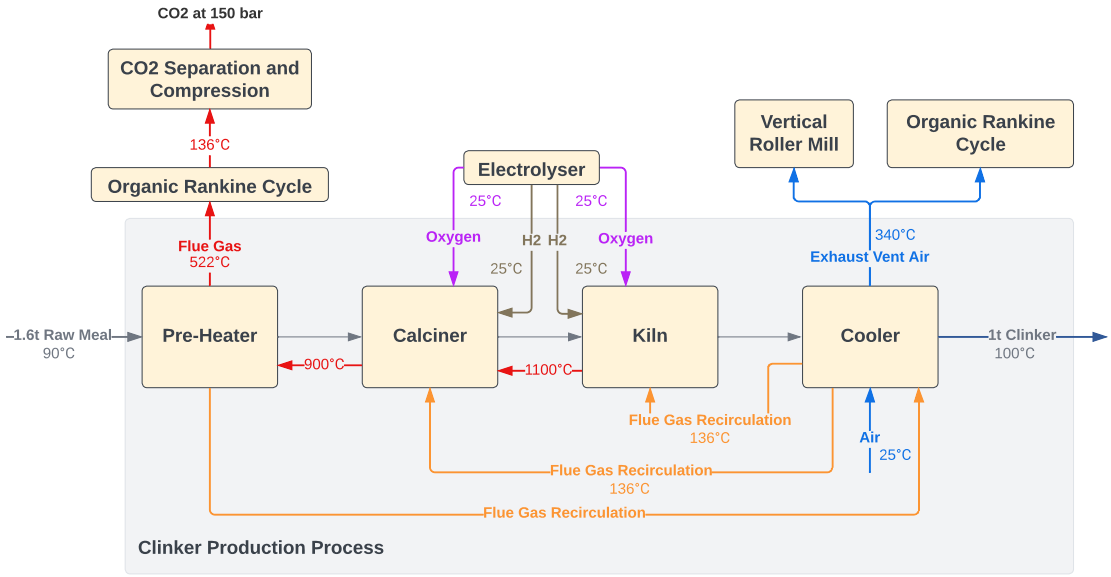


***Figure 3.6. $H_2$-d cement production process flow diagram*** *(100% hydrogen replacement of natural-gas and combustion with oxygen), with $CO_2$ separation and compression (See Figure A.6 for Aspen Flowsheet).*

Aspen Plus was identified as the most suitable tool for modelling and simulating the clinker production process. Its flow sheet simulation provides a graphical representation of each clinker production stage from raw meal pre-heating and calcination to sintering and cooling, allowing for modifications to be made without the need to develop new models for each change (John, 2020). Additionally, the software features a diverse databank and the capacity to simulate chemical reactions in solid, liquid, and vapour phases (Technology, 2001), suitable for determining the clinker chemistry, thermodynamics, material and energy balances and reaction stoichiometries. Moreover, Aspen Plus provides accurate simulations of the clinker chemistry, material and energy balances, and reaction stoichiometries (Technology, 2001). In addition, its reliability has been established through adoption in similar cement process studies as per (Nhuchhen, Sit and Layzell, 2022a), and (Faria *et al.*, 2022). Model verification was achieved through comparing simulated values of the reference cases, such as fuel consumption, key temperatures, and $CO_2$ with literature and plant benchmarks, confirming consistency within acceptable ranges.

The SOLIDS property method in Aspen Plus was selected for the clinker production process simulation, to provide relevant correlations (such as heat capacity, enthalpy, Gibbs energy), and model the high-temperature solid-phase interactions in the process. To account for the thermodynamic requirements of the phase streams, the sub-stream type of CISOLID was adopted for solid components (such as raw meal and clinker minerals). For conventional gas components (such as gas streams and air) or components containing a mixture of solids with either liquid or gas the sub-stream type of MIXED was adapted. This ensures that the phase contributions to the overall heat and mass balance are modelled accurately.

The fundamental principles and methodology underpinning Aspen modelling calculations are presented as follows where the unit operations are presented in Table 3.2 and equations in Table 3.3 and Table 3.4, respectively:

1) **Property methods** set to determine the thermodynamic properties of the components (including solid and conventional components) in different streams accounting for phase behaviour, heat capacities, and other crucial properties of components.
2) **Mass and energy balances** modelled in every unit module (see Table 3.2) to represent specific stages in the clinker production process (pre-heating, calcination, kiln, and cooling) through conservation of material and energy ensuring the simulated flows and energy requirements reflect the behaviour of an actual process.
3) **Chemical reactions** in the combustors (calciner and kiln) for fuel combustion, $CaCO_3$ decomposition and formation of clinker mineral components are simulated through stoichiometric reactor units (see Table 3.2).
4) **Temperature fluctuations** of streams are simulated through heat exchange units (see Table 3.2).

5) **Integration of process modules** with ORC and $CO_2$ capture to determine the overall energy consumption and $CO_2$ production.

Specific details of Aspen modelling for each process are further discussed in Sections 3.2.3, 3.2.4, 3.2.5, and 3.2.6.

***Table 3.2. Aspen Plus unit operation models*** *and their respective functions (Technology, 2001).*

| **Aspen Plus unit operation model** | **Function** |
|---|---|
| RStoic | Stoichiometric reactors are used to simulate reactions defined by stoichiometry and conversion, notably, the reactions of calcination (decomposition of $CaCO_3$), $CH_4$ combustion, and reaction of formation of clinker mineral components (i.e., alite, belite, ferrite and aluminate) in three kiln stages (including decomposition, transition, and sintering). |
| Heater | Heat exchange unit is employed to increase or decrease the temperature of a specific stream (including the pre-heating of raw materials, clinker cooling, simulation of an ORC and carbon capture). |
| FSplit | A splitter is used to divide a single feed stream into multiple streams to route a fraction of a process stream different units and recover excess heat through an ORC. |
| Flash2 | A flash separation unit splits a feed stream into vapor and liquid phases, notably, to separate the $H_2O$ from $CO_2$ in the compression and separation of $CO_2$. |
| Compr | Compressor unit is utilised to raise the pressure of a specific stream in the compression and separation of $CO_2$. |

***Table 3.3. Aspen Plus equations for pure components**, respective abbreviations and their purposes (Technology, 2001).*

| Equation | Aspen Abbreviation | Purpose |
|---|---|---|
| Solid heat capacity polynomial | CPSP01 | Temperature-dependent heat capacity which calculates the energy requirements for processes involving solids (enthalpy, entropy, and Gibbs energy of solids). |
| Watson heat of vaporisation | DHVLWT | Determines a substance's heat of vaporisation at a specific temperature. |
| Liquid thermal conductivity | KLDIP | Measures the ability of a material to conduct heat. |
| Andrade liquid viscosity | MULAND | Determines the relationship between viscosity of liquids and its absolute temperature. |
| Surface Tension | SIGDIP | Determines the liquid surface tension. |
| Polynomial for solids | VSPOLY | Calculate the solid molar volume. |

***Table 3.4. Aspen Plus equations for binary interactions**, respective abbreviations and their purposes (Technology, 2001).*

| Equation | Aspen Abbreviation | Purpose |
|---|---|---|
| Andrade liquid mixture viscosity | ANDKIJ/ANDMIJ | Describes the relationship between a liquid's viscosity and its temperature. |
| Viscosity Quadratic Mixing Rule | MLQKIJ | Calculates the mixture viscosity from the pure component viscosities. |
| Henry's Law | HENRY-1 | Represents the behaviour of dissolved gases or other components in a mixture. |

### 3.2.3. Reference (NG) process for clinker production

In the reference process (NG) depicted in Figure 3.1 and with its Aspen flowsheet presented in Figure A.1, natural gas combustion in the presence of air was used to supply thermal energy for clinker production (NG-C and NG-K in Figure A.1). Both combustors, for the calciner and the kiln, were modelled as a stoichiometric reactor (RStoic), (CALCINER and COMB-K in Figure A.1). Series of solid reactions occurring in the kiln were simulated using three RStoic reactors, representing decomposition, transition (i.e., exothermic reaction zone), and sintering stages (DECOMP, TRANSI, and SINTER in Figure A.1). Details of the modelled reactions at each stage are provided in Table 3.5 with conversion rates set to ensure that the resulting clinker maintains the expected chemical compositions, including tricalcium silicate ($C_3S$), dicalcium silicate ($C_2S$), tricalcium aluminate ($C_3A$), and tetra-calcium aluminoferrite ($C_4AF$), within the specified range (Nhuchhen, Sit and Layzell, 2022a). That is, these conversions were calculated based on the assumed raw meal composition and the anticipated composition of the calcined meal and clinker. Specifically, the resulting mass fractions of these components in the clinker were 0.691, 0.111, 0.072, and 0.126, respectively.

*Table 3.5. Major reactions considered in the production process and the fractional conversions.*

| Reaction | Fractional Conversion of Component | Fractional Conversion |
|---|---|---|
| 2 CaO(CISOLID) + $SiO_2$(CISOLID) --> $C_2S$(CISOLID) | $SiO_2$ | 1 |
| $C_2S$(CISOLID) + CaO(CISOLID) --> $C_3S$(CISOLID) | $C_2S$ | 0.825 |
| 3 CaO(CISOLID) + $Al_2O_3$(CISOLID) --> $C_3A$(MIXED) | $Al_2O_3$ | 0.507 |
| 4 CaO(CISOLID) + $Al_2O_3$(CISOLID) + $Fe_2O_3$(CISOLID) --> $C_4AF$(CISOLID) | $Fe_2O_3$ | 1 |

In the NG process as per Figure 3.1, primary and secondary air were introduced into the combustor of the kiln (COMB-K), while tertiary air was supplied to the combustor of the calciner (COMB-C). Secondary and tertiary air were pre-heated to temperatures of 1050 °C and 900 °C, respectively (Nhuchhen, Sit and Layzell, 2022a), by recovering heat from the hot clinker. The exhaust vent air (output of the cooler in Figure 3.1) was effectively utilised to recycle energy back into the system for operating the VRM. In the NG process with the CCS implementation, the exhaust vent air was initially used to provide heat to the CCS operation. Afterwards, the airflow was separated, with one portion dedicated to meeting the VRM requirements (VRM-IN), and the other excess flow was used to operate the ORC (ORC-IN) for heat recovery. Additionally, the pre-heater flue gas was harnessed to operate the ORC for heat recovery.

Heat losses were considered in the model, consistent with (Faria *et al.*, 2022), for both the calciner and different stages of the kiln. The heat loss values are as follows; 42.99 MJ/t clinker for the calciner, 30.60 MJ/t clinker for the decomposition stage, 59.40 MJ/t clinker

for the transition stage, and 90 MJ/t clinker for the sintering stage, respectively. These same heat loss values were assumed for all subsequent process options.

The reference model developed and simulated here in the Aspen Plus process simulation software was based on the Excel-based model presented by (Nhuchhen, Sit and Layzell, 2022a), for a natural gas-fired cement plant. Aspen Plus was utilised in this work instead of an excel-based model as per (Nhuchhen, Sit and Layzell, 2022a), to more accurately represent the combustion stages and the kinetics between the unit operations (see Table 3.2). The excel-based model specified in (Nhuchhen, Sit and Layzell, 2022a), was primarily used to perform techno-economic, energetic, and scenario based assessments by incorporating the following key elements: (1) mass and energy balance calculations for both the reference and oxy-combustion based processes from an Aspen based thermal energy flow model, whilst accounting for process specific energy demands, (2) cost estimations, including capital (CAPEX) and operational (OPEX) expenditures were determined from scaling equations and levelised costs, (3) scenario and sensitivity analysis comparing ASU's with electrolysis for oxygen production from specific electricity consumption values amongst literature, and (4) evaluation of $CO_2$ emissions related to cement production. This study incorporated three key modifications from the model presented by Nhuchhen et al.: i) the kiln stage was modelled with three distinct stages (decomposition, transition, and sintering), considering heat losses. In contrast, the previous model in (Nhuchhen, Sit and Layzell, 2022a), treated the kiln as a single stage; ii) the $O_2$ concentrations in the flue gases for the kiln and calciner exits were adjusted to 6.5% and 1.0% (molar basis), respectively, in the reference paper (Nhuchhen, Sit and Layzell, 2022a), whereas in this study, the supply of $O_2$ was set to achieve more complete consumption, resulting in $O_2$ concentrations at 3.7% and 0.3%

(molar basis) for these two streams, respectively; iii) this work did not consider the leakage air, a factor taken into account in (Nhuchhen, Sit and Layzell, 2022a).

### 3.2.4. Modified process for clinker production using oxy-combustion

To model the process referred to as Oxy (as shown in Figure 3.2, and detailed in Figure A.2 for the Aspen flowsheet in the Appendix), the Aspen model used for the process NG was adapted. This adaptation involved replacing the air input to the kiln and calciner combustors with $O_2$ at 25 °C as per Figure 3.2, for natural gas combustion (O2-IN-KILN and O2-IN-CALCINER in Figure A.1). Flue gas recirculation (FGR) at 136 °C was employed to maintain adequate gas flows throughout the system, following the approach outlined in (Nhuchhen, Sit and Layzell, 2022a). More specifically, the flue gas exiting the preheater tower was divided into three separate streams. Two of these streams were designed to mimic the role of secondary air and tertiary air in the process NG, maintaining the same molar flow rates and target temperatures as in that process. The third flow became an exhaust stream.

All $O_2$ required for this process was assumed to be provided by a cryogenic distillation-based ASU at an electrical energy demand of 0.81 GJ/tonne $O_2$ as indicated in (Nhuchhen, Sit and Layzell, 2022a) (though not explicitly modelled in this study). The natural gas feeds to the calciner and the kiln, along with the corresponding $O_2$ feeds, were adjusted to meet the temperature targets set for these units. The flow rates of exhaust vent air were more than sufficient to operate the VRM. Excess flows and the flows from the pre-heater flue gas were both incorporated into the system to operate the ORC for heat recovery. Pre-heating of the $O_2$ input in both the calciner and kiln, achieved through heat recovery from the pre-heater flue gas, was set to 136 °C, in accordance with (Nhuchhen, Sit and Layzell, 2022a).

### 3.2.5. Modified processes for clinker production using hydrogen

The four processes involving the use of $H_2$ were modelled by adapting the model of Process Oxy (refer to Figures 3.1 – 3.6, and Appendix Figures A.3 – A.6). For processes $H_2$-a, $H_2$-c and $H_2$-d, a direct replacement of natural gas by $H_2$ was implemented according to the degrees of substitution described earlier (as detailed in Table 3.1), without altering the process design. For process $H_2$-b, indirect calcination was modelled by (1) feeding the calciner's combustor (COMB-C in Figure A.3) with air instead of $O_2$, removing the need for an ASU; (2) assuming a heat flow to the calciner from its combustor to the effect of bringing the temperature of the combustor's exhaust to 800 °C to meet pre-heating demands; and (3) injecting the tertiary air equivalent flow and the kiln exhaust into the calciner (as opposed to its combustor), to avoid the mixing of $CO_2$ in these two flows with $N_2$ brought in by the calciner's combustion air. As such, there are two separate exhaust gas flows arising from the calcination subsystem, one from the combustor (containing no $CO_2$), and another from the outlet of the calciner (as a mixture of $CO_2$ and water steam), therefore a modified heat recovery arrangement (specific novel component) was adopted for process $H_2$-b. Whilst studies have utilised indirect combustion (Ozcan, Brandani and Ahn, 2014) with fossil fuel combustion, there is yet to be research on the use of $H_2$ for indirect calcination in the cement production process.

In all four processes, the supply of $H_2$ was assumed to be via on-site water electrolysis, which also produces $O_2$ to meet the demand for oxyfuel combustion either partially ($H_2$-a, $H_2$-c) or fully ($H_2$-b, $H_2$-d). The remaining $O_2$ demand in $H_2$-a and $H_2$-c was met by an ASU. The electricity consumption by electrolysis was considered at two efficiency levels based on the ratio of the lower heating value of produced $H_2$ and the electricity input: 60%

(reflecting the efficiency of contemporary industrial alkaline electrolysers (Institute of Power Engineering, 2022)) and 84% (achievable with more efficient technologies such as solid-oxide electrolysers (Salzgitter, 2022)), corresponding to 50 and 40 kWh/kg $H_2$, respectively.

### 3.2.6. $CO_2$ separation and compression

In process NG, a standard amine-based system for $CO_2$ capture, which was not explicitly modelled, was assumed to have 100% capture efficiency as it allows for a direct and clear comparison of the different processes without having to adjust the capture rates in each scenario. Amine-based capture efficiencies typically range at 90% or over (Hills *et al.*, 2016; Mathisen *et al.*, 2018; Voldsund *et al.*, 2019), and both the overall energy use and net emissions would slightly differ according to the capture efficiency, however, the comparative results in terms of energy and $CO_2$ savings would remain largely identical. This system was employed to produce a pure $CO_2$ stream at 1 bar, which was subsequently compressed to 150 bar as reported in (Energy Equipment and Infrastructure Alliance, 2019), a pressure commonly chosen to facilitate the transportation of captured $CO_2$. The energy demand for CCS in process NG was calculated, and the results can be found in Table 3.8. For all the other processes, the flue gas consisted of a mixture of $CO_2$ and water due to oxyfuel combustion. In these cases, $CO_2$ separation was integrated with compression, as illustrated in Figure 3.7. The flue gas exiting from each process underwent a cooling process, using cooling water as a refrigerant within the Aspen simulation. Liquid water resulting from the cooling process was removed in a liquid-vapor separator module. The flue gas then entered a four-stage compression process, with the same cooling and water separation steps repeated between stages while maintaining a temperature of 35 °C for the cooler output.

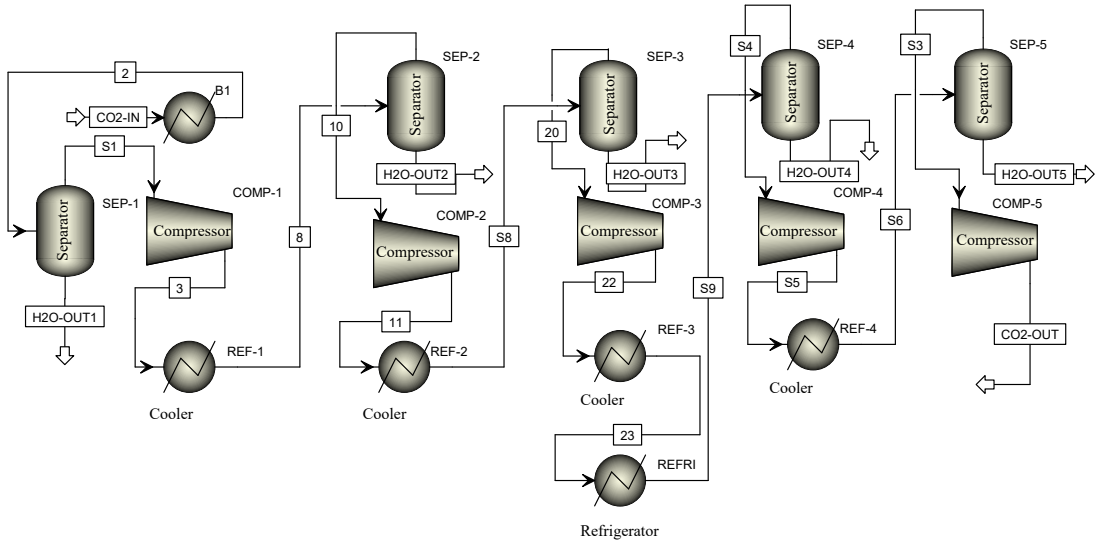


***Figure 3.7. $CO_2$ Separation and Compression model from Aspen simulations.*** *This includes four stages of separation, compression and cooling.*

An exception was introduced after the third stage of water cooling (REF-3), where an additional refrigeration step (REFRI) was included to further reduce the temperature to 6 °C. This extra cooling facilitated additional water removal, ensuring that the final $CO_2$ product achieved a purity greater than 99.95 mol%. The output temperature leaving the final cooling stage (REF-4) was 35 °C. Following the fourth stage of water separation (SEP-4) and compression (COMP-4), the flow exited the process for transport and storage.

The simulation employed a pressure ratio of 2.72 and assumed isentropic and mechanical efficiencies of 0.85 and 0.95, respectively (Nhuchhen, Sit and Layzell, 2022b). The electricity consumption (W) for the refrigeration cycle was estimated from the heat removed (Q) using a coefficient of performance (COP) value of 3.7 (Smith, 2005).

### 3.2.7. Energy recovery and consumption

The key components affecting the net energy consumption or production of the processes are summarised in Table 3.6. These components include natural gas fuel, fans, auxiliary

equipment, CCS, and an ORC, which were present in all the process options. The energy consumption associated with the ASU and electrolysis was detailed in Section 3.3. Further explanations of the calculation of the other components are provided below.

***Table 3.6. Key energy users and providers.***

| **Energy users or providers** | **Processes** | **Energy Type** | **Contribution** |
|---|---|---|---|
| Natural Gas Fuel | All | Thermal | Consumption |
| Fans | All | Electrical | Consumption |
| Auxiliary Equipment | All | Electrical | Consumption |
| Carbon Capture and Storage (CCS) | All | Electrical and Thermal | Consumption |
| Organic Rankine Cycle (ORC) | All | Electrical | Production |
| Air Separation Unit (ASU) | Oxy, $H_2$-a, $H_2$-c | Electrical | Consumption |
| Electrolysis | $H_2$-a, $H_2$-b, $H_2$-c, and $H_2$-d | Electrical | Consumption |

The natural gas fuel input for each process was obtained from the Aspen simulation, and the thermal energy content was calculated using the lower heating value of methane, 50 MJ/kg (Wan, 2004). The power consumption for each fan *($W_{fan}$),* as described as below in Equation 3.1, was estimated by scaling the reported reference fan power consumption in (Nhuchhen, Sit and Layzell, 2022a). Here, $q_{ref}$ and $W_{ref}$ represent the volumetric gas flow and the power consumption of a reference fan, while q is the volumetric gas flow of the fan.

*Equation 3.1. Power consumption of fans.*

$$W_{fan} = W_{ref} \times \left(\frac{q}{q_{ref}}\right)^3$$

The auxiliary power consumption was assumed to remain constant across all processes as extracted from (Nhuchhen, Sit and Layzell, 2022a), at 245 MJ/t of clinker for auxiliary equipment.

The thermal energy required to operate amine-based carbon capture at 1 bar in process NG was primarily for operating the reboiler of the regeneration column at a temperature of 128.4 °C, requiring a heat input of $Q_{reb}$ = 3.8 MJ/kg of $CO_2$ (Voldsund *et al.*, 2019). In the Aspen Plus simulation of process NG, the maximum coverage of heat demand through waste heat was achieved via heat recovery ($Q_{rec}$) from the flue gas and exhaust vent air by cooling the hot streams to 148.4 °C (allowing a 20 °C temperature difference for heat transfer with the reboiler). The net thermal energy demand ($Q_{net} = Q_{reb} - Q_{rec}$) for carbon capture was assumed to be supplied by natural gas combustion, and its $CO_2$ emissions were included in the total $CO_2$ to be captured from the process NG (refer to Figure A.1). Additional power consumption for carbon capture, ($P_{add}$) was assumed to be 0.55 MJ/kg of $CO_2$ (Voldsund *et al.*, 2019). The electricity consumption by the subsequent $CO_2$ compression in the process NG and that of $CO_2$ separation and compression in other processes were calculated based on the modelling described in Section 3.3.

An organic Rankine cycle (ORC) was integrated into the simulated processes for waste heat recovery to generate electricity in support of the processes. The ORC power ($W_{ORC} = Q_{in} \times \eta$) was calculated using the recovered waste heat from the hot gas stream ($Q_{in}$). $Q_{in}$ was obtained from the results of the Aspen simulation of each cooler, mimicking the evaporator of the ORC, on the waste heat source streams cooled to 130 °C, which was 20 °C higher (to provide a heat transfer driving force) than the working fluid's temperature within the ORC. It is typically around 110 °C, as presented in the ORC design from (Moreira

and Arrieta, 2019). The efficiency ($\eta_{th}$) of the ORC was set to 0.225 according to the assumed organic working fluid (Moreira and Arrieta, 2019).

### 3.2.8. Additional assumptions

Different assumptions and inputs applied for conducting the technical and energetic analysis are discussed below:

- The natural-gas molar composition consists of 100% methane, with a lower heating value (LHV) of 50 MJ/kg.
- The molar composition of air was assumed to be 78.12% $N_2$; 20.95% $O_2$; and 0.93% Ar as per (Nhuchhen, Sit and Layzell, 2022a).
- The clinker composition by weight percentage (13% $C_4AF$, 11% $C_2S$, 69% $C_3S$, and 7% $C_3A$) and raw meal input (refer to Table A.7) were kept constant across all processes as per (Nhuchhen, Sit and Layzell, 2022a).
- The pressure was assumed to be 1 bar throughout the clinker production system to represent near atmospheric conditions.
- Complete combustion was assumed for all combustors, with $O_2$ molar percentage less than 1%, minimising unburned gases.

Although real-world (industrial use) natural gas varies in composition from 94 – 96% (mol.) of $CH_4$ (Nhuchhen, Sit and Layzell, 2022a; Jokar *et al.*, 2023), natural gas was assumed to be compromised of 100% $CH_4$ which allowed the combustion reactions and thermodynamic properties to be represented in Aspen Plus straightforwardly. This simplification reduces model complexity while having a modest impact on results as deviations are minute and would not impact the comparative conclusions of the energetic and $CO_2$ performance.

Moreover, this study assumes that the electricity required for hydrogen production (via electrolysis) and for operating the ASU is derived entirely from carbon free (renewable) sources. As a result, upstream (indirect) $CO_2$ emissions for both hydrogen generation and ASU operation are taken as zero, since no emissions are attributed to the electricity used. assuming that electricity is net-zero, the results highlight process emissions from calcination and fuel combustion, without conflating them with emissions from power generation. In real-world cases where upstream (indirect) emissions are considered through the adaptation of a grid electricity mix with a specific level of $CO_2$ intensity, the total $CO_2$ savings in the hydrogen replacement and oxy-combustion cases may be lower. Therefore, it is worth noting that the use of grid electricity would introduce an associated carbon footprint under the current system. Other properties such as the temperature of the raw meal, clinker minerals, and mass and energy flows were taken from (Nhuchhen, Sit and Layzell, 2022a).

## 3.3. Results and discussion

This section presents and discusses the modelling results in three interconnected parts. Firstly, we provide the key results of Aspen Plus simulation, focusing on materials flows and essential process parameters, particularly temperatures, in Section 3.3.1. Subsequently, we delve into an analysis of two critical aspects of process performance used for comparing the six technical options, namely energy consumption and $CO_2$ production, in Sections 3.3.2 and 3.3.3, respectively.

### 3.3.1. Simulated material flows and key process conditions

The key temperatures for calcination and sintering play a vital role in ensuring the intended chemical conversions occur in various stages of the system. As presented in Table 3.7, the simulated results show that they were tightly controlled for all processes around the target values of 900 °C and 1500 °C, respectively. These critical process temperatures were consequences of the fuel input in these processes. Furthermore, Table 3.7 indicates that the kiln exhaust temperatures, influenced by the control of the calcination and sintering temperatures, are slightly higher in the Oxy and $H_2$ processes compared to the reference process (NG). This difference is not expected to pose any significant operational issues. Detailed material flows in the major streams of all six processes examined here are provided in Appendix Tables A.1 – A.6.

***Table 3.7. Key temperatures, flowrates, and thermal energy input from Aspen Plus modelling.***

| **System Input** | **Key Temperatures (°C)** | | **Natural Gas-In (kg/t clinker)** | | **Oxygen-In (kg/t clinker)** | | **Oxygen from air separation unit (kg/t clinker)** | **Hydrogen-In (kg/t clinker)** | | **Lower heating value of fuel input** |
|---|---|---|---|---|---|---|---|---|---|---|
| | ***Calcination*** | ***Sintering*** | ***Calciner*** | ***Kiln*** | ***Calciner*** | ***Kiln*** | | ***Calci-ner*** | ***Kiln*** | ***MJ/t clinker*** |
| ***NG*** | 898.55 | 1500.03 | 47.00 | 30.54 | N/A | N/A | 0.00 | N/A | N/A | 3877.05 |
| ***Oxy*** | 899.24 | 1501.61 | 45.47 | 35.52 | 181.37 | 141.68 | 323.05 | N/A | N/A | 4049.08 |
| ***$H_2$-a*** | 899.76 | 1498.75 | 45.60 | 28.41 | 181.91 | 136.69 | 295.34 | N/A | 2.91 | 4049.32 |
| ***$H_2$-b*** | 899.68 | 1499.23 | N/A | 28.41 | 0.00 | 140.00 | 0.00 | 21.04 | 3.04 | 4310.34 |
| ***$H_2$-c*** | 903.14 | 1498.24 | N/A | 28.41 | 165.00 | 132.00 | 119.35 | 19.47 | 2.736 | 4085.19 |
| ***$H_2$-d*** | 899.01 | 1502.61 | 0.00 | 0.00 | 144.00 | 132.00 | 0.00 | 19.08 | 14.94 | 4082.40 |

As shown in Table 3.8, the reference case (NG) consumes 77.54 kg/t clinker of natural gas (equivalent to 3877 MJ in fuel LHV) per tonne clinker, which falls within the anticipated range of fuel consumption by conventional cement plants (Pamenter and Myers, 2021). The thermal energy required for the NG case was seen to be in line with literature (Nhuchhen, Sit and Layzell, 2022a). In comparison, there is a modest increase of 4.9% GJ in the natural gas fuel consumption in process Oxy. This increase is primarily due to changes in the composition of the combustion products and the gaseous flows within the system (Nhuchhen, Sit and Layzell, 2022a). Electrical energy required for the Oxy case was 580.03 MJ/t clinker and was near identical with the reported value of ~561 MJ/t clinker from literature (Nhuchhen, Sit and Layzell, 2022a). An alignment with literature (Nhuchhen, Sit and Layzell, 2022a), regarding the electrical energy required for $CO_2$ separation and compression was also seen in the Oxy case at 289.75 MJ/t clinker, where the literature reported value is 241.2 MJ/t clinker.

***Table 3.8. Component of thermal and electrical energy consumptions/production of all six process options for cement production decarbonisation.***

| **Processes** | | **NG** | **Oxy** | **$H_2$-a** | **$H_2$-b** | **$H_2$-c** | **$H_2$-d** |
|---|---|---|---|---|---|---|---|
| **Electrical Energy for production (MJ/t)** | Fans | 540.99 | 432.32 | 424.75 | 401.97 | 439.99 | 509.44 |
| | Auxiliary | 244.80 | 244.80 | 244.80 | 244.80 | 244.80 | 244.80 |
| | Electrolysis (60% Efficiency) | 0.00 | 0.00 | 523.26 | 4334.76 | 3997.03 | 6123.60 |
| | Electrolysis (84% Efficiency) | 0.00 | 0.00 | 418.61 | 3467.81 | 3197.63 | 4898.88 |
| | Air Separation Unit (ASU) | 0.00 | 261.67 | 239.23 | 0.00 | 96.68 | 0.00 |
| | Organic Rankine Cycle (ORC) | -105.02 | -349.76 | -349.71 | -403.00 | -360.68 | -359.09 |
| | *Subtotal (60% Electrolysis* Efficiency) | 680.77 | 580.03 | 1082.32 | 4578.53 | 4417.83 | 6318.75 |
| | *Subtotal (84% Electrolysis* Efficiency) | 680.77 | 580.03 | 977.67 | 3711.58 | 3618.42 | 5294.03 |
| **Thermal Energy for production (MJ/t)** | Natural Gas | 3880.15 | 4052.32 | 3703.44 | 1421.64 | 1421.64 | 0.00 |
| **Energy for $CO_2$ capture (MJ/t)** | Amine-based capture: Electrical Energy | 492.08 | 0.00 | 0.00 | 0.00 | 0.00 | 0.00 |
| | Amine-based capture: Carbon Capture and Storage (CCS) Thermal Energy | 2233.93 | 0.00 | 0.00 | 0.00 | 0.00 | 0.00 |
| | $CO_2$ Separation and Compression: Electrical energy | 282.55 | 289.75 | 282.73 | 237.08 | 237.13 | 208.79 |
| | ***Sub Total (MJ/t)*** | 3008.56 | 289.75 | 282.73 | 237.08 | 237.13 | 208.79 |
| **Net Total Energy (MJ/t) with 60% electrolysis efficiency** | | 7569.48 | 4922.09 | 5068.50 | 6237.25 | 6076.59 | 6727.54 |
| **Net Total Energy (MJ/t) with 84% electrolysis efficiency** | | 7569.48 | 4922.09 | 4963.84 | 5370.29 | 5277.19 | 5502.82 |

The fuel mix varies in cases involving $H_2$, as expected. Process $H_2$-a exhibits modest $H_2$ substitution for natural gas, while processes $H_2$-b and $H_2$-c demonstrate greater substitution. Finally, process $H_2$-d achieves complete substitution of $H_2$ for natural gas. Despite variations in the fuel input composition, the total fuel LHV remains similar, approximately 4067 MJ/t clinker, for processes Oxy, $H_2$-a, $H_2$-c, and $H_2$-d. This represents a 4.8% increase compared to the process NG (reference case). However, $H_2$-b requires considerably higher fuel input, approximately 4310 MJ/t clinker, which is roughly ~11% more than the reference case. This increase is mainly attributed to the use of air (rather than $O_2$) in the calciner combustor as part of the indirect calcination process. This results in a greater amount of flue gas, about 1471 kg/tonne clinker (~35% more) compared to the process Oxy, leading to greater heat loss.

As expected, $H_2$-b requires the least $O_2$ supply due to indirect calcination; eliminating the need for an ASU as electrolytic $O_2$ exceeds the demand. In the other processes, increased $H_2$ usage generally translates to reduced demand for $O_2$, determined by the combustion requirement. Process Oxy relies entirely on the ASU for $O_2$ supply. Conversely, process $H_2$-d achieves an $O_2$ balance between the electrolysis energy generation and the consumption by 100% $H_2$-based fuel combustion. Processes $H_2$-a and $H_2$-c fall between these extremes, relying on the ASU to varying degrees.

### 3.3.2. Energy consumption

As indicated in Table 3.8, the overall energy consumption encompasses both thermal energy input from fuels (natural gas and hydrogen), and electrical energy input for operating fans, including the auxiliary components of the cement plant, electrolysers, ASU, and $CO_2$ capture and separator units. The energetics is important to be considered as: (1) fuel consumption

drives $CO_2$ emissions, (2) every unit of energy consumed adds cost, and (3) alternatives fuels such as hydrogen depend on reliable, large-scale renewable energy supply. This summary provides a comparative analysis of the energetic performance across different processes, considering both thermal and electrical energy demands, which are influenced by the energy efficiency of water electrolysis ($\eta_{ely}$). First, we analyse the results assuming $\eta_{ely}$ = 60%, and we present an energy flow diagram in Figure 3.8 to illustrate the distribution of electrical (el) and thermal energy (th) distribution across all the processes. It is worth noting that approximately 10% to 13% of the energy consumption is attributed to fans while 3% to 6% is attributed to $CO_2$ separation and compression, consistently across all processes. In the first three processes (NG, Oxy, and $H_2$-a), the majority of the energy demand (>50%) comes from natural gas in the form of thermal energy. In contrast, in processes $H_2$-b, $H_2$-c, and $H_2$-d, electrolysis dominates the energy demand, primarily in the form of electrical energy.

Additionally, the environmental aspect of energy use in cement production is mainly linked to $CO_2$ emissions from fuel combustion, which can be reduced through the use of cleaner energy sources such as hydrogen. However, emissions from the calcination of limestone remain unavoidable and require alternative clinker materials. Although higher energy demand increases operating costs, this chapter focuses on the relationship between energy use and emissions rather than detailed economic analysis.

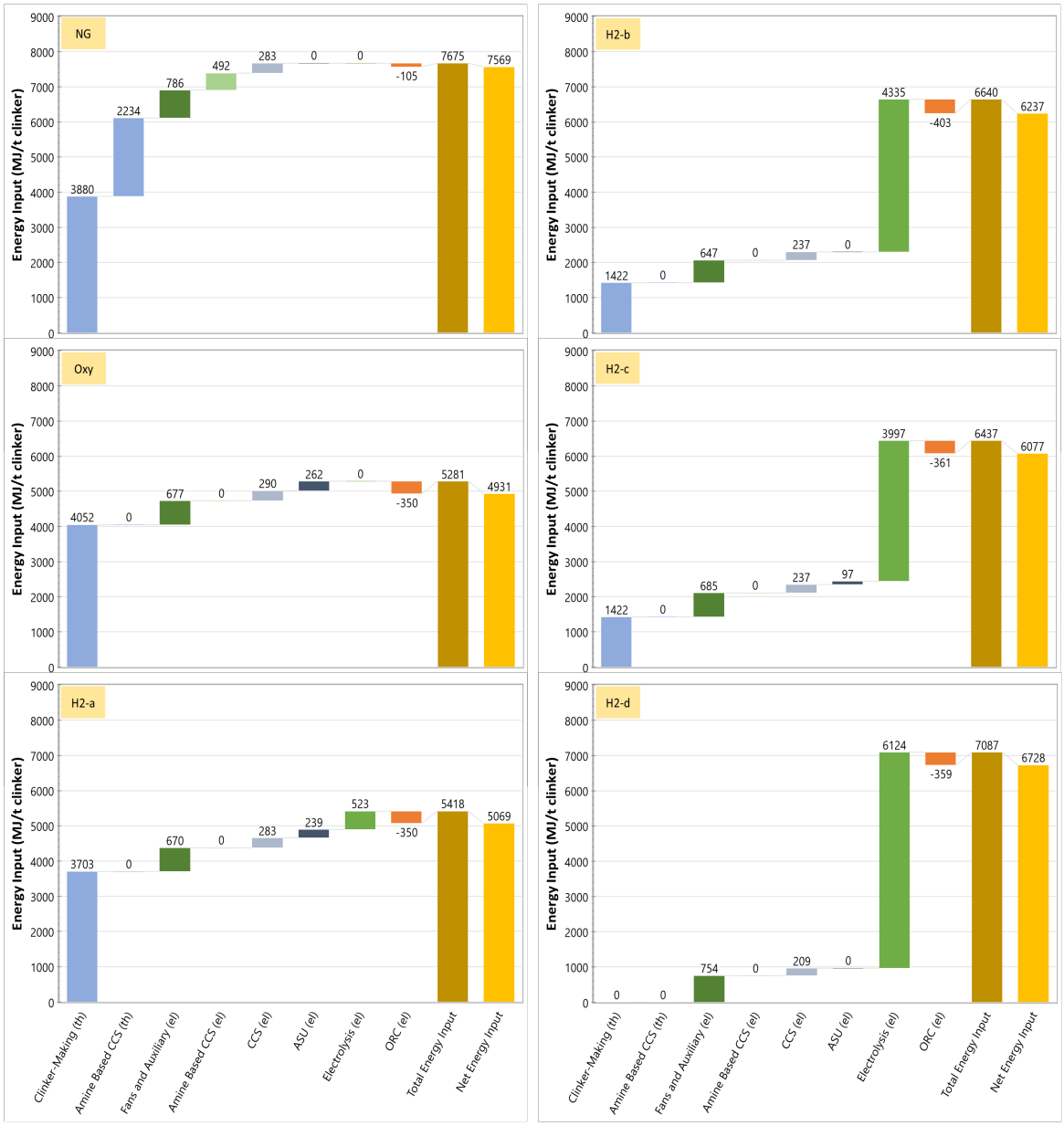


***Figure 3.8. Total and net energy flows in simulated processes*** *(electrolysis efficiency = 60%) [Note: Electricity sources were assumed to be 100% renewable ($GJ_{el}$=$GJ_{th}$)].*

In a previous study (Nhuchhen, Sit and Layzell, 2021), it was found that half of the thermal energy demand was from natural-gas-infused $H_2$. In the $H_2$ processes ($H_2$-a – $H_2$-d), all the thermal energy demand is supplied by natural gas, as $H_2$ is sourced from electrolysis. Moreover, the thermal energy consumption in an oxy-combustion-based production process from the literature consumed around 560 MJ/tonne of clinker (Faria *et al.*, 2022); the thermal energy consumption in the simulated Oxy process was higher, at 4052 MJ/tonne of clinker; the difference could be attributed to result from the variation in adopted fuel type and

modelling assumptions. More importantly, according to (Nhuchhen, Sit and Layzell, 2022a), the thermal energy demand was 7% higher compared to the NG-based process in the literature. This work confirmed the comparative trend between the two process options, although the difference is slightly lower, at 4.3%.

The most energy-intensive is process NG, where $CO_2$ capture using amine-absorption (including purification and compression) imposes a significant energy burden, accounting for approximately 40% (3008.56 MJ/t clinker) of the total energy input. This is despite partial coverage of the thermal energy requirement for solvent regeneration by heat recovery from the clinker production process. In contrast, process Oxy stands out as the most energy-efficient option. Although operating the ASU requires additional electrical energy, it constitutes only a small portion (~5% or 261.67 MJ/t clinker) of the total energy demand of the process Oxy. The use of oxyfuel combustion significantly simplifies $CO_2$ separation. Even with the ASU's energy requirement (261.67 MJ/t clinker) added to the energy consumption by $CO_2$ separation and compression (289.75 MJ/t clinker), the sum of the two energy demands is still much lower than the energy demand for the $CO_2$ capture of the process NG through amine-absorption (3008.56 MJ/t clinker), resulting in substantial energy savings that offset the slight increase in its natural gas or thermal energy consumption during clinker production.

Across the hydrogen-involving processes ($H_2$-a, $H_2$-c, and $H_2$-d), clear trends for electricity and natural gas demand emerge. As the level of $H_2$ substitution increases, electricity demand becomes significantly higher, driven by the requirement of electrolysis. Although natural gas demand decreases, the total fuel energy input in process $H_2$-a is similar to that of the process Oxy (as shown in Table 3.8). The energy loss in electrolysis during the conversion from electricity to $H_2$ means that the greater the $H_2$ substitution, the greater the electrolytic

energy demand for producing 1 tonne of clinker. Increased use of electrolytic $H_2$ results in i) more electrolytic $O_2$, reducing ASU operation and its energy demand, and ii) lower $CO_2$ production, reducing the energy demand for $CO_2$ separation and compression (also discussed in Section 3.2). Nonetheless, these savings are not significant enough to offset the energy demand of electrolysis. As shown in Table 3.8 if $\eta_{ely}$ = 60%, the energy demand for the entire system in the $H_2$-using processes ranges from 5068.60 – 6727.54 MJ/t clinker, with electrolysis accounting for 10% to 91% of the net total energy consumption. On the other hand, these $H_2$-using processes reduce the energy demand by 11% to 33% compared to the reference process NG.

However, achieving a significantly higher electrolysis efficiency would be required for a process with significant $H_2$ substitution to energetically outperform process Oxy. The energetic performance of process $H_2$-b is about 6% less than $H_2$-c (despite having the same level of $H_2$ substitution as $H_2$-b). This difference is primarily due to the higher fuel input requirement caused by the use of air in the calciner combustor as part of indirect calcination. It managed to eliminate the need for an ASU while allowing the clinker to operate with 80% of natural gas and oxyfuel combustion. Conversely, the relative insignificance of the ASU in total energy consumption means that the increase in the higher fuel input requirement leads to an overall energy penalty. It is important to note that this process recovers approximately 15% more electricity compared to the other oxyfuel processes, due to the higher waste heat content in the flue gas from the calciner combustor. Nonetheless, the low efficiency of ORC (20%) results in a considerable energy loss, highlighting the need for more energy-efficient energy recovery to improve the overall energetics of process $H_2$-b.

### 3.3.3. $CO_2$ production and capture

The $CO_2$ produced for all the processes were calculated using the Aspen Plus simulations and are listed in Table 3.9. The findings from Table 3.9, show that replacing natural gas with hydrogen and adopting oxyfuel-combustion presents promising $CO_2$ reduction potential of up to 27.6%, whilst offering a more concentrated molar fraction of $CO_2$ for a more energy efficient carbon capture. It is evident that the introduction of oxyfuel-combustion in the processes effectively eliminates nitrogen from the flue gases, with the exception of the calciner combustor exhaust from process $H_2$-b. This exception occurred because air was introduced to burn $H_2$ in the indirect calcination combustor, as described earlier, resulting in only water vapour and nitrogen. The highest $CO_2$ molar fraction was 74% in the flue gas from the $H_2$-b process. Furthermore, increasing the replacement of natural gas with $H_2$ led to a reduction in the flue gas flow in processes $H_2$-a, $H_2$-c, and $H_2$-d. This reduction in the flue gas flow subsequently reduces the need for $CO_2$ capture and separation, along with its associated electrical energy demand, from 283 MJ/t clinker in process $H_2$-a to 209 MJ/t clinker in process $H_2$-d (as indicated in Table 3.8).

***Table 3.9. Flue gas composition and $CO_2$ produced.*** *Compares the flue gas characteristics (flow-rate, temperature, molar compositions of gases, and total $CO_2$ produced) for different fuel and combustion cases of the modelled clinker production process.*

| Processes | Location | Flue gas (kmol/h) | Flue Gas (kg/h) | Flue Gas (°C) | $CO_2$ mol fraction | $H_2O$ mol fraction | $N_2$ mol fraction | $CO_2$ (kg/t clinker) |
|---|---|---|---|---|---|---|---|---|
| **NG** | Preheater exhaust | 64.67 | 2001.46 | 130 | 0.27 | 0.15 | 0.57 | 771.82 |
| **Oxy** | Preheater exhaust | 27.85 | 963.14 | 130 | 0.64 | 0.36 | 0.00 | 781.26 |
| **$H_2$-a** | Preheater exhaust | 28.00 | 954.61 | 130 | 0.62 | 0.38 | 0.00 | 762.13 |
| **$H_2$-b** | Preheater exhaust | 19.60 | 730.56 | 130 | 0.74 | 0.26 | 0.00 | 637.04 |
| **$H_2$-b** | Calciner combustor exhaust | 30.07 | 741.04 | 130 | 0.00 | 0.35 | 0.65 | 0.00 |
| **$H_2$-c** | Preheater exhaust | 29.26 | 906.73 | 130 | 0.49 | 0.50 | 0.00 | 637.04 |
| **$H_2$-d** | Preheater exhaust | 29.59 | 863.49 | 130 | 0.43 | 0.57 | 0.00 | 559.11 |

As indicated in Table 3.9, even in the process $H_2$-d where the fuel-related emissions were entirely eliminated by replacing natural gas with $H_2$, limestone calcination still contributed to about 559 kg$CO_2$/t clinker. This was similar to the values reported in literature of 510 kg$CO_2$/t clinker (Juangsa *et al.*, 2022), utilising 100% $H_2$ to replace conventional fossil fuels, and near identical with the $CO_2$ produced from feedstock (excluding fuel-induced emissions) reported in (Nhuchhen, Sit and Layzell, 2022a), of 557 kg $CO_2$/t clinker. Limestone calcination accounted for 72.4% of the total $CO_2$ production, in the reference case (process

NG), in line with literature at about 76% (Nhuchhen, Sit and Layzell, 2022a). This highlights a limitation of fuel substitution as a decarbonisation strategy for the cement industry, particularly if the goal is to achieve deep decarbonisation in alignment with the Paris Agreement.

## 3.4. Conclusions

Energy consumption and $CO_2$ production modelling using Aspen Plus was carried out for six technological options aimed at decarbonising the cement production process. Concerning total energy consumption, the oxyfuel combustion process (Oxy) fuelled by natural gas was found to be the most efficient, requiring approximately 35% less energy input compared to the reference process, which assumed the use of amine-based post-combustion $CO_2$ capture in a conventional cement plant powered by natural gas. This highlights the significant potential benefit of oxyfuel combustion, which outweighs the energy requirements of the ASU necessary for the process Oxy.

In the processes using $H_2$ (i.e., $H_2$-a, $H_2$-b, and $H_2$-c), the total energy reduction achieved was between 11 – 33% compared to the reference process. The lower energy reduction percentages are primarily due to energy losses from water electrolysis, which became more significant on a per-tonne clinker basis as the level of $H_2$ substitution increased. Improved electrolysis efficiencies were shown to lead to a significant reduction in total energy in these processes. The process with indirect calcination (in $H_2$-b) required higher $H_2$ fuel input and eventually consumed more total energy than its counterpart, despite eliminating the need for ASU for $O_2$ supply.

In terms of $CO_2$ production, the natural gas-powered oxyfuel-combustion (Oxy) process resulted in slightly higher $CO_2$ generation than the reference plant due to the minor increase in natural gas requirements. The processes utilising $H_2$ achieved a 17.5% to 27.6% reduction in $CO_2$ generation compared to the reference plant, depending on the level of $H_2$ substitution, with the highest reduction corresponding to 100% replacement of natural gas with $H_2$ in process $H_2$-d. Noteworthily, the hydrogen based processes in this study were analysed under the assumption that hydrogen is produced on site via electrolysis, but any associated $CO_2$ emissions from electricity generation for electrolysis were not included in the reported results. Utilising $H_2$ has the potential to increase cradle-to-gate $CO_2$ emissions, depending on the energy source of $H_2$ production. As a consequence, the findings reflect only the direct process emissions (e.g., from fuel combustion inside the kiln or calciner and from limestone decarbonation), along with the in-plant energy requirements. This underscores the potential of $H_2$, or other low-carbon alternative fuels, in reducing $CO_2$ generation and emphasises the importance of integrating energy-focused solutions with efforts targeting raw materials to achieve more comprehensive decarbonisation of cement production. In particular, future research should explore new forms of raw meal for clinker production that reduce the fraction of limestone, a major source of $CO_2$ generation due to calcination and investigate alternative cementitious materials to reduce the use of conventional clinkers.

This work primarily focused on assessing the energy and emissions performance of different hydrogen-based options supported by oxy-combustion for decarbonising the cement production process. Energy use is linked to $CO_2$ emissions and represents a key challenge for achieving deep emission reductions. While the economic dimension is an important factor in determining the feasibility and scalability of hydrogen replacement, it was not the main emphasis of this study. Nonetheless, the analysis of energy demand provides an indirect

connection to economics, as higher energy requirements imply increased operational costs. Future work should therefore include a comprehensive techno-economic assessment to fully evaluate the cost-effectiveness and practical implementation of the proposed hydrogen replacement options.

# Chapter 4. Substituting fossil fuels from cement production with solar energy to reduce carbon emissions

## Summary

This chapter features an under review manuscript which was edited to include further clarifications: Williams, F., & Yang, A. (2025). Substituting fossil fuels from cement production with solar energy to reduce carbon emissions. The corresponding Supplementary Information can be found in Appendix B.

Among the authors who contributed to this chapter, Franco Williams conceptualised the study involving the methodology, developed the models, analysed the results, and wrote the manuscript; Aidong Yang supported with the conceptualisation, supervision, provided feedback on the modelling, and revised the manuscript.

The second original work chapter builds on the first research project to assess the decarbonisation extent of directly using renewable energy (as opposed to relying on conversion to $H_2$) to reduce fossil-based $CO_2$ emissions. This chapter investigates the potential of solar energy-based decarbonisation options in clinker production, with the focus on solar calcination, followed by kiln electrification powered by photovoltaics.

Optimisation models which are parametrised by process simulation results were utilised to assess the economic costs and carbon emission reduction performance of the solar driven

processes. The findings with reference to retrofitting a natural gas fuelled clinker plant indicate that the solar driven processes can achieve $CO_2$ savings of ~26%, through nearly complete replacement of fossil fuels with solar energy. The location dependent analysis of illustrative sites in three countries (including the United States, China and Brazil), showed that regions with higher solar energy quality benefit from up to ~47% lower costs to implement the proposed retrofitting. Across the analysed sites, the solar calciner achieves cost competitiveness once natural gas price exceeds 30 USD/MWh at the Brazil site and 50 USD/MWh for the other two sites. In contrast, the photovoltaics (PV)-based kiln electrification costs are significantly higher, which undermines its economic viability under current cost assumptions. The results underscore the critical role of local solar energy characteristics in influencing the costs, whilst emphasising the necessity for future cost reduction in renewables-based decarbonisation of industrial heating for clinker production and other sectors.

## 4.1. Introduction

ement ranks as the most prevalently used man-made material on earth (Global Cement and Concrete Association, 2024), with its widespread use propelled by rapid infrastructure development, urbanisation, and population growth (Shah *et al.*, 2022). The primary component of cement, Portland cement clinker, reached an annual production of 4.1 billion metric tonnes in 2023 (Tkachenko *et al.*, 2023), with a projection to increase to 12–23% above 2020 levels by 2050 (Cheng *et al.*, 2023). Clinker production exerts a significant contribution to global climate change, emitting an average of 866 kg of $CO_2$ per tonne of clinker produced (Summerbell, Barlow and Cullen, 2016), contributing to 1.6 billion metric tonnes or 8% of annual global

carbon emissions (Moumin *et al.*, 2020; Tiseo, 2023a), driven by both the fuel used and the calcination of limestone. Beyond greenhouse gas (GHG) emissions, the energy consumption in the production of clinker accounts for 7% of global energy demand (Uratani and Griffiths, 2023), responsible for 50–60% of overall manufacturing costs (Sahoo, Kumar and Samsher, 2022). To align with the Paris Agreement and limit global warming to 1.5 °C above pre-industrial levels, society must achieve net-zero GHG emissions by 2050 (UNFCCC, 2015), therefore, it is imperative for the cement industry to find pathways for effective $CO_2$ mitigation. Clinker is a product of raw meal after being subjected to calcination at 900 °C and fuel combustion at high temperatures, reaching up to 1500 °C (Nhuchhen, Sit and Layzell, 2022a), where the primary constituents of raw meal involve calcium oxide (CaO), commonly derived from limestone, along with silicon dioxide ($SiO_2$), aluminium oxide ($Al_2O_3$) and iron oxide ($Fe_2O_3$).

The environmental impacts from clinker production can be mitigated through technical options, addressing energy usage, emissions, and economic costs, including the use of alternative fuels (Juangsa *et al.*, 2022), energy efficiency (Supriya *et al.*, 2023), alternative clinkers (Sahu and Meininger, 2019; Yang *et al.*, 2022), carbon capture utilisation and storage (CCUS) (Wang *et al.*, 2022), and $CO_2$ mineralisation (Strunge, Renforth and der Spek, 2022). Among the array of promising options, substitution of fossil fuels such as coal and natural gas (Juangsa *et al.*, 2022), is a promising option to tackle fuel emissions (Chatterjee and Sui, 2019; Nhuchhen, Sit and Layzell, 2022a), followed by using alternative clinkers to reduce calcination related emissions (Antunes *et al.*, 2022). Together, these measures can potentially account for ~80% of total $CO_2$ emissions from the clinker production process (Moumin *et al.*, 2020; Williams, Yang and Nhuchhen, 2024). Although the utilisation of CCUS could potentially capture up to 90% of the total $CO_2$ emissions from

clinker production, the thermal energy demand and economic costs are high and hence currently hindering its wide adoption (Hills *et al.*, 2016). Concentrated solar power (CSP) and low-carbon energy-based electrification (Moumin *et al.*, 2020; Quevedo Parra and Romano, 2023), providing heating in the calcination and kiln stages, respectively, can potentially replace fossil fuels for mitigating the fuel combustion emissions (Naqi and Jang, 2019), while reducing costs associated with rising carbon taxes (Tsai and Lin, 2024). In a CSP system, solar radiant energy is captured by using multiple reflective mirrors (known as heliostats) to concentrate the heat energy onto a specific focal point, which is typically a solar reactor (Sahoo, Kumar and Samsher, 2023). Implementation of the CSP system for calcination involves two distinct tower designs, top of tower (TT) option and the beam down (BD) option (Moumin *et al.*, 2020). In the TT option, the solar calcination reactor (i.e., the solar calciner) is placed on top of a tower. In the BD option the reactor is placed on the ground where solar radiation is received through a tower reflector. To deal with the variability and intermittency of solar energy input, an energy storage mechanism is imperative to allow continuous supply of calcined meal to the kiln (Gonzalez, Switzerland and Flamant, 2013; Tregambi *et al.*, 2018; Moumin *et al.*, 2020). This can be provided by thermal energy storage (TES) with molten salts to allow continued heating to be supplied to a solar calciner (Moumin *et al.*, 2020). Alternatively, calcined meal storage may be adopted (Moumin *et al.*, 2020), where over-produced calcined meal during daylight hours is stored at 700 °C (Sahoo, Kumar and Samsher, 2023). During hours with insufficient solar input, the stored calcined meal is re-heated to 900 °C using natural gas to ensure stable supply to the kiln (Sahoo, Kumar and Samsher, 2023). These additional components compared to the conventional calciner contribute to increased capital costs (González and Flamant, 2014). Several studies have shown that a CSP-based solar calciner can be used to reduce fossil fuel use in cement production while adhering to the temperature conditions of the cement

calciner and kiln (González and Flamant, 2014; Tomatis et al., 2020; Nikolakopoulos et al., 2022; Sahoo, Kumar and Samsher, 2023). The estimated $CO_2$ emissions reduction ranges from 35.5% (Nikolakopoulos *et al.*, 2022) to 48% (Tomatis *et al.*, 2020). These underscore the potential of utilising CSP to decarbonise cement production in the calcination stage.

On electrification, although its potential in cement production in general has previously been discussed (Antunes *et al.*, 2022; Quevedo Parra and Romano, 2023), of particular interest is the application in the kiln stage following calcination. In the CemZero project, it was shown that producing cement clinker using plasma technology is not only feasible but also allows for the generation of temperatures up to 2000 °C (Antunes *et al.*, 2022). This scheme has been modelled by (Quevedo Parra and Romano, 2023), revealing the feasibility of employing plasma generators to supply the requisite temperature of 1500 °C for the kiln stage. If the electricity supply is based on renewables such as solar energy, energy storage will also be needed to ensure continuous and stable power provision.

Despite these previous investigations of using solar energy in different parts of cement plants, an assessment of solar-driven designs for the entire clinker production process, particularly one that is based on detailed optimisation modelling, is still lacking. This work presents a technoeconomic analysis to quantify economic costs and reduction potential of $CO_2$ emissions of retrofitting a conventional clinker production process with: (1) a solar calciner to replace the conventional calciner heated by natural gas combustion, and (2) a photovoltaics (PV)-powered plasma generator to supply heating to the kiln, replacing its natural gas combustor (shown in Figure 4.1). To capture the challenges of variable solar energy supply, this study uses cost-minimising optimisation models to determine the sizing of key technical components based on detailed hourly solar energy data. Unlike previous techno-economic studies of the solar calciner (Moumin *et al.*, 2020; Sahoo, Kumar and

Samsher, 2023), and the electrified kiln subsystem (Jacob and Tokheim, 2023), this study, to the best of the authors knowledge, is the first to use optimisation models with high resolution renewable energy data (author's concept). Since the quality of the location-specific solar power plays a major role in the economic performance of the solar and electrified option (Quevedo Parra and Romano, 2023), the assessment is performed for three sites in major cement production countries, namely the United States (US), China (CN), and Brazil (BR), to show the impact of the solar energy characteristics on the performance of the assessed system. As such, this work provides a more rigorous and comprehensive assessment of the decarbonisation potential of renewable energy-based cement production, proposing a solar-based energy solution to replace fossil fuels while detailing its operational and implementation aspects.

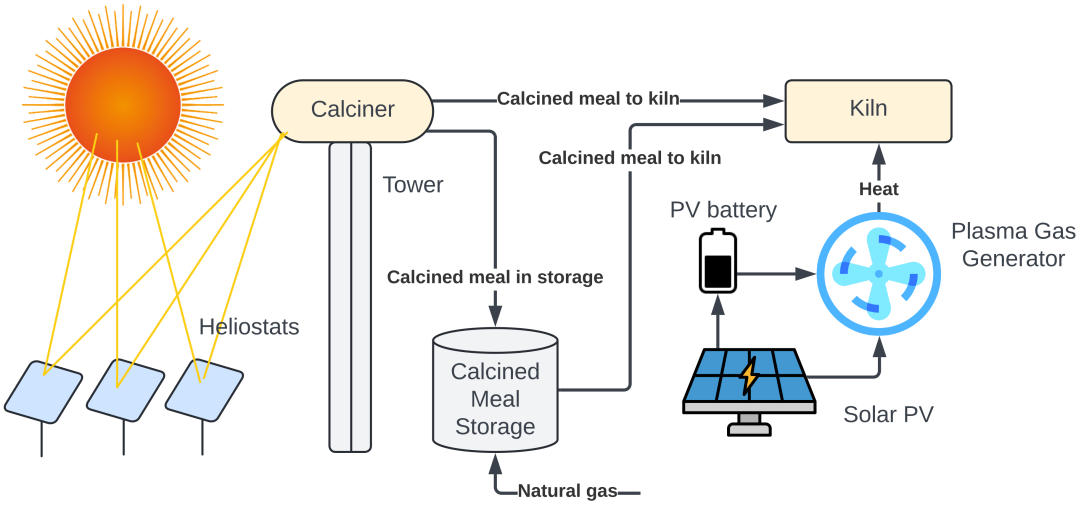


***Figure 4.1. Conceptual representation of the solar calciner and electrified kiln subsystems.*** *The calciner receives concentrated solar energy and kiln receives high-temperature plasma gas powered by solar photovoltaics (PV); both systems involve storage for operation during non-daylight hours.*

## 4.2. Methodology

### 4.2.1. Overview of optimisation modelling and case study locations

Linear programming optimisation models of the calciner and kiln subsystems within the cement production process were developed and solved using General Algebraic Modelling System (GAMS (Rejani *et al.*, 2022)) (see Figure 4.2). With an hourly resolution over a representative year, the optimisation models determined the energy and material flows and the capacity of each key system component (including the heliostat, solar calciner and calcined meal storage in the calcination subsystem, PV and battery storage in the kiln subsystem). The model solution was driven by the objective function that minimises the total annualised cost over 8760 hours for a plant lifetime of 30 years. The optimisation models evaluated the techno-economic costs of retrofitting an existing conventional clinker plant to replace heating based on natural gas combustion with solar-based supply. The plant is assumed to be based on clinker production capacity of 1 tonne per hour, in alignment with prior work detailed in (Williams, Yang and Nhuchhen, 2024). Process simulation using Aspen Plus V12.1 was utilised to determine the boundary conditions such as temperatures and flowrates of streams exchanged between the calciner and the kiln subsystems and the temperature of the exhaust gas from the calciner subsystem, to ensure that these retrofitted subsystems would operate in a clinker production plant without mismatches. Aspen simulation was also used to determine the plasma gas flow rate at a pre-specified temperature (see Section 4.2 for further details) to ensure that this gas flow meets the requirement of operating the kiln. The other economic costing and physical parameters for the calciner and kiln optimisation models were taken from literature. Costs associated with raw material procurement, labour, training, land procurement, component degradation, and long-term

maintenance were excluded in this study due to the lack of real-world operational data for solar cement plants.

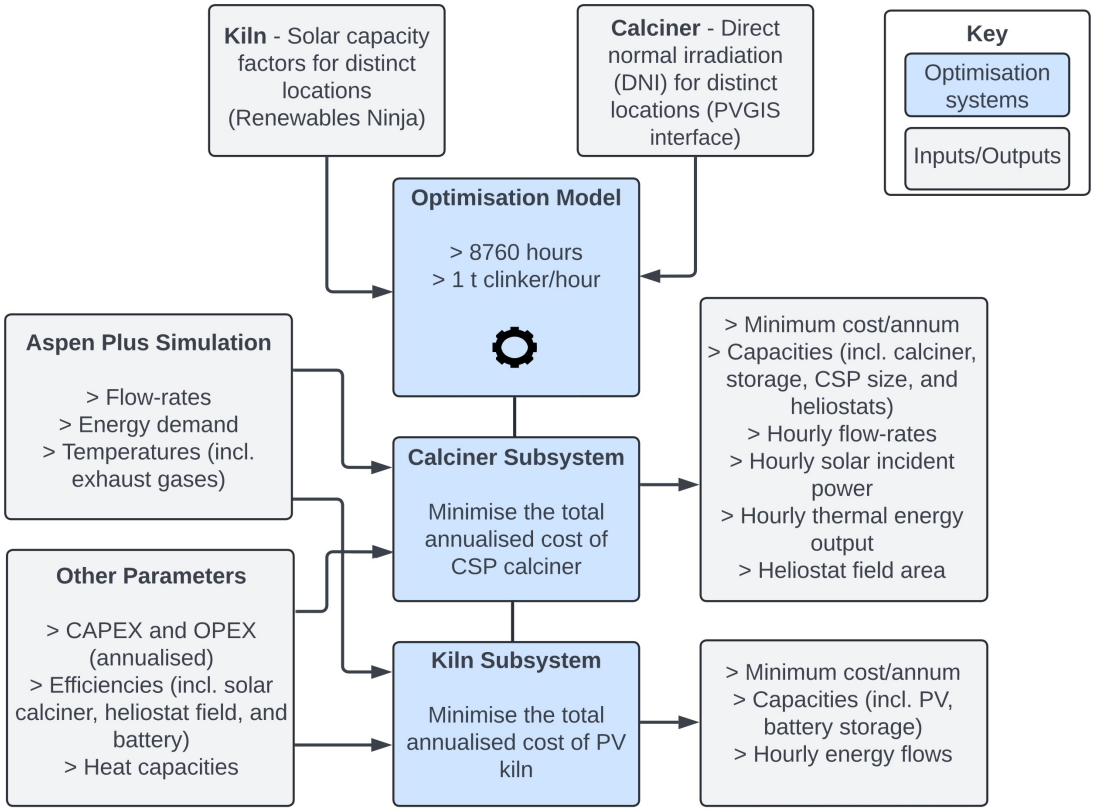


***Figure 4.2. Overview of the optimisation model development of the calciner and kiln subsystems.*** *Optimisation was conducted for three geospatial locations (including US, CN, and BR) to determine the lowest annualised costs for each subsystem, namely the calciner and kiln. Blue boxes represent the optimisation system, whilst the grey boxes indicate the inputs and outputs as per the key.*

Each model targeted specific plant sites in three countries from the world's top ten cement producers, namely, the United States, China, and Brazil (shown in Table 4.1). This enabled a diverse selection, capturing distinctive climatic conditions while representing three different sites for total installed renewable energy capacities. The analysis specifically used the sites of the largest cement production plants within these countries (refer to Table B.6).

***Table 4.1. Site specific locations of the solar driven process across three countries*** *(Pfenninger and Staffell, 2016; European Commission, 2022).*

| Location | Country | Company | Plant ID | Coordinates |
|---|---|---|---|---|
| 1 | United States | Holcim | Genevieve Cement Plant | 38.1113, -90.2586 |
| 2 | China | Anhui Conch Cement | Baimashan Cement Factory | 30.4264, 117.2427 |
| 3 | Brazil | Votorantim Cimentos RI | Edealina Plant | -17.2593, -49.7882 |

Hourly PV capacity factors and direct normal irradiation (DNI) for the selected locations were sourced from Renewables Ninja (Pfenninger and Staffell, 2016) and PVGIS interface from the European Commission (European Commission, 2022), respectively, providing hourly data from 2019 and 2015, respectively. The hourly solar energy data averaged to monthly PV capacity factors and DNI are shown in Figure 4.3a and Figure 4.3b, respectively. Correspondingly, the average annual values of the PV capacity factor and DNI are shown in Figure 4.3c and Figure 4.3d, respectively, for an overall comparison between the three locations. Among the three sites, the one in Brazil possesses superior solar energy quality in terms of both PV capacity factor and DNI. The US site has visibly better DNI than that in China; the overall PV capacity factor profiles of the two sites are closer.

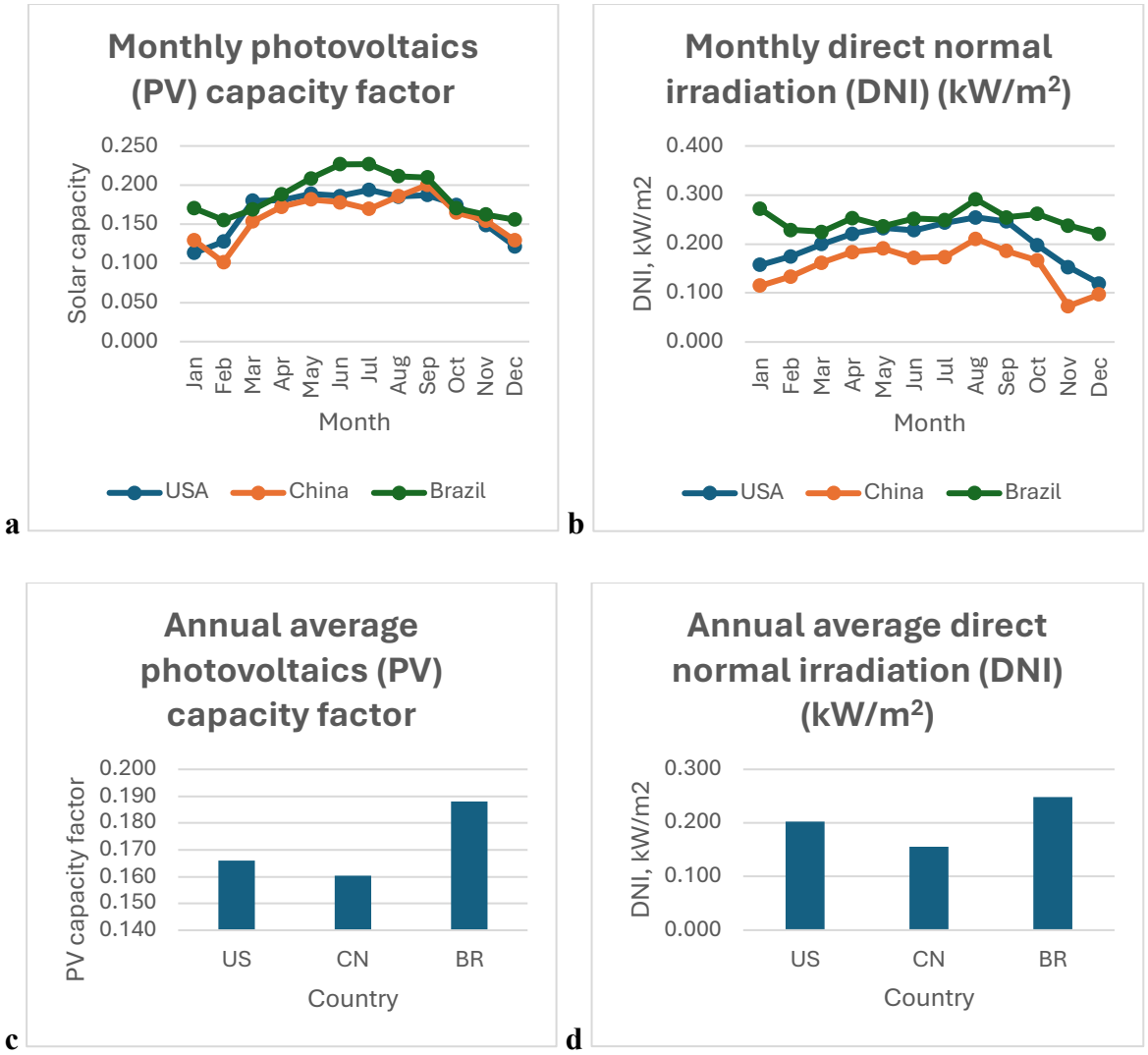


***Figure 4.3. PV capacity factors and DNI.*** *Monthly (a and b) and annual (c and d) solar photovoltaics (PV) capacity factors and direct normal irradiation (DNI) for sites in three countries, United States (US), China (CN), and Brazil (BR) are presented with a and b denoting the average monthly values whilst c and d denote the average annual values.*

### 4.2.2. Optimisation Model for the Calciner Subsystem

Figure 4.4 shows the key gas and solid material flows in the calciner subsystem, where the temperature of each stream (as well as the flowrates of calcined meal, tertiary air, and kiln gas) were determined in accordance with the conventional clinker production plant as previously studied (Williams, Yang and Nhuchhen, 2024). The objective function of the optimisation model aimed at minimising the subsystem's total annualised cost ($k_{total}$), covering both the capital expenditure (CAPEX) and operational expenditure (OPEX). The costing of the solar calciner was based on the TT option as it provides high efficiency and

low optical losses due to better sunlight exposure and reduced shading (Moumin *et al.*, 2020). Besides, calcined meal storage was adopted as a solution simpler than TES that involves intermediate fluids (molten salts) (Gonzalez, Switzerland and Flamant, 2013). Time-dependent decision variables involved the material and gas flows in this subsystem, notably the raw meal, calcined meal, kiln gas, tertiary air, and natural gas flowrates (in kg/h). More importantly, decision variables determining the sizing of key system components include the total area of the heliostats, capacities of the calciner and calcined meal storage. The cost and technical parameters of the calciner subsystem were determined based on literature (Moumin *et al.*, 2020), and by employing Aspen Plus simulations of the cement production process, respectively (see Appendix Tables B.1 – B.5).

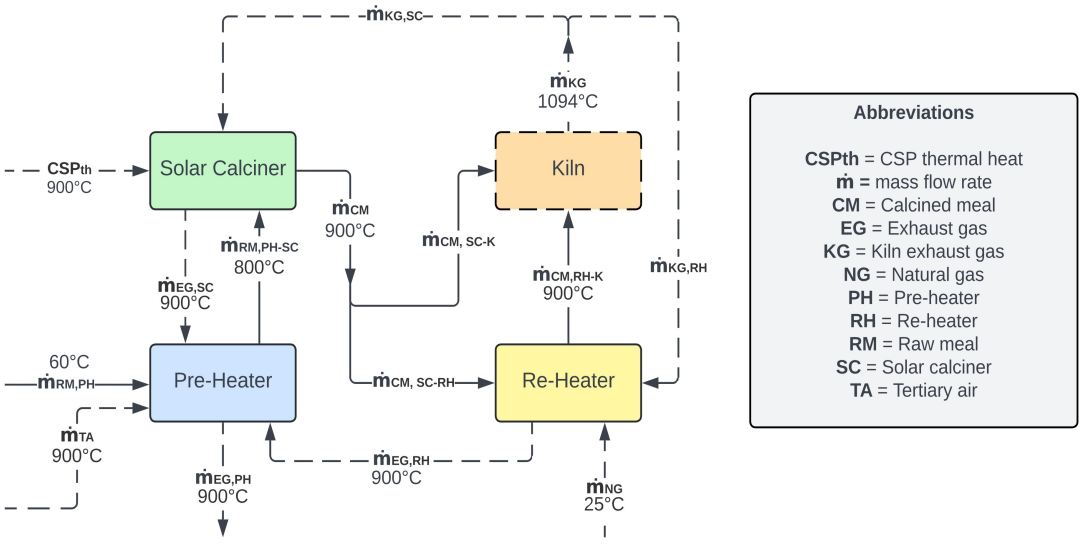


***Figure 4.4. Diagram of the calciner subsystem.*** *The material (shown in solid lines) and gas flows (shown in dashed lines) are determined by the optimisation model to minimise total annualised costs. The temperatures of the respective flows are represented in degrees Celsius. The decision variables include time dependent material and gas flows, along with the sizing of the components (modelled in GAMS), corresponding to individual hours, to collectively capture time-dependent fluctuations.*

The calciner subsystem is subjected to several constraints involving the mass and heat balance of the solar calciner system (see Equation 4.1), where $\dot{m}_{CM,SC-RH}(t)$, $\dot{m}_{CM,SC-K}(t)$, and $\dot{m}_{KG,SC}(t)$ denotes the flowrates (in kg/h) of the calcined meal in storage, calcined meal in kiln, and solar calciner kiln gas, respectively. $q_{CM,cal}(t)$ and $Q_{KG,SC}$ represents the

calcination energy demand per kg of calcined meal and solar calciner kiln gas energy in MJ/kg, where $Q_{th,SC}(t)$ denotes the calciner thermal energy output (kW). $Q_{th,SC}(t)$ is determined by Equation 4.2, as per (Moumin *et al.*, 2020), where $\eta_{SC}$ and $Q_{sol}(t)$ denotes the solar calciner (efficiency at 50% (Moumin *et al.*, 2020)), and solar incident power, respectively. As $Q_{th,SC}(t)$ is in kW, it was converted to MJ/h in Equation 4.1. The solar incident power $Q_{sol}(t)$ at time (t) is determined by Equation 4.3, where $A_{helio}$, $\eta_{helio}$, and $DNI(t)$, denote the heliostat reflective area (decision variable), heliostat field efficiency, and hourly DNI (in kW/m$^2$), respectively.

*Equation 4.1. Solar calciner mass and heat balance.*

$$(\dot{m}_{CM,SC-RH}(t) + \dot{m}_{CM,SC-K}(t)) * q_{CM,cal} \leq \left(\dot{m}_{KG,SC}(t) * Q_{KG,SC}\right) + \left(\left(\frac{Q_{th,SC}(t)}{1000}\right) * 3600\right)$$

*Equation 4.2. Calciner thermal energy output over time (t).*

$$Q_{th,SC}(t) = \eta_{SC} * Q_{sol}(t)$$

*Equation 4.3. Solar incident power subject to time (t).*

$$Q_{sol}(t) = A_{helio} * \eta_{helio} * DNI(t)$$

Further constraints involve the heat balance of the re-heater (Equation 4.4), responsible for the re-heating of calcined meal during non-daylight hours. This involves mass flows (in kg/h) of $\dot{m}_{CM,RH-K}(t)$, $\dot{m}_{KG,RH}(t)$, and $\dot{m}_{NG}$, defining calcined meal out of storage, re-heater kiln gas, and natural-gas input, respectively. $q_{RM,rhe}$ denotes the re-heating energy demand per kg of raw meal, whilst $Q_{KG,RH}$ denotes the re-heater kiln gas energy in MJ/kg. The lower heating value of natural gas is represented as $LHV_{NG}$ (with natural gas assumed to be 100% methane).

*Equation 4.4. Re-heater heat balance.*

$$\dot{m}_{CM,RH-K}(t) * q_{RM,rhe} \leq \left(\dot{m}_{KG,RH}(t) * Q_{KG,RH}\right) + (\dot{m}_{NG} * LHV_{NG})$$

Additionally, the heat balance for the raw meal pre-heater was identified as a constraint (Equation 4.5) where the solar calciner, pre-heater and re-heater subsystems are denoted as SC, PH, and RH, respectively. Furthermore, $q_{RM,phe}$ denotes the pre-heating energy demand per kg of raw meal in MJ/kg. The gas flows involving kiln gas, pre-heater tertiary air (parameter shown in Table B.1), and exhaust gas are represented by KG, TA, and EG, respectively. Mass balances for the exhaust gases were calculated based on the fraction of components in the kiln gas or tertiary air ($O_2$, $N_2$, $CO_2$ and $H_2O$) and amount of each gas required to support respective combustion stages (see Appendix B, Equations (B.1) – (B.17)). The heat capacity values for various gases ($O_2$, $N_2$, $CO_2$ and $H_2O$) are denoted by $C_p$ (see Table B.4). The variable T represents the temperature of respective flows (see Table B.3). Moreover, a heat transfer feasibility constraint was placed in Equation 4.5, to ensure the exhaust temperature of $T_{EG,PH}$ is 30 °C ($\Delta\ T$) greater (to provide a heat transfer driving force (Moreira and Arrieta, 2019)) than the temperature of the raw meal input $\left(T_{RM,feed}\right)$. The exhaust gas temperatures of the solar calciner ($T_{EG,SC}$) and re-heater ($T_{EG,RH}$), were determined from Aspen Plus simulations (in conformation with the conventional clinker process) shown in Table B.3. Conversely, the pre-heater exhaust temperature ($T_{EG,PH}$) was determined from the optimisation models, providing the maximum temperature for feasible operation.

*Equation 4.5. Raw meal pre-heater heat balance.*

$$\dot{m}_{RM,PH}(t) * q_{RM,phe} = (\dot{m}_{TA}(t) * Q_{TA}) + \Big(\big(\dot{m}_{O2,exhaust,SC}(t) * Cp_{O2}\big) + \big(\dot{m}_{N2,exhaust,SC}(t) * Cp_{N2}\big) + \big(\dot{m}_{CO2,exhaust,SC}(t) * Cp_{CO2}\big) + \big(\dot{m}_{H2O,exhaust,SC}(\mathrm{t}) * Cp_{H2O}\big)\Big) * T_{EG,SC} + \Big(\big(\dot{m}_{O2,exhaust,RH}(t) * Cp_{O2}\big) + \big(\dot{m}_{N2,exhaust,RH}(t) * Cp_{N2}\big) + \big(\dot{m}_{CO2,exhaust,RH}(t) * Cp_{CO2}\big) + \big(\dot{m}_{H2O,exhaust,RH}(t) * Cp_{H2O}\big)\Big) * T_{EG,RH} - \Big(\big(\dot{m}_{O2,exhaust,PH}(t) * Cp_{O2}\big) + \big(\dot{m}_{N2,exhaust,PH}(t) * Cp_{N2}\big) + \big(\dot{m}_{CO2,exhaust,PH}(t) * Cp_{CO2}\big) + \big(\dot{m}_{H2O,exhaust,PH}(t) * Cp_{H2O}\big)\Big) * T_{EG,PH};\ T_{EG,PH} \geq \dot{m}_{RM,PH}\ \Delta T + \Delta T$$

The mass balances of the solid and gas flows in the calciner subsystem (see Figure 4.4), are listed in the following Equations (4.6) – (4.10), where Equation 4.6 governs the total amount of calcined meal entering the kiln at a given time $\dot{m}_{CM,total}$(t) (parameter shown in Table B.1). The total amount of kiln gas ($\dot{m}_{KG,total}$(t)), is equal to the sum of the solar calciner ($\dot{m}_{KG,SC}(t)$) and re-heater kiln ($\dot{m}_{KG,RH}(t)$) gases, respectively (see Equation 4.7 and Table B.1 for parameter).

*Equation 4.6. Mass flow of calcined meal to kiln subject to time (t).*

$$\dot{m}_{CM,SC-K}(t) + \dot{m}_{CM,RH-K}(t) = \dot{m}_{CM,total}(\mathrm{t})$$

*Equation 4.7. Mass flow of kiln gas over time (t).*

$$\dot{m}_{KG,SC}(t) + \dot{m}_{KG,RH}(t) = \dot{m}_{KG,total}(t)$$

The conversion of raw meal to calcined meal is depicted in Equation 4.8 where $\dot{m}_{RM,PH}(t)$ denotes the amount of raw meal input in kg/h, and $Conversion_{RM-CM}$ represents the conversion from raw meal to calcined meal, fixed at 0.668. Equation 4.9 ensures that the $O_2$ content in the kiln exhaust gas (determined by the $O_2$ mass fraction, $O_{2fraction}$) is sufficient for the combustion of natural gas in the re-heater according to the required natural gas to $O_2$ mass ratio, $r_{NG,O2}$ which was taken as 4.

*Equation 4.8. Raw meal to calcined meal conversion.*

$$\dot{m}_{CM,SC-K}(t) + \dot{m}_{CM,SC-RH}(t) = (Conversion_{RM-CM}) * \dot{m}_{RM,PH}(t)$$

*Equation 4.9. Re-heater kiln gas over time (t).*

$$\dot{m}_{KG,RH}(t) * O_{2,fraction} \geq r_{NG,O2} * \dot{m}_{NG}(t)$$

Equation 4.10 denotes an equality constraint where, over a year, the sum of the calcined meal fed into the storage $\left(\dot{m}_{CM,SC-RH}\right)$ is equal to that of the calcined meal output from the storage $\left(\dot{m}_{CM,RH-K}\right)$.

*Equation 4.10. Equality constraint.*

$$\sum\left(\dot{m}_{CM,SC-RH}(t), t = 1\ to\ 8760\right) = \sum\left(\dot{m}_{CM,RH-K}(t), t = 1\ to\ 8760\right)$$

The objection function from the annualised cost constraint (Equation 4.13), involving both the capital expenditure (CAPEX) and operational expenditure (OPEX) is denoted as $k_{annual,total}$. The CAPEX costs of the calciner subsystem (Equation 4.11) involves the compound parabolic concentrator (CPC, a device needed to facilitate the solar calciner), solar calciner (SC), storage, heliostats, and solar tower were represented as $k_{cpc}$, $k_{SC,CAPEX}$, $k_{storage,CAPEX}$, $k_{heliostats}$, and $k_{tower}$, respectively (see Table B.5), along with the annualisation factor as $annual_{factor}$ (see Appendix Equation B.20). The OPEX costs were taken to be 2% of the CAPEX (a standard assumption in solar thermal based techno-economic analyses) (see Equation 4.12) as per (Moumin *et al.*, 2020), plus the natural gas costs ($k_{NG,OPEX}$). It is worth noting that the actual cost (although the influence is expected to be minute) may deviate from this simplifying treatment, given the nature of a solar energy driven system where the cost is dominated by the capital investment due to the unnecessity of operating with fuels.

Within the subsystem, the solar calciner's capacity ($Cap_{SC}$) in Equation 4.14 defines the maximum amount of calcined meal that can be stored and is thus equivalent to the maximum input of raw meal over 1 – 8760 hours. The calcined meal storage over time (t) ($Storage_{CM}$(t)) in Equation 4.15 is determined by the difference between the sum of the calcined meal in minus the sum of the calcined meal out at a given time (t). The storage capacity (Equation 4.16) is then assessed by the peak value minus the valley of $Storage_{CM}$(t) over 1 – 8760 hours.

*Equation 4.11. CAPEX of the solar calciner subsystem.*

$$k_{CAPEX,total} = (\left(\left(CSP_{th} * k_{cpc,variable}\right) + k_{cpc,fixed}\right) + \left(k_{SC_{CAPEX}} * Cap_{SC} * 24\right) + \left(k_{storage,CAPEX} * Cap_{storage} * q_{CM,cal}\right) + (k_{heliostats} * A_{helio}) + k_{tower}) * annual_{factor}$$

*Equation 4.12. OPEX of the solar calciner subsystem.*

$$k_{OPEX,total} = (k_{CAPEX,total} * 0.02) + (k_{NG,OPEX} * CM_{RH})$$

*Equation 4.13. Objective function of the solar calciner subsystem.*

$$k_{annual,total} = k_{CAPEX,total} + k_{OPEX,total}$$

*Equation 4.14. Solar calciner capacity.*

$$Cap_{SC} = \max(\dot{m}_{RM,PH}(t), t = 1\ to\ 8760)$$

*Equation 4.15. Calcined meal storage over time (t).*

$$Storage_{CM}(\mathrm{t}) = \sum\left(\dot{m}_{CM,SC-RH}(t'), t' = 1\ to\ t\right) - \sum\left(\dot{m}_{CM,RH-K}(t'), t' = 1\ to\ t\right)$$

*Equation 4.16. Storage capacity.*

$$Cap_{storage} = max(Storage_{CM}(t), t = 1\ to\ 8760) - min(Storage_{CM}(t), t = 1\ to\ 8760)$$

The energy consumed from natural gas ($Q_{NG}$) in the solar driven process for calcination is obtained from Equation 4.17 where $NG_{flow}$ is determined from the optimisation model where $NG_{energy}$ is per (Commission, 2023), (see Table B.2). This was compared to the

energy demand from natural gas consumption for calcination in the conventional process, given in (Williams, Yang and Nhuchhen, 2024).

*Equation 4.17. Energy consumed by natural gas.*

$$Q_{NG} = NG_{flow} * NG_{energy}$$

### 4.2.3. Optimisation model for the kiln subsystem

The purpose of the plasma generator is to provide a hot air stream at 453.45 kg/hour and 3470 ˚C, determined by Aspen plus simulation of the kiln for sufficient heat provision for producing clinker at 1 tonne/hour. The plasma generator is to be powered by constant electricity input supplied by a combination of direct power input from solar PV and electricity retrieved from Li-ion battery-based storage. The objective function in the kiln subsystem aimed at minimising the total annualised costs for replacing natural gas combustion with the generation of plasma gas ($k_{PV,total}$), influenced by the decision variables (shown in Figure 4.5), and given cost parameters for PV and battery storage (International Renewable Energy Agency, 2017; Renewable Energy Agency, 2023). The decision variables that correspond to energy flows (in kW) includes the PV electricity input ($P_g$), direct energy to the plasma generator ($P_{d,d}$), energy into storage ($P_{s,in}$), energy out of storage (to the plasma generator) ($P_{s,out}$), all respective of time (t) (see Figure 4.5). Additionally, decision variables involving the battery storage capacity ($C_{battery,storage}$) and PV capacity ($C_{pv}$) were defined.

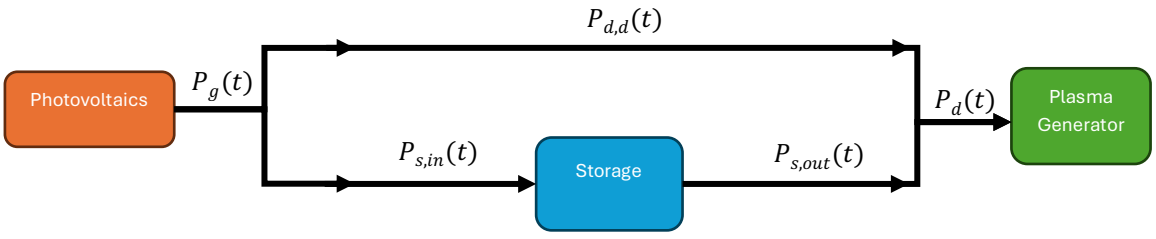


***Figure 4.5. Diagram of the kiln subsystem.***

Assuming an electricity conversion efficiency of 0.85 (Quevedo Parra and Romano, 2023), Aspen simulation determined a power demand by the plasma generator of 621.91 kW ($P_d$). This was set as the sum of the direct energy to the plasma generator ($P_{d,d}(t)$) and electricity drawn from storage ($P_{s,out}(t)$) (see Equation 4.18 and Figure 4.5). The PV electricity generation ($P_g(t)$) needs to be no less than the sum of $P_{d,d}(t)$ and power input to storage, $P_{s,in}(t)$ (see Equation 4.19). $P_g(t)$ is quantified by the installed PV capacity ($C_{pv}$) multiplied by the hourly (location-dependent) PV capacity factor ($a(t)$), as per Equation 4.20. Finally, the storage inputs and outputs were balanced by Equation 4.21 where $\eta_{battery}$ is the round-trip efficiency of the battery storage.

*Equation 4.18. Energy supply to the kiln over time (t).*

$$P_d(t) = P_{d,d}(t) + P_{s,out}(t)$$

*Equation 4.19. Energy supply from plasma gas.*

$$P_g(t) \geq P_{d,d}(t) + P_{s,in}(t)$$

*Equation 4.20. Energy supply from plasma gas.*

$$P_g(t) = C_{pv} * a(t)$$

*Equation 4.21. Storage input and output balance.*

$$\sum\left(P_{s,in}(t), t\right) = \sum\left(P_{s,out}(t), t\right)/\eta_{battery}$$

The total cost is derived from the sum of the costs of the PV and storage capacity (see Equation 4.22). The cost parameters in the kiln subsystem, namely the costs of the PV system ($k_{pv}$) and PV battery storage ($k_{battery}$) were obtained from International Renewable Energy Agency (IRENA) (International Renewable Energy Agency, 2017; Renewable Energy Agency, 2023), which were then annualised according to Appendix Equation B.20 (see Table B.5). The typical cost of the plasma generator, which is size dependent, ranges from ~1,230 – 4,180 USD/kWh when supported by grid electricity (Quevedo Parra and Romano, 2023). However, due to the lack of data on the costs associated with solar based

plasma generators, plasma generator costs are not included in this study. The electricity storage level over time (t) ($Storage_{elec}(t)$) is determined according to Equation 4.23. The battery storage efficiency is shown in Table B.5 as per (Sepúlveda *et al.*, 2023). The electricity storage capacity is then assessed by the peak value minus the valley of $Storage_{elec}(t)$ over 1 – 8760 hours, corresponding to the highest and lowest level of stored energy, respectively (see Equation 4.24):

*Equation 4.22. Total cost constraint of the kiln subsystem.*

$$T_{cost} = \left(C_{pv} * k_{pv}\right) + (C_{elec,storage} * \ k_{battery})$$

*Equation 4.23. Electricity storage over time (t).*

$$Storage_{elec}(t) = \sum\left(P_{s,in}(t'), t' = 1\ to\ t\right) - \frac{\sum\left(P_{s,out}(t'), t' = 1\ to\ t\right)}{\eta_{battery}}$$

*Equation 4.24. Electricity storage capacity.*

$$C_{elec,storage} = \max(Storage_{elec}(t), t = 1\ to\ 8760) - \min(Storage_{elec}(t), t = 1\ to\ 8760)$$

### 4.2.4. Performance comparison between solar-driven and conventional systems

The mass and energy flows along with the $CO_2$ emissions of the conventional system were quantified through process simulation in Aspen Plus as reported earlier (Williams, Yang and Nhuchhen, 2024). The Aspen simulation was then adapted to support the assessment of the solar-driven system, where the natural gas combustor in the kiln subsystem was replaced by plasma gas assumed to be generated using electricity from solar PV. Simulation models ensured that key process temperatures (such as the sintering temperature and the kiln exhaust gas temperature) are preserved, and that the resulting clinker maintains the expected mass flow and chemical compositions, including tricalcium silicate ($C_3S$), dicalcium silicate

($C_2S$), tricalcium aluminate ($C_3A$), and tetra-calcium aluminoferrite ($C_4AF$), within the specified range (Williams, Yang and Nhuchhen, 2024). Details of the Aspen Plus flowsheet are presented in Appendix Table B.1.

The retrofitted process and the conventional process were firstly compared in fuel-derived carbon emissions. $CO_2$ produced by the solar driven process was assumed to be zero from fuel use, with the exception of the natural gas required to re-heat the calcined meal during non-daylight hours. The reduction in natural gas use derived $CO_2$ emissions ($\dot{m}_{CO2,reduced}$) achieved by the solar-driven process was calculated by Equation 4.25.

*Equation 4.25. Reduction in $CO_2$ produced.*

$$\dot{m}_{CO2,reduced} = \dot{m}_{CO2,conventional} - \dot{m}_{CO2,solar}$$

$\dot{m}_{CO2,conventional}$ and $\dot{m}_{CO2,solar}$ denotes the amount of $CO_2$ (in kg/t clinker) from natural gas used in the conventional process and solar-driven processes and were determined by the previously established Aspen simulation (Williams, Yang and Nhuchhen, 2024), and the natural gas consumption suggested by the optimisation model, respectively. This study quantifies the direct $CO_2$ emissions from the use of natural gas within the clinker production plant; emissions arising from the supply chain of natural gas were not included.

Additionally, the total retrofitting cost to introduce the solar-driven processes, including the costs of the calciner ($k_{annual}$) and kiln subsystems ($T_{cost}$), was determined as per Section 4.2, normalised on a per tonne of clinker basis. To facilitate the understanding of the economic implications, the levelised costs for "fuel" supply of the retrofitted and the conventional plants, with and without carbon capture, were compared at a range of natural gas prices. Natural gas prices were varied from 5 – 100 USD/t clinker. To include natural gas consumption for $CO_2$ capture, natural gas demand (at a lower heating value of 50 MJ/kg

(Wan, 2004)) for carbon capture was taken at 3.8 MJ/kg of $CO_2$ with reference to an amine-based absorption process (Voldsund *et al.*, 2019). As the focus of this assessment was on fuel consumption, the potential savings by the retrofitted system on electricity consumption by the $CO_2$ capture process was not included.

## 4.3. Results and discussion

### 4.3.1. Optimal design of the calciner subsystem

The optimal sizing of the key components of the calciner subsystem is shown in Table 4.2. For a plant producing clinker at 1 tonne/hour, the nominal capacity of the calciner is ~1.54 tonne raw meal/hour. Even facilitated by the calcined meal storage, the solar calciners in all locations needed to be significantly oversized to between 6.25 (BR) and 13.26 (CN) tonne raw meal/hour, to cope with the intermittent solar energy supply; the heliostat area and hence the CSP capacity were sized accordingly. Among the three locations, the BR site is the clear winner with the lowest capacities (including calciner, calcined meal storage and heliostat/CSP). This was attributed to the fact that it experienced higher annual average (0.249 kW/m$^2$) and least fluctuating solar DNI values throughout the entire year in contrast with the US and CN sites (see Figure 4.3), thanks to Brazil's tropical climate and proximity to the equator. On the other hand, the CN site had the lowest annual average DNI value (0.155 kW/m$^2$) with most significant fluctuation, leading to the need for increased calciner and calcined meal storage capacities, to capture more energy and store more calcined meal for non-daylight hours, respectively. The DNI quality of the US site falls in between the BR and CN sites, hence the capacities of its key components.

***Table 4.2. Calciner capacities and heliostat field area.*** *The capacity of the calciner and calcined meal storage capacities (in tonnes) are shown along with the CSP size and heliostat field areas for each respective country (including US, CN, and BR).*

| | Country | Value | Unit |
|---|---|---|---|
| **Heliostat field area** | United States | 9,217.39 | $m^2$ |
| | China | 12,649.52 | $m^2$ |
| | Brazil | 4,723.51 | $m^2$ |
| **Calciner capacity** | United States | 10.23 | tonne raw meal/hour |
| | China | 13.26 | tonne raw meal/hour |
| | Brazil | 6.25 | tonne raw meal/hour |
| **Calcined meal storage capacity** | United States | 147.58 | tonne |
| | China | 220.97 | tonne |
| | Brazil | 83.31 | tonne |
| **Concentrated solar power size, $CSP_{th}$** | United States | 6.41 | MW |
| | China | 8.26 | MW |
| | Brazil | 3.19 | MW |

The optimal sizing for each site was accompanied by optimised hourly material and energy flows driven by DNI to produce the fixed output of ~1.03 tonne calcined meal/hour. Figure 4.6 shows hourly flows during a typical day on the site located in the US. The mass flow rates of $\dot{m}_{RM,ph}$, $\dot{m}_{CM,sc-k}$, and $\dot{m}_{CM,sc-rh}$ increase along with the DNI. This suggests an over-production of calcined meal during daylight hours, which is subsequently utilised during night-time operations. During this period, the majority, if not all of the calcined meal required in the kiln is directly from the calciner. Conversely, $\dot{m}_{CM,rh-k}$, $\dot{m}_{NG}$, and $\dot{m}_{KG,rh}$, exhibits an inverse trend to the DNI, as these flows are predominantly active during periods

characterised by low to no solar irradiation, specifically from 0:00 (midnight) to 08:00 and again from 16:00 to 24:00. During this period, calcined meal is retrieved from the storage, and heating through natural gas is required to reach the calcined meal temperature of 900 °C. In contrast, the flow rate of $\dot{m}_{KG,sc}$ is fairly constant throughout the entire day, with only a marginal reduction by ~6% during periods of low to no sunshine, for $\dot{m}_{KG,rh}$ to support natural gas combustion.

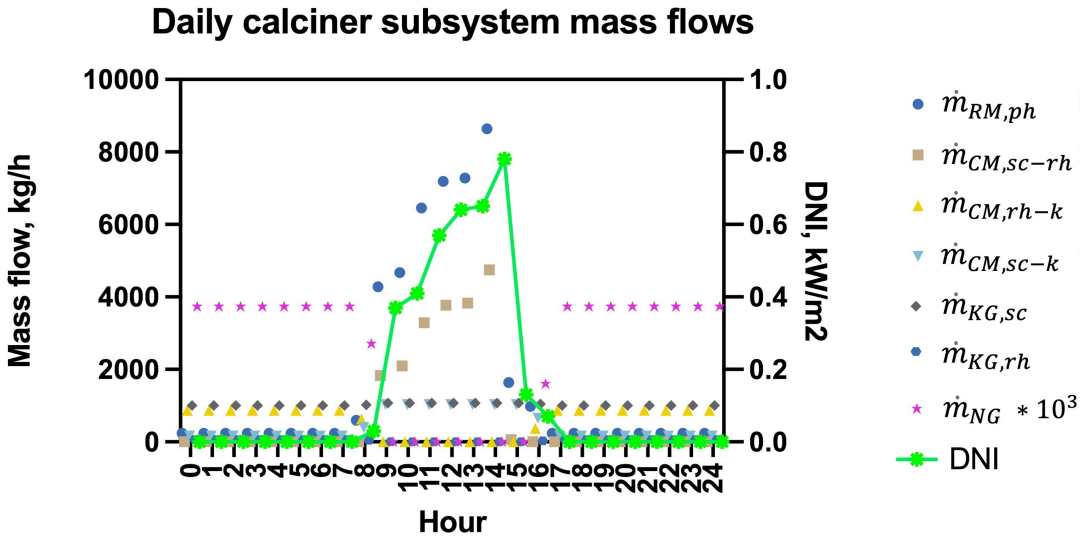


***Figure 4.6. Calciner subsystem daily mass flows.*** *Daily mass flow values of the materials (including $\dot{m}_{RM,ph}$, $\dot{m}_{CM,sc-rh}$, $\dot{m}_{CM,rh-k}$, and $\dot{m}_{CM,sc-k}$) and gases (including $\dot{m}_{KG,sc}$, $\dot{m}_{KG,rh}$, and $\dot{m}_{NG}$) are derived from hourly values (from the calciner optimisation model), with the hours ranging from 0 – 24, displayed in the x-axis. The natural gas flow ($\dot{m}_{NG}$) was scaled to $10^3$. The y-axes display the mass flows (in kg/h) and DNI(t). This was respective of the reference site in the United States (US).*

### 4.3.2. Optimal design of the kiln subsystem

The optimal sizing of the retrofitted kiln subsystem involves PV and battery storage which collectively need to meet the constant power demand of the plasma generator at ~0.62 MW. As shown in Table 4.3, the significant oversizing observed earlier with the calciner subsystem also manifests here, with the PV capacity of the three locations ranging from 6.03 MW (BR) to 15.03 MW (US). This is accompanied by significant battery storage capacities

between 14.21 MWh (BR) and 23.05 (CN). Dictated by the PV capacity factor data, the BR site is again the best location and significantly outperforms the other two sites, thanks to its high and consistent PV capacity factors across the year.

***Table 4.3. Kiln subsystem PV and electricity storage capacities.*** *The total capacities associated with energy in the respective sites located in three countries (US, CN, and BR) are represented, where the key contributors are the PV capacity and electricity storage.*

| Capacities | United States | China | Brazil | Unit |
|---|---|---|---|---|
| Kiln Electricity Storage | 19.54 | 23.05 | 14.21 | MWh |
| Kiln PV Capacity | 15.03 | 10.07 | 6.03 | MW |

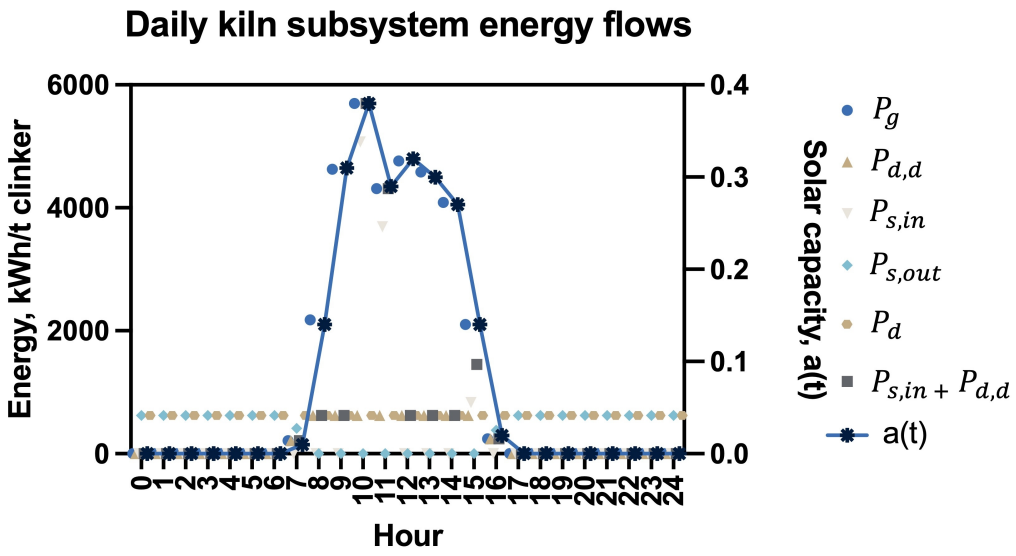


***Figure 4.7. Kiln subsystem hourly energy flows.*** *Hourly flow data from the kiln optimisation model is averaged and grouped into hours ranging from 0 – 24 hours, represented in the x-axis of the figure, where the energy (in kWh/t clinker), and PV capacity factor (a(t)) from Renewables Ninja are represented in the y-axes. The PV electricity input, energy demand, and direct energy to the plasma generator are represented as $P_g$, $P_d$, and $P_{d,d}$, respectively. $P_{s,in}$ and $P_{s,out}$ represents the energy into storage and energy out of storage, respectively. Utilised power is represented as $P_{d,d} + P_{s,in}$.*

In terms of the detailed behaviour of this subsystem under optimised conditions, Figure 4.7 shows how the power flows are driven by the PV capacity factor on an hourly basis for a typical day on the US site. As expected, PV power generation ($P_g$) basically follows the PV capacity factor (a) during the daylight times. The constant energy demand ($P_d$) is fully met by direct supply from PV ($P_{d,d}$) throughout the hours of 08:00 – 15:00 (during periods of

high solar irradiance). During this period, part of the surplus electricity is sent to storage ($P_{s,in}$) which increases in parallel with the solar irradiance. In hours with low or no PV output, electricity is withdrawn from storage ($P_{s,out}$). From the huge gap between PV power generation ($P_g$) and the utilised power ($P_{d,d}$+$P_{s,in}$), one can see significant power curtailment, which is dictated by the economics of power supply (see Section 4.3.3 for further details).

### 4.3.3. Costs of the solar-driven processes

Here, the economic assessment of the calciner and kiln subsystems are presented, where both subsystems provide solar based energy; CSP for the calciner and PV for the kiln, and when combined provide an integrated system for continuous renewable energy. The costs in the calciner subsystem (retrofitting) were conducted across three distinct sites, involving both the annualised CAPEX and OPEX. It is worth noting that as the DNI increases, the OPEX decreases since less calcined meal is reheated during low to non-daylight hours. As shown in Figure 4.8a, the contributors to the costs of the calciner subsystem include the solar calciner, calcined meal storage, and the CSP components (heliostats, tower and CPC). The heliostats and storage costs are collectively responsible for ~57% of the total costs, with heliostats alone accounting for over 35%, relatively consistently amongst all sites. In contrast, the cost of the solar calciner is rather insignificant. Among the analysed sites, BR emerged as the most cost-effective location, as a direct result of reduced capacities of calcined meal storage and the $CSP$ components (shown in Table 4.2). Conversely, China exhibited the highest costs.

The costs associated with the kiln subsystem (retrofitting) across the three sites are shown in Figure 4.8b. Again, the BR site was identified as the most cost-effective location, followed by CN, while the US site incurred the highest costs. These cost comparisons are dictated by the sizing of PV and battery storage (shown in Table 4.3) and their unit costs. Between the CN and US sites, whilst the annual average PV capacity factor was slightly higher (by ~3%) at the US site, its higher standard deviation (at hourly resolution) (by ~6%) increased the electricity storage capacity (by ~18%), resulting in a higher total cost from greater daily variability in solar irradiation. In terms of the total costs for the solar-driven solution with both subsystems, Brazil is the most cost effective at 126.07 USD/t clinker, followed by China at 217.95 USD/t clinker, with the United States holding the highest costs at 238.48 USD/t clinker. The kiln subsystem incurs a higher cost compared to the calciner subsystem due to the higher costs of the kiln subsystem components (PV) relative to the components of the calciner subsystem (CSP) (as per Appendix B, Table B.5).

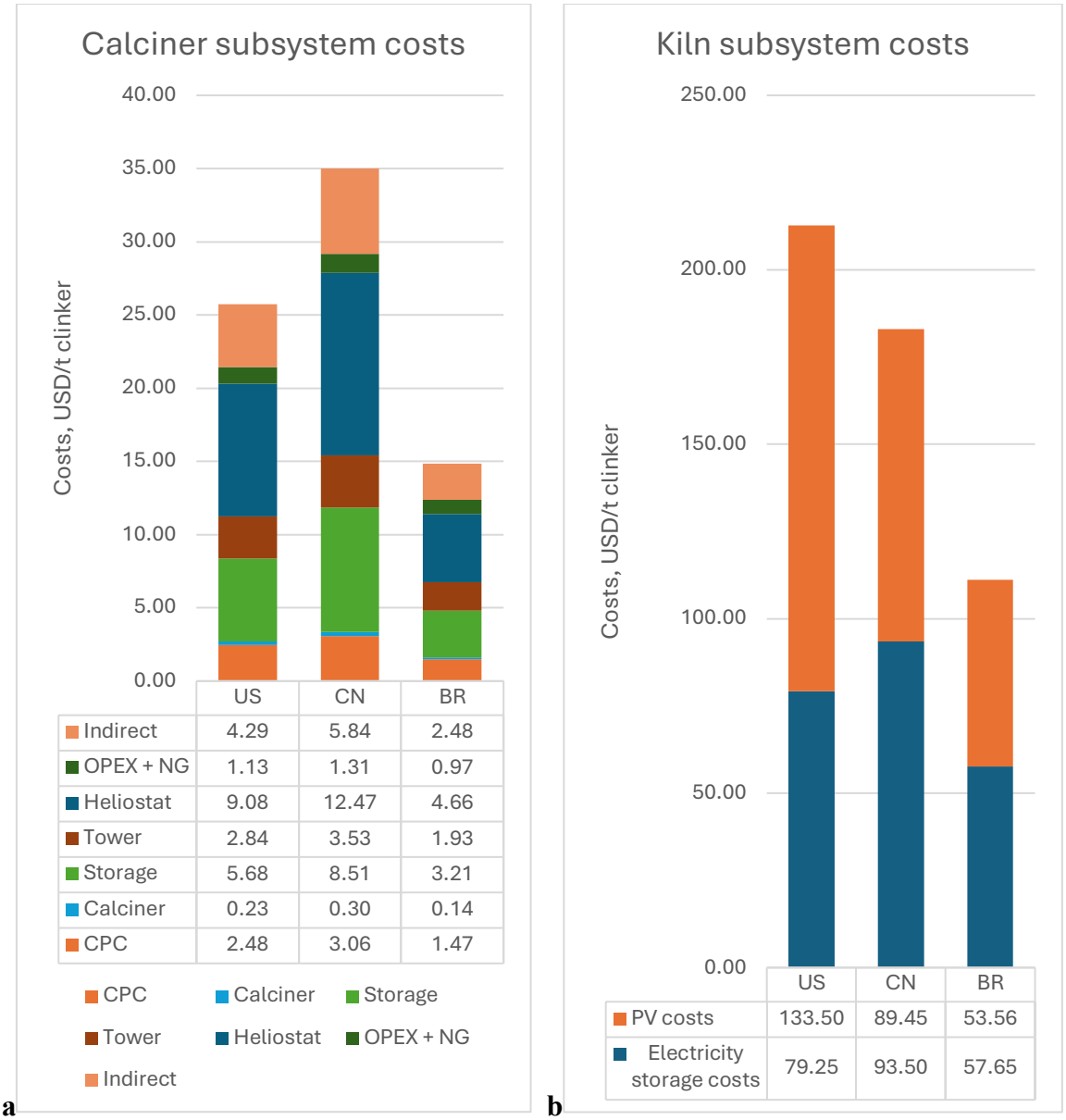


***Figure 4.8. Calciner and kiln subsystem economics.*** *The levelised cost of clinker production (in USD/t clinker) of the solar driven calciner and kiln subsystems in three distinct sites (including US, CN, and BR) are displayed for the year 2020. The key cost contributors in the calciner involve the solar calciner, calcined meal storage, tower, heliostats, CPC, natural gas, operational costs (OPEX), and indirect costs. In contrast, the key cost contributors in the kiln consist of the PV and the electricity storage.*

It is worth mentioning that the cost of the calciner subsystem, although a relatively minor fraction of the total cost, is heavily affected by the thermal energy efficiency of the solar calciner. A sensitivity analysis (Table 4.4) shows that the economic results vary against variations of the three solar calciner efficiencies ($\eta_{sc}$), at 50% (reference efficiency), 65% and 86%. An increase in $\eta_{sc}$, resulted in the decrease of the total costs, predominantly from less energy losses in the reactor and thus requiring significantly less energy input from

heliostats. Here, the findings suggest that an increased reactor efficiency is key to lowering economical costs associated with the solar calciner subsystem and cost reductions of up to ~26% can be achieved.

***Table 4.4. Sensitivity analysis of calciner subsystem.*** *The economic impact and capacity variances of three calciner reactor efficiencies (including 50%, 65%, and 86%) are presented for the reference country (i.e., United States).*

| Reactor Efficiency | 50% | 65% | 86% | Unit |
|---|---|---|---|---|
| **Compound Parabolic Concentrator Cost** | 2.48 | 2.02 | 1.64 | USD/t clinker |
| **Calciner Cost** | 0.23 | 0.23 | 0.22 | USD/t clinker |
| **Storage Cost** | 5.68 | 5.68 | 5.68 | USD/t clinker |
| **Tower Cost** | 2.84 | 2.41 | 2.06 | USD/t clinker |
| **Heliostat Cost** | 9.08 | 6.99 | 5.29 | USD/t clinker |
| **OPEX + Natural Gas Cost** | 1.13 | 1.07 | 1.02 | USD/t clinker |
| **Indirect Cost** | 4.29 | 3.68 | 3.18 | USD/t clinker |
| **Total Cost** | 25.73 | 22.07 | 19.09 | USD/t clinker |

***Table 4.5. Sensitivity analysis of the kiln subsystem.*** *The economic impact across three kiln efficiencies (including 85%, 90%, and 86%) are presented for the reference country (i.e., United States).*

| Kiln Efficiency | 85% | 90% | 95% |
|---|---|---|---|
| Electricity storage costs, USD/t clinker | 79.25 | 74.84 | 70.91 |
| Photovoltaics costs, USD/t clinker | 133.50 | 126.04 | 119.47 |
| Total costs, USD/t clinker | 212.75 | 200.89 | 190.37 |

On the side of the kiln subsystem, its cost is similarly impacted by the efficiency of the plasma generator ($\eta_k$). As shown in the sensitivity analysis in Table 4.5, increasing it from

the base case of 85% (adopted from (Quevedo Parra and Romano, 2023)) to 90% and 95% leads to notable reductions in the total subsystem cost of up to ~11%, including those for electricity storage and PV.

### 4.3.4. Natural gas consumption and $CO_2$ emissions

As the first aspect of comparison between the solar-driven retrofitted system and the conventional system for clinker production, Table 4.6 shows natural gas consumption and $CO_2$ emissions arising from it.

***Table 4.6. Comparison of the natural gas consumption and the corresponding $CO_2$ emissions.***

| | **Conventional process** | **Solar driven process** | | | **Unit** |
|---|---|---|---|---|---|
| | | United States | China | Brazil | |
| **Natural gas consumption** | 74.49 | 2.28 | 2.37 | 2.34 | kg/t clinker |
| **$CO_2$ from natural gas consumption** | 204.86 | 6.27 | 6.53 | 6.44 | kg$CO_2$/t clinker |

One can see a considerable reduction of ~97% in fuel (natural-gas) related $CO_2$ emissions in the solar driven clinker process compared to the conventional (fossil-based) process (Williams, Yang and Nhuchhen, 2024), amongst all sites. This is a direct result of the substantially reduced natural gas demand (averaging at 2.33 kg/t clinker among the three sites) in the solar driven process in contrast to the conventional process (at 74.49 kg/t clinker). The conventional process primarily relies on natural gas as fuel to support combustion in calcination and kiln operations. In contrast, the solar driven process minimises the reliance on natural gas, using it only for re-heating the calcined meal from 700 °C to 900 °C during low or non-solar hours. Our previous work (Williams, Yang and

Nhuchhen, 2024), indicated that the conventional clinker process produces in total 771.82 kg $CO_2$/t clinker. Assuming that the $CO_2$ from calcination remains unchanged, the solar driven process offers a reduction in total $CO_2$ emissions of ~26%.

### 4.3.5. Market competitiveness and future achievable trends

From Section 4.3.3, a levelised retrofitting cost between 126.07 – 238.48 USD/t clinker is incurred for replacing natural gas combustion-based heating with (primarily) solar-driven options, depending on the location.

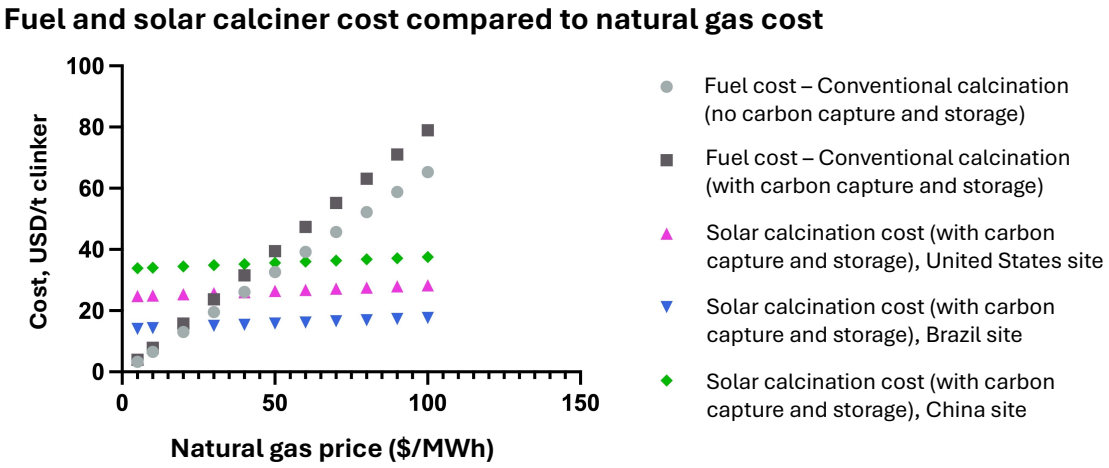


***Figure 4.9. Fuel and solar calciner costs responding to changes in natural gas price.*** *The solar calcination costs without carbon capture and storage (CCS) are slightly lower than those with CCS and are not shown.*

Understandably, the economic competitiveness of the retrofitted system depends on the cost of natural gas supply. Here, the cost of heating conventional calcination was compared to that of solar calcination over natural gas prices ranging from 5 to 100 USD/MWh, with or without $CO_2$ capture. As shown in Figure 4.9, the solar calciner subsystem costs across the three sites remain largely unaffected by the increase in the natural gas price due to the minimal consumption for re-heating stored calcined meal. In contrast, the heating cost of conventional calcination increases linearly with the natural gas price, hence showing

significant vulnerability of price spikes on the international market. While the solar calciner is more costly when the natural gas price is very low, its implementation at the BR site starts to be competitive when natural gas reaches 30 USD/MWh; it can be economically attractive when natural gas price exceeds 50 USD/MWh.

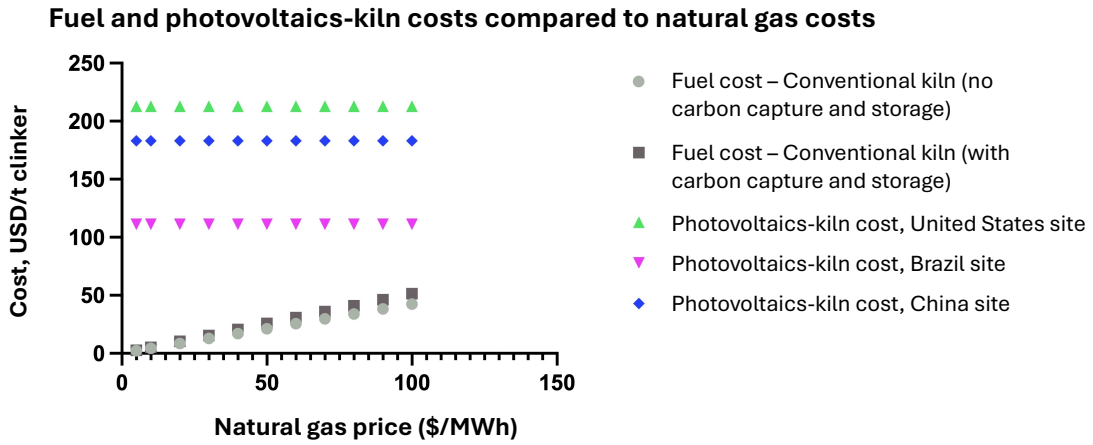


***Figure 4.10. Fuel and PV kiln costs compared with fluctuations in natural gas costs.*** *Including fuel costs of the conventional kiln system with and without carbon capture and storage (CCS), and PV based kiln costs with CCS in three different sites in the US, CN, and BR.*

On the side of the kiln subsystem, the solar-driven option struggles to gain competitiveness across the whole studied range of natural gas prices, even at the optimal location (BR), as shown in Figure 4.10. This lack of attractiveness is hardly surprising, given the high costs of solar PV and battery storage. The levelised cost for electricity supply to the plasma generator (based on the costing results shown in Section 4.3.3) was 212.75 USD/MWh, 182.95 USD/MWh, and 111.21 USD/MWh for US, CN, and BR, respectively. One can see that even at the BR site, the per MWh (firm) energy cost (174 USD) is still significantly higher than the top end of the assessed natural gas price (100 USD). To improve the economics of the solar-driven kiln subsystem, a more favourable location with greater PV capacity factors and/or much reduced technology costs for PV and storage would be required.

## 4.4. Discussion

The results presented above shows that the adoption of solar driven processes in clinker production can play a key role in reducing $CO_2$ emissions, achieving reductions of ~26% through the integration of solar calcination and PV-driven plasma-based electrified kilns. This decrease in emissions is primarily attributed to the replacement of natural gas with solar energy to provide energy for process heating. Unlike previous studies that utilised grid sourced electrical energy (Quevedo Parra and Romano, 2023), this study sourced solar energy, reducing the climate change impacts associated with energy use. Furthermore, the solar driven process not only offers reductions in $CO_2$ emissions but also mitigates the release of pollutants such as sulphur dioxide ($SO_2$) and nitrogen oxides ($NO_x$), commonly emitted during the combustion of fossil fuels, which contributes to health and environmental hazards (Barbhuiya *et al.*, 2024). In addition, the availability of abundant and renewable solar energy is advantageous compared to the finite nature of fossil fuels.

The solar-powered retrofitting options considered in this work adds to other decarbonisation options for clinker production and may be adopted in combination with existing ones. It is evident that alternative fuels, including both the solar driven (this work) and hydrogen (Williams, Yang and Nhuchhen, 2024) options can yield comparable $CO_2$ reductions of 26%, primarily due to both options replacing natural gas by up to 100%. Alternatively, the use of alternative clinkers, when product properties are not compromised, could achieve up to 35% $CO_2$ savings from the mitigation of emissions related to limestone calcination (Williams and Yang, 2024). In contrast, the utilisation of supplementary cementitious materials (SCMs) produced through $CO_2$ mineralisation can reduce $CO_2$ produced by ~45%, from replacing ~25% of clinker and reuse of captured $CO_2$ (Williams and Yang, 2024). Finally, carbon

capture and storage (CCS) with technologies such as anime-based capture (Jiang *et al.*, 2024) and calcium looping (Lena, Spinelli and Romano, 2018) could further minimise $CO_2$ emissions from cement production.

The techno-economics of the solar calciner across the studied sites ranged from 14.85 – 35.01 USD/t clinker, aligning closely with literature reported values for solar calcination at 13.60 – 22.05 USD/t clinker (González and Flamant, 2014; Moumin *et al.*, 2020; Sahoo, Kumar and Samsher, 2023). To the authors' knowledge, a PV-based kiln coupled with a plasma generator has not been assessed previously. Economically, these retrofits will have to complete with the conventional system. Higher fossil fuel prices, along with policy instruments such as carbon taxes and credits (Barbhuiya *et al.*, 2024), would make the former more attractive, but cost reduction in the technical components in the solar-driven solution is much needed. Notably, global average prices for solar PV have experienced significant cost reductions by 4.2-fold over the last decade (Timilsina, 2021), with the levelised costs of electricity dropping by ~40% in 2024, compared to 2018 (International Energy Agency, 2023). Similarly, capital costs for CSP systems have fallen by ~50% in the last decade and expected to achieve further reductions of ~40% by 2030, with the levelised costs of electricity decreasing by 68% comparing 2010 and 2022 levels (Khan *et al.*, 2024). Both PV and CSP based solar energy are projected to achieve further cost reductions through 2050 (Hernández-Moro and Martínez-Duart, 2013), exhibiting promising signs of economic competitiveness in the long-term. While technological cost reduction is progressing, favourable locations with high quality of renewable energy available, such as the BR site studied in this work, holding potential to host early economically viable adoptions.

As a final note, this work has focused on replacing fossil fuel-based process heating, without considering the electricity demand for fans and auxiliary systems. In a typical cement plant,

this untrivial demand is ~0.23 MWh/tonne of clinker (Williams, Yang and Nhuchhen, 2024); supplying this demand from a poorly decarbonised grid constitutes part of the carbon footprint of cement production. Future work could expand the scope by incorporating electricity demand in the optimal design of renewables-based energy supply.

## 4.5. Conclusions

Through a combined use of process simulation and optimisation modelling, this study explores the feasibility of retrofitting an existing fossil fuel dependent clinker plant with solar calcination and PV-powered kiln electrification, to reduce $CO_2$ emissions. The results show that these retrofitting measures can reduce the consumption of fuel combustion by ~97% and achieve ~26% reduction in the total $CO_2$ emissions of a national gas-powered clinker plant. Location dependent analysis underscores the economic advantages of locating solar driven processes in regions with high solar energy quality. In terms of the total retrofitting cost, the site in Brazil emerged as the most cost effective at 126.07 USD/t clinker, significantly better than the site in China (217.95 USD/t clinker) and the site in the United States (238.48 USD/t clinker). Between the two subsystems, solar calcination accounts for only 10 – 20% of the total cost and can become competitive when the natural gas price exceeds 30 USD/MWh at the Brazil site and 50 USD/MWh at the other two sites. In contrast, PV-powered plasma generation is significantly more expensive due to the high electricity demand combined with the current high cost of solar based PV systems and hence requires significant cost reduction to become attractive. In future work, research should explore more cost-effective options for kiln electrification powered by clean energy, possibly integrating with alternative clinkers to achieve a more markedly decreased carbon footprint of clinker production.

# Chapter 5. Potential of reducing $CO_2$ emissions in cement production through altering clinker compositions

## Summary

This chapter features a published manuscript which was edited to include further clarifications: Williams, F., & Yang, A. (2024). Potential of reducing $CO_2$ emissions in cement production through altering clinker compositions. *Industrial & Engineering Chemistry Research 2024 63 (40), 17158-17167.* DOI: 10.1021/acs.iecr.4c01885. The corresponding Supplementary Information can be found in Appendix C.

Among the authors who contributed to this chapter, Franco Williams conceptualised the study involving the methodology, developed the models, analysed the results, and wrote the manuscript; Aidong Yang supported with the conceptualisation, supervision, provided feedback on the modelling, and revised the manuscript.

Whilst the first two pieces of original work address decarbonisation measures through the reduction of fuel related $CO_2$ emissions, this third chapter shifts its attention to calcination induced emissions. Notably, this chapter assesses seven cases of distinct raw material compositions with the aid of process simulation using Aspen Plus V12.1, focusing on reducing carbon dioxide emissions ($CO_2$) and energy demands from clinker production. Material and energy flows for the raw meal mixes were simulated in a natural gas-fuelled

plant. The results indicated up to 45.5% of energy, and 35.1% of $CO_2$ reduction using alternative clinkers compared to ordinary Portland cement (OPC) clinker. Calcium silicate clinker (CSC) had the lowest energy consumption and $CO_2$ emissions, resulting from raw meal limestone reduction and lowered sintering temperature. Partially replacing OPC clinker with a supplementary cementitious materials (SCMs) from $CO_2$ mineralisation reduced $CO_2$ emissions by ~45% compared to OPC. Location-dependent $CO_2$ emissions analysis revealed that Brazil yielded the least emissions compared to the United States and China. These findings underscore the imperative for cement industries to adopt alternative clinkers, coupled with SCMs, as decarbonisation measures.

## 5.1. Introduction

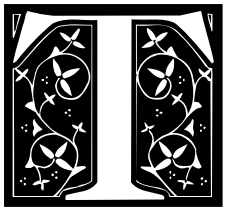

he global production of cement, the most used material in the world after water (Scrivener, John and Gartner, 2018), reached 4.4 billion tonnes in 2021 and reduced slightly to 4.1 billion tonnes in 2023 (Jaganmohan, 2024b). Cement production was responsible for 2.9 billion tonnes of $CO_2$ emissions in 2021 (Supriya *et al.*, 2023), or about 8% of global anthropogenic carbon dioxide ($CO_2$) emissions (Cormos, 2022). Towards the Net Zero targets by 2050 and aligning with the objectives established in the Paris Agreement, the World Business Council for Sustainable Development (WBCSD) has urged the cement industry to achieve 20 – 25% $CO_2$ emission reductions by 2030 (Scrivener, John and Gartner, 2018).

Most of the $CO_2$ emissions of cement production arises from the process of producing clinker, the main component of ordinary Portland cement (OPC) which accounts for 95% of cement (British Geological Survey, 2005). Clinker production involves calcination, in which

limestone is decomposed to calcium oxide and $CO_2$ (Faria *et al.*, 2022), and the subsequent operation of the kiln where clinker is formed (Cement Association, 2018). Both the calciner and the kiln require heating which represents the main energy consumption in clinker production (Williams, Yang and Nhuchhen, 2024), along with electricity for grinding raw material (known as raw meal) (Ghalandari *et al.*, 2021), driving gas flows in the production process and other auxiliary uses (Nhuchhen, Sit and Layzell, 2022a). In addition to the above-mentioned $CO_2$ production from calcination which accounts for ~60% of total emissions (Cavalett *et al.*, 2024), the combustion of fuels (predominantly coal or natural gas) in the calciner and kiln leads to about 28 – 35% of $CO_2$ emissions from clinker production (Klee, 2009; Antunes *et al.*, 2022; Williams, Yang and Nhuchhen, 2024).

To tackle $CO_2$ emissions produced from cement production, carbon capture utilisation and storage (CCUS) have been typically considered as a strategy to be applied to the flue gas of clinker production which typically contains about 20% of $CO_2$ (Baker *et al.*, 2018). CCUS has previously been reported to offer carbon capture efficiencies of 90% (Gardarsdottir *et al.*, 2019), 94% (Rolfe *et al.*, 2018), and 99.7% (Jiang *et al.*, 2024), through the use of MEA-based absorption, calcium looping, and advanced amine-based $CO_2$ capture, respectively. To aid CCUS, oxygen combustion (hereafter oxy-combustion) offers more concentrated $CO_2$ to be produced from cement flue gases (Faria *et al.*, 2022), leading to higher capture efficiencies of up to 100% (Rolfe *et al.*, 2018), and yield high-purity $CO_2$ streams, hence easing carbon capture (Guo *et al.*, 2024). Although substantial $CO_2$ emissions can be removed from the cement production process, the implementation of CCUS demands higher energy (Jiang *et al.*, 2024). While CCUS offers removal of $CO_2$ emissions from the cement production process, it does not prevent the generation of $CO_2$ but mitigates its release to the atmosphere.

Deep decarbonisation in the cement sector necessitates the transition to cleaner production by reducing both the dependency on fossil fuels (Chatterjee and Sui, 2019a), and calcination induced emissions (Cavalett *et al.*, 2024). Alternative fuels that have been considered for clinker production include hydrogen ($H_2$) (El-Emam and Gabriel, 2021; Juangsa *et al.*, 2022; Williams, Yang and Nhuchhen, 2024) and biomass (Kusuma *et al.*, 2022). Notably, a prior modelling study by (Williams, Yang and Nhuchhen, 2024) achieved $CO_2$ reductions of ~28% in contrast with the conventional fossil fuel (natural gas based) process from the combustion with $H_2$ fuel. In the industry, a report by Hanson Cement (Hanson, 2022), successfully demonstrated the replacement of fossil fuels with a combination of $H_2$, biomass, and plasma-based energy supply at Hanson's Ribblesdale plant in the United Kingdom (UK) where it saved about 180,000 tonnes of $CO_2$ annually at Ribblesdale, Lancashire. Amongst alternative fuels, biomass demonstrated climate change mitigation of up to ~30% in contrast with fossil fuels (Cavalett *et al.*, 2024). Modelling work by (Association and Ltd, 2019) demonstrated alternative fuel replacement in the kiln with 50% hydrogen and 50% biomass while 83.3% biomass and 16.7% plasma were used in the calciner, leading to removal of fuel related $CO_2$ emissions. Despite these results, fuel-oriented measures alone can only achieve a limited extent of carbon abatement, since they do not address emissions from calcination (Williams, Yang and Nhuchhen, 2024).

The raw meal of Portland clinker consists of calcium carbonate (in the form of limestone, the main source of $CO_2$), argillaceous clays (silicon), aluminium and iron, where the chemical compositions are $CaCO_3$, $SiO_2$, $Al_2O_3$, and $Fe_2O_3$ (Mikulčić *et al.*, 2016). The clinker product compositions include $C_3S$ (alite), $C_2S$ (belite), $C_3A$ (calcium aluminate), and $C_4AF$ (ferrite) (Faria *et al.*, 2022), in which $C_3S$ (alite) is the most carbon intensive component (Scrivener, John and Gartner, 2018). Targeting $CO_2$ reductions in calcination

involves the use of different clinker types deviating from the conventional OPC clinker as follows:

- Belite ye'elimite ferrite (BYF) clinker, which is produced from a raw meal with reduced limestone content (Morin *et al.*, 2017) and increased aluminate and sulfur content, leads to a product containing ye'elimite ($C_4A_3S$) (one of the main clinker phases in BYF) with higher belite and ferrite quantities, whilst in the absence of alite (Wang *et al.*, 2023). BYF also offers a reduction in the sintering temperature from the typical 1500 °C in the kiln for producing OPC clinkers to the range of 1300 to 1350 °C (Sabbah and Zhutovsky, 2022). BYF clinker displayed energy and $CO_2$ savings of 20% and 20 – 40% compared to OPC clinker, respectively (Sabbah and Zhutovsky, 2022). Ye'elimite is formed between 950 – 1000°C, where its rapidly hydrated in under 24 hours (Sabbah and Zhutovsky, 2022) with gypsum to form ettringite, contributing to the early age strength and assists with setting. Moreover, belite forms at 1050 – 1150°C, where its hydration produces calcium silicate hydrate (C–S–H), the primary component driving late strength development (Wang *et al.*, 2023). Additionally, ferrite is formed between 1150 – 1200 °C which contributes to the development of early-age and long-term mechanical properties whilst reducing the combustion temperature (Wang *et al.*, 2023). The high porosity of BYF clinkers make them easier to ground compared to OPC clinkers (Sabbah and Zhutovsky, 2022).
- High-ferrite clinker (HFC), produced from a raw meal with increased $Fe_2O_3$ content, leads to a product containing increased ferrite ($C_4AF$) content. HFC decreases the combined proportion of $C_2S$ and $C_3S$, offering a reduced sintering temperature by approximately 100 °C compared to traditional OPC clinker (Elakneswaran *et al.*, 2019; Zhang *et al.*, 2021). HFC demonstrated up to 20% energy and 18% $CO_2$ savings to be

achieved relative to OPC clinker (Elakneswaran *et al.*, 2019; Zhang *et al.*, 2021; Yang *et al.*, 2022). High-ferrite clinker exhibits accelerated hydration reactivity (Yang *et al.*, 2022) and higher early compressive strength (Elakneswaran *et al.*, 2019; Zhang *et al.*, 2021) when produced at lower combustion temperatures. Despite its lower $C_3S$ content compared to OPC, HFC presents excellent compressive strength to OPC from its high hydration reactivity (Elakneswaran *et al.*, 2019). Under lower temperatures, the ferrite phase shows higher reactivity, and increases the pH value whilst accelerating the $C_3S$ hydration, driven by the synergistic interaction of the $C_3S$ and $C_4AF$ phases (Zhang *et al.*, 2021). The hydration process of HFC does not produce a new phase and is identical to OPC (Elakneswaran *et al.*, 2019; Yang *et al.*, 2022), therefore the setting time is also identical to OPC (Elakneswaran *et al.*, 2019). HFC exhibits better sulfate resistance to OPC, primarily due to its lower $C_3A$ and $C_3S$ contents, reducing the potential for the formation of ettringite (AFt) and gypsum (Yang *et al.*, 2022).

- Calcium silicate cement (CSC) clinker adopts a raw meal with increased silica content to displace limestone, resulting in a product containing low-lime calcium silicate phases whilst having a significantly reduced sintering temperature of 1200 °C (Sahu and Meininger, 2019). $CO_2$ and energy savings of 30% can be realised from the use of CSC clinker, relative to OPC clinker (Sahu and Meininger, 2019). CSC sets through carbonation rather than hydration, where the low-lime components (i.e., wollastonite, rankinite) and amorphous phases react with $CO_2$ under aqueous conditions and produce calcite ($CaCO_3$) and silica ($SiO_2$) resulting in a net increase in solid volume, forming a stable calcium carbonate binder (Ashraf, Olek and Sahu, 2019; Sahu and Meininger, 2019). The calcite functions similarly to the C-S-H phase in Portland cement by contributing to strength and refining the pore structure (Seifu *et al.*, 2023), where the silica contributes to increased sulfate resistance (Sahu and Meininger, 2019). Melilite is

responsible for making the texture of cement denser through carbonisation and for strength development (Kurokawa *et al.*, 2013).

More details about these alternative clinkers, particularly in terms of their hydration, setting process, and the development of compressive strength, are provided in Appendix C and Table C.1. As well as holding potential in energy and $CO_2$ savings compared to OPC clinker, these BYF, HFC and CSC clinkers have been reported to offer sufficient mechanical properties needed for replacing OPC, as shown in (Wang *et al.*, 2023), (Elakneswaran *et al.*, 2019; Zhang *et al.*, 2021; Yang *et al.*, 2022), and (Sahu and Meininger, 2019) respectively.

In addition, the use of supplementary cementitious materials (SCMs) which exhibit hydraulic or pozzolanic properties allows $CO_2$ emissions reductions by reducing the required amount of (carbon-intensive) clinker in a cement product (Lothenbach, Scrivener and Hooton, 2011; Skibsted and Snellings, 2019). SCMs are typically industrial by-products, including fly ash (from coal combustion), blast furnace slag (from pig iron production), silica fume, as well as natural pozzolans such as limestone power and volcanic rock ashes (Ndahirwa *et al.*, 2022). The reaction of SCMs typically occurs at a slower rate compared to conventional clinker phases. Their reactivity depends on the chemical composition, fineness, amount of reactive phases present, and alkalinity of the pore solution (Lothenbach, Scrivener and Hooton, 2011). Most SCMs exhibit limited hydraulic reactivity, however, when fine powered SCMs are exposed to alkaline aqueous conditions or calcium hydroxide, they undergo a chemical reaction known as pozzolanic reaction, forming hydration products such as calcium silicate hydrate (C–S–H), similar to those produced during cement hydration (Skibsted and Snellings, 2019). Hydration is the reaction between an anhydrous compound and water, forming a new compound known as a hydrate (Lea, Hewlett and Liska, 2019). The hydration process is responsible for the strength development of cement, primarily

involving the formation of calcium silicate hydrate (C-S-H) and calcium hydroxide (portlandite, $Ca(OH)_2$) (Gonnon and Lootens, 2023). Moreover, SCMs also undergo physical effects for inert fine powders or fillers, known collectively as the filler effect (Skibsted and Snellings, 2019). During the early stages of hydration, this filler effect dominates, enhancing the reactions of clinker phases by providing additional space relative to the clinker content and increasing nucleation rates (Lothenbach, Scrivener and Hooton, 2011).

While the above-mentioned alternative clinkers are promising for the reduction of the inherent $CO_2$ emissions from calcination, it is to our knowledge that their production processes are yet to be systematically assessed and compared, to quantify their potential on a consistent basis. Through modelling these processes in the Aspen Plus V12.1 process simulator, this study aims to fill the gap and provide a comparative evaluation of these options in terms of energy consumption and $CO_2$ emissions. Additionally, recognising the emerging proposal of SCMs derived from $CO_2$ mineralisation that absorbs $CO_2$ emissions from cement production (Bremen *et al.*, 2022; Strunge, Renforth and der Spek, 2022), a further option incorporating partial replacement of clinkers with SCMs is also evaluated in parallel with the alternative clinkers for comparison. The focus is placed on process-level performance during the *production* of cement, including the energy performance, waste heat recovery, and $CO_2$ emissions, with the assumption that these different material options all lead to a viable cement product according to the relevant literature (see Table 5.2); the modelling work thus does not address processes important during the *application* of cement, such as hydration kinetics or long-term concrete behaviour, which falls outside the scope of this analysis. The results from the study are poised to bring new insights on the carbon

abatement potential of interventions from a materials perspective, complementing energy-oriented studies of cement production to promote deep decarbonisation of this sector.

## 5.2. Methods

This study is centred on seven technical options for producing clinkers or equivalent products, which are introduced in Section 5.2.1. The evaluation of these options is fundamentally based on computer simulations of the clinker production processes, presented in Section 5.2.2; the simulation results then inform the quantification of energy consumption and $CO_2$ emissions following the approaches described in Sections 5.2.3 and 5.2.4.

### 5.2.1. Cases for evaluation

Seven cases were selected to scrutinise the effects of material composition on energy demand and $CO_2$ production, as shown in Table 5.1, where six cases contained distinct raw meal compositions for producing clinkers and one involved 25 wt.% replacement of a clinker with a SCM produced through $CO_2$ mineralisation. In all cases, natural gas was the assumed fuel for providing thermal energy.

The alternative clinkers evaluated in this study were selected according to four key criteria: (1) demonstrated potential in scientific literature to reduce $CO_2$ emissions without compromising the clinker's compressive strength, (2) shown compatibility with existing clinker manufacturing methods without requiring significant process modifications, (3) primarily reliant on limestone without significant changes in raw materials, and (4) sufficient data availability on mineral composition and sintering temperature. Certain alternative clinkers, such as MgO-based clinker and amorphous low-calcium hydraulic clinker, were

excluded despite their potential to achieve $CO_2$ reductions of up to 25% compared to OPC clinker (Song *et al.*, 2021; Antunes *et al.*, 2022). The former requires significant changes in raw material composition and resultant decline in compressive strength (Song *et al.*, 2021), whilst the latter was not considered as it necessitates modifications to the production process (Antunes *et al.*, 2022).

For the reference case (Case 1), the raw meal compositions were established following the parameters outlined in (Williams, Yang and Nhuchhen, 2024), to produce traditional ordinary Portland cement (OPC). Cases two to four featured three variations of HFC based on literature, with various $Fe_2O_3$ contents at 4.34 wt% (Case 2) (Zhang *et al.*, 2021), 3.72 wt% (Case 3) (Yang *et al.*, 2022), and 3.93 wt% (Case 4) (Elakneswaran *et al.*, 2019). Furthermore, according to these references, the sintering temperatures of these HFC cases are 100 – 150 °C lower than that of OPC clinker. BYF clinker was adopted for Case 5, with a lower lime (CaO) content and a greater alumina content in the raw meal. BYF required a lower sintering temperature, similar to the HFC cases, whilst containing a noticeably higher content of $C_2S$ compared to the other clinkers (Sabbah and Zhutovsky, 2022). Case 6 was introduced to represent the CSC clinker (Sahu and Meininger, 2019), characterised by the lowest $CaCO_3$ content, and the highest silica content in the raw meal amongst all clinker options. This was accompanied by the lowest sintering temperature of 1250 °C. Case 7 integrated $CO_2$ mineralisation (not explicitly modelled in this work) based on (Strunge, Renforth and der Spek, 2022), with the utilisation of $CO_2$ from the cement flue gas to produce a SCM which contains 40% $SiO_2$, 50% $MgCO_3$, and 10% moisture, replacing 25% of OPC clinker.

In terms of the product properties, the literature-reported compressive strengths of the clinkers are shown in Table 5.1. Although deviations are present between OPC clinker and

the alternative clinkers, the latter can offer compressive strengths comparable to OPC. The same comparability has been deemed valid for Case 7 (Strunge, Renforth and der Spek, 2022), although no specific measurements of mechanical strengths were reported. The properties of each clinker are largely determined by its chemical composition. Table 5.3 shows the chemical reactions leading to the key components of the clinkers where the composition of each clinker is shown in Table 5.1. Note that the composition of the raw meal for each of the cases (shown in Table 5.1) was determined according to its literature-reported clinker composition (shown in Table 5.4) by mass balance. The conditions of the alternative clinkers, including the curing time, water to cement ratio (w/c), curing conditions, and material property impacting compressive strength was shown in Table 5.2.

Simulations in Aspen using these calculated raw meal inputs showed that the resultant clinker mineral compositions were consistent with the literature values (Elakneswaran *et al.*, 2019; Sahu and Meininger, 2019; Zhang *et al.*, 2021; Sabbah and Zhutovsky, 2022; Yang *et al.*, 2022).

***Table 5.1. Chemical compositions of raw materials (wt%) in six different simulated clinker cases.*** *This includes $CaCO_3$, $SiO_2$, $Al_2O_3$, $Fe_2O_3$, and $CaSO_4$; with the addition of a case where clinker is mixed with SCM; including the combustion temperature of seven simulated cases (°C), ranging from 1250 – 1500 °C, with their respective mechanical strengths, where the compressive strength of clinkers in Case 7 were not identified as it was integrated with $CO_2$ mineralisation but are assumed to be adequate as it shares similar raw material compositions as that of Case 1, respectively. It is worth noting that the lower water to cement (w/c) ratio of CSC increases the compressive strength as less water relative to the amount of clinker is present (Kondraivendhan and Bhattacharjee, 2016).*

| | **Chemical composition of raw materials (wt%)** | | | | | | | |
|---|---|---|---|---|---|---|---|---|
| **Case ID** | **$CaCO_3$** | **$SiO_2$** | **$Al_2O_3$** | **$Fe_2O_3$** | **$CaSO_4$** | **Sintering Temperature (°C)** | **Compressive Strength (MPa)** | **References** |
| **1. OPC** | 79.47 | 14.34 | 3.49 | 2.70 | 0.00 | 1500 | 32.5 – 55 | (Svinning, Høskuldsson and Justnes, 2010; Standards, 2011) |
| **2. HFC-a (4.34)** | 77.08 | 14.81 | 3.77 | 4.34 | 0.00 | 1375 | 73 | (Zhang *et al.*, 2021) |
| **3. HFC-b (3.72)** | 77.33 | 15.80 | 3.14 | 3.72 | 0.00 | 1350 | 60 | (Yang *et al.*, 2022) |
| **4. HFC-c (3.93)** | 78.46 | 12.85 | 4.73 | 3.93 | 0.00 | 1350 | 45 | (Elakneswaran *et al.*, 2019) |
| **5. BYFC** | 64.20 | 12.50 | 13.80 | 4.70 | 4.81 | 1350 | 45.9 | (Wang *et al.*, 2023) |
| **6. CSC** | 61.86 | 35.61 | 1.93 | 0.59 | 0.00 | 1250 | 63 | (Sahu and Meininger, 2019) |
| **7. SCM + OPC** | 75% OPC + 25% SCM | | | | | | Not specified; properties considered comparable with OPC | (Strunge, Renforth and der Spek, 2022) |

***Table 5.2. Conditions of the alternative clinkers**. Including the curing time, water to cement ratio (w/c), curing conditions, and material property impacting compressive strength. These are the required properties of cement from the user perspective which should not be compromised. The key criteria for the property was the compressive strength and additional properties (hydration and setting) of cement are provided in Appendix C and Table C.1.*

| Clinker Type | Curing time | w/c ratio | Curing conditions | Material property impacting compressive strength | References |
|---|---|---|---|---|---|
| **OPC** | 28 days | 0.5 | Initial storage in moist air followed by curing with $H_2O$. | $C_3S$ for the primary strength development and $C_2S$ for late strength development. The hydration of both $C_3S$ and $C_2S$ forms C–S–H which is the key contributor to the strength. | (Svinning, Høskuldsson and Justnes, 2010; Standards, 2011; Lea, Hewlett and Liska, 2019) |
| **HFC-a** | 28 days | n/a | n/a | High ferrite reactivity and elevated pH accelerates $C_3S$ hydration and increases the C–S–H microstructure, contributing to the cement compressive strength. | (Zhang *et al.*, 2021) |
| **HFC-b** | 28 days | 0.5 (water-to-binder) | In $H_2O$ | Ferrite offers high early-age compressive strength but slows later strength development. | (Yang *et al.*, 2022) |
| **HFC-c** | 28 days | 0.5 | Poured into cylindrical molds and sealed for curing at 20°C. | Ferrite offers high early-age compressive strength but slows later strength development. | (Elakneswaran *et al.*, 2019) |
| **BYF** | 28 days | 0.3 | Curing chambers maintained at 20 ± 2°C with a relative humidity of 95 ± 3%. | Ye'elimite hydration results in the formation of ettringite and contributes to the development of early-age strength.<br><br>Ferrite phases and over-burned anhydrite show potential for enhancing strength development and durability.<br><br>Hydration of $C_2S$ to form C–S–H is mainly responsible for the later-age strength. | (Wang *et al.*, 2023) |
| **CSC** | 3 days | 0.39 | Cured in an environment of pure $CO_2$ for 72 hours at temperatures below 100°C. | $CaCO_3$ and $SiO_2$ formation incorporates $CO_2$, increasing solid volume and strength in CSC. | (Sahu and Meininger, 2019) |

*Table 5.3. Chemical reactions for the formation of clinker components.*

| Cases | Mineral component | Chemical reaction |
|---|---|---|
| 1 – 6 | Belite | $2\ CaO + SiO_2 \rightarrow C_2S$ (Sahu and Meininger, 2019) |
| 1 – 4 | Alite | $C_2S + CaO \rightarrow C_3S$ (Sahu and Meininger, 2019) |
| 1 – 4 | Aluminate | $3\ CaO + Al_2O_3 \rightarrow C_3A$ (Sahu and Meininger, 2019) |
| 1 – 5 | Ferrite | $4\ CaO + Al_2O_3 + Fe_2O_3 \rightarrow C_4AF$ (Sahu and Meininger, 2019) |
| 5 | Calcium Sulfoaluminate | $3\ Al_2O_3 + 3\ CaO + CaSO_4 \rightarrow Ca_4Al_6O_{12}SO_4$ ($C_4A_3S$) (Dong *et al.*, 2020) |
| 6 | Wollastonite | $CaO + SiO_2 \rightarrow CaSiO_3$ (CS) (Sahu and Meininger, 2019) |
| 6 | Rankinite | $3\ CaO + 2\ SiO_2 \rightarrow Ca_3Si_2O_7$ ($C_3S_2$) (Sahu and Meininger, 2019) |
| 6 | Gehlenite/Melilite | $2\ CaO + Al_2O_3 + SiO_2 \rightarrow Ca_2Al_2SiO_7$ (Sabbah and Zhutovsky, 2022) |

***Table 5.4. Mineral composition of six clinker cases (wt%)*** *(Svinning, Høskuldsson and Justnes, 2010; Standards, 2011; Elakneswaran* et al.*, 2019; Sahu and Meininger, 2019; Zhang* et al.*, 2021; Sabbah and Zhutovsky, 2022; Yang* et al.*, 2022).*

| | Mineral composition of clinker cases (wt%) | | | | | | | | |
|---|---|---|---|---|---|---|---|---|---|
| **Case ID** | **$C_3S$** | **$C_2S$** | **$C_3A$** | **$C_4AF$** | **$C_4A_3S$** | **CS** | **$C_3S_2$** | **Melilite** | **Amorphous** |
| **1. OPC** | 57.60 | 18.00 | 9.00 | 9.30 | 0 | 0 | 0 | 0 | 0 |
| **2. HFC-a (4.34)** | 42.10 | 28.40 | 2.80 | 18.10 | 0 | 0 | 0 | 0 | 0 |
| **3. HFC-b (3.72)** | 37.06 | 32.86 | 4.32 | 15.17 | 0 | 0 | 0 | 0 | 0 |
| **4. HFC-c (3.93)** | 59.10 | 8.60 | 8.50 | 17.20 | 0 | 0 | 0 | 0 | 0 |
| **5. BYFC** | 0 | 49.70 | 0 | 19.90 | 28.80 | 0 | 0 | 0 | 0 |
| **6. CSC** | 0 | 2.96 | 0 | 0 | 0 | 52.30 | 13.38 | 7.12 | 24.20 |

### 5.2.2. Process simulation

The mathematical modelling work of the clinker production process was based on adapting the Aspen Plus V12.1 simulation model established in an earlier study (Williams, Yang and Nhuchhen, 2024). The modelling itself was originally based on a plant producing 4,200 tonnes of clinker daily in Alberta, Canada (Nhuchhen, Sit and Layzell, 2022a). The process utilises natural gas combustion in air, serving as a primary source of thermal energy which is accompanied by electrical energy from the grid. A schematic representation of the production process is shown in Figure 5.1 with the Aspen Plus flowsheet provided in Appendix Figure C.1. To produce OPC clinker, the process begins as raw materials are crushed, milled and blended to create a homogeneous raw meal before entering the pre-heating stage (Lea, Hewlett and Liska, 2019; Faria *et al.*, 2022). Homogenisation involves the process of mixing and blending materials to achieve a uniform composition to reduce the variations in composition to ensure consistent quality (Cao and Zhou, 2024), and is generally conduced in the vertical roller mill (Pareek and Sankhla, 2020). The homogenised raw meal enters the pre-heater and is processed in the calciner where limestone is decomposed at 900 °C to attain 95% calcination (Vikström, 2021). The calciner output then proceeds to the kiln, where decomposition, transition and sintering reactions occur, with the sintering temperature reaching 1500 °C. As the material moves down the hotter zones of the kiln toward the flame, intense heat triggers chemical and physical reactions, causing partial melting of the material into clinker (Cembureau, 2024). The material is being cooled to 100 °C in the cooler and exiting the process. In the process, primary air (PA) and secondary air (SA) enter the kiln's combustor at 25 °C and 1050 °C, respectively, whereas tertiary air (TA) enters the calciner's combustor at 900 °C following heat recovery (Nhuchhen, Sit and Layzell, 2022a). The cooling vent air progresses through heat recovery phases which supply

a hot gas flow of 1,762 kg/tonne clinker at 176.85 °C to satisfy the operation of the vertical roller mill (VRM) (Ghalandari *et al.*, 2021). The remaining cooling exhaust coupled by the pre-heater exhaust then provides heat to operate the Organic Rankine Cycle (ORC) for further heat recovery.

The calciner and kiln combustors were modelled as stoichiometric reactors (RStoic), where a series of three RStoic reactors represented the three stages in the kiln. Heat losses were modelled for the combustors including the calciner, kiln decomposition, kiln transition, and kiln sintering at 42.99 MJ/t clinker, 30.60 MJ/t clinker, 59.40 MJ/t clinker and 90 MJ/t clinker, respectively in accordance with (Faria *et al.*, 2022). To simulate the production of an alternative clinker, the above Aspen Plus model was adapted by using a clinker-specific raw meal composition (Table 5.1), chemical reactions (Table 5.3), and their conversions as needed to attain the clinker composition (Table 5.4). Physical properties of new clinker components which are not present in the OPC clinker are summarised in Table C.2. Clinker-specific sintering temperatures (Table 5.1) were also applied through adjusting the supply of natural gas and combustion air.

The physical property modelling of all the cases was also based on the previously established Aspen model for OPC clinker production (Williams, Yang and Nhuchhen, 2024). The enthalpy and other data needed for simulation was available in the Aspen database for the majority of the clinker phases, data for the clinker phases not covered (i.e., $C_4AF$, $C_3A$, $C_4A_3S$, $Ca_2Al_2SiO_7$) were obtained from literature (see Table C.2).

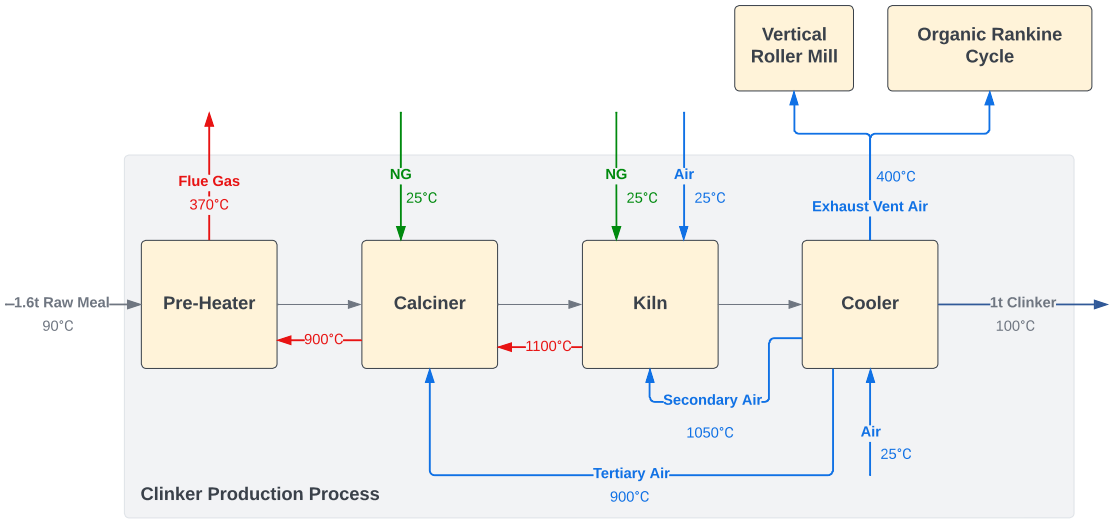


***Figure 5.1. Schematic of the clinker production process.*** *Air is represented in blue, natural gas in green, flue-gas in red and material flows in grey. The raw meal mass flowrate and temperatures refer to the case of OPC clinker production.*

### 5.2.3. Quantification of energy demand and $CO_2$ emissions of clinker production (Cases 1–6)

Principal components responsible for the net energy consumption of the clinker production processes include the consumption of electrical (fans, raw meal preparation, auxiliary) and thermal energy (natural gas), along with the recovery of thermal energy into electricity through an ORC. The natural gas consumptions values were extracted from the Aspen simulations. The following assumptions were taken in energetic analyses:

- The scope of energy consumption modelling was set to “gate to gate”; processes that occur before or after the clinker production process were not included as per (Williams, Yang and Nhuchhen, 2024).
- Natural gas was assumed to be 100% methane in accordance with prior work (Williams, Yang and Nhuchhen, 2024), with a lower heating value (LHV) of 50 MJ/kg (Wan, 2004).

- The auxiliary electricity consumption was assumed constant across all cases as 68 kWh/t clinker according to (Williams, Yang and Nhuchhen, 2024).
- Electricity required for raw meal preparation was presumed to be constant among the cases at 25.2 kWh/t clinker as per (Meng *et al.*, 2021).

The electrical energy demand for each fan ($W_{fan}$) was determined by scaling the reference fan power consumption as per (Nhuchhen, Sit and Layzell, 2022a), where $q_{ref}$ and $W_{ref}$ denotes the volumetric gas flow and the power consumption of a reference fan, and q is the volumetric gas flow of the fan, shown below in Equation 5.1:

*Equation 5.1. Electrical energy demand of fans.*

$$W_{fan} = W_{ref} \times \left(\frac{q}{q_{ref}}\right)^3$$

The heat of reactions was automatically calculated in Aspen Plus through the use of RStoic reactors by inputting the stoichiometry and fractional conversion of components, yielding results comparable to literature values (i.e., for calcination its 178 kJ/mol in literature (Svensson, 2021) and 178.32 kJ/mol in Aspen). The required heat for phase changes (latent heat) was also calculated automatically in Aspen.

An ORC was incorporated into each clinker production process for waste heat recovery which produces electricity to partially offset the process electricity demand. The ORC electricity output ($W_{ORC} = Q_{in} \times \eta th$) was calculated using the recovered waste heat from the hot gas stream ($Q_{in}$) which was acquired from the Aspen simulation results of each cooler. This represented the evaporator of the ORC, where waste heat streams were cooled to 130 °C, providing a 20 °C temperature difference (to drive heat transfer) compared to the working fluid of the ORC (at 110 °C), as per the design presented in (Ahmed *et al.*, 2018).

The ORC's efficiency, $\eta_{th}$, was set to 0.225 according to the assumed organic working fluid (Moreira and Arrieta, 2019).

$CO_2$ emissions were assessed from two main sources: direct emissions from the clinker production process (resulting from both calcination and natural gas combustion, as quantified by Aspen simulations) and indirect emissions from the supply of grid electricity consumed in the clinker production process. Other $CO_2$ emissions in the cement supply chain, such as transportation of materials were not included. The $CO_2$ demand of transportation is minimal (Mikulčić, Vujanović and Duić, 2013), and any transportation-relate $CO_2$ emissions would be similar across all scenarios (i.e., on a $CO_2$ per tonne of material transported). Therefore, excluding them would not change the relative $CO_2$ performance among the simulated processes.

The carbon footprint of grid electricity depends on geographical locations. Consequently, three out of the top-10 cement producing countries with low, medium, and high carbon intensities (on a basis of kg of $CO_2$eq per MWh), namely Brazil (Our World in Data, 2023), the United States (Our World in Data, 2023), and China (Tiseo, 2023b) were chosen to calculate location-sensitive emissions from electricity.

### 5.2.4. Quantification of energy demand and $CO_2$ emissions for the option involving $CO_2$ mineralisation (Case 7)

The $CO_2$ mineralisation process was incorporated in Case 7, involving the blending of 250 kilograms (kg) of supplementary cementitious material (SCM), derived from the mineralisation of $CO_2$, with 750 kg of clinker. This facilitates the production of 1 tonne of final product in accordance with (Strunge, Renforth and der Spek, 2022). $CO_2$ was sourced

by a monoethanolamide (MEA)-based process applied to the flue gas from clinker production with a capture efficiency of 90% (Strunge, Renforth and der Spek, 2022). The $CO_2$ mineralisation process produced a stream of SCM consisting of 40% $SiO_2$, 50% $MgCO_3$, and 10% moisture (on a weight basis) (Strunge, Renforth and der Spek, 2022). To determine the electrical and thermal energy requisites for the production of 750 kg of clinker, 75% of the corresponding values of OPC (Case 1) were taken, illustrated in Figure 5.2.

For the production of 250 kg of SCM containing 40% or 100 kg of $SiO_2$, the $CO_2$ demand was stoichiometrically determined to be 146.50 kg $CO_2$ according to the reaction equation of magnesium silicate carbonation (see Equation 5.2). The thermal and electrical energy demands for MEA-based carbon capture were 3.8 MJ/kg of $CO_2$ captured (thermal), and 0.55 MJ/kg of $CO_2$ captured (electrical) (Voldsund *et al.*, 2019). The electrical and thermal energy required for the $CO_2$ mineralisation process leading to the production of 250 kg SCM were 115.97 kWh and 31.24 kWh, on a per tonne of product basis, respectively (Strunge, Renforth and der Spek, 2022).

The quantification of $CO_2$ emissions for Case 7 included (see Figure 5.2) 75% of $CO_2$ emissions from the production of 1 tonne OPC clinker in Case 1. This was determined according to; (1) deduction of 146.50 kg $CO_2$ consumed by mineralisation; (2) $CO_2$ emissions by the supply of thermal energy required for mineralisation and MEA-based carbon capture, at 241 kg $CO_2$/MWh (Strunge, Renforth and der Spek, 2022), and (3) carbon footprint of the electricity consumed by mineralisation and MEA-based carbon capture, based on the location-specific carbon intensities of grid electricity in the three chosen countries.

*Equation 5.2. Chemical reaction of SCM production.*

$$Mg_2SiO_4 + 2CO_2 \longrightarrow 2MgCO_3 + SiO_2$$

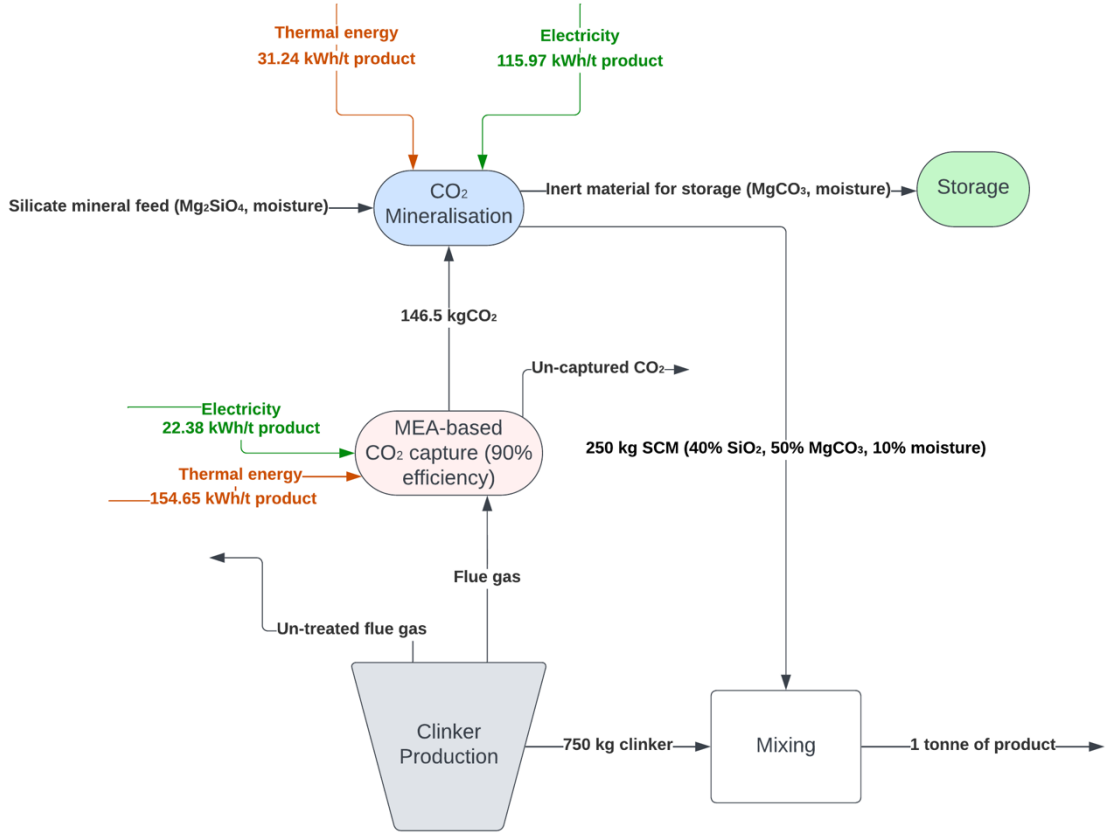


***Figure 5.2. Process diagram for cases involving $CO_2$ mineralisation.*** *The electrical and thermal energy inputs were calculated based on (Elakneswaran* et al.*, 2019); the compositions of SCM were based on literature (Strunge, Renforth and der Spek, 2022).*

## 5.3. Results and discussion

This section presents and discusses the results pertaining to energy consumption and carbon intensity, offering a comparative analysis of various cases. Specifically, we examine the thermal energy input from natural gas and the electrical energy requirement. The carbon intensity assessment involves determining the amount of $CO_2$ produced and the carbon footprint associated with electricity, which extends across three distinct locations, namely the United States, China, and Brazil.

### 5.3.1. Energy intensity

The energy consumption results are presented in Table 5.5. All alternative clinkers (Cases 2–6) were predicted to gain energy savings compared to the OPC clinker (Case 1) as projected in previous studies (Elakneswaran *et al.*, 2019; Sahu and Meininger, 2019; Zhang *et al.*, 2021; Sabbah and Zhutovsky, 2022; Yang *et al.*, 2022). In particular, Case 6 (CSC clinker) is the most energy efficient, with a total energy intensity of 665.1 kWh/tonne clinker, which represents a ~46% reduction in thermal and total energy, respectively, compared to Case 1 (OPC). Its energy savings can be attributed to its significantly lower sintering temperature (1250 °C), and $CaCO_3$ input (989.7 kg/tonne clinker) corresponding to significantly lower contents of $C_3S$ and $C_2S$. In comparison, Case 1 (OPC) had a sintering temperature of 1500 °C and a $CaCO_3$ input 1271.5 kg/tonne clinker, both demanding greater thermal energy input.

Case 5 (BYF) shared a similar $CaCO_3$ content with Case 6, but with a higher sintering temperature (by 100 °C) and substantial amount of $C_2S$ in the clinker composition, making it the second most energy-efficient alternative clinker, saving thermal energy and total energy by 29.4% and 31.3% compared to OPC clinker, respectively. Among the high-ferrite cases (Cases 2 – 4), electrical and thermal energy consumption were comparable, with differences below 10%, resulting from minor variations in the raw meal and clinker compositions. Notably, among the high-ferrite options, Case 3 (HFC-b), with the lowest alite content, exhibited the lowest thermal and total energy consumption with 12.3% and 16.5% savings compared to OPC clinker, respectively. The case involving SCM (Case 7) was the most energy intensive process, even more demanding than Case 1 which supplied 75% of its product. This suggests that, on a basis of 1 kg of product (SCM or clinker), the energy

required for mineralisation and MEA-based carbon capture (1.30 kWh/kg SCM) was greater than that of OPC clinker production (1.22 kWh/kg).

Finally, it is worth noting that thermal energy from natural gas emerged as the key contributor to the total energy demand, contributing 63 – 89% of the total energy demand across all the cases. Besides, it was observed that Case 1 had the highest and Case 6 had the lowest heat recovery value from ORC as the amount of recoverable waste heat was corelated with the natural gas input in the processes.

***Table 5.5. Key players for the electrical and thermal energy demand of all cases**; as $CO_2$ mineralisation was only applicable to Case 7, $CO_2$ mineralisation energy (thermal and electrical) was not applicable to Cases 1 – 6.*

| | **Case 1 OPC** | **Case 2 HFC-4.34** | **Case 3 HFC-3.72** | **Case 4 HFC-3.93** | **Case 5 BYF** | **Case 6 CSC** | **Case 7 SCM + OPC** |
|---|---|---|---|---|---|---|---|
| **Electrical Energy for clinker (kWh/t clinker)** | | | | | | | |
| Fans (kWh/t) | 165.66 | 86.65 | 77.76 | 91.63 | 62.28 | 37.20 | 124.25 |
| Auxiliary (kWh/t) | 68.00 | 68.00 | 68.00 | 68.00 | 68.00 | 68.00 | 51.00 |
| Organic Rankine Cycle (kWh/t) | -73.79 | -61.09 | -59.33 | -62.69 | -48.15 | -24.07 | -55.34 |
| Raw Meal Preparation (kWh/t) | 25.20 | 25.20 | 25.20 | 25.20 | 25.20 | 25.20 | 18.90 |
| MEA Capture (electrical) | N/A | | | | | | 22.38 |
| Mineralisation (electrical) | | | | | | | 115.97 |
| **Total electrical energy (kWh/t clinker)** | 185.07 | 118.76 | 111.63 | 122.14 | 107.33 | 106.33 | 277.16 |
| **Thermal Energy for clinker (kWh/t clinker)** | | | | | | | |
| Natural Gas (kWh/t) | 1035.37 | 924.54 | 907.81 | 971.83 | 731.03 | 558.78 | 776.53 |
| MEA Capture (thermal) | N/A | | | | | | 154.65 |
| Mineralisation (thermal) | | | | | | | 31.24 |
| **Total thermal energy (kWh/t clinker)** | 1035.37 | 924.54 | 907.81 | 971.83 | 731.03 | 558.78 | 962.41 |
| **Net total energy (kWh/t clinker)** | 1220.44 | 1043.30 | 1019.45 | 1093.97 | 838.36 | 665.11 | 1239.57 |

*Table 5.6. $CO_2$ emissions for seven simulated cases in three different geographical locations of the United States (USA), China, and Brazil.*

| | | OPC Clinker Production | | SCM - MEA Capture | | SCM - $CO_2$ Mineralisation | | Net Total $CO_2$ |
|---|---|---|---|---|---|---|---|---|
| | | $CO_2$ Produced ($kgCO_2$/t clinker) - from Aspen | Net Electrical ($kgCO_2$/t clinker) | Electrical ($kgCO_2$/t clinker) | Thermal ($kgCO_2$/t clinker) | Electrical ($kgCO_2$/t clinker) | Thermal ($kgCO_2$/t clinker) | Total ($kgCO_2$/t clinker) |
| **Case 1** | **USA** | 741.50 | 67.92 | | | | | 809.42 |
| **OPC** | **China** | 741.50 | 98.30 | | | | | 839.80 |
| | **Brazil** | 741.50 | 18.88 | | | | | 760.38 |
| **Case 2** | **USA** | 695.80 | 43.58 | | | | | 739.38 |
| **HFC-a (4.34)** | **China** | 695.80 | 63.08 | | | | | 758.88 |
| | **Brazil** | 695.80 | 12.11 | | | | | 707.91 |
| **Case 3** | **USA** | 694.43 | 40.97 | | | | | 735.40 |
| **HFC-b (3.72)** | **China** | 694.43 | 59.29 | | | | | 753.72 |
| | **Brazil** | 694.43 | 11.39 | | | | | 705.82 |
| **Case 4** | **USA** | 718.62 | 44.83 | | | | | 763.45 |
| **HFC-c (3.93)** | **China** | 718.62 | 64.88 | | | | | 783.50 |
| | **Brazil** | 718.62 | 12.46 | | | | | 731.08 |
| **Case 5** | **USA** | 537.28 | 39.39 | | | | | 576.67 |
| **BYF** | **China** | 537.28 | 57.01 | | | | | 594.29 |
| | **Brazil** | 537.28 | 10.95 | | | | | 548.23 |
| **Case 6** | **USA** | 481.34 | 39.02 | | | | | 520.36 |
| **CSC** | **China** | 481.34 | 56.48 | | | | | 537.81 |
| | **Brazil** | 481.34 | 10.85 | | | | | 492.18 |
| **Case 7** | **USA** | 409.63 | 50.94 | 8.21 | 37.27 | 42.56 | 7.53 | 556.14 |
| **SCM + OPC** | **China** | 409.63 | 73.73 | 11.89 | 37.27 | 61.60 | 7.53 | 601.63 |
| | **Brazil** | 409.63 | 14.16 | 2.28 | 37.27 | 11.83 | 7.53 | 482.69 |

N/A

### 5.3.2. Carbon intensity

As shown in Table 5.6, all the non-OPC options (Cases 2 – 7) were predicted to have a carbon intensity lower than the OPC clinker (Case 1). Among the alternative clinkers (Cases 2 – 6), the trend in carbon intensity agrees well with that in thermal energy consumption, where reduced natural gas consumption was coupled with a reduced $CaCO_3$ content in the raw meal, both contributing to the reduction of $CO_2$ emissions. Case 6 (CSC) was projected to achieve 35.1% reduction in direct emissions (i.e., excluding carbon footprint of electricity) compared to Case 1, followed by 27.5% and 3.1–6.4% reduction by Case 5 (BYF) and Cases 2 – 4 (HFC clinkers), respectively. These values of $CO_2$ savings were comparable to literature suggesting 30%, 20 – 40% and of up to 18% in contrast with OPC clinker for CSC, BYF and HFC clinkers, respectively (Elakneswaran *et al.*, 2019; Sahu and Meininger, 2019; Zhang *et al.*, 2021; Sabbah and Zhutovsky, 2022; Yang *et al.*, 2022) (shown in Table 5.8). When the carbon footprint of electricity is included, results differ between the three countries, although their difference was within 10% despite the significant gap in the carbon intensity of grid electricity. This was a result of the relatively low share of electricity in the total energy consumption. Comparing Case 6 with Case 1, the reductions of total carbon intensity for producing 1 tonne clinker were 35.7%, 36% and 35.3% for the US, China, and Brazil, respectively.

For the option involving $CO_2$ mineralisation (Case 7), the impact of replacing 250 kg of clinker with SCM on total carbon intensity was dictated by the combined effect of three elements, namely: (1) $CO_2$ removal through the mineralisation process, (2) avoided $CO_2$ emissions from the replaced 250 kg clinker, and (3) the $CO_2$ emissions associated with the supply of electrical and thermal energy for $CO_2$ capture and mineralisation. The second and

the third elements are differentially affected by the carbon intensity of the grid electricity in different locations. Compared to Case 1 (OPC), Case 7 clearly shows, for all the three countries, that the benefit of $CO_2$ savings (elements 1 and 2) outweighs the $CO_2$ burden of additional energy consumption (element 3), leading to 31.3%, 28.4% and 36.5% reduction in total carbon intensity for US, China, and Brazil, respectively (shown in Table 5.6). These findings were comparable to literature, where $CO_2$ savings of 33% were realised from substitution of 25% SCMs from $CO_2$ mineralisation (Strunge, Renforth and der Spek, 2022). However, the comparison of Case 7 with Case 6 shows that, while Brazil was predicted to marginally benefit from the SCM replacement from its rather "green" electricity grid, the higher energy consumption in the case involving the replacement resulted in a higher overall carbon intensity for the US and China, compared to a low-carbon clinker (CSC).

### 5.3.3. Further discussions

From the results presented above on alternative clinkers, the lowering of the sintering temperature and $CaCO_3$ content in raw meal both played a role in reducing energy consumption and $CO_2$ emissions. A less understood aspect was the relative contributions from these two factors. To shed light on this, additional supporting simulation of OPC clinker production at 1400 $^oC$ (which is the lower end of the practical range as specified by (Stadler, Poland and Gallestey, 2011)) was conducted as per Table 5.7. Furthermore, two hypothetical lower sintering temperatures for OPC clinker, 1350 $^oC$ and 1250 $^oC$, directly corresponding to those adopted for BYF and CSC clinkers, respectively, were simulated (See Table 5.7, Table C.3, and Table C.4). These additional simulations showed, reductions between 7.0% and 17.5% in total energy consumption and between 1.0% to 2.6% in average $CO_2$ emissions, all in contrast with Case 1 (OPC). In comparison and as shown earlier, the

assessed alternative clinkers achieved between up to 45.5% energy reductions and up to 35.1% $CO_2$ reductions. The contrast of these percentage savings suggests that adopting a low-limestone raw meal plays a more significant role in $CO_2$ and energy reductions than lowering the sintering temperature.

The alternative clinkers studied in this work have previously been considered being able to achieve energy and $CO_2$ savings (shown in Table 5.8). Here, we can compare the previously stated $CO_2$ and energy performances with what was predicted in this study through consistent modelling. As shown in Table 5.8, both Cases 5 (BYF) and 6 (CSC) demonstrates a notable agreement with existing literature (Sahu and Meininger, 2019; Sabbah and Zhutovsky, 2022) regarding $CO_2$ savings, however the findings of this study indicate higher energy savings in comparison with literature. This difference may be caused by the assessment's consideration of various energy types and distinct comparison baselines. Whist existing studies provide a comparison with coal-combusted Ordinary Portland Cement (OPC) (Elakneswaran *et al.*, 2019; Sahu and Meininger, 2019; Zhang *et al.*, 2021; Sabbah and Zhutovsky, 2022; Yang *et al.*, 2022), this study uses natural gas-combusted OPC as a benchmark. In contrast, the HFC cases in the results only exhibited modest $CO_2$ savings of up to 6.4% from the calcination process in contrast with literature which projected $CO_2$ savings of up to 18% (Zhang *et al.*, 2021) (shown in Table 5.8). This was predominantly a result of the minor reductions in $CaCO_3$ content in the raw meal.

Examining the underlying chemical and physical mechanisms, the decomposition of $CaCO_3$ to CaO involves the decomposition reaction, $CaCO_3 \rightarrow CaO + CO_2$, releasing 0.44 $kgCO_2$ per tonne of $CaCO_3$ converted. Additionally, the reaction requires an input of 179.4 kJ/kmol of heat at 900 °C (Faria *et al.*, 2022). This emphasises that both $CO_2$ and energy savings can be realised from the reduction of the $CaCO_3$ content in the raw material composition, a key

target that has been aimed at by all the alternative clinkers. In the kiln processes, silica ($SiO_2$) reacts with CaO to form alite ($C_3S$) and belite ($C_2S$), which are the primary components of clinker, requiring 12.0 kJ/kmol and releasing 135.0 kJ/kmol of heat, respectively (Faria *et al.*, 2022). Furthermore, the clinker raw materials of iron oxide ($Fe_2O_3$) and aluminium oxide ($Al_2O_3$) demand conversion temperatures of up to 1280 °C, releasing heat of 41.3 kJ/kmol and requiring 19.7 kJ/kmol, respectively for the formation of $C_4AF$ and $C_3A$ (Faria *et al.*, 2022). Energetically, the above suggests that $C_2S$ and $C_4AF$ would be preferred over $C_3S$ and $C_3A$, respectively, which have been broadly reflected in the contrast of compositions between OPC clinker and the alterative clinkers studied in this work.

On the use of SCMs, the main study presented above assumed 25% of replacement, although a lower-level replacement may be favoured due to concerns such as product workability (Skocek, Zajac and Ben Haha, 2020). If 20% of clinker were to be replaced with SCMs, an additional option suggested by (Strunge, Renforth and der Spek, 2022), our additional assessment showed that $CO_2$ reductions in the results observed in Case 7 compared with Case 1 would be 25.1%, 22.8%, and 29.2% for the United States, China, and Brazil, respectively. These reductions represent a 6.2%, 5.6%, and 7.3% decrease in $CO_2$ savings compared to the scenario with 25% SCM replacement in these respective countries. Despite these decreases, the $CO_2$ saving potential of this technical option remains significant.

As a final comment, although the electricity consumption is relatively minor compared to the thermal energy demand in clinker production that is dominated by thermal processes (i.e., the operation of the calciner and the kiln), the introduction of a SCM could potentially alter the picture, depending on the production method of the SCM. In the example included in this study, 22.4% of the total energy consumption of the $CO_2$ mineralisation processes is electricity, higher than that of OPC production. A higher share of electricity in total energy

consumption, among other impacts, will lead to greater differentiation in the total carbon emissions between countries with diverse carbon intensities in their electricity supply, potentially making some options more suitable for certain countries than the others.

***Table 5.7. Reference OPC case compared to a lower sintering temperature scenario**, (1400 °C) and hypothetical additional simulations with changes to the sintering temperatures of 1350 °C (H1-OPC) and 1250 °C (H2-OPC).*

| Reference OPC vs Hypothetical supporting simulations | Sintering temperature (°C) | Energy consumption (kWh/t clinker) | $CO_2$ produced ($kgCO_2$/t clinker) |
|---|---|---|---|
| OPC (reference) | 1500 | 1220.4 | 741.5 |
| OPC (low sintering T) | 1400 | 1134.5 | 733.8 |
| H1-OPC | 1350 | 1063.8 | 730.1 |
| H2-OPC | 1250 | 1006.9 | 722.3 |

***Table 5.8. Energy and $CO_2$ savings from literature compared to traditional OPC clinker**, with corresponding literature references, and energy and $CO_2$ savings from the results compared to the reference Case 1.*

| Alternative Clinkers | Energy Savings (Literature) | $CO_2$ Savings (Literature) | Energy Savings (Results) | $CO_2$ Savings (Results) | Literature References |
|---|---|---|---|---|---|
| **HFC-a** | 17 – 20% | 15 – 18% | 14.5% | 6.2% | (Zhang *et al.*, 2021) |
| **HFC-b** | N/A | N/A | 16.5% | 6.4% | (Yang *et al.*, 2022) |
| **HFC-c** | 5% | 5% | 10.4% | 3.1% | (Elakneswaran *et al.*, 2019) |
| **BYF** | 20% | 20 – 40% | 31.3% | 27.5% | (Sabbah and Zhutovsky, 2022) |
| **CSC** | 30% | 30% | 45.5% | 35.1% | (Sahu and Meininger, 2019) |

## 5.4. Conclusions

With the aid of process simulation, this work has quantified how $CO_2$ emissions and energy consumption of the cement production process can be reduced through altering the clinker composition. The energy demand and $CO_2$ production in 7 evaluated cases were found to vary according to four key factors: limestone content in the raw meal, alite ($C_3S$) content in the clinker, sintering temperature, and substituting conventional clinker with SCMs from $CO_2$ mineralisation.

(1) The limestone ($CaCO_3$) content in the raw meal plays a key role, as the chemical reaction of calcination is a significant source of both thermal energy demand and direct $CO_2$ emissions. All the cases alternative to OPC clinker featured a reduction in the use of $CaCO_3$ to different extents, which led to reduced fuel consumption for calcination.

(2) Reduction of the alite content of the clinker is advantageous in achieving a lower $CO_2$ output from the cement production process, which is particularly demonstrated by Cases 5 (BYC) and 6 (CSC). This is in-line with literature, which determined that alite was the most carbon intensive clinker mineral when compared to the rest.

(3) The alternative clinkers were accompanied with a lower sintering temperature compared to OPC, which was a contributing factor to the lower energy demand and $CO_2$ emissions, although more significant contributions were shown to stem from the alternation of the raw meal and hence the clinker compositions.

(4) The use of a SCM derived through $CO_2$ mineralisation to partially substitute OPC clinkers demonstrated a significant reduction of $CO_2$. However, it did not lead to the

lowering of energy demand due to the high energy (thermal and electrical) requirement of $CO_2$ mineralisation.

Overall, Case 6 (CSC) emerges as the winner in energy efficiency (45.5% energy reduction compared to Case 1, OPC), with the lowest $CaCO_3$ content in the raw meal, zero alite in the clinker, lowest sintering temperature and the absence of the energy demand associated with SCM. In terms of direct $CO_2$ emissions from the production process (i.e., excluding the carbon footprint of electricity), CSC clinker achieved 35.1% of reduction from the OPC clinker, which is the second best, next to Case 7 (SCM+OPC) which achieved 44.8% of reduction. However, when the carbon footprint of electricity is included in the total $CO_2$ emissions, the SCM+OPC case retains its superiority over the CSC case only in Brazil from its low-carbon grid, but not in China and the United States. This indicates the importance of decarbonising electricity generation particularly in production options where the electrical energy demand is significant. Whilst this study quantifies the energy and carbon intensity of the *production* of alternative clinkers, it does not simulate aspects important for the *application* of clinkers, such as hydration reactions, setting times, or concrete properties made from these clinkers. Future work is recommended to extend this modelling framework to include hydration modelling and concrete performance with mechanical testing to evaluate the trade-offs between environmental performance and final concrete characteristics, particularly for widespread adoption in structural applications. The encouraging results of this modelling study on alternative clinkers warrant further experimental testing of these products as well as their production processes, so that their potential in decarbonising the cement industry can be firmly established.

# Chapter 6. Conclusions

## 6.1. Summary of research and key contributions

This thesis provides academic research to facilitate decarbonisation options in clinker production, evaluating their energetic, $CO_2$, and techno-economic performances across distinct geospatial regions. The research meets the aim of the thesis by focusing on the emissions stemming from cement production, namely from fuel combustion and limestone calcination, offering comparative performance assessments through three original research projects that examine different decarbonisation options by using theoretical models. The initial phase of the project investigates the energetic and $CO_2$ performance impact of substituting fossil fuels with $H_2$ at various ratios, supported by oxy-combustion through process simulation models detailed in Chapter 3. This is followed by optimisation models in Chapter 4 which evaluates the techno-economic implications and subsystem capacities of replacing conventional fossil fuels with solar energy sources, specifically through concentrated solar power (CSP) and photovoltaics (PV). Finally, the thesis tackles calcination induced emissions in Chapter 5 by identifying alternative clinkers with distinctive limestone contents, whilst assessing their effects on energetic and $CO_2$ performance through process simulation models. Both Chapters 4 and 5 carried out investigations with reference to three regions: the United States, China, and Brazil.

The initial research project (Chapter 3) demonstrated that utilising $H_2$ from water electrolysis coupled with oxy-combustion enabled $CO_2$ savings of up to ~28%. This is attributed to the complete replacement of fossil fuels in both the calciner and kiln combustors, highlighting

the potential of $H_2$ and other low-carbon fuels in reducing $CO_2$ emissions. Although $CO_2$ savings were realised, the energy demand associated with the $H_2$ processes was notably higher compared to the fossil-based process. This increase was attributed to the energy losses in water electrolysis, which became increasingly significant on a per-tonne clinker basis as the level of hydrogen substitution increased. Notably, among the distinct $H_2$ cases explored, it was observed that improvements in electrolysis efficiencies could lead to greater energy savings. Moreover, the findings showed that while indirect calcination allowed for the production of purer $CO_2$ streams from the clinker flue gas, it required significantly more energy and $H_2$ fuel compared to its direct calcination counterpart.

Building upon decarbonisation through fuel replacement, the subsequent project on the solar based option (Chapter 4) demonstrated $CO_2$ savings of ~26% through nearly complete replacement of fossil fuels with renewable solar energy. Furthermore, regions with high DNI and solar PV capacity factors such as Brazil, show economic benefits from an all-year-round high solar radiation. This climatic advantage substantially dictates the required storage capacities of the subsystems, where greater sunshine availability directly correlates with reduced storage capacities, higher efficiencies, and, consequently, lower economic costs. Techno-economic analyses within this project reveal that the cost of the kiln subsystem represents 80 – 90% of the solar driven process costs due to the high electricity demand combined with the current high cost of solar PV and the associated energy storage systems, limiting the economic feasibility under current assumptions. Conversely, the solar calciner subsystem becomes economically attractive once natural gas prices surpass 30 USD/MWh at the Brazil site and 50 USD/MWh for the United States and China sites. The results convey the impact of local solar energy characteristics on the techno-economics, whilst emphasising the need for cost reductions in renewables-based decarbonisation options.

The final project (Chapter 5) shifts the focus from fuel related emissions to calcination induced emissions where the findings reveal a substantial $CO_2$ reduction of up to ~35% through alternative clinkers in contrast with the conventional fossil-based process without compromising the compressive strength. This reduction further increased to ~45% when 25% of the clinker was substituted with SCMs from $CO_2$ mineralisation, which partially captures $CO_2$ from clinker flue gases. Although all alternative clinkers showed energy savings over conventional clinker, the clinker incorporating SCMs exhibited a minute increase in the total energy demand, due to the additional energy required for MEA-based $CO_2$ capture and $CO_2$ mineralisation. The factors influencing the $CO_2$ and energy intensities in these alternative clinkers were the limestone content, alite concentration (which is the most carbon intensive clinker component), and the reduction in sintering temperatures to as low as 1250 °C (decreasing the total enthalpy of formation). Despite the slight increase in energy requirements by a margin of only 1.5% using the SCM containing cement, the substantial $CO_2$ savings of ~45% offsets this higher energy demand, underscoring the potential of this clinker formulation in achieving sustainable clinker production.

Overall, the cumulative contribution of this thesis is the fresh insights it offers on the carbon abatement potential of both the materials and process perspectives, complementing energy-oriented studies of clinker production to promote deep decarbonisation of the cement industry. This study is the first of its kind to holistically assess the energetic, carbon and techno-economics of operating specific renewable fuels and different raw meal mixes, underpinned by process simulations and optimisation models. Additionally, the work in this thesis demonstrates the feasibility and level of $CO_2$ mitigation attainable in three distinct regions for a geospatial analysis when utilising alternative clinkers or solar based energy sources. The original research chapters collectively provide technical insights for

researchers and industry practitioners to make informed decisions in decarbonising the clinker production process whilst complying with the Paris Agreement to limit global warming to 1.5 °C above pre-industrial levels.

## 6.2. Limitations and future work

Whilst this thesis has contributed to a performance assessment of technical decarbonisation options for the clinker production process, notable limitations remain that merit further work. Firstly, the solar driven optimisation models and $CO_2$ assessment of alternative clinkers were constrained to the investigation of three countries. Investigation of additional countries could offer a deeper understanding of the variability in costs and capacities, whilst underscoring how differences in solar capacity factors and DNI influence the economic viability of implementing the solar driven option.

Secondly, the use of solar capacity factors and DNI data from a single year limits the representation of long-term trends in annual variations of solar radiation. The inclusion of additional yearly data would improve the optimisation results by providing a broader account of the fluctuations across several years while leading to more precise results. As a result, the optimisation model would be able to develop more robust designs.

Thirdly, the techno-economic analyses were limited to the solar driven option, therefore, introducing optimisation models that specifically targets cost minimisation for the alternative clinkers and $H_2$ options would enable a more robust comparative cost assessment across the decarbonisation options examined in this work. Correspondingly, this approach would determine the key contributors to the overall costs and risks, identifying potential strategies for reducing the costs of other decarbonisation options.

Finally, it is worth noting that, the modelling results are based on standardised assumptions and validated process parameters and further experimental validation, and pilot scale research are recommended to confirm the practical feasibility of the proposed systems under real-world operating conditions.

A logical progression from this study is to assess the feasibility of integrating the decarbonisation options presented, namely the combination of utilising alternative clinkers with either $H_2$ based fuels or solar based energy. This approach could substantially enhance the $CO_2$ savings by addressing emissions from both fuel combustion and calcination. It would be of interest to determine the maximum extent of $CO_2$ reductions achievable through these decarbonisation options without compromising the product properties of clinker or incurring excessive costs.

# Appendix A. Supplementary Information to Chapter 3

All conversions in the heat exchangers are modelled through two separate heaters and coolers connected by a heat flow.

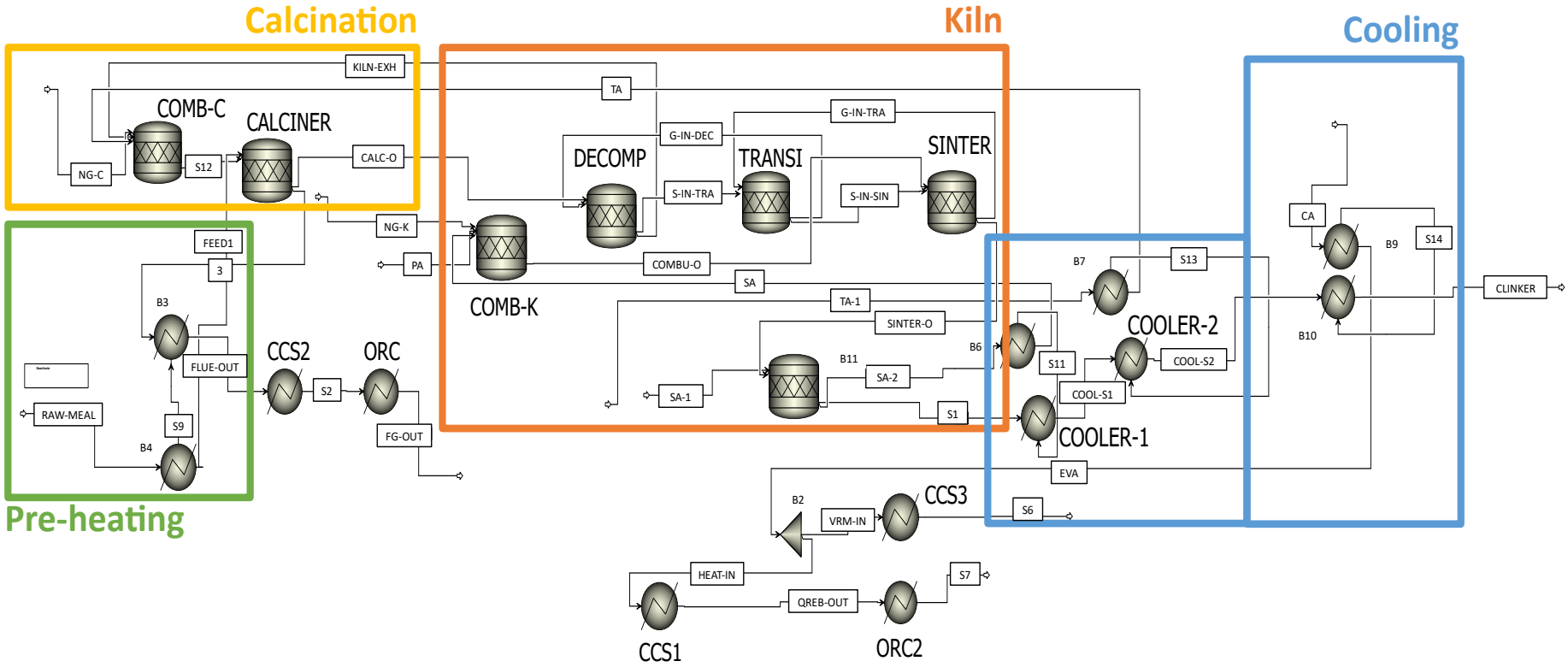


***Figure A.1. Aspen model of the NG process*** *(natural-gas based) with four major stages: i) Preheating of raw meal to 800 °C; ii) Calcination at 900 °C; iii) Kiln combustion at 1500 °C followed by operation with three stages (decomposition, transition, and sintering); and iv) Cooling of clinker to 100 °C using cold air.*

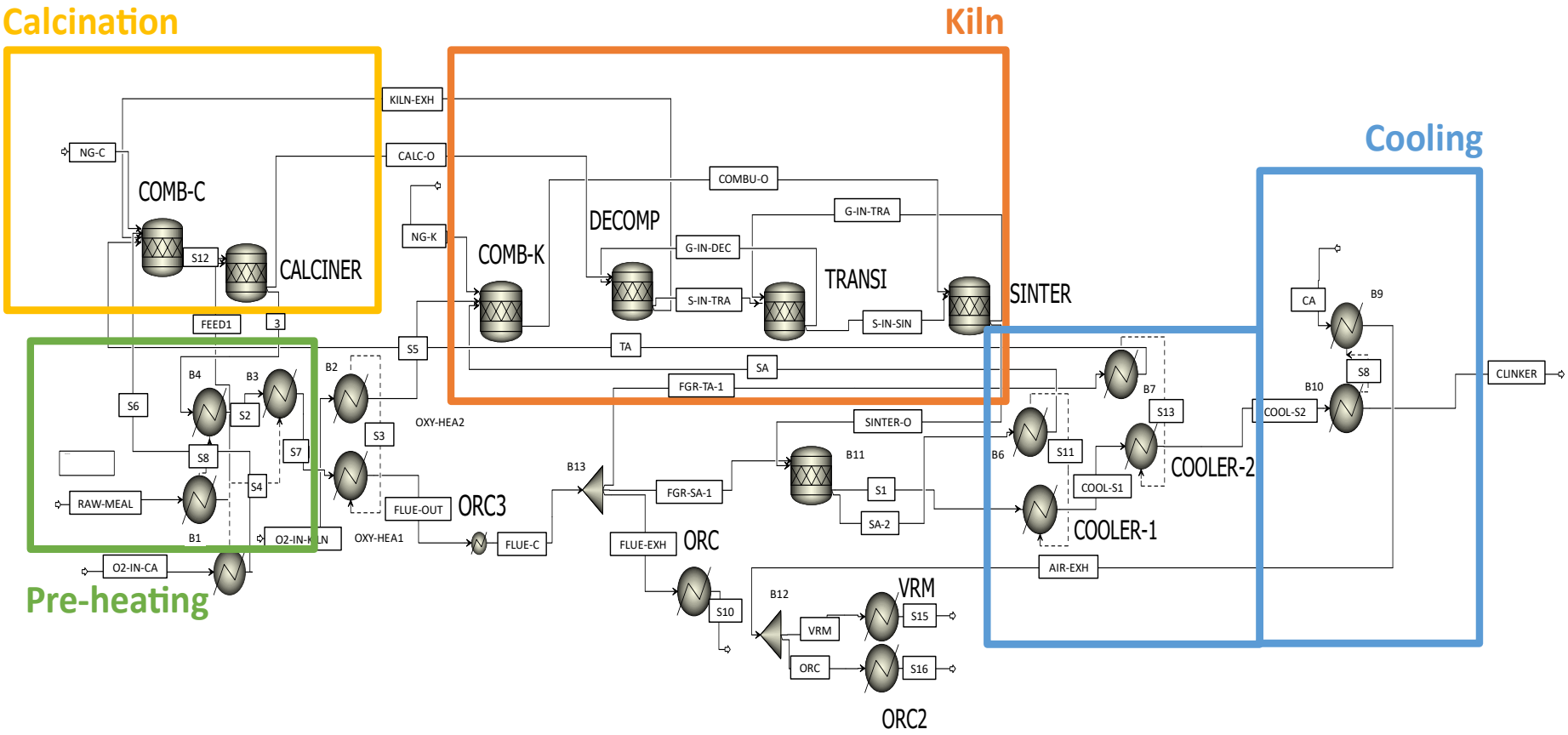


***Figure A.2. Aspen model of the Oxy process*** *(oxy-combustion) with four major stages: i) Preheating of raw meal to 800 °C; ii) Calcination at 900 °C; iii) Kiln combustion at 1500 °C followed by operation with three stages (decomposition, transition, and sintering); and iv) Cooling of clinker to 100 °C using cold air.*

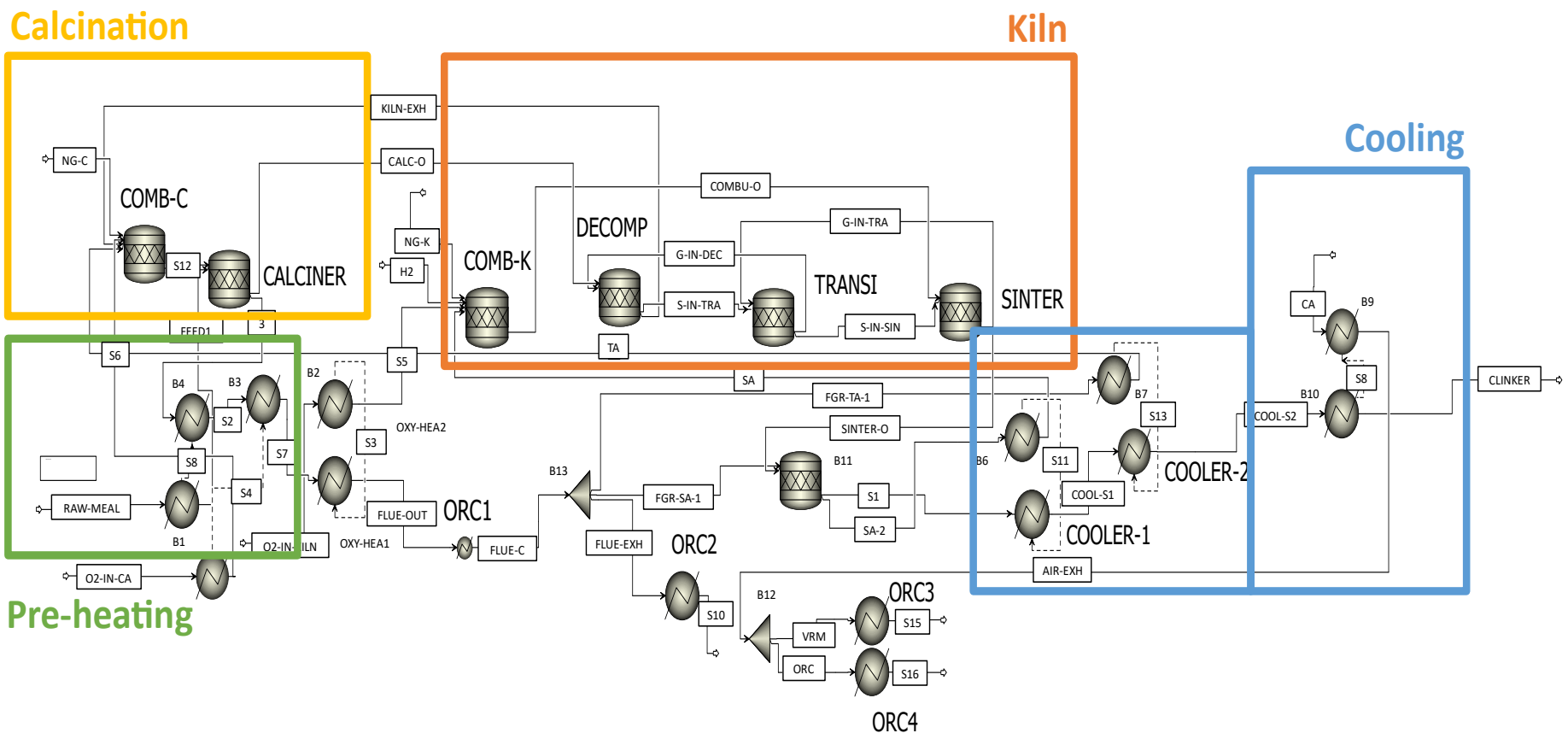


***Figure A.3. Aspen model of the $H_2$-a process*** *(20% hydrogen in the kiln coupled with oxy-combustion) separated into four major stages: i) Preheating of raw meal to 800 °C; ii) Calcination at 900 °C; iii) Kiln combustion at 1500 °C followed by operation with three stages (decomposition, transition, and sintering); and iv) Cooling of clinker to 100 °C using cold air.*

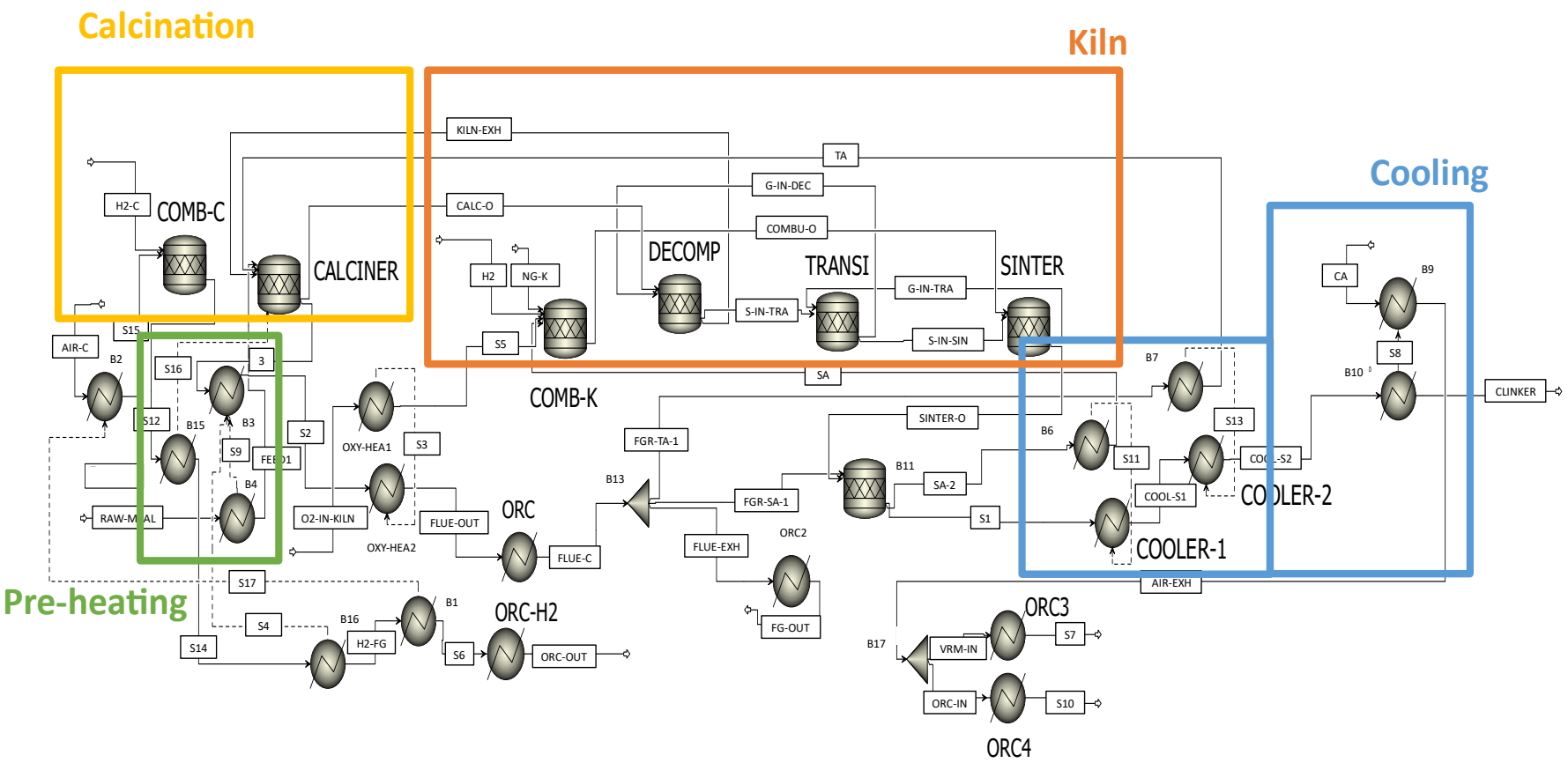


***Figure A.4. Aspen model of the $H_2$-b process*** *(indirect calcination of hydrogen) with four key stages: i) Preheating of raw meal to 800 °C; ii) Calcination at 900 °C; iii) Kiln combustion at 1500 °C followed by operation with three stages (decomposition, transition, and sintering); and iv) Cooling of clinker to 100 °C using cold air.*

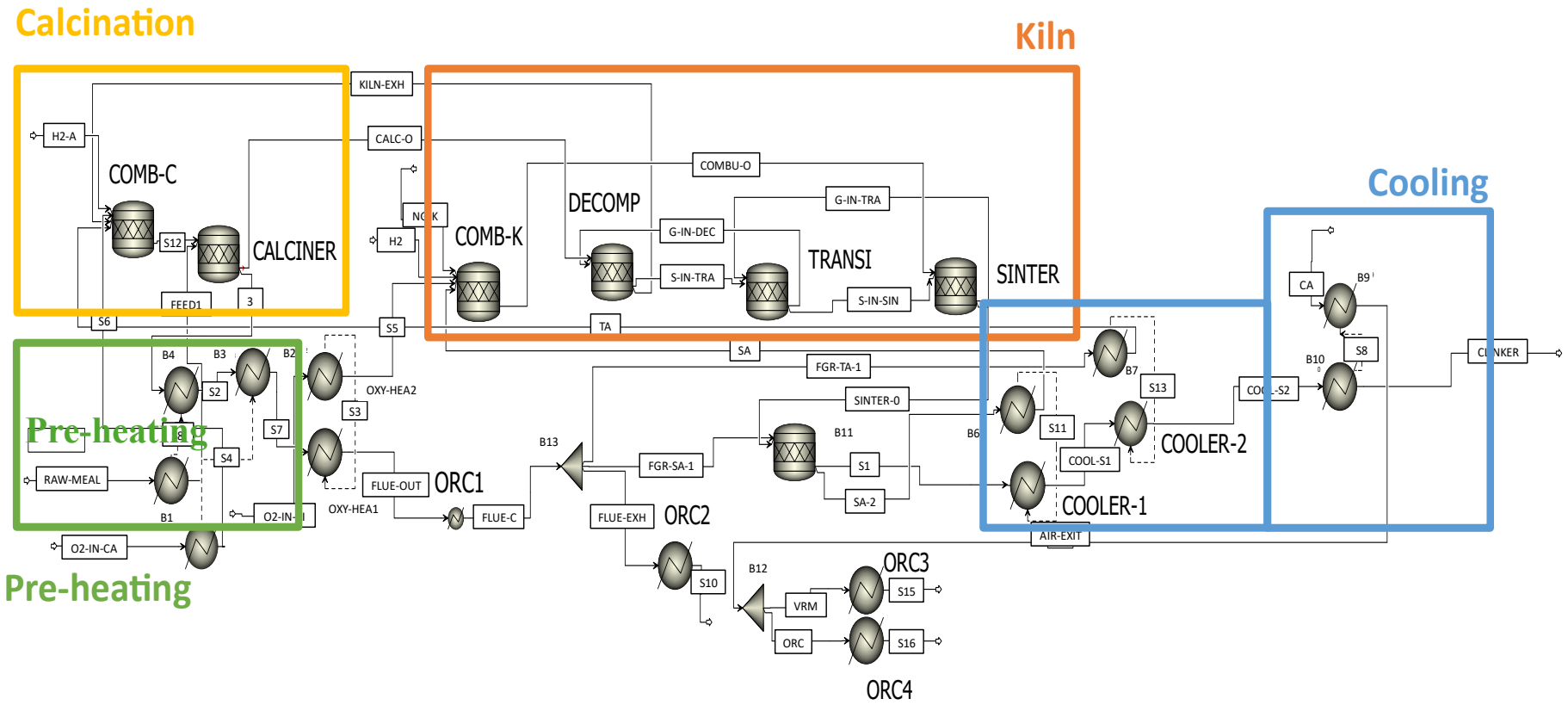


***Figure A.5. Aspen model of the $H_2$-c process*** *(20% hydrogen replacement of natural-gas in both the calciner and kiln) with four key stages: i) Preheating of raw meal to 800 °C; ii) Calcination at 900 °C; iii) Kiln combustion at 1500 °C followed by operation with three stages (decomposition, transition, and sintering); and iv) Cooling of clinker to 10 0°C using cold air.*

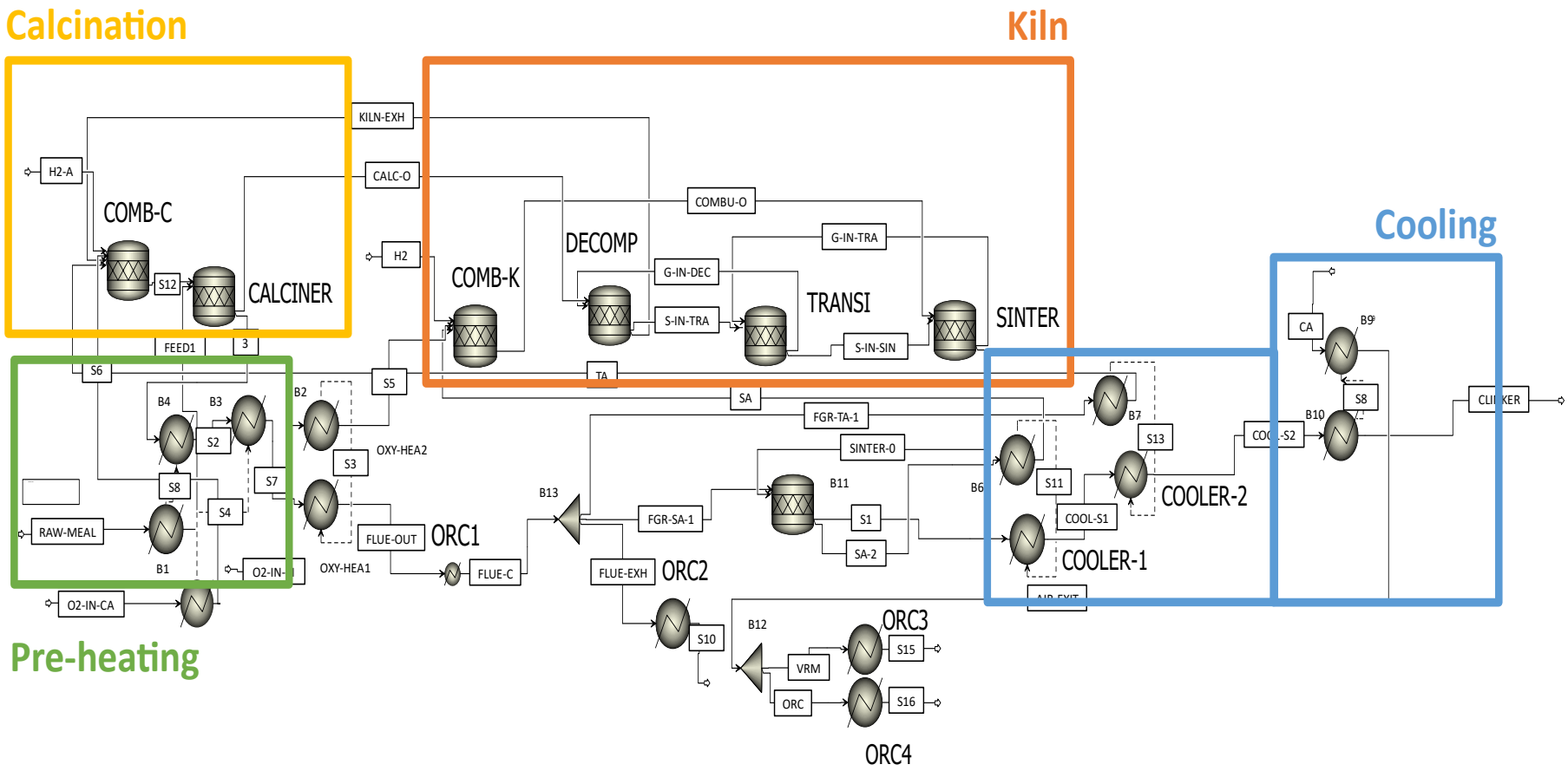


***Figure A.6. Aspen $H_2$-d process*** *(100% hydrogen combustion with oxygen) including four key stages: i) Preheating of raw meal to 800 °C; ii) Calcination at 900 °C; iii) Kiln combustion at 1500 °C followed by operation with three stages (decomposition, transition, and sintering); and iv) Cooling of clinker to 100 °C using cold air.*

***Table A.1.*** *Material flow data of major streams in the NG process.*

| | | | | Molar composition | | | | |
|---|---|---|---|---|---|---|---|---|
| **Stream** | **Temperature (°C)** | **Mass Flow (kg/t clk)** | **Molar Flow (kmol/t clk)** | **CO2** | **N2** | **O2** | **H2O** | **AR** |
| **Primary Air** | 25.00 | 40.29 | 1.39 | 0.00 | 0.78 | 0.21 | 0.00 | 0.01 |
| **Secondary Air** | 1060.00 | 615.60 | 21.26 | 0.00 | 0.78 | 0.21 | 0.00 | 0.01 |
| **Tertiary Air** | 900.00 | 708.93 | 24.48 | 0.00 | 0.78 | 0.21 | 0.00 | 0.01 |
| **Cooling Air** | 25.00 | 2674.00 | 92.34 | 0.00 | 0.78 | 0.21 | 0.00 | 0.01 |
| **Exhaust Vent Air** | 400.00 | 2674.00 | 92.34 | 0.00 | 0.78 | 0.21 | 0.00 | 0.01 |
| **Kiln Exhaust** | 1019.48 | 714.39 | 25.19 | 0.10 | 0.70 | 0.04 | 0.15 | 0.00 |
| **Calciner Flue Gas** | 898.54 | 2001.46 | 64.67 | 0.27 | 0.57 | 0.00 | 0.15 | 0.01 |
| **Pre-heater Flue Gas** | 377.64 | 2001.46 | 64.67 | 0.27 | 0.57 | 0.00 | 0.15 | 0.01 |

***Table A.2.*** *Material flow data of major streams in the Oxy process.*

| | | | | Molar composition | | | | |
|---|---|---|---|---|---|---|---|---|
| **Streams** | **Temperature (°C)** | **Mass Flow (kg/t clk)** | **Molar Flow (kmol/t clk)** | **CO2** | **N2** | **O2** | **H2O** | **AR** |
| **Secondary Air** | 1060.00 | 734.60 | 21.24 | 0.64 | 0.00 | 0.00 | 0.36 | 0.00 |
| **Tertiary Air** | 900.00 | 846.66 | 24.48 | 0.64 | 0.00 | 0.00 | 0.36 | 0.00 |
| **Cooling Air** | 25.00 | 2216.00 | 76.49 | 0.00 | 0.78 | 0.21 | 0.00 | 0.01 |
| **Exhaust Vent Air** | 298.40 | 2216.00 | 76.49 | 0.00 | 0.78 | 0.21 | 0.00 | 0.01 |
| **Kiln Exhaust** | 1124.20 | 939.75 | 28.52 | 0.57 | 0.00 | 0.00 | 0.43 | 0.00 |
| **Calciner Flue Gas** | 899.24 | 2544.41 | 73.57 | 0.64 | 0.00 | 0.00 | 0.36 | 0.00 |
| **Pre-heater Flue Gas** | 528.93 | 2544.41 | 73.57 | 0.64 | 0.00 | 0.00 | 0.36 | 0.00 |

***Table A.3.*** *Material flow data of major streams in the $H_2$-a process.*

| | | | | Molar composition | | | | |
|---|---|---|---|---|---|---|---|---|
| **Streams** | **Temperature (°C)** | **Mass Flow (kg/t clk)** | **Molar Flow (kmol/t clk)** | **CO2** | **N2** | **O2** | **H2O** | **AR** |
| **Secondary Air** | 1060.00 | 724.27 | 21.24 | 0.62 | 0.00 | 0.00 | 0.38 | 0.00 |
| **Tertiary Air** | 900.00 | 834.75 | 24.48 | 0.62 | 0.00 | 0.00 | 0.38 | 0.00 |
| **Cooling Air** | 25.00 | 2216.00 | 76.49 | 0.00 | 0.78 | 0.21 | 0.00 | 0.01 |
| **Exhaust Vent Air** | 300.38 | 2216.00 | 76.49 | 0.00 | 0.78 | 0.21 | 0.00 | 0.01 |
| **Kiln Exhaust** | 1122.84 | 920.23 | 28.64 | 0.54 | 0.00 | 0.00 | 0.46 | 0.00 |
| **Calciner Flue Gas** | 899.76 | 2513.63 | 73.71 | 0.62 | 0.00 | 0.00 | 0.38 | 0.00 |
| **Pre-heater Flue Gas** | 528.48 | 2513.63 | 73.71 | 0.62 | 0.00 | 0.00 | 0.38 | 0.00 |

***Table A.4.*** *Material flow data of major streams in the $H_2$-b process.*

| | | | | Molar composition | | | | |
|---|---|---|---|---|---|---|---|---|
| **Streams** | **Temperature (°C)** | **Mass Flow (kg/t clk)** | **Molar Flow (kmol/t clk)** | **CO2** | **N2** | **O2** | **H2O** | **AR** |
| **Secondary Air** | 1060.00 | 791.51 | 21.24 | 0.74 | 0.00 | 0.00 | 0.26 | 0.00 |
| **Tertiary Air** | 900.00 | 912.25 | 24.48 | 0.74 | 0.00 | 0.00 | 0.26 | 0.00 |
| **Cooling Air** | 25.00 | 2216.00 | 76.49 | 0.00 | 0.78 | 0.21 | 0.00 | 0.01 |
| **Exhaust Vent Air** | 277.66 | 2216.00 | 76.49 | 0.00 | 0.78 | 0.21 | 0.00 | 0.01 |
| **Kiln Exhaust** | 1128.33 | 990.92 | 28.78 | 0.63 | 0.00 | 0.00 | 0.37 | 0.00 |
| **Calciner Flue Gas** | 899.95 | 2434.33 | 65.32 | 0.74 | 0.00 | 0.00 | 0.26 | 0.00 |
| **Pre-heater Flue Gas** | 639.61 | 2434.33 | 65.32 | 0.74 | 0.00 | 0.00 | 0.26 | 0.00 |
| **Indirect Combustor Out** | 2523.56 | 741.04 | 30.07 | 0.00 | 0.64 | 0.00 | 0.35 | 0.00 |
| **Indirect Combustor Flue Gas** | 530.00 | 741.04 | 30.07 | 0.00 | 0.64 | 0.00 | 0.35 | 0.00 |

***Table A.5.*** *Material flow data of major streams in the $H_2$-c process.*

| | | | | Molar composition | | | | |
|---|---|---|---|---|---|---|---|---|
| **Streams** | **Temperature (°C)** | **Mass Flow (kg/t clk)** | **Molar Flow (kmol/t clk)** | **CO2** | **N2** | **O2** | **H2O** | **AR** |
| **Secondary Air** | 1060.00 | 658.10 | 21.24 | 0.49 | 0.00 | 0.00 | 0.50 | 0.00 |
| **Tertiary Air** | 900.00 | 758.49 | 24.48 | 0.49 | 0.00 | 0.00 | 0.50 | 0.00 |
| **Cooling Air** | 25.00 | 2216.00 | 76.49 | 0.00 | 0.78 | 0.21 | 0.00 | 0.01 |
| **Exhaust Vent Air** | 324.84 | 2216.00 | 76.49 | 0.00 | 0.78 | 0.21 | 0.00 | 0.01 |
| **Kiln Exhaust** | 1118.50 | 849.20 | 28.45 | 0.45 | 0.00 | 0.00 | 0.54 | 0.00 |
| **Calciner Flue Gas** | 903.14 | 2323.31 | 74.98 | 0.49 | 0.00 | 0.00 | 0.50 | 0.00 |
| **Pre-heater Flue Gas** | 531.51 | 2323.31 | 74.98 | 0.49 | 0.00 | 0.00 | 0.50 | 0.00 |

***Table A.6.*** *Material flow data of major streams in the $H_2$-d process.*

| | | | Molar composition | | | | | |
|---|---|---|---|---|---|---|---|---|
| **Streams** | **Temperature (°C)** | **Mass Flow (kg/t clk)** | **Molar Flow (kmol/t clk)** | **CO2** | **N2** | **O2** | **H2O** | **AR** |
| **Secondary Air** | 1060.00 | 619.79 | 21.24 | 0.43 | 0.00 | 0.00 | 0.57 | 0.00 |
| **Tertiary Air** | 900.00 | 714.34 | 24.48 | 0.43 | 0.00 | 0.00 | 0.57 | 0.00 |
| **Cooling Air** | 25.00 | 2216.00 | 76.49 | 0.00 | 0.78 | 0.21 | 0.00 | 0.01 |
| **Exhaust Vent Air** | 340.16 | 2216.00 | 76.49 | 0.00 | 0.78 | 0.21 | 0.00 | 0.01 |
| **Kiln Exhaust** | 1121.48 | 792.65 | 29.64 | 0.33 | 0.00 | 0.00 | 0.66 | 0.00 |
| **Calciner Flue Gas** | 899.84 | 2197.62 | 75.31 | 0.43 | 0.00 | 0.00 | 0.57 | 0.00 |
| **Pre-heater Flue Gas** | 522.99 | 2197.62 | 75.31 | 0.43 | 0.00 | 0.00 | 0.57 | 0.00 |

***Table A.7.*** *Raw Meal Composition (Faria et al., 2022).*

| **Raw Meal Composition** | **$CaCO_3$** | **$SiO_2$** | **$Al_2O_3$** | **$Fe_2O_3$** |
|---|---|---|---|---|
| Composition (wt%) | 79.47 | 14.34 | 3.49 | 2.70 |

***Table A.8.*** *Solid Properties (Nhuchhen, Sit and Layzell, 2021).*

| **Solid Properties** | **Type** | **Component Name** | **Alias** |
|---|---|---|---|
| $C_2S$ | Solid | Olivine | $Ca_2SiO_4$ |
| $C_3S$ | Solid | Tricalcium-silicate | $Ca_3SiO_5$ |
| $C_3A$ | Solid | Tricalcium-aluminate | $Ca_3Al_2O_6$ |
| $C_4AF$ | Solid | Tetracalcium-aluminoferrite | $Ca_4Al_2Fe_2O_{10}$ |

# Appendix B. Supplementary Information to Chapter 4

***Table B.1. Mass flowrates for the calciner subsystem.*** *Where the fixed values from Aspen simulations in the decision variables are shown.*

| Equations | Abbreviation | Mass flowrates (kg/h) | Reference |
|---|---|---|---|
| $\dot{\boldsymbol{m}}_{\boldsymbol{CM,sc-k}}(\boldsymbol{t}) + \dot{\boldsymbol{m}}_{\boldsymbol{CM,rh-k}}(\boldsymbol{t})$ | $\dot{m}_{CM,total}$(t) | 1026.85 | Aspen Simulation |
| $\dot{\boldsymbol{m}}_{\boldsymbol{KG,sc}}(\boldsymbol{t}) + \dot{\boldsymbol{m}}_{\boldsymbol{KG,rh}}(\boldsymbol{t})$ | $\dot{m}_{KG,total}$(t) | 1071.73 | Aspen Simulation |
| $\dot{\boldsymbol{m}}_{\boldsymbol{TA}}(\boldsymbol{t})$ | $\dot{m}_{TA}(t)$ | 681.07 | Aspen Simulation |

The energy demand in the calciner subsystem regarding the solid materials and gases were analysed using Aspen Plus simulations. For solid materials, the energy demands associated with calcination per kg of calcined meal ($q_{CM,cal}$), re-heating per kg of raw meal ($q_{RM,rhe}$), pre-heating per kg of raw meal ($q_{RM,phe}$), were determined by running Aspen Plus models of each specific subsystem (solar calciner, re-heater, and pre-heater) and determining the energy required to output 1 kg of required material (see Table B.2). Conversely, for the gases, the heat energy (Q, in MJ/kg) of the solar calciner kiln gas ($Q_{KG,SC}$), re-heater kiln gas ($Q_{KG,RH}$), and pre-heater tertiary air ($Q_{TA}$) were determined based on Appendix Equation B.18.

***Table B.2. Energy parameters in the calciner subsystem.*** *The energy demand per kilograms (kg) of material was determined from Aspen Simulations, and the LHV denotes the lower heating value of natural gas, in this case 100% methane. $Q_{KG,sc}$, $Q_{KG,rh}$, and $Q_{TA}$ were calculated by using the heat equation: $Q = C_p * T_{chg}$, where $C_p$ is the heat capacity of the gas, and $T_{chg}$ is the temperature difference between the input and output flows.*

| Energy parameters in calciner | Abbreviation | Value | Unit | Reference |
|---|---|---|---|---|
| **Calcination energy demand per kg of calcined meal** | $q_{CM,cal}$ | 1.422 | MJ/kg | Aspen Simulation |
| **Re-heating energy demand per kg of raw meal** | $q_{RM,rhe}$ | 0.233 | MJ/kg | Aspen Simulation |
| **Pre-heating energy demand per kg of raw meal** | $q_{RM,phe}$ | 0.817 | MJ/kg | Aspen Simulation |
| **Solar calciner kiln gas energy** | $Q_{KG,sc}$ | 0.266 | MJ/kg | Aspen Simulation |
| **Re-heater kiln gas energy** | $Q_{KG,rh}$ | 0.266 | MJ/kg | Aspen Simulation |
| **Pre-heater kiln gas energy** | $Q_{TA}$ | 0.951 | MJ/kg | Aspen Simulation |
| **LHV of natural gas** | $LHV_{NG}$ | 50 | MJ/kg | (Wan, 2004) |
| **Energy per kg of natural gas** | $NG_{energy}$ | 13.9 | kWh/kg | (Commission, 2023) |

***Table B.3. Temperatures of exhaust gases in the optimisation model*** *for the calciner subsystem, where the values were obtained from Aspen simulations represented in Kevin (K).*

| Exhaust gases | Abbreviation | Temperatures of exhaust gases | Unit | Reference |
|---|---|---|---|---|
| **Solar calciner exhaust** | $T_{EG,sc}$ | 1172.98 | K | Aspen Simulations |
| **Re-heater exhaust** | $T_{EG,rh}$ | 1172.98 | K | Aspen Simulations |
| **Pre-heater exhaust** | $T_{EG,ph}$ | 1172.98 | K | Calciner Optimisation Model |

Where the exhaust gas flows of the calciner, re-heater, and pre-heater were determined from Appendix B Equations (B.1)–(B.17), where the fractions of each gas component (i.e., $O_2$, $N_2$, $CO_2$ and $H_2O$) are multiplied by the gas flowrate. SC, RH and PH, denotes the solar calciner, re-heater, and pre-heater, respectively.

*Equation B.1. Solar calciner oxygen exhaust.*

$$\dot{m}_{O2,exhaust,sc} = \dot{m}_{KG,sc}(t) * 0.225$$

*Equation B.2. Solar calciner nitrogen exhaust.*

$\dot{m}_{N2,exhaust,sc} = \dot{m}_{KG,sc}(t) * 0.735$

*Equation B.3. $CO_2$ per kg of raw meal.*

$CO2/kg\ of\ raw\ meal$ = 1062.96/3200= 0.332 kg $CO_2$/kg RM

*Equation B.4. Solar calciner $CO_2$ exhaust.*

$\dot{m}_{CO2,exhaust,sc} = [0.025 * \dot{m}_{KG,sc}(t)] + (\dot{m}_{RM,ph}(t) * 0.332)$

*Equation B.5. Solar calciner water exhaust.*

$\dot{m}_{H2O,exhaust,sc} = \dot{m}_{KG,sc}(t) * 0.003$

Before determining the re-heater gas flows, we calculated the amount of each gas needed to support natural gas (NG) combustion:

*Equation B.6. $CH_4$ for natural gas combustion.*

$CH_{4,mol} = \dot{m}_{NG}(t)$ g / 16.04 g/mol = 0.062 * $\dot{m}_{NG}(t)$ mol

*Equation B.7. $O_2$ needed by natural gas combustion.*

$\dot{m}_{O2,NG,comb}$ = 2 * $\dot{m}_{NG}(t)$ mol * 32 g/mol = 0.064 * $\dot{m}_{NG}(t)$ kg/h

*Equation B.8. $CO_2$ produced by natural gas combustion.*

$\dot{m}_{CO2,NG,comb}$= $\dot{m}_{NG}(t)$mol * 44.01 g/mol = 0.044 * $\dot{m}_{NG}(t)$ kg/h

*Equation B.9. $H_2O$ produced by natural gas combustion.*

$\dot{m}_{H2O,NG,comb}$ = 2 * $\dot{m}_{NG}(t)$ mol * 18.016 g/mol = 0.036 * $\dot{m}_{NG}(t)$ kg/h

*Equation B.10. Re-heater oxygen exhaust.*

$\dot{m}_{O2,exhaust,rh}$ = ($\dot{m}_{KG,rh}(t)$ * 0.225) - $O_{2,NG,combustion}$

*Equation B.11. Re-heater nitrogen exhaust.*

$\dot{m}_{N2,exhaust,rh}$ = (0.735 * $\dot{m}_{KG,rh}(t)$)

*Equation B.12. Re-heater water exhaust.*

$\dot{m}_{H2O,exhaust,rh}$ = (0.003 * $\dot{m}_{KG,rh}(t)$) + $H_2O_{NG,combustion}$

*Equation B.13. Re-heater carbon dioxide exhaust.*

$\dot{m}_{CO2,exhaust,rh}$ = (0.025 * $\dot{m}_{KG,rh}(t)$) + $CO_{2,NG,combustion}$

*Equation B.14. Pre-heater oxygen exhaust (excluding contribution of tertiary air, same below).*

$\dot{m}_{O2,exhaust,ph} = \dot{m}_{O2,exhaust,sc} + \dot{m}_{O2,exhaust,rh}$

*Equation B.15. Pre-heater nitrogen exhaust.*

$\dot{m}_{N2,exhaust,ph} = \dot{m}_{N2,exhaust,sc} + \dot{m}_{N2,exhaust,rh}$

*Equation B.16. Pre-heater carbon dioxide exhaust.*

$$\dot{m}_{CO2,exhaust,ph} = \dot{m}_{CO2,exhaust,sc} + \dot{m}_{CO2,exhaust,rh}$$

*Equation B.17. Pre-heater water exhaust.*

$$\dot{m}_{H2O,exhaust,ph} = \dot{m}_{H2O,exhaust,sc} + \dot{m}_{H2O,exhaust,rh}$$

*Equation B.18. Heat energy.*

$$Q = C_p * T_{change}$$

***Table B.4. Heat capacity (Cp) of relevant gases*** *in the calciner subsystem where they are represented in units of kJ/kg-K. Where Cp of a particular gas ($C_{p,gas}$) was calculated based on the mass fraction of $CO_2$, $N_2$, $O_2$, and $H_2O$ in each respective gas as per Equation B.19.*

| Gas | Abbreviation | Heat capacity | Unit | Reference |
|---|---|---|---|---|
| **Carbon dioxide, $CO_2$** | $Cp_{N2}$ | 1.270 | kJ/kg-K | (Poling, Prausnitz and O'Connell, 2020) |
| **Oxygen, $O_2$** | $Cp_{O2}$ | 1.109 | kJ/kg-K | (Poling, Prausnitz and O'Connell, 2020) |
| **Nitrogen, $N_2$** | $Cp_{N2}$ | 1.196 | kJ/kg-K | (Poling, Prausnitz and O'Connell, 2020) |
| **Water, $H_2O$** | $Cp_{H2O}$ | 4.187 | kJ/kg-K | (Poling, Prausnitz and O'Connell, 2020) |

*Equation B.19. Heat capacity ($C_p$).*

$$C_{p,gas} = \left(C_{p,CO2} * mass\ fraction_{CO2}\right) + \left(C_{p,O2} * mass\ fraction_{O2}\right) + \left(C_{p,N2} * mass\ fraction_{N2}\right) + \left(C_{p,H2O} * mass\ fraction_{H2O}\right)$$

This study utilised GAMS which is a mathematical programming and modelling system designed to solve both linear and nonlinear optimisation problems, aiding in decision making on optimising resources effectively (Rejani *et al.*, 2022). GAMS has been previously applied in engineering research, including pavement management to optimise the costs and utilise resources effectively (Rejani *et al.*, 2022), and to optimise pump and value schedules in complex large scale water distribution networks from a distinct range of constraints (Skworcow *et al.*, 2014). In this study, GAMS was utilised to optimise the costs of a solar driven clinker process.

A linear programming model was used as the constraints, mass and energy balances, vary linearly with the respective mass and energy flowrates between different process units, constituting to the majority of the decision variables. This implies that where multiplication occurs in the model, it involves only one decision variable (and one constant parameter). Moreover, the objective function itself is linear and does not contain non-linear relationships.

The reference year is 2020, and inflation is excluded to simplify the economic analysis, focusing on a relative comparison between the solar driven and conventional processes. It is assumed to equally affect clinker production costs, resulting in a neutral net impact that does not influence the techno-economic analysis. Moreover, it is worth noting that the use of alternative energy sources such as plasma-based electrification or solar energy currently remains limited to research and pilot scale plants due to the present high production and storage costs as detailed in Table B.5.

***Table B.5. Cost parameters for the calciner and kiln subsystems.*** *Where the GAMS abbreviation and the units are displayed; the calciner subsystem includes the compound parabolic concentrator (CPC) which supplies solar energy to the calciner, solar tower (tower), heliostats, solar calciner (SC), and calcined meal stored (storage). The annualised CAPEX (see Equation 4.11) was calculated using the annual factor from Equation B.20, where r denotes the interest rate at 8%, and n denoting the lifetime of the plant as 30 years. The kiln subsystem involves the natural gas, PV, and PV battery storage costs. The total costs of the solar tower (k_tower_total) was calculated using Equation B.21, where k_tower_ref, k_tower, and A_helio_ref are given, whilst A_helio is determined in the optimisation model of the calciner subsystem.*

| Cost parameters | Abbreviation | Value | Unit | Reference |
|---|---|---|---|---|
| **Solar calciner CAPEX** | $k_{SC,CAPEX}$ | 91.937 | USD/t RM-day | (Moumin *et al.*, 2020) |
| **Calcined meal stored CAPEX** | $k_{storage,CAPEX}$ | 9.612 | USD/kWh | (Moumin *et al.*, 2020) |
| **CAPEX of heliostats** | $k_{heliostats}$ | 97.20 | USD/m$^2$ | (Moumin *et al.*, 2020) |
| **Fixed CAPEX of solar tower** | $k_{tower}$ | 19.937 | USD/m$^2$ | (Moumin *et al.*, 2020) |
| **Fixed Compound parabolic concentrator (CPC)** | $k_{CPC\_fixed}$ | 47,067.48 | USD | (Moumin *et al.*, 2020) |
| **Variable Compound parabolic concentrator (CPC)** | $k_{CPC\_variable}$ | 30,849.12 | USD/MW | (Moumin *et al.*, 2020) |
| **Reference costs of the solar tower** | $k_{tower\_ref}$ | 195,000.00 | USD | (Meier, Gremaud and Steinfeld, 2005) |
| **Reference area of heliostats** | $A_{helio\_ref}$ | 4,955.00 | m$^2$ | (Meier, Gremaud and Steinfeld, 2005) |
| **Natural gas** | $k_{NG}$ | 1.42 | USD/t RH-CM | (Our World in Data, 2024) |
| **Photovoltaics (PV)** | $k_{pv}$ | 77.81 | USD/kW | (Renewable Energy Agency, 2023) |
| **Photovoltaics (PV) battery storage** | $k_{battery}$ | 35.53 | USD/kWh | (Cole and Karmakar, 2030) |
| **Battery storage efficiency** | $\eta_{batt,storage}$ | 0.95 | n/a | (Sepúlveda *et al.*, 2023) |

*Equation B.20. Annualisation factor for CAPEX.*

$$annual_{factor} = (\frac{r}{1-(1+r)^{-n}})$$

*Equation B.21. Total costs of the solar tower.*

$$k_{tower\_total} = k_{tower\_ref} + (\left(A_{helio} - A_{helio_{ref}}\right) * k_{tower})$$

***Table B.6. Countries selected for the location dependent analysis.*** *Where their annual cement production and ranking (from the top ten global cement producers) are identified.*

| Country | Cement production, 2023 (million metric tonnes) | Ranking, from top ten | Reference |
|---|---|---|---|
| **China** | 2100 | #1 | (Jaganmohan, 2024a) |
| **United States** | 91 | #4 | (Jaganmohan, 2024a) |
| **Brazil** | 63 | #7 | (Jaganmohan, 2024a) |

It is worth noting that, this study quantifies the direct $CO_2$ emissions avoided from replacing fossil fuels in the combustion stages, however, indirect emissions (i.e., from material production, transport, life cycle of cement) are not within the scope of this work due to the lack of reliable data for solar-based cement production and need for a cradle-to-grave assessment. Moreover, minor components (i.e., $K_2O$, $Na_2O$, $SO_3$, $TiO_2$, and MgO) were not considered based on literature (John, 2020; Wang and Shi, 2024) as their concentrations typically range between >0.01 – 1.22 wt.%. Although these components can slightly reduce the melting temperature and form solid solutions with major components (Lea, Hewlett and Liska, 2019), the overall impact is minimal due to their low concentrations. For instance, $SO_3$ and $Na_2O$ can influence the burnability of the raw meal during solid-state reactions (Segata *et al.*, 2019), affecting the combustion temperatures, whilst high levels of $TiO_2$ can reduce the compressive strength (Blotevogel *et al.*, 2021). Conversely $K_2O$ can lower the calcination temperature by 10 – 23°C if 0.50 – 0.80 wt.% is used (Weibo *et al.*, 2017). Similarly, MgO can reduce the combustion temperature, however, leads to lower

compressive strength (José *et al.*, 2020). However, the overall impact of these minor components on chemical reactions, $CO_2$ emissions, and energy consumption in clinker production is assumed to be minimal (John, 2020; Wang and Shi, 2024), without substantially influencing the clinker formation, fuel consumption, or energy efficiency.

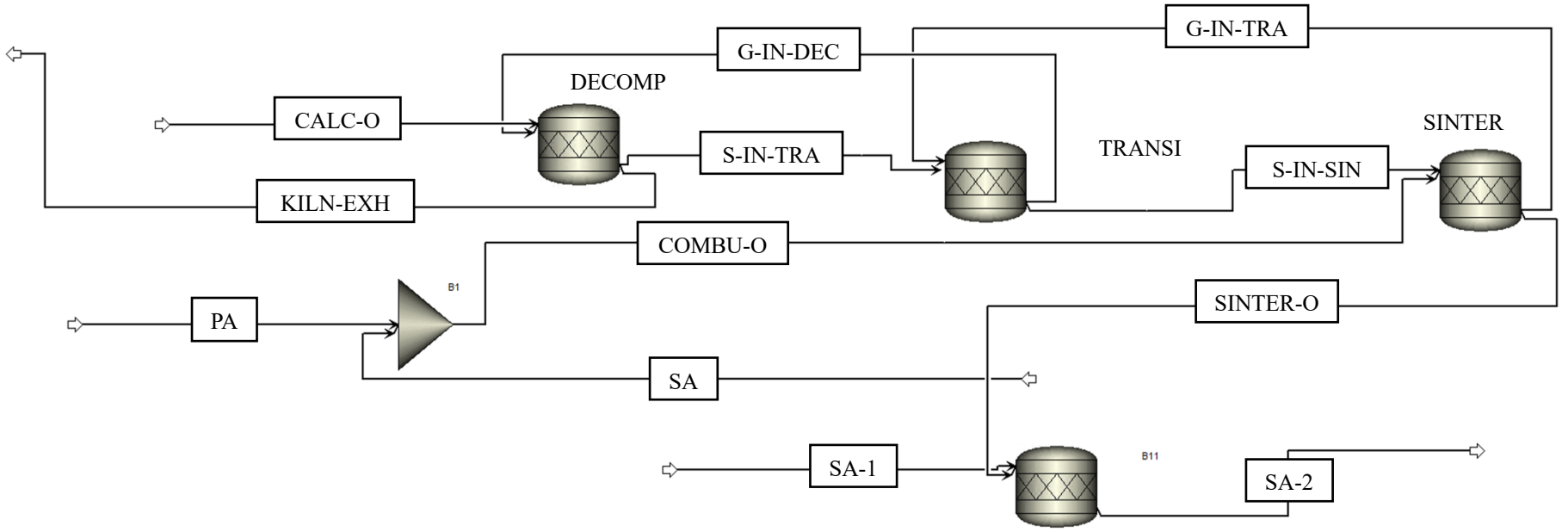


***Figure B.1. Aspen simulation of the kiln subsystem*** *as modelled in (Williams, Yang and Nhuchhen, 2024), with the focus of simulating the kiln subsystem to determine the plasma flow-rate (PA) in the kiln. In contrast, the solar calciner energy and mass flows were modelled through GAMS optimisation.*

# Appendix C. Supplementary Information to Chapter 5

The primary strength contributing minerals in clinker are $C_3S$ and $C_2S$, responsible for the early and the later stages of strength development, respectively (Neville and Brooks, 2010; Lea, Hewlett and Liska, 2019). The strength development of cement is typically attributed to hydration, during which the formation of the stable hydration product (C-S-H) fills pores and voids, thereby enhancing strength and initiating cement setting (Lea, Hewlett and Liska, 2019; Pareek and Sankhla, 2020). Calcium silicate hydrate (C-S-H) is formed when $C_3S$ or $C_2S$ reacts with water which is the primary strength contributor in cement. C-S-H typically contains twice as much CaO compared to $SiO_2$, along with water. Alongside C-S-H, hydration of $C_3S$ and $C_2S$ releases additional CaO, forming calcium hydroxide (CH), where free lime, reacting with water, also contributes to CH formation. Furthermore, AFt phases form continuously as long as $C_3A$, sulfate and water are present (Lea, Hewlett and Liska, 2019).

Calcium sulfate ($SO_3$) regulates the setting time by controlling the rapid reaction rate of $C_3A$. Without $SO_3$, the rapid hydration of $C_3A$ would result in the stiffening of the cement paste, known as flash set, which is irreversible and renders the concrete unplaceable. The presence of $SO_3$ modifies the above reaction, forming a calcium sulfoaluminate hydrate and thereby controlling the setting behaviour (Neville and Brooks, 2010; Lea, Hewlett and Liska, 2019). The filler effect influences cement hydration through the incorporation of inert fine powders or fillers. This facilitates early hydration of cement by increasing the water and space for the formation of hydration products in the clinker phases due to a higher water to clinker ratio

whilst also providing enhanced nucleation (Lothenbach, Scrivener and Hooton, 2011; Skibsted and Snellings, 2019; Snellings, Suraneni and Skibsted, 2023).

Through the pozzolanic reaction, SCMs produce hydration products of C-S-H which is responsible for strength development and contributes to a denser microstructure. Compared to the primary clinker phase (alite), SCMs typically reacts slower, resulting in lower early-age strength when higher SCM replacement levels (30 – 50% wt.) are used. The primary contribution to strength development from SCMs occurs from prolonged hydration, allowing the cement to reach or surpass the strength of OPC after 28 – 90 days (Skibsted and Snellings, 2019). The following (see Table C.1) further explains the properties of clinker, how it leads to the formation of cement, cement paste, mortar and concrete.

It should be noted that alternative clinkers are primarily in the research and pilot-scale stages. Given the limited industrial-scale data and long-term performance validation, additional experimental investigations are required to assess their practical viability for large-scale structural applications.

***Table C.1. Properties of clinker, cement, cement paste, mortar, and concrete.***

| | Composition | Properties | References |
|---|---|---|---|
| Clinker | $C_3S + C_2S + C_4AF + C_3A$ | • **$C_3S$** – Primary mineral responsible for strength development.<br>• **$C_2S$** – Contributes to later strength development.<br>• **$C_4AF$** – Reacts with gypsum, accelerating the hydration of silicates.<br>• **$C_3A$** – Contributes to the initial setting characteristics from rapid hydration, facilitating the combination of lime and silica. | (Neville and Brooks, 2010; Lea, Hewlett and Liska, 2019; Pareek and Sankhla, 2020) |
| Cement | Clinker + Gypsum | • **Gypsum** (calcium sulfate) – Regulates the setting time and controls the rapid reaction rate of $C_3A$. | (Neville and Brooks, 2010; Lea, Hewlett and Liska, 2019; Cembureau, 2024) |
| Cement paste | Cement + $H_2O$ | • **$H_2O$** – Water addition (i.e., hydration) initiates the formation of stable hydration products (C-S-H and $Ca(OH)_2$), which contributes to the strength development, filling pores and voids, whilst triggering the setting of cement. | (Lea, Hewlett and Liska, 2019). |
| Mortar | Cement paste + fine aggregate (i.e., sand) | • **Fine aggregate** – Improves workability, reduces water demand, and improves the compressive strength. | (Lea, Hewlett and Liska, 2019; Pareek and Sankhla, 2020) |
| Concrete | Mortar + coarse aggregates (i.e., gravel, crushed stone, etc.) | • **Coarse aggregate** – Improves the strength, durability, load-bearing capacity, and crack resistance whilst providing structural mass which are crucial for durability and structural performance. | (Neville and Brooks, 2010; Lea, Hewlett and Liska, 2019; Pareek and Sankhla, 2020) |

***Table C.2. Physical properties of user inputted clinker minerals among cases****, including the chemical formula, molecular weight, enthalpy of formation, heat capacity, and their respective sources; the heat capacity ($C_p$) was calculated with reference to the temperature, where the temperature (T) is 298K among the cases, and the equation is $C_p = C_{1i} + C_{2i}*T + C_{3i}*T^2 + C_{4i}*T^{-1} + C_{5i}*T^{-2} + C_{6i}*T^{-0.5}$, where i is the constant specified in the table.*

| Name | Chemical Formula | Molecular Weight (g/mol) | Enthalpy of Formation (J/kmol) | $C_{1i}$ | $C_{2i}$ | $C_{3i}$ | $C_{4i}$ | $C_{5i}$ | $C_{6i}$ | Source |
|---|---|---|---|---|---|---|---|---|---|---|
| Calcium aluminoferrite | $Ca_4Al_2Fe_2O_{10}$ ($C_4AF$) | 485.96 | -5.08e3 | 3.74e2 | 7.30e-2 | 0 | 0 | 0 | 0 | (Faria *et al.*, 2022) |
| Tricalcium aluminate | $Ca_3Al_2O_6$ ($C_3A$) | 270.19 | -3.56e3 | 2.61e2 | 1.90e-2 | 0 | 0 | -5.06e6 | 0 | (Faria *et al.*, 2022) |
| Calcium Sulfoaluminate | $Ca_{12}Al_6O_{12}SO_4$ ($C_4A_3S$) | 610.26 | -8.38e9 | 6.93e2 | 1.80e-2 | 0 | 0 | -2.92e7 | 0 | (Lothenbach *et al.*, 2022) |
| Gehlenite/ Melilite | $Ca_2Al_2SiO_7$ | 274.20 | -3.99e9 | 5.88e2 | -6.72e-2 | 3.89e5 | 0 | 1.51e6 | -6.27e3 | (Hanein, Glasser and Bannerman, 2020) |

***Table C.3. The energy demand (thermal and electrical) and $CO_2$ produced from the hypothetical cases****, including H-1 (sintering temperature of 1350 °C) and H-2 (sintering temperature of 1250 °C), where only the kiln's sintering temperature was modified from Case 1 (reference).*

| | **Case H-1** | **Case H-2** |
|---|---|---|
| **Hypothetical Cases Energy Demand (kWh/t clinker)** | **OPC - 1350** | **OPC - 1250** |
| Fans (kWh/t clinker) | 56.69 | 32.87 |
| Auxiliary (kWh/t clinker) | 68.00 | 68.00 |
| Organic Rankine Cycle (kWh/t clinker) | -63.87 | -57.37 |
| Raw Meal Preparation (kWh/t clinker) | 25.20 | 25.20 |
| Electrical Energy Total (kWh/t clinker) | 86.03 | 68.71 |
| Natural Gas (kWh/t clinker) | 977.74 | 938.18 |
| **Net Total Energy (kWh/t clinker)** | 1063.77 | 1006.88 |
| **$CO_2$ Produced ($kgCO_2$/t clinker)** | 730.10 | 722.29 |

***Table C.4. The net $CO_2$ emissions of the hypothetical cases*** *(H1 – H2), including the carbon intensity of the electricity grid simulated in three distinctive countries, namely the Unites States (US), China, and Brazil.*

| | | Fans ($kgCO_2$/t clinker) | Auxiliary ($kgCO_2$/t clinker) | Organic Rankine Cycle ($kgCO_2$/t clinker) | Raw Meal Preparation ($kgCO_2$/t clinker) | $CO_2$ produced ($kgCO_2$/t clinker) | Net total $CO_2$ ($kgCO_2$/t clinker) |
|---|---|---|---|---|---|---|---|
| **H1** | **United States** | 20.81 | 24.96 | -23.44 | 9.25 | 730.10 | 761.67 |
| | **China** | 30.11 | 36.12 | -33.92 | 13.38 | 730.10 | 775.79 |
| | **Brazil** | 5.78 | 6.94 | -6.51 | 2.57 | 730.10 | 738.87 |
| **H2** | **United States** | 12.07 | 24.96 | -21.05 | 9.25 | 722.29 | 747.51 |
| | **China** | 17.46 | 36.12 | -30.47 | 13.38 | 722.29 | 758.78 |
| | **Brazil** | 3.35 | 6.94 | -5.85 | 2.57 | 722.29 | 729.30 |

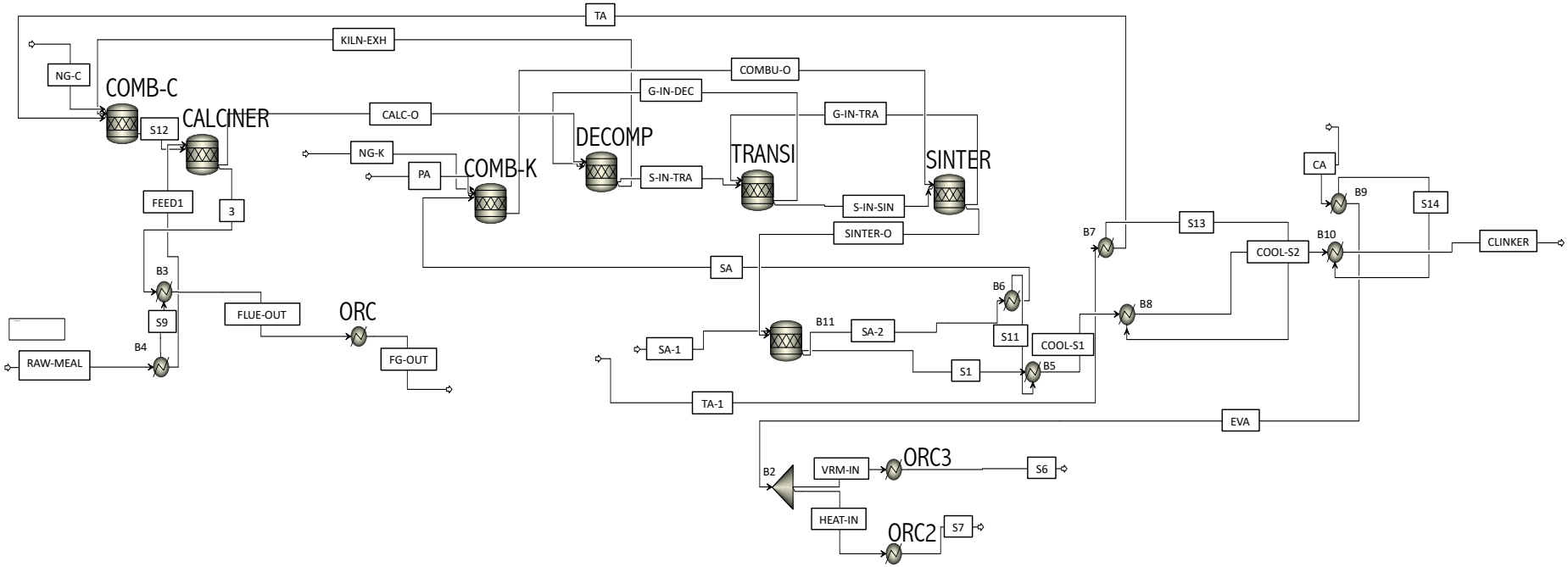


***Figure C.1. Aspen model of the cement production process*** *(natural gas based) with four major stages: i) Preheating of raw meal to 800 °C; ii) Calcination at 900 °C; iii) Kiln combustion at 1500 °C followed by operation with three stages (decomposition, transition, and sintering).*

# References


Abbasi, T. and Abbasi, S.A. (2010) 'Biomass energy and the environmental impacts associated with its production and utilization', *Renewable and Sustainable Energy Reviews*, 14(3), pp. 919–937. Available at: https://doi.org/10.1016/j.rser.2009.11.006.

Abdin, Z. *et al.* (2020) 'Hydrogen as an energy vector', *Renewable and Sustainable Energy Reviews*. Elsevier Ltd. Available at: https://doi.org/10.1016/j.rser.2019.109620.

Adeniran, J.A. *et al.* (2019) 'Exergetic analysis and pollutants emission from a rotary kiln system in a major cement manufacturing plant', *Energy and Environment*, 30(4), pp. 601–616. Available at: https://doi.org/10.1177/0958305X18802766.

Agico Cement (2024) *Cyclone preheater in cement plant*, *Agico Cement*. Available at: https://cement-plants.com/clinker-production/cyclone-preheater/ (Accessed: 5 March 2025).

Ahmed, A. *et al.* (2018) 'Design methodology of organic Rankine cycle for waste heat recovery in cement plants', *Applied Thermal Engineering*, 129, pp. 421–430. Available at: https://doi.org/10.1016/j.applthermaleng.2017.10.019.

Alfè, M. *et al.* (2022) 'Pyrolysis and Gasification of a Real Refuse-Derived Fuel (RDF): The Potential Use of the Products under a Circular Economy Vision', *Molecules*, 27(23). Available at: https://doi.org/10.3390/molecules27238114.

Al-Rawashdeh, H.A. *et al.* (2019) 'Efficiency and exergy enhancement of ORC powered by recovering flue gases-heat system in cement industrials: A case study', *International Review of Mechanical Engineering*, 13(3), pp. 185–197. Available at: https://doi.org/10.15866/ireme.v13i3.16713.

Anacleto, T.F. *et al.* (2021) 'Chemical exergy influence in the exergetic analysis of a real clinker rotary kiln', *Brazilian Journal of Chemical Engineering*, 38(1), pp. 197–214. Available at: https://doi.org/10.1007/s43153-020-00084-0.

Antunes, M. *et al.* (2022) 'Alternative clinker technologies for reducing carbon emissions in cement industry: A critical review', *Materials*, 15(1). Available at: https://doi.org/10.3390/ma15010209.

Aranda Usón, A. *et al.* (2013) 'Uses of alternative fuels and raw materials in the cement industry as sustainable waste management options', *Renewable and Sustainable Energy Reviews*. Elsevier Ltd, pp. 242–260. Available at: https://doi.org/10.1016/j.rser.2013.02.024.

Ariyaratne, W.K.H. *et al.* (2015) 'CFD modelling of meat and bone meal combustion in a cement rotary kiln - Investigation of fuel particle size and fuel feeding position impacts', *Chemical Engineering Science*, 123, pp. 596–608. Available at: https://doi.org/10.1016/j.ces.2014.10.048.

Ashraf, W., Olek, J. and Sahu, S. (2019) 'Phase evolution and strength development during carbonation of low-lime calcium silicate cement (CSC)', *Construction and Building Materials*, 210, pp. 473–482. Available at: https://doi.org/10.1016/j.conbuildmat.2019.03.038.

Association, M.P. and Ltd, C. (2019) *Options for switching UK cement production sites to near zero CO2 emission fuel: Technical and financial feasibility*. Available at: https://assets.publishing.service.gov.uk/government/uploads/system/uploads/attachment_data/file/866365/Phase_2_-_MPA_-_Cement_Production_Fuel_Switching.pdf (Accessed: 11 July 2023).

Awan, A.B. *et al.* (2019) 'Design and comparative analysis of photovoltaic and parabolic trough based CSP plants', *Solar Energy*, 183, pp. 551–565. Available at: https://doi.org/10.1016/j.solener.2019.03.037.

Baker, R.W. *et al.* (2018) 'CO2 Capture from Cement Plants and Steel Mills Using Membranes', *Industrial and Engineering Chemistry Research*, 57(47), pp. 15963–15970. Available at: https://doi.org/10.1021/acs.iecr.8b02574.

Barbhuiya, S. *et al.* (2024) 'Decarbonising cement and concrete production: Strategies, challenges and pathways for sustainable development', *Journal of Building Engineering*, 86. Available at: https://doi.org/10.1016/j.jobe.2024.108861.

Benhelal, E. *et al.* (2013) 'Global strategies and potentials to curb CO2 emissions in cement industry', *Journal of Cleaner Production*. Elsevier Ltd, pp. 142–161. Available at: https://doi.org/10.1016/j.jclepro.2012.10.049.

Benhelal, E., Shamsaei, E. and Rashid, M.I. (2021) 'Challenges against CO2 abatement strategies in cement industry: A review', *Journal of Environmental Sciences (China)*, 104, pp. 84–101. Available at: https://doi.org/10.1016/j.jes.2020.11.020.

Blotevogel, S. *et al.* (2021) 'Effect of TiO2 and 11 minor elements on the reactivity of ground-granulated blast-furnace slag in blended cements', *Journal of the American Ceramic Society*, 104(1), pp. 128–139. Available at: https://doi.org/10.1111/jace.17431.

Boesch, M.E., Koehler, A. and Hellweg, S. (2009) 'Model for cradle-to-gate life cycle assessment of clinker production', *Environmental Science and Technology*, 43(19), pp. 7578–7583. Available at: https://doi.org/10.1021/es900036e.

Bouaissi, A. *et al.* (2020) 'Fly Ash as a Cementitious Material for Concrete', in *Zero-Energy Buildings - New Approaches and Technologies*. IntechOpen. Available at: https://doi.org/10.5772/intechopen.90466.

Bradbury, J., Clement, Z. and Down, A. (2015) *Greenhouse Gas Emissions and Fuel Use within the Natural Gas Supply Chain-Sankey Diagram Methodology Acknowledgements*.

Bremen, A.M. *et al.* (2022) 'Direct Olivine Carbonation: Optimal Process Design for a Low-Emission and Cost-Efficient Cement Production', *Industrial and Engineering*

*Chemistry Research*, 61(35), pp. 13177–13190. Available at: https://doi.org/10.1021/acs.iecr.2c00984.

British Geological Survey (2005) *Cement Raw Materials British Geological Survey Mineral Profile*. United Kingdom.

Brożek, P. *et al.* (2022) 'Study of the Combustion Process for Two Refuse-Derived Fuel (RDF) Streams Using Statistical Methods and Heat Recovery Simulation', *Energies*, 15(24). Available at: https://doi.org/10.3390/en15249560.

Canvi Climatic, O.C. del (2019) *Practical Guide for Calculating Greenhouse Gas Emissions (GHG)*.

Cao, L. and Zhou, Y. (2024) 'Evaluation and Analysis of Cement Raw Meal Homogenization Characteristics Based on Simulated Equipment Models', *Materials*, 17(12). Available at: https://doi.org/10.3390/ma17122993.

Carrasco-Maldonado, F. *et al.* (2016) 'Oxy-fuel combustion technology for cement production - State of the art research and technology development', *International Journal of Greenhouse Gas Control*. Elsevier Ltd, pp. 189–199. Available at: https://doi.org/10.1016/j.ijggc.2015.12.014.

Cavalett, O. *et al.* (2024) 'Paving the way for sustainable decarbonization of the European cement industry', *Nature Sustainability*, 7(5), pp. 568–580. Available at: https://doi.org/10.1038/s41893-024-01320-y.

Cembureau (2023) *Activity Report 2023*. Brussels. Available at: www.cembureau.eu.

Cembureau (2024) *The Story of Cement Manufacture*. Brussels. Available at: www.cembureau.eu.

Cement Association, E. (2018) *The Story of Cement Manufacture*, *Cembureau*. Available at: https://cembureau.eu/media/wm0jmdwl/cementmanufacturing.pdf (Accessed: 9 January 2024).

Chandra Kahawalage, A., Melaaen, M.C. and Tokheim, L.-A. (2017) 'Numerical modeling of the calcination process in a cement kiln system', in *Proceedings of the 58th Conference on Simulation and Modelling (SIMS 58) Reykjavik, Iceland, September 25th – 27th, 2017*. Linköping University Electronic Press, pp. 83–89. Available at: https://doi.org/10.3384/ecp1713883.

Chatterjee, A. and Sui, T. (2019) 'Alternative fuels – Effects on clinker process and properties', *Cement and Concrete Research*, 123. Available at: https://doi.org/10.1016/j.cemconres.2019.105777.

Chaves, G. de L.D. *et al.* (2022) 'The Potential of Refuse-Derived Fuel Production in Reducing the Environmental Footprint of the Cement Industry', in *Environmental Footprints and Eco-Design of Products and Processes*. Springer, pp. 35–64. Available at: https://doi.org/10.1007/978-981-16-8426-5_2.

Cheng, D. *et al.* (2023) 'Projecting future carbon emissions from cement production in developing countries', *Nature Communications*, 14(1). Available at: https://doi.org/10.1038/s41467-023-43660-x.

Churkina, G. *et al.* (2020) 'Buildings as a global carbon sink', *Nature Sustainability*, 3(4), pp. 269–276. Available at: https://doi.org/10.1038/s41893-019-0462-4.

Clark, G. *et al.* (2024) 'Assessment of fuel switching as a decarbonization strategy in the cement sector', *Energy Conversion and Management*, 312. Available at: https://doi.org/10.1016/j.enconman.2024.118585.

Climate Friendly (2024) *Benefits Beyond Carbon Reduction*. Thailand. Available at: www.climatefriendly.com.

Cole, W. and Karmakar, A. (2030) *Cost Projections for Utility-Scale Battery Storage: 2023 Update*. Available at: www.nrel.gov/publications.

Commission, E.T. (2023) *Making the Hydrogen Economy Possible: Accelerating Clean Hydrogen in an Electrified Economy*.

Cormos, C.C. (2022) 'Decarbonization options for cement production process: A techno-economic and environmental evaluation', *Fuel*, 320. Available at: https://doi.org/10.1016/j.fuel.2022.123907.

Cumbrera, F. de Q. (2023) *Thermal energy intensity of clinker production worldwide from 2010 to 2022, by type of energy*, *Statista*. Available at: https://www.statista.com/statistics/1399841/global-energy-intensity-of-clinker-production-by-type-of-energy/ (Accessed: 7 August 2024).

Damtoft, J.S. *et al.* (2008) 'Sustainable development and climate change initiatives', *Cement and Concrete Research*, 38(2), pp. 115–127. Available at: https://doi.org/10.1016/j.cemconres.2007.09.008.

Desideri, U. and Campana, P.E. (2014) 'Analysis and comparison between a concentrating solar and a photovoltaic power plant', *Applied Energy*, 113, pp. 422–433. Available at: https://doi.org/10.1016/j.apenergy.2013.07.046.

Ding, Y., Dai, J.G. and Shi, C.J. (2016) 'Mechanical properties of alkali-activated concrete: A state-of-the-art review', *Construction and Building Materials*, 127, pp. 68–79. Available at: https://doi.org/10.1016/j.conbuildmat.2016.09.121.

Ditaranto, M. and Bakken, J. (2019) 'Study of a full scale oxy-fuel cement rotary kiln', *International Journal of Greenhouse Gas Control*, 83, pp. 166–175. Available at: https://doi.org/10.1016/j.ijggc.2019.02.008.

Domingues, B.C. *et al.* (2023) 'Techno-Economic Analysis of Cement Decarbonization Techniques: Oxygen Enrichment vs. Hydrogen Fuel'. Available at: https://doi.org/10.20944/preprints202310.0856.v1.

Dong, K. *et al.* (2020) 'Calcination of calcium sulphoaluminate cement using pyrite-rich cyanide tailings', *Crystals*, 10(11), pp. 1–13. Available at: https://doi.org/10.3390/cryst10110971.

Duchesne, J. (2021) 'Alternative supplementary cementitious materials for sustainable concrete structures: a review on characterization and properties', *Waste and Biomass Valorization*. Springer Science and Business Media B.V., pp. 1219–1236. Available at: https://doi.org/10.1007/s12649-020-01068-4.

Elakneswaran, Y. *et al.* (2019) 'Characteristics of ferrite-rich portland cement: Comparison with ordinary portland cement', *Frontiers in Materials*, 6. Available at: https://doi.org/10.3389/fmats.2019.00097.

El-Emam, R.S. and Gabriel, K.S. (2021) 'Synergizing hydrogen and cement industries for Canada's climate plan–case study', *Energy Sources, Part A: Recovery, Utilization and Environmental Effects*, 43(23), pp. 3151–3165. Available at: https://doi.org/10.1080/15567036.2021.1936699.

Energy Equipment and Infrastructure Alliance (2019) *Meeting the Dual Challenge: A Roadmap to At-Scale Deployment of Carbon Capture, Use, and Storage Key Excerpts from National Petroleum Council Report:* United States.

European Commission (2022) *Photovoltaic Geographical Information System (PVGIS)*, *European Commission*. Available at: https://re.jrc.ec.europa.eu/pvg_tools/en/ (Accessed: 21 August 2024).

Fantilli, A.P. and Jóźwiak-Niedźwiedzka, D. (2021) 'Special issue: Supplementary cementitious materials in concrete, part I', *Materials*, 14(9). Available at: https://doi.org/10.3390/ma14092291.

Faria, D.G. *et al.* (2022) 'Integrating oxy-fuel combustion and power-to-gas in the cement industry: A process modeling and simulation study', *International Journal of Greenhouse Gas Control*, 114. Available at: https://doi.org/10.1016/j.ijggc.2022.103602.

Faridmehr, I. *et al.* (2021) 'Life-cycle assessment of alkali-activated materials incorporating industrial byproducts', *Materials*, 14(9). Available at: https://doi.org/10.3390/ma14092401.

Fearnely, N., Robinson, G. and Leonard, J. (2023) *Global Construction Futures - A global forecast for the construction industry to 2037*. London. Available at: www.oxfordeconomics.com.

Flamant, G. (2020) *The next solar revolution could power cement production with sunlight*, *European Commission*. Available at: https://cordis.europa.eu/article/id/421794-the-next-solar-revolution-could-power-cement-production-with-sunlight (Accessed: 30 July 2024).

Flower, D.J.M. and Sanjayan, J.G. (2007) 'Green house gas emissions due to concrete manufacture', *International Journal of Life Cycle Assessment*, 12(5), pp. 282–288. Available at: https://doi.org/10.1065/lca2007.05.327.

Fode, T.A., Chande Jande, Y.A. and Kivevele, T. (2023) 'Effects of different supplementary cementitious materials on durability and mechanical properties of cement composite – Comprehensive review', *Heliyon*. Elsevier Ltd. Available at: https://doi.org/10.1016/j.heliyon.2023.e17924.

Franco, A. and Giovannini, C. (2023) 'Recent and Future Advances in Water Electrolysis for Green Hydrogen Generation: Critical Analysis and Perspectives', *Sustainability (Switzerland)*, 15(24). Available at: https://doi.org/10.3390/su152416917.

Gagg, C.R. (2014) 'Cement and concrete as an engineering material: An historic appraisal and case study analysis', *Engineering Failure Analysis*, 40, pp. 114–140. Available at: https://doi.org/10.1016/j.engfailanal.2014.02.004.

García-Lodeiro, I., Fernández-Jiménez, A. and Palomo, A. (2013) 'Alkali-activated based concrete', in *Eco-Efficient Concrete*. Elsevier Ltd., pp. 439–487. Available at: https://doi.org/10.1533/9780857098993.4.439.

Gardarsdottir, S.O. *et al.* (2019) 'Comparison of technologies for CO2 capture from cement production—Part 2: Cost analysis', *Energies*, 12(3). Available at: https://doi.org/10.3390/en12030542.

Gartner, E. and Sui, T. (2018) 'Alternative cement clinkers', *Cement and Concrete Research*. Elsevier Ltd, pp. 27–39. Available at: https://doi.org/10.1016/j.cemconres.2017.02.002.

Georgiades, M. *et al.* (2023) 'Prospective life cycle assessment of European cement production', *Resources, Conservation and Recycling*, 194. Available at: https://doi.org/10.1016/j.resconrec.2023.106998.

Georgiopoulou, M. and Lyberatos, G. (2018) 'Life cycle assessment of the use of alternative fuels in cement kilns: A case study', *Journal of Environmental Management*, 216, pp. 224–234. Available at: https://doi.org/10.1016/j.jenvman.2017.07.017.

Ghalandari, V. *et al.* (2021) 'A case study on energy and exergy analyses for an industrial-scale vertical roller mill assisted grinding in cement plant', *Advanced Powder Technology*, 32(2), pp. 480–491. Available at: https://doi.org/10.1016/j.apt.2020.12.027.

Global Carbon Budget (2023) *Annual $CO_2$ emissions from cement*, *Our World in Data*. Available at: https://ourworldindata.org/grapher/annual-co2-cement (Accessed: 23 July 2024).

Global Cement and Concrete Association (2023) 'CEMEX – Solar Clinker', *Global Cement and Concrete Association* [Preprint]. Available at:

https://gccassociation.org/2050-net-zero-roadmap-one-year-on/action-progress-case-study-cemex/ (Accessed: 29 July 2024).

Global Cement and Concrete Association (2024) *About Cement & Concrete*, *Global Cement and Concrete Association*. Available at: https://gccassociation.org/our-story-cement-and-concrete/ (Accessed: 1 July 2024).

Gonnon, P. and Lootens, D. (2023) 'Toward net zero carbon for concrete and mortar: Clinker substitution with ground calcium carbonate', *Cement and Concrete Composites*, 142. Available at: https://doi.org/10.1016/j.cemconcomp.2023.105190.

González, R.S. and Flamant, G. (2014) 'Technical and economic feasibility analysis of using concentrated solar thermal technology in the cement production process: Hybrid approach-a case study', *Journal of Solar Energy Engineering, Transactions of the ASME*, 136(2). Available at: https://doi.org/10.1115/1.4026573.

Gonzalez, R.S., Switzerland, C. and Flamant, G. (2013) *Technical and Economic Feasibility Analysis of Using Concentrated Solar Thermal Technology in the Cement Production Process: Hybrid Approach - A Case Study*. Available at: http://asmedigitalcollection.asme.org/ES/proceedings-pdf/ES2013/55515/V001T03A005/4447516/v001t03a005-es2013-18143.pdf.

Gulyurtlu, I. *et al.* (2005) 'Co-combustion of coal and meat and bone meal', in *Fuel*, pp. 2137–2148. Available at: https://doi.org/10.1016/j.fuel.2005.04.024.

Guo, Y. *et al.* (2024) 'A review of low-carbon technologies and projects for the global cement industry', *Journal of Environmental Sciences (China)*, 136, pp. 682–697. Available at: https://doi.org/10.1016/j.jes.2023.01.021.

Habib, M.A. *et al.* (2024) 'Hydrogen combustion, production, and applications: A review', *Alexandria Engineering Journal*. Elsevier B.V., pp. 182–207. Available at: https://doi.org/10.1016/j.aej.2024.05.030.

Hamada, H.M. *et al.* (2023) 'Effect of silica fume on the properties of sustainable cement concrete', *Journal of Materials Research and Technology*, 24, pp. 8887–8908. Available at: https://doi.org/10.1016/j.jmrt.2023.05.147.

Hanein, T. *et al.* (2021) 'Decarbonisation of calcium carbonate at atmospheric temperatures and pressures, with simultaneous CO2 capture, through production of sodium carbonate', *Energy and Environmental Science*, 14(12), pp. 6595–6604. Available at: https://doi.org/10.1039/d1ee02637b.

Hanein, T., Glasser, F.P. and Bannerman, M.N. (2020) 'Thermodynamic data for cement clinkering', *Cement and Concrete Research*, 132. Available at: https://doi.org/10.1016/j.cemconres.2020.106043.

Hanson (2022) *Hydrogen trial | Hanson UK*. Available at: https://www.hanson.co.uk/en/socialvalue/climate/hydrogen-trial (Accessed: 9 May 2023).

Harder, J. (2023) *Retrospective: Cement industry development*, *ZKG Cement.* Available at: https://www.zkg.de/en/artikel/zkg_Retrospective_Cement_industry_development-3786043.html (Accessed: 24 July 2024).

Hernández-Moro, J. and Martínez-Duart, J.M. (2013) 'Analytical model for solar PV and CSP electricity costs: Present LCOE values and their future evolution', *Renewable and Sustainable Energy Reviews*, pp. 119–132. Available at: https://doi.org/10.1016/j.rser.2012.11.082.

Hills, T. *et al.* (2016) 'Carbon Capture in the Cement Industry: Technologies, Progress, and Retrofitting', *Environmental Science and Technology*, 50(1), pp. 368–377. Available at: https://doi.org/10.1021/acs.est.5b03508.

Hiromi Ariyaratne, W.K. *et al.* (2014) 'Mathematical Model for Alternative Fuel Combustion in a Rotary Cement Kiln Burner', *International Journal of Modeling and Optimization*, 4(1), pp. 56–61. Available at: https://doi.org/10.7763/ijmo.2014.v4.347.

Hökfors, B., Eriksson, M. and Viggh, E. (2014) 'Modelling the cement process and cement clinker quality', *Advances in Cement Research*, 26(6), pp. 311–318. Available at: https://doi.org/10.1680/adcr.13.00050.

Huismans, M. and Voswinkel, F. (2023) 'Electrification', *IEA* [Preprint]. Available at: https://www.iea.org/energy-system/electricity/electrification (Accessed: 31 July 2024).

Hulst, N. van (2019) *The clean hydrogen future has already begun*, *IEA*. Available at: https://www.iea.org/commentaries/the-clean-hydrogen-future-has-already-begun (Accessed: 11 April 2025).

ICR Newsroom (2024) *Thailand's low-carbon transition*, *Cemnet*. Available at: https://www.cemnet.com/Articles/story/176194/thailand-s-low-carbon-transition.html (Accessed: 27 July 2024).

IEA (2024) *Solar PV*, *IEA*. Available at: https://www.iea.org/energy-system/renewables/solar-pv (Accessed: 29 July 2024).

Institute of Power Engineering (2022) *Basic information on hydrogen*. Available at: https://www.ien.com.pl/tl_files/pliki/CPE/FAQ_final_EN.pdf (Accessed: 26 April 2023).

International Energy Agency, I. (2023) *Renewable Energy Market Update - June 2023*. Available at: www.iea.org (Accessed: 15 July 2025).

International Renewable Energy Agency (2017) *Electricity storage and renewables : costs and markets to 2030*.

Jacob, R.M. and Tokheim, L.-A. (2023) *Electrified calciner concept for CO2 capture in pyro-2 processing of a dry process cement plant*.

Jaganmohan, M. (2024a) *Major countries in worldwide cement production in 2023*, *Statista*. Available at: https://www.statista.com/statistics/267364/world-cement-production-by-country/ (Accessed: 5 July 2024).

Jaganmohan, M. (2024b) *Production volume of cement worldwide from 1995 to 2023*, *Statista*. Available at: https://www.statista.com/statistics/1087115/global-cement-production-volume/ (Accessed: 1 July 2024).

Jain, J.A., Seth, A. and DeCristofaro, N. (2019) 'Environmental impact and durability of carbonated calcium silicate concrete', *Proceedings of Institution of Civil Engineers: Construction Materials*, 172(4), pp. 179–191. Available at: https://doi.org/10.1680/jcoma.17.00004.

Jiang, K. *et al.* (2024) 'Zero-Emission Cement Plants with Advanced Amine-Based CO2 Capture', *Environmental Science and Technology*, 58(16), pp. 6978–6987. Available at: https://doi.org/10.1021/acs.est.4c00197.

Jibran, J.A. and Mahat, C. (2023) 'Application of green hydrogen for decarbonization of cement manufacturing process: A technical review', in *Journal of Physics: Conference Series*. Institute of Physics. Available at: https://doi.org/10.1088/1742-6596/2629/1/012027.

John, J.P. (2020) 'Parametric Studies of Cement Production Processes', *Journal of Energy*, 2020, pp. 1–17. Available at: https://doi.org/10.1155/2020/4289043.

Jokar, S.M. *et al.* (2023) 'The recent areas of applicability of palladium based membrane technologies for hydrogen production from methane and natural gas: A review', *International Journal of Hydrogen Energy*. Elsevier Ltd, pp. 6451–6476. Available at: https://doi.org/10.1016/j.ijhydene.2022.05.296.

José, N. *et al.* (2020) 'Magnesia (Mgo) production and characterization, and its influence on the performance of cementitious materials: A review', *Materials*. MDPI AG, pp. 1–31. Available at: https://doi.org/10.3390/ma13214752.

Juangsa, F.B. *et al.* (2022) 'Thermodynamic analysis of hydrogen utilization as alternative fuel in cement production', *South African Journal of Chemical Engineering*, 42, pp. 23–31. Available at: https://doi.org/10.1016/j.sajce.2022.07.003.

Juenger, M.C.G. and Siddique, R. (2015) 'Recent advances in understanding the role of supplementary cementitious materials in concrete', *Cement and Concrete Research*. Elsevier Ltd, pp. 71–80. Available at: https://doi.org/10.1016/j.cemconres.2015.03.018.

Juenger, M.C.G., Snellings, R. and Bernal, S.A. (2019) 'Supplementary cementitious materials: New sources, characterization, and performance insights', *Cement and Concrete Research*, 122, pp. 257–273. Available at: https://doi.org/10.1016/j.cemconres.2019.05.008.

Kääntee, U. *et al.* (2004) 'Cement manufacturing using alternative fuels and the advantages of process modelling', *Fuel Processing Technology*, 85(4), pp. 293–301. Available at: https://doi.org/10.1016/S0378-3820(03)00203-0.

Kaddatz, K.T., Rasul, M.G. and Rahman, A. (2013) 'Alternative fuels for use in cement kilns: Process impact modelling', in *Procedia Engineering*. Elsevier Ltd, pp. 413–420. Available at: https://doi.org/10.1016/j.proeng.2013.03.141.

Karpan, B., Abdul Raman, A.A. and Taieb Aroua, M.K. (2021) 'Waste-to-energy: Coal-like refuse derived fuel from hazardous waste and biomass mixture', *Process Safety and Environmental Protection*, 149, pp. 655–664. Available at: https://doi.org/10.1016/j.psep.2021.03.009.

Khadka, D. (2021) *Calcination applying H2 combustion in O2 in a CO2 rich atmosphere*, *University of South Eastern Norway*. Available at: https://openarchive.usn.no/usnxmlui/bitstream/handle/11250/2765115/no.usn%3Awiseflow%3A2636125%3A43485478.pdf?sequence=1&isAllowed=y (Accessed: 11 July 2023).

Khan, M.I. *et al.* (2024) 'The economics of concentrating solar power (CSP): Assessing cost competitiveness and deployment potential', *Renewable and Sustainable Energy Reviews*. Elsevier Ltd. Available at: https://doi.org/10.1016/j.rser.2024.114551.

Khurana, S., Banerjee, R. and Gaitonde, U. (2002) 'Energy balance and cogeneration for a cement plant', pp. 486–494. Available at: www.elsevier.com/locate/apthermeng.

Kian, K. *et al.* (2021) *Recent Advances in Structural Engineering and Construction Management*.

Klee, H. (2009) *The Cement Sustainability Initiative - Cement Industry Energy and CO2 Performance*.

Kondraivendhan, B. and Bhattacharjee, B. (2016) 'Strength and w/c ratio relationship of cement based materials through pore features', *Materials Characterization*, 122, pp. 124–129. Available at: https://doi.org/10.1016/j.matchar.2016.10.036.

Kouchaki-Penchah, H. *et al.* (2023) 'Impact of Biogenic Carbon Neutrality Assumption for Achieving a Net-Zero Emission Target: Insights from a Techno-Economic Analysis', *Environmental Science and Technology*, 57(29), pp. 10615–10628. Available at: https://doi.org/10.1021/acs.est.3c00644.

Kurkute, N. and Priyam, A. (2022) 'A thorough review of the existing concentrated solar power technologies and various performance enhancing techniques', *Journal of Thermal Analysis and Calorimetry*, 147(24), pp. 14713–14737. Available at: https://doi.org/10.1007/s10973-022-11634-8.

Kurokawa, D. *et al.* (2013) 'Quality design of belite-melilite clinker', *Cement and Concrete Research*, 54, pp. 126–132. Available at: https://doi.org/10.1016/j.cemconres.2013.09.004.

Kusuma, R.T. *et al.* (2022) 'Sustainable transition towards biomass-based cement industry: A review', *Renewable and Sustainable Energy Reviews*, 163. Available at: https://doi.org/10.1016/j.rser.2022.112503.

Lea, F.M., Hewlett, P.C. and Liska, Martin. (2019) *Lea's chemistry of cement and concrete*. Butterworth-Heinemann.

Lechtenböhmer, S. *et al.* (2016) 'Decarbonising the energy intensive basic materials industry through electrification – Implications for future EU electricity demand', *Energy*, 115, pp. 1623–1631. Available at: https://doi.org/10.1016/j.energy.2016.07.110.

Lena, E. De, Spinelli, M. and Romano, M.C. (2018) 'CO2 capture in cement plants by "tail-End" Calcium Looping process', in *Energy Procedia*. Elsevier Ltd, pp. 186–193. Available at: https://doi.org/10.1016/j.egypro.2018.08.049.

Lin, Z., Lyu, G. and Fang, K. (2025) 'Carbon emissions assessment of concrete and quantitative calculation of CO2 reduction benefits of SCMs: A case study of C30-C80 ready-mixed concrete in China', *Case Studies in Construction Materials*, 22. Available at: https://doi.org/10.1016/j.cscm.2025.e04287.

Lothenbach, B. *et al.* (2022) 'Thermodynamic properties and hydration behavior of ye'elimite', *Cement and Concrete Research*, 162. Available at: https://doi.org/10.1016/j.cemconres.2022.106995.

Lothenbach, B., Scrivener, K. and Hooton, R.D. (2011) 'Supplementary cementitious materials', *Cement and Concrete Research*, pp. 1244–1256. Available at: https://doi.org/10.1016/j.cemconres.2010.12.001.

Luo, Z. *et al.* (2024) 'Recent Advances on the Uses of Biomass Alternative Fuels in Cement Manufacturing Process: A Review', *Energy and Fuels*. American Chemical Society, pp. 7454–7479. Available at: https://doi.org/10.1021/acs.energyfuels.3c04535.

Lv, L. *et al.* (2021) 'Prehydration of calcium sulfoaluminate (CSA) clinker at different relative humidities', *Cement and Concrete Research*, 144. Available at: https://doi.org/10.1016/j.cemconres.2021.106423.

Madlool, N.A. *et al.* (2011) 'A critical review on energy use and savings in the cement industries', *Renewable and Sustainable Energy Reviews*, 15(4), pp. 2042–2060. Available at: https://doi.org/10.1016/j.rser.2011.01.005.

Mastorakos, E. *et al.* (1998) *CFD predictions for cement kilns including flame modelling, heat transfer and clinker chemistry*. Greece. Available at: https://doi.org/10.1016/S0307-904X(98)10053-7.

Mathisen, A. *et al.* (2018) *CO2 capture scenarios for a cement plant*. Available at: https://ssrn.com/abstract=3365874.

Meier, A., Gremaud, N. and Steinfeld, A. (2005) 'Economic evaluation of the industrial solar production of lime', *Energy Conversion and Management*, 46(6), pp. 905–926. Available at: https://doi.org/10.1016/j.enconman.2004.06.005.

Mendes, B.C. *et al.* (2021) 'Application of eco-friendly alternative activators in alkali-activated materials: A review', *Journal of Building Engineering*. Elsevier Ltd. Available at: https://doi.org/10.1016/j.jobe.2020.102010.

Meng, R. *et al.* (2021) 'A survey and analysis on electricity consumption of raw material mill system in china cement industry between 2014 and 2019', *Sustainability (Switzerland)*, 13(3), pp. 1–11. Available at: https://doi.org/10.3390/su13031126.

Middleton, L. *et al.* (2025) 'Energy and exergy analysis of liquid piston compression for small-scale methane liquefaction', *Energy*, 330. Available at: https://doi.org/10.1016/j.energy.2025.136933.

Mikulčić, H. *et al.* (2012) 'The application of CFD modelling to support the reduction of CO2 emissions in cement industry', *Energy*, 45(1), pp. 464–473. Available at: https://doi.org/10.1016/j.energy.2012.04.030.

Mikulčić, H. *et al.* (2016) 'Reducing greenhouse gasses emissions by fostering the deployment of alternative raw materials and energy sources in the cleaner cement manufacturing process', *Journal of Cleaner Production*, 136, pp. 119–132. Available at: https://doi.org/10.1016/j.jclepro.2016.04.145.

Mikulčić, H., Vujanović, M. and Duić, N. (2013) 'Reducing the CO2 emissions in Croatian cement industry', *Applied Energy*, 101, pp. 41–48. Available at: https://doi.org/10.1016/j.apenergy.2012.02.083.

Miller, S.A. (2018) 'Supplementary cementitious materials to mitigate greenhouse gas emissions from concrete: can there be too much of a good thing?', *Journal of Cleaner Production*, 178, pp. 587–598. Available at: https://doi.org/10.1016/j.jclepro.2018.01.008.

Mohamad, N. *et al.* (2021) 'Environmental impact of cement production and Solutions: A review', in *Materials Today: Proceedings*. Elsevier Ltd, pp. 741–746. Available at: https://doi.org/10.1016/j.matpr.2021.02.212.

Moreira, L.F. and Arrieta, F.R.P. (2019) 'Thermal and economic assessment of organic Rankine cycles for waste heat recovery in cement plants', *Renewable and Sustainable Energy Reviews*, 114. Available at: https://doi.org/10.1016/j.rser.2019.109315.

Morin, V. *et al.* (2017) 'Impact of quantity of anhydrite, water to binder ratio, fineness on kinetics and phase assemblage of belite-ye'elimite-ferrite cement', *Cement and Concrete Research*, 99, pp. 8–17. Available at: https://doi.org/10.1016/j.cemconres.2017.04.014.

Moseman, A. and Surendranath, Y. (2023) *How can burning one ton of fuel create more than one ton of CO2?*, *MIT Climate Portal*. Available at: https://climate.mit.edu/ask-mit/how-can-burning-one-ton-fuel-create-more-one-ton-co2 (Accessed: 24 July 2024).

Moumin, G. *et al.* (2020) 'CO2 emission reduction in the cement industry by using a solar calciner', *Renewable Energy*, 145, pp. 1578–1596. Available at: https://doi.org/10.1016/j.renene.2019.07.045.

Mujumdar, K.S. *et al.* (2007) 'Rotary Cement Kiln Simulator (RoCKS): Integrated modeling of pre-heater, calciner, kiln and clinker cooler', *Chemical Engineering Science*, 62(9), pp. 2590–2607. Available at: https://doi.org/10.1016/j.ces.2007.01.063.

Naqi, A. and Jang, J.G. (2019) 'Recent progress in green cement technology utilizing low-carbon emission fuels and raw materials: A review', *Sustainability (Switzerland)*, 11(2). Available at: https://doi.org/10.3390/su11020537.

Ndahirwa, D. *et al.* (2022) 'The role of supplementary cementitious materials in hydration, durability and shrinkage of cement-based materials, their environmental and economic benefits: A review', *Cleaner Materials*. Elsevier Ltd. Available at: https://doi.org/10.1016/j.clema.2022.100123.

Nehdi, M.L., Marani, A. and Zhang, L. (2024) 'Is net-zero feasible: Systematic review of cement and concrete decarbonization technologies', *Renewable and Sustainable Energy Reviews*, 191. Available at: https://doi.org/10.1016/j.rser.2023.114169.

Neville, A.M. and Brooks, J.J. (2010) *Concrete Technology*. Second. Edited by Pearson.

Nhuchhen, D.R., Sit, S.P. and Layzell, D.B. (2021) 'Alternative fuels co-fired with natural gas in the pre-calciner of a cement plant: Energy and material flows', *Fuel*, 295. Available at: https://doi.org/10.1016/j.fuel.2021.120544.

Nhuchhen, D.R., Sit, S.P. and Layzell, D.B. (2022a) 'Decarbonization of cement production in a hydrogen economy', *Applied Energy*, 317. Available at: https://doi.org/10.1016/j.apenergy.2022.119180.

Nhuchhen, D.R., Sit, S.P. and Layzell, D.B. (2022b) 'Towards net-zero emission cement and power production using Molten Carbonate Fuel Cells', *Applied Energy*, 306. Available at: https://doi.org/10.1016/j.apenergy.2021.118001.

Nie, S. *et al.* (2022) 'Analysis of theoretical carbon dioxide emissions from cement production: Methodology and application', *Journal of Cleaner Production*, 334. Available at: https://doi.org/10.1016/j.jclepro.2021.130270.

Nikolakopoulos, A. *et al.* (2022) 'Solar-aided calcination of limestone: First modeling of the SOLCEMENT process', in *AIP Conference Proceedings*. American Institute of Physics Inc. Available at: https://doi.org/10.1063/5.0085791.

Nozaki, T., Kim, D.Y. and Chen, X. (2024) 'Plasma-enabled electrification of chemical processes toward decarbonization of society', *Japanese Journal of Applied Physics*, 63(3). Available at: https://doi.org/10.35848/1347-4065/ad280f.

Okeke, I.J. *et al.* (2024) *Role of Hydrogen as Fuel in Decarbonizing US Clinker Manufacturing for Cement Production: Costs and CO2 Emissions Reduction Potentials*. Colorado.

Olsson, J.A., Miller, S.A. and Kneifel, J.D. (2024) 'A review of current practice for life cycle assessment of cement and concrete', *Resources, Conservation and Recycling*. Elsevier B.V. Available at: https://doi.org/10.1016/j.resconrec.2024.107619.

Ostovari, H. *et al.* (2021) 'From Unavoidable CO2 Source to CO2 Sink? A Cement Industry Based on CO2 Mineralization', *Environmental Science and Technology*, 55(8), pp. 5212–5223. Available at: https://doi.org/10.1021/acs.est.0c07599.

Our World in Data (2023) *Carbon intensity of electricity, 2022*, *Our World in Data*. Available at: https://ourworldindata.org/grapher/carbon-intensity-electricity (Accessed: 11 January 2024).

Our World in Data (2024) *Natural gas prices*. Available at: https://ourworldindata.org/grapher/natural-gas-prices (Accessed: 5 July 2024).

Ozcan, D.C., Brandani, S. and Ahn, H. (2014) 'A hybrid carbon capture system of indirect calcination and amine absorption for a cement plant', in *Energy Procedia*. Elsevier Ltd, pp. 6428–6439. Available at: https://doi.org/10.1016/j.egypro.2014.11.678.

Pal, A. *et al.* (2024) 'Powering squarely into the future: A strategic analysis of hydrogen energy in QUAD nations', *International Journal of Hydrogen Energy*. Elsevier Ltd, pp. 16–41. Available at: https://doi.org/10.1016/j.ijhydene.2023.06.169.

Palanivel, T.M. and Sulaiman, H. (2014) 'Generation and Composition of Municipal Solid Waste (MSW) in Muscat, Sultanate of Oman', *APCBEE Procedia*, 10, pp. 96–102. Available at: https://doi.org/10.1016/j.apcbee.2014.10.024.

Pamenter, S. and Myers, R.J. (2021) 'Decarbonizing the cementitious materials cycle: A whole-systems review of measures to decarbonize the cement supply chain in the UK and European contexts', *Journal of Industrial Ecology*, 25(2), pp. 359–376. Available at: https://doi.org/10.1111/jiec.13105.

Pareek, P. and Sankhla, V.S. (2020) 'Review on vertical roller mill in cement industry & its performance parameters', in *Materials Today: Proceedings*. Elsevier Ltd, pp. 4621–4627. Available at: https://doi.org/10.1016/j.matpr.2020.10.916.

Parida, B., Iniyan, S. and Goic, R. (2011) 'A review of solar photovoltaic technologies', *Renewable and Sustainable Energy Reviews*, 15(3), pp. 1625–1636. Available at: https://doi.org/10.1016/j.rser.2010.11.032.

Perilli, D. (2024) *Update on hydrogen use at cement plants, July 2024*, *Global Cement*. Available at: https://www.globalcement.com/news/item/17589-update-on-hydrogen-use-at-cement-plants-july-2024 (Accessed: 26 July 2024).

Pfenninger, S. and Staffell, I. (2016) 'Long-term patterns of European PV output using 30 years of validated hourly reanalysis and satellite data', *Energy*, 114, pp. 1251–1265. Available at: https://doi.org/10.1016/j.energy.2016.08.060.

Pitre, V., La, H. and Bergerson, J.A. (2024) 'Impacts of alternative fuel combustion in cement manufacturing: Life cycle greenhouse gas, biogenic carbon, and criteria air contaminant emissions', *Journal of Cleaner Production*, 475, p. 143717. Available at: https://doi.org/10.1016/j.jclepro.2024.143717.

Poggianti, B., Palazzolo, R. and Moliner, C. (2024) 'Rotary kiln simulation for energy recovery: The precalciner cement kiln case', *Thermal Science and Engineering Progress*, 54. Available at: https://doi.org/10.1016/j.tsep.2024.102806.

Pol Segura, I. *et al.* (2023) 'A review: Alkali-activated cement and concrete production technologies available in the industry', *Heliyon*. Elsevier Ltd. Available at: https://doi.org/10.1016/j.heliyon.2023.e15718.

Poling, B.E., Prausnitz, J.M., and O'Connell, J.P. (2020) *Properties of Gases and Liquids, Fifth Edition*. McGraw-Hill Education.

Popescu, C.D., Muntean, M. and Sharp, J.H. (2003) 'Industrial trial production of low energy belite cement', *Cement and Concrete Composites*, 25(7), pp. 689–693. Available at: https://doi.org/10.1016/S0958-9465(02)00097-5.

Psomopoulos, C.S. and Themelis, N.J. (2014) *Use of alternative fuels in cement industry*. Available at: https://www.researchgate.net/publication/263714046.

Quevedo Parra, S. and Romano, M.C. (2023) 'Decarbonization of cement production by electrification', *Journal of Cleaner Production*, 425. Available at: https://doi.org/10.1016/j.jclepro.2023.138913.

Rahman, A. *et al.* (2013) 'Impact of alternative fuels on the cement manufacturing plant performance: An overview', in *Procedia Engineering*. Elsevier Ltd, pp. 393–400. Available at: https://doi.org/10.1016/j.proeng.2013.03.138.

Rahman, A. *et al.* (2015) 'Recent development on the uses of alternative fuels in cement manufacturing process', *Fuel*, 145, pp. 84–99. Available at: https://doi.org/10.1016/j.fuel.2014.12.029.

Rahman, A. *et al.* (2016) 'Cement Kiln Process Modeling to Achieve Energy Efficiency by Utilizing Agricultural Biomass as Alternative Fuels', in *Thermofluid Modeling for Energy Efficiency Applications*. Elsevier Inc., pp. 197–225. Available at: https://doi.org/10.1016/B978-0-12-802397-6.00009-9.

Rahman, A. *et al.* (2017) 'Assessment of energy performance and emission control using alternative fuels in cement industry through a process model', *Energies*, 10(12). Available at: https://doi.org/10.3390/en10121996.

Ramzi, S. and Hajiloo, H. (2023) 'The Effects of Supplementary Cementitious Materials (SCMs) on the Residual Mechanical Properties of Concrete after Exposure to High Temperatures—Review', *Buildings*. MDPI. Available at: https://doi.org/10.3390/buildings13010103.

Rejani, V.U. *et al.* (2022) 'A Network Level Pavement Maintenance Optimisation Approach Deploying GAMS', *International Journal of Pavement Research and Technology*, 15(4), pp. 863–875. Available at: https://doi.org/10.1007/s42947-021-00058-6.

Renewable Energy Agency, I. (2023) *Renewable Power Generation Costs In 2022*. Available at: www.irena.org.

Research Department, S. (2023) *Major countries in worldwide cement production in 2022*, *Statista*.

Ritchie, H., Samborska, V. and Roser, M. (2024) *Urbanization across the world today*, *Our World in Data*. Available at: https://ourworldindata.org/urbanization (Accessed: 23 July 2024).

Rodgers, L. (2018) *Climate change: The massive CO2 emitter you may not know about*, *BBC News*. Available at: https://www.bbc.co.uk/news/science-environment-46455844 (Accessed: 29 November 2023).

Roelofsen, O. *et al.* (2020) *Plugging in: What electrification can do for industry*. Amsterdam.

Rolfe, A. *et al.* (2018) 'Technical and environmental study of calcium carbonate looping versus oxy-fuel options for low CO2 emission cement plants', *International Journal of Greenhouse Gas Control*, 75, pp. 85–97. Available at: https://doi.org/10.1016/j.ijggc.2018.05.020.

Sabbah, A. and Zhutovsky, S. (2022) 'Effect of sulfate content and synthesis conditions on phase composition of belite-ye'elimite-ferrite (BYF) clinker', *Cement and Concrete Research*, 155. Available at: https://doi.org/10.1016/j.cemconres.2022.106745.

Sahoo, N., Kumar, A. and Samsher (2022) 'Review on energy conservation and emission reduction approaches for cement industry', *Environmental Development*, 44. Available at: https://doi.org/10.1016/j.envdev.2022.100767.

Sahoo, N., Kumar, A. and Samsher (2023) 'Design of solar cement plant for supplying thermal energy in cement production', *Journal of Cleaner Production*, 426. Available at: https://doi.org/10.1016/j.jclepro.2023.139151.

Sahu, S. and Meininger, R.C. (2019) 'Performance of CO2-reducing cement based on calcium silicates 15 th International Congress on the Chemistry of Cement', in *International Congress on the Chemistry of Cement*.

Saidur, R. *et al.* (2011) 'A review on kiln system modeling', *Renewable and Sustainable Energy Reviews*, pp. 2487–2500. Available at: https://doi.org/10.1016/j.rser.2011.01.020.

Salzgitter (2022) *World's largest high-temperature electrolyzer achieves record efficiency*, *Sunfire*. Available at: https://www.sunfire.de/en/news/detail/worlds-largest-high-temperature-electrolyzer-achieves-record-efficiency# (Accessed: 26 April 2023).

Samad, S. and Shah, A. (2017) 'Role of binary cement including Supplementary Cementitious Material (SCM), in production of environmentally sustainable concrete: A critical review', *International Journal of Sustainable Built Environment*. Elsevier B.V., pp. 663–674. Available at: https://doi.org/10.1016/j.ijsbe.2017.07.003.

Sanaye, S. *et al.* (2020) 'A comprehensive approach for designing, modeling and optimizing of waste heat recovery cycle and power generation system in a cement plant: A thermo-economic and environmental assessment', *Energy Conversion and Management*, 205. Available at: https://doi.org/10.1016/j.enconman.2019.112353.

Schneider, M. *et al.* (2023) 'The cement plant of tomorrow', *Cement and Concrete Research*, 173. Available at: https://doi.org/10.1016/j.cemconres.2023.107290.

Schoeck, M. (2023) *Cement manufacturer to generate 75% of onsite power with 25 MW solar array*, *PV Magazine*. Available at: https://pv-magazine-usa.com/2023/06/15/cement-manufacturer-to-generate-75-of-onsite-power-with-25-mw-solar-array/ (Accessed: 30 July 2024).

Schumacher, G. and Juniper, L. (2023) 'Coal utilization in the cement and concrete industries', in *The Coal Handbook: Volume 2: Towards Cleaner Coal Utilization, 2nd Edition*. Elsevier, pp. 627–663. Available at: https://doi.org/10.1016/B978-0-12-824327-5.00017-X.

Scrivener, K.L., John, V.M. and Gartner, E.M. (2018) 'Eco-efficient cements: Potential economically viable solutions for a low-CO2 cement-based materials industry', *Cement and Concrete Research*, 114, pp. 2–26. Available at: https://doi.org/10.1016/j.cemconres.2018.03.015.

Segata, M. *et al.* (2019) 'The effects of MgO, Na2O and SO3 on industrial clinkering process: phase composition, polymorphism, microstructure and hydration, using a multidisciplinary approach', *Materials Characterization*, 155. Available at: https://doi.org/10.1016/j.matchar.2019.109809.

Seifu, M.N. *et al.* (2023) 'Exploring reaction and carbonation products of calcium silicate cement', *Journal of CO2 Utilization*, 71. Available at: https://doi.org/10.1016/j.jcou.2023.102471.

Sepúlveda, F.J. *et al.* (2023) 'Efficiency evaluation of photovoltaic systems with batteries considering different voltage levels', *Journal of Energy Storage*, 63. Available at: https://doi.org/10.1016/j.est.2023.106971.

Shah, I.H. *et al.* (2022) 'Cement substitution with secondary materials can reduce annual global CO2 emissions by up to 1.3 gigatons', *Nature Communications*, 13(1). Available at: https://doi.org/10.1038/s41467-022-33289-7.

Shahbaz, M. *et al.* (2021) 'A comprehensive review of biomass based thermochemical conversion technologies integrated with CO2 capture and utilisation within BECCS networks', *Resources, Conservation and Recycling*, 173. Available at: https://doi.org/10.1016/j.resconrec.2021.105734.

Sharma, P., Sheth, P.N. and Sen, S. (2023) 'Aspen plus simulation of an inline calciner for white cement production with a fuel mix of petcoke and producer gas', *Energy*, 282. Available at: https://doi.org/10.1016/j.energy.2023.128892.

Shehata, N. *et al.* (2022) 'Role of refuse-derived fuel in circular economy and sustainable development goals', *Process Safety and Environmental Protection*. Institution of Chemical Engineers, pp. 558–573. Available at: https://doi.org/10.1016/j.psep.2022.05.052.

Simoni, M. (2022) *Towards more sustainable cement production: a no-combustion approach for the decarbonisation of CaCO3*.

Singh, A. and Singh, N. (2024) 'Mechanical properties of silica fume based concrete: A review', *Materials Today: Proceedings* [Preprint]. Available at: https://doi.org/10.1016/j.matpr.2024.05.037.

Skibsted, J. and Snellings, R. (2019) 'Reactivity of supplementary cementitious materials (SCMs) in cement blends', *Cement and Concrete Research*. Elsevier Ltd. Available at: https://doi.org/10.1016/j.cemconres.2019.105799.

Skocek, J., Zajac, M. and Ben Haha, M. (2020) 'Carbon Capture and Utilization by mineralization of cement pastes derived from recycled concrete', *Scientific Reports*, 10(1). Available at: https://doi.org/10.1038/s41598-020-62503-z.

Skworcow, P. *et al.* (2014) 'Optimisation of pump and valve schedules in complex large-scale water distribution systems using GAMS modelling language', in *Procedia Engineering*. Elsevier Ltd, pp. 1566–1574. Available at: https://doi.org/10.1016/j.proeng.2014.02.173.

Ślosarczyk, A. *et al.* (2023) 'A literature review of the latest trends and perspectives regarding alkali-activated materials in terms of sustainable development', *Journal of Materials Research and Technology*, 25, pp. 5394–5425. Available at: https://doi.org/10.1016/j.jmrt.2023.07.038.

Smith, R. (2005) *Chemical Process Design and Integration*. Wiley. Available at: https://nitsri.ac.in/Department/Chemical%20Engineering/PEDB1.pdf (Accessed: 11 July 2023).

Snellings, R., Suraneni, P. and Skibsted, J. (2023) 'Future and emerging supplementary cementitious materials', *Cement and Concrete Research*, 171. Available at: https://doi.org/10.1016/j.cemconres.2023.107199.

Song, Q. *et al.* (2021) 'The occurrence of MgO and its influence on properties of clinker and cement: A review', *Construction and Building Materials*. Elsevier Ltd. Available at: https://doi.org/10.1016/j.conbuildmat.2021.123494.

Song, Q., Guo, M.Z. and Ling, T.C. (2022) 'A review of elevated-temperature properties of alternative binders: Supplementary cementitious materials and alkali-activated materials', *Construction and Building Materials*. Elsevier Ltd. Available at: https://doi.org/10.1016/j.conbuildmat.2022.127894.

Stadler, K.S., Poland, J. and Gallestey, E. (2011) 'Model predictive control of a rotary cement kiln', *Control Engineering Practice*, 19(1), pp. 1–9. Available at: https://doi.org/10.1016/j.conengprac.2010.08.004.

Standards, B. (2011) *BS EN 197-1:2011*, *BSI Standards Publication*.

Strunge, T., Renforth, P. and der Spek, V. (2022) 'Towards a business case for CO2 mineralisation in the cement industry', *Communications Earth and Environment* [Preprint]. Available at: https://doi.org/10.1038/s43247-022.

Summerbell, D.L., Barlow, C.Y. and Cullen, J.M. (2016) 'Potential reduction of carbon emissions by performance improvement: A cement industry case study', *Journal of Cleaner Production*, 135, pp. 1327–1339. Available at: https://doi.org/10.1016/j.jclepro.2016.06.155.

Supriya *et al.* (2023) 'Low-CO2 emission strategies to achieve net zero target in cement sector', *Journal of Cleaner Production*, 417. Available at: https://doi.org/10.1016/j.jclepro.2023.137466.

Svensson, M. (2021) *Numerical Modelling of Calcination of Limestone: An evaluation of existing calcination model*. Umea University.

Svinning, K., Høskuldsson, A. and Justnes, H. (2010) 'Prediction of potential compressive strength of Portland clinker from its mineralogy', *Cement and Concrete Composites*, 32(4), pp. 300–311. Available at: https://doi.org/10.1016/j.cemconcomp.2009.12.004.

Sztekler, K. *et al.* (2016) 'Utilization of waste heat from rotary kiln for burning clinker in the cement plant', *E3S Web of Conferences* [Preprint]. Available at: https://doi.org/10.1051/2016.

Tan, T.H. *et al.* (2023) 'An Overview of the Utilization of Common Waste as an Alternative Fuel in the Cement Industry', *Advances in Civil Engineering*. Hindawi Limited. Available at: https://doi.org/10.1155/2023/7127007.

Technology, A. (2001) *APLUS 111 User Guide*. Cambridge: Aspen Technology Inc.

Teixeira, E.R. *et al.* (2016) 'Comparative environmental life-cycle analysis of concretes using biomass and coal fly ashes as partial cement replacement material', *Journal of Cleaner Production*, 112, pp. 2221–2230. Available at: https://doi.org/10.1016/j.jclepro.2015.09.124.

Terán-Cuadrado, G. *et al.* (2024) 'Current and potential materials for the low-carbon cement production: Life cycle assessment perspective', *Journal of Building Engineering*, 96. Available at: https://doi.org/10.1016/j.jobe.2024.110528.

Timilsina, G.R. (2021) 'Are renewable energy technologies cost competitive for electricity generation?', *Renewable Energy*, 180, pp. 658–672. Available at: https://doi.org/10.1016/j.renene.2021.08.088.

Tiseo, I. (2023a) *Carbon dioxide emissions from the manufacture of cement worldwide from 1960 to 2022*, *Statista*. Available at: https://www.statista.com/statistics/1299532/carbon-dioxide-emissions-worldwide-cement-manufacturing/ (Accessed: 1 July 2024).

Tiseo, I. (2023b) *Carbon intensity of the power sector in China from 2000 to 2022*, *Statista*. Available at: https://www.statista.com/statistics/1300419/power-generation-emission-intensity-china/ (Accessed: 24 November 2023).

Tkachenko, N. *et al.* (2023) 'Global database of cement production assets and upstream suppliers', *Scientific Data*, 10(1). Available at: https://doi.org/10.1038/s41597-023-02599-w.

Tomatis, M. *et al.* (2020) 'Assessing the environmental sustainability of an emerging energy technology: Solar thermal calcination for cement production', *Science of the Total Environment*, 742. Available at: https://doi.org/10.1016/j.scitotenv.2020.140510.

Tregambi, C. *et al.* (2018) 'Solar-driven production of lime for ordinary Portland cement formulation', *Solar Energy*, 173, pp. 759–768. Available at: https://doi.org/10.1016/j.solener.2018.08.018.

Tsai, W.H. and Lin, W.H. (2024) 'Production Decision Model for the Cement Industry in Pursuit of Carbon Neutrality: Analysis of the Impact of Carbon Tax and Carbon Credit Costs', *Sustainability (Switzerland)* , 16(6). Available at: https://doi.org/10.3390/su16062251.

UNFCCC (2015) *Key aspects of the Paris Agreement*. Available at: https://unfccc.int/key-aspects-of-the-paris-agreement (Accessed: 1 July 2024).

Uratani, J.M. and Griffiths, S. (2023) ‘A forward looking perspective on the cement and concrete industry: Implications of growth and development in the Global South’, *Energy Research and Social Science*, 97. Available at: https://doi.org/10.1016/j.erss.2023.102972.

Uwasu, M., Hara, K. and Yabar, H. (2014) ‘World cement production and environmental implications’, *Environmental Development*, 10(1), pp. 36–47. Available at: https://doi.org/10.1016/j.envdev.2014.02.005.

Valderrama, C. *et al.* (2013) ‘Comparative LCA of sewage sludge valorisation as both fuel and raw material substitute in clinker production’, *Journal of Cleaner Production*, 51, pp. 205–213. Available at: https://doi.org/10.1016/j.jclepro.2013.01.026.

Vaquerizo, L. and Cocero, M.J. (2018) ‘CFD–Aspen Plus interconnection method. Improving thermodynamic modeling in computational fluid dynamic simulations’, *Computers and Chemical Engineering*, 113, pp. 152–161. Available at: https://doi.org/10.1016/j.compchemeng.2018.03.019.

Velpuri, V.S.B., Jyothishya, B.C.K. and Vinod, Y. (2021) ‘Experimental studies on durability properties of Sustainable and Eco-friendly materials of GGBS and Fly ash in reinforced cement concrete’, in *IOP Conference Series: Earth and Environmental Science*. IOP Publishing Ltd. Available at: https://doi.org/10.1088/1755-1315/796/1/012070.

Vermeiren, J. *et al.* (2024) ‘Electrification of clinker and calcination treatments in the cement sector by microwave technology – A review’, *Construction and Building Materials*, 428. Available at: https://doi.org/10.1016/j.conbuildmat.2024.136271.

Vikström, A. (2021) *Separate Calcination in Cement Clinker Production: A laboratory scale study on how an electrified separate calcination step affects the phase composition of cement clinker*. Dissertation.

Voldsund, M. *et al.* (2019) ‘Comparison of technologies for CO2 capture from cement production—Part 1: Technical evaluation’, *Energies*, 12(3). Available at: https://doi.org/10.3390/en12030559.

Wan, B. (2004) *Energy Density of Methane - The Physics Factbook*, *The Physics Factbook*. Available at: https://hypertextbook.com/facts/2004/BillyWan.shtml (Accessed: 13 January 2023).

Wang, F. *et al.* (2023) ‘A new perspective on Belite-ye’elimite-ferrite cement manufactured from electrolytic manganese residue: Production, properties, and environmental analysis’, *Cement and Concrete Research*, 163. Available at: https://doi.org/10.1016/j.cemconres.2022.107019.

Wang, H. *et al.* (2015) ‘Organic Rankine cycle saves energy and reduces gas emissions for cement production’, *Energy*, 86, pp. 59–73. Available at: https://doi.org/10.1016/j.energy.2015.03.112.

Wang, L. and Shi, B. (2024) ‘Coupled Oxygen-Enriched Combustion in Cement Industry CO2 Capture System: Process Modeling and Exergy Analysis’, *Processes*, 12(4). Available at: https://doi.org/10.3390/pr12040645.

Wang, X., Guo, M.Z. and Ling, T.C. (2022) ‘Review on CO2 curing of non-hydraulic calcium silicates cements: Mechanism, carbonation and performance’, *Cement and Concrete Composites*, 133. Available at: https://doi.org/10.1016/j.cemconcomp.2022.104641.

Wang, Y. *et al.* (2022) ‘A novel carbon dioxide capture system for a cement plant based on waste heat utilization’, *Energy Conversion and Management*, 257. Available at: https://doi.org/10.1016/j.enconman.2022.115426.

Weibo, S. *et al.* (2017) ‘Effect of K2O and MgO on the formation and hydration activity of ba-bearing calcium sulfoaluminate’, *Ceramics - Silikaty*, 61(1), pp. 6–13. Available at: https://doi.org/10.13168/cs.2016.0053.

Williams, F. and Yang, A. (2024) ‘Potential of Reducing CO2 Emissions in Cement Production through Altering Clinker Compositions’, *Industrial and Engineering Chemistry Research* [Preprint]. Available at: https://doi.org/10.1021/acs.iecr.4c01885.

Williams, F., Yang, A. and Nhuchhen, D.R. (2024) ‘Decarbonisation pathways of the cement production process via hydrogen and oxy-combustion’, *Energy Conversion and Management*, 300, p. 117931. Available at: https://doi.org/10.1016/j.enconman.2023.117931.

Wiloso, E.I. *et al.* (2016) ‘Effect of biogenic carbon inventory on the life cycle assessment of bioenergy: Challenges to the neutrality assumption’, *Journal of Cleaner Production*, 125, pp. 78–85. Available at: https://doi.org/10.1016/j.jclepro.2016.03.096.

Wojtacha-Rychter, K., Kucharski, P. and Smolinski, A. (2021) ‘Conventional and alternative sources of thermal energy in the production of cement—an impact on CO2 emission’, *Energies*, 14(6). Available at: https://doi.org/10.3390/en14061539.

Yang, H.M. *et al.* (2022) ‘High-ferrite Portland cement with slag: Hydration, microstructure, and resistance to sulfate attack at elevated temperature’, *Cement and Concrete Composites*, 130. Available at: https://doi.org/10.1016/j.cemconcomp.2022.104560.

Yang, K.H. *et al.* (2015) ‘Effect of supplementary cementitious materials on reduction of CO2 emissions from concrete’, *Journal of Cleaner Production*, 103, pp. 774–783. Available at: https://doi.org/10.1016/j.jclepro.2014.03.018.

Ying, Z. *et al.* (2018) ‘Simulating the Process of Oxy-Fuel Combustion in the Sintering Zone of a Rotary Kiln to Predict Temperature, Burnout, Flame Parameters and the Yield of Nitrogen Oxides’, *Chemistry and Technology of Fuels and Oils*, 54(5), pp. 650–660. Available at: https://doi.org/10.1007/s10553-018-0971-2.

Zajac, M. *et al.* (2022) ‘CO2 Mineralization Methods in Cement and Concrete Industry’, *Energies*, 15(10). Available at: https://doi.org/10.3390/en15103597.

Zhang, K. *et al.* (2021) ‘Development of high-ferrite cement: Toward green cement production’, *Journal of Cleaner Production*, 327. Available at: https://doi.org/10.1016/j.jclepro.2021.129487.

Zhang, Y. *et al.* (2011) ‘Aspen Plus-based simulation of a cement calciner and optimization analysis of air pollutants emission’, *Clean Technologies and Environmental Policy*, 13(3), pp. 459–468. Available at: https://doi.org/10.1007/s10098-010-0328-y.

Ziaee, E. *et al.* (2016) ‘Utilization of Refuse-Derived Fuel (RDF) from Urban Waste as an Alternative Fuel for Cement Factory: a Case Study’, *International Journal of Renewable Energy Research*, 6(2). Available at: https://doi.org/10.1234/ijrer.v6i2.3170.

Zieri, W. and Ismail, I. (2018) ‘Alternative Fuels from Waste Products in Cement Industry’, in *Handbook of Ecomaterials*. Springer International Publishing, pp. 1–24. Available at: https://doi.org/10.1007/978-3-319-48281-1_142-1.